Port of Rotterdam

TU Delft Delft University of Technology

Sailing through the fluid mud

AUTHOR

A.P.K. Goda

Rheological and plate's hydrodynamic resistance in fluid mud measurements for the nautical bottom applications

An experimental study for sailing through fluid mud applications

Author: Aditya Pavan Kumar Goda

Student number: 5005574

A thesis submitted to Delft University of Technology to demonstrate attainment of a professional level within his Offshore and Dredging Engineering MSc Degree program.

Chair: Dr. ir. G.H. Keetels

Department of Mechanical, Maritime and Materials Engineering

Delft University of Technology
Academic year: 2019 - 2021

TU Delft Delft University of Technology

EVALUATION COMMITTEE

Dr.ir. G.H. Keetels (TU Delft)

Dr.ir. A.M. Talmon (TU Delft, Deltares)

Dr. Alex Kirichek (TU Delft)

MSc. Stefano Lovato (TU Delft)

This master's project was conducted at the

Water & Soil Flume and Physics Laboratory

Deltares

PERMISSION FOR USAGE

STUDENT’S NAME: Aditya Pavan Kumar Goda

SUMMARY

Ships are considered the best mode of transport throughout the human history. The demand of the goods transportation across the world increased exponentially from the past few decades. Therefore, the ships size are increasing and also demanding better infrastructure at ports and harbours.

When a ship reaches the shore, the water depth reduces and thus the under keel clearance also reduces. The ship keel clearance influences the maneuverability of the sailing ship. Scientists and engineers are keenly studying the impact of very low under keel clearance and defining nautical bottom.

In this thesis project, the link between the fluid mud rheology and its density is first investigated. The exponential relation reformulated between the density and yield stress necessitates the direct measurement of rheology for navigability. It was confirmed true that the yield strength grows exponentially with the density of the fluid mud. However, at higher densities of mud, more thixotropy is observed in the flow curves. Besides, the Power-law relations were found for the relation with volumetric concentration, for yield stress in agreement with fractal dimension theory.

Second, quantification of the thixotropy effect of fluid mud is conducted to justify the importance of the time-dependency effect in the rheological modeling. We found that an unremolded fluid mud has high thixotropy even at high shear rates. However, diluted and remolded fluid mud at high shear rates found a negligible thixotropy effect. We also observed that Houska's modeling curve coincides perfectly with the flow curve of fluid mud at high shear rates, and also it integrates the thixotropy into the modeling.

Third, the total resistance of a plate moving through fluid mud is measured and compared to the frictional forces calculated using the available analytical formulas of a plate moving in Bingham fluids and Power-law fluids. The moving plate is an abstraction of a vessel's keel sailing through the fluid mud. We found that the total resistance of the plate moved in fluid mud at low velocity agrees with the frictional force of a plate moved in Bingham fluids. As the velocity increases, the stagnation pressure becomes significant, and the deviation of the total resistance of plate and frictional force of a plate increases. Thus, to estimate the total resistance of a plate moved in mud, normal forces (stagnation pressure) and vortices at edges should be investigated because these need to be subtracted.

The experimental data in this thesis are made resourceful to help researchers validate their Computational fluid dynamics(CFD) models in the application of sailing through the mud.

Keywords

Fluid mud, total resistance, Rheology, Rheometry, Flat plates, Thixotropy, Non-Newtonian Modelling, Houska thixotropy, Port of Rotterdam, Beerkanaal, Calandkanaal, 8e Petroleumhaven.

Contents

Nomenclature

Acronyms

CFD	Computational Fluid Dynamics
CSR	Controlled Shear Rate
CSS	Controlled Shear Stress
EFC	Equilibrium Flow Curve
PIANC	Permanent International Association of Navigation Congresses
PSD	Particle Size Distribution
UKC	Under Keel Clearance

Greek Symbols

δ	Boundary layer thickness	m
λ	Structural parameter in Houska model	–
τ_0	Yield stress of fully structured fluid in Houska model	Pa
τ_∞	Yield stress of totally destructed fluid in Houska model	Pa
η	Dynamic viscosity	Pa · s
$\dot{\gamma}$	Shear rate	$1/\mathrm{s}$
γ	Shear strain	
κ	Consistency in Herschel-Bulkley model	
τ	Shear stress	Pa
τ_y	Bingham yield stress	Pa

Roman Symbols

a	Structural growth parameter in Houska model	–
b	Structural decay parameter in Houska model	–
Bi	Bingham number	–
C_D	Drag coefficient	–
F_d	Frictional force exerted on a plate	N
n_f	Fractal dimension	–
Re	Reynolds number of the fluid flow	–
m	Coefficient of fluid consistency in power-law model	$\mathrm{Pas^n}$
n	Flow index in the power-law model	–

Chapter 1

Introduction

1.1 Background

For many millennia, humans have been using the waterways for the movement of goods and people. However, after the first industrial revolution, the infrastructure of ships was significantly improved. For example, sail-powered to steam-powered, oil-powered, to digital support transport. Therefore the transport rates at ports are increasing, and so the vessel size.

The Port authorities are concerned with the safe navigation of ships and ever-changing sea bathymetry (Rodrigue, 2020). In the Netherlands, Rijkwaterstaat maintains the waterways and provides updates of water levels for safe navigation. Shippers use these water level data to determine the load capacity for safe shipping. However, the increased shipping business led to larger draughts of vessels. Therefore, during the design of canals, water depth- draught ratios are used for safe navigation. However, such guidelines are not available for natural water bodies because of fluctuating water levels and changing bathymetry.

The Port of Rotterdam is looking to improve the port infrastructure and facilities with emerging technology that enables the ship to sail safely through the fluid mud. This master thesis is part of the PRISMA project conducted in collaboration with Hamburg Port Authority, Rijkwaterstaat, TU Delft, Hamburg University of Technology, MARIN and Deltares.

1.2 Problem definition

The growing dimensions of vessels demand more significant drafts for safe navigation. Sea-going vessels do not have these problems because of extensive water depths. However, for the ships reaching ports or harbors, the ship's and bed's clearance becomes essential. Therefore, to increase the water depth, seaports and harbors often do the dredging.

Instead of maintenance dredging, another alternative option is to adopt the nautical bottom approach (PIANC, 2014), where can use fluid mud layers for the Under Keel Clearance (UKC) estimations (see Figure 1.1). PIANC (2014) defined nautical depth as "the level where physical characteristics of the bottom reach a critical limit beyond which contact with a ship's keel causes either damage or unacceptable effects on controllability and maneuverability." So, the density and yield stress of the fluid mud are considered as the physical characteristics of nautical bottom estimations. However, it is not clear in the literature which of the fluid mud properties (density/ yield strength) should be considered for the nautical bottom approach and how these two parameters are related Kirichek et al. (2018).

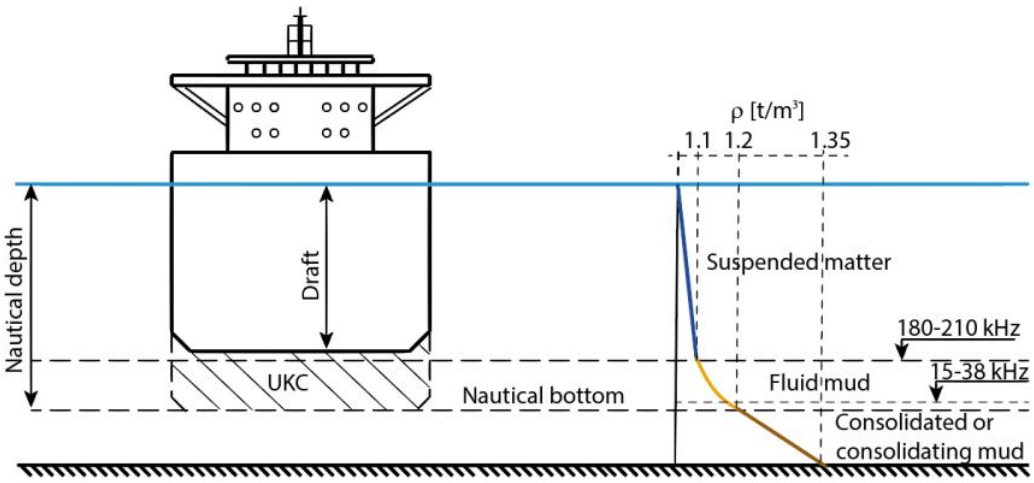

Figure 1.1: Nautical bottom concept. Schematic sketch is taken from Kirichek et al. (2018)

The fluid mud is defined as a mixture of fine sand, silt, clay, organic matter and water. Thus, the composition of fluid mud can depend on the geographical location (Mehta, 2013). Therefore, the nautical bottom criteria can also change within the port or harbor area. The conventional method to determine the bottom is by identifying the interface of the bed sediments and water layers using the hydrography surveys. To analyse the fluid mud density and rheology on-site, Kirichek et al. (2020) provided more information on advanced in-situ tools.

When a ship sails through the fluid mud, there will be a predominant influence on the ship's resistance. In order to determine the criteria and type of nautical depth for safe navigation, the composition and the effect of fluid mud rheology on the ship's maneuverability also should be known.

Some of the full-scale experiments can be found in Sellmeijer & van Oortmerssen (1984) and Barth et al. (2016). They provided the relations between the mud and water interface, effect on ship behavior by the maneuverability and speed of the ship. However, full-scale tests are challenging to perform because the situation and observed conditions change. Some of the controlled model tests can be found in Delefortrie (2007), Vantorre (1991), and Brossard et al. (1991) on the implications of the thickness of the mud layer, depth, and speed on the ship maneuverability. A numerical analysis is another way to look into the impact of fluid mud properties on ship maneuverability. Kaidi et al. (2020) studied the influence of density and viscosity of fluid mud on the resistance of the ship and Gao et al. (2015) studied the effects of ship speed and mud layer thickness on the ship resistance. Leijs (2021) found that the yield stress of the fluid mud mainly affects pressure component in total resistance of the ship. It is still unclear which fluid mud characteristic is affecting the ship resistance.

In addition to the laboratory and full scale experiments, different analytical models, empirical models, and numerical models are developed to predict the non-Newtonian flow behavior of mud (Fitton et al., 2007). It can replicate a wide range of water bodies and can also model highly concentrated non-Newtonian flows. However, there is lack of non-Newtonian rheological modelling which takes fluid mud properties like shear-thinning and time-dependency (thixotropy) into account.

1.3 Objective

This thesis intends to study the rheological behavior of fluid mud from the Port of Rotterdam, investigate the link between the yield stress and density, and verify the available analytical formulas in the literature for the frictional force of plate dragged in non-Newtonian fluids with the total resistance of a plate moved in fluid mud.

The research questions of this thesis are:

1. What is the link between the presence of clay and the rheological properties of mud? And how it can link to the density and the yield stress of mud?
2. How thixotropy of fluid mud can be quantified and taken into account in the non-Newtonian rheological modeling?
3. What is the relation between towing forces for a plate dragged in fluid mud and rheology? What existing analytical formulas for non-Newtonian fluids can be used for estimating the plate resistance measured in the flume experiments?

1.4 Approach

This thesis consists of three main parts. First a literature study was done to have an understanding of the rheological experiments. Second a rheological study of fluid mud from different locations of Port of Rotterdam is conducted. This experiment is also helpful to design the test matrix for flume experiments for measuring the plate resistance dragged in fluid mud. Third is the flume experiments in which total resistance of the plate moved in fluid mud is measured and then compared to the analytical formulas available for Bingham fluids and power-law fluids.

Part 1 - Literature study

A literature study was done to describe the fluid mud behaviour. This includes:

1. Elaboration of fluid mud characterization, formation and in-situ testing tools.
2. Providing the available theories for describing the link between the density and rheology.
3. Describing the rheology of non-Newtonian fluids and its measurements through rheometry practice. This includes:
    - Yield stress measurement,
    - Thixotropy effect quantification
4. Understanding the rheological models that also includes time-dependent properties of the fluid mud.
5. Elaboration of analytical formulas to find the frictional force of a plate moved in Bingham fluids and power-law fluids.
6. Conclusions and knowledge gaps.

Part 2 - Rheology study of mud samples from different Port locations

Rheology tests are performed on fluid mud samples from Beerkanaal, Calandkanaal, and 8e Petroleumhaven by diluting with seawater and freshwater. The tests concerns:

1. Investigating the influence of salt content on the rheology of fluid mud.
2. Analysing the applicability of fractal dimension theory relating volumetric solids concentration and yield stresses.
3. Standardizing the rheometry test protocols for the flume experiments.

Part 3 - Flume experiments for studying the plate resistance in fluid mud

The flume experiments are performed using the fluid mud from the Calandkanaal. In the tests, a plate was dragged in the fluid mud at different velocities. During the tests, the fluid mud samples were collected for rheology tests before and after the towing experiments. The tests concern:

1. Performing experiments by moving a plate in mud at different velocities and recording the total resistance of a plate in mud.
2. Conducting the rheological tests on the fluid mud samples collected during the tests.
3. Comparing the total resistance of the plate moved in mud to the frictional force of a plate calculated using analytical formulas moved in a Bingham fluid and power-law fluid.
4. Fitting the Houska model to the flow curves of the mud samples collected during the flume experiments.
5. Quantifying the fluid mud thixotropy effect using the hysteresis loop method and the sensitivity method.

1.5 Contributions

This thesis is a part of Port of Rotterdam's PRISMA project, which collaborated with Hamburg Port Authority, MARIN, TU Delft, TU Hamburg, Rijkwaterstaat and Deltares. The rheology tests and flume experiments are performed at Deltares. A towed object borrowed from Hamburg Port Authority and also another towed object was designed and built at Deltares.

Chapter 2

Literature review

2.1 Fluid mud

Fluid mud is a highly concentrated aqueous suspension of fine sediment particles. The settling is hindered substantially in fluid mud by the proximity of flocs and fine grains (McAnally et al., 2007). The other names of the fluid mud are cremes de vase (French) and slib (Dutch). Another definition of fluid mud defined by Foda et al. (1993) is, the fluid mud is a reverse process of consolidation in which water quantity is increased in the mud and form suspension of particles.

2.1.1 Characterization of fluid mud

Characterization is essential in understanding the fluid mud processes and presenting information available in the literature on fluid mud. Some of the fluid mud characteristics are:

1. **Composition:** Water, fine sand, clay, silt, and organic materials make up fluid mud. As per the Went-worth scale for sediment sizes, the particle size of fluid mud is less than 62.5 microns in diameter (McAnally et al., 2007). Here, particle size refers to the individual grain constituents but not the loosely bound flocs present in the mud.
2. **Density:** Near the bottom of the mud beds, different layers of mud like fluid mud, pre-consolidated, and consolidated mud can be found which means the density increases with the depth. In addition, these mud layers with varying densities have different rheological properties and composition (Shakeel et al., 2021). Figure 2.1 taken from Shakeel et al. (2021), represented the relation between the fluidic yield stress as a function of density. In addition, they concluded that the rheological behavior is significantly dependent on the fluid mud density and total organic content (see Figure 2.1b.

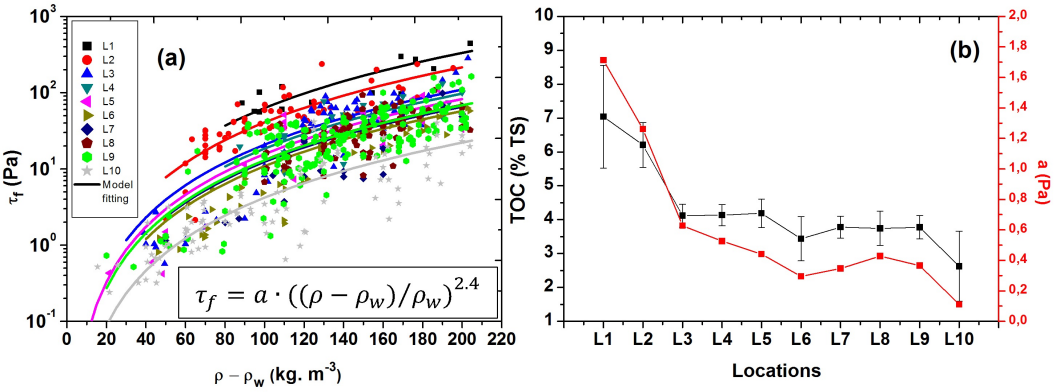

Figure 2.1: (a) Relation between the density and fluidic yield stress of fluid mud samples from port of Hamburg. (b) Relation between the total organic content and different river locations of port of Hamburg. Image taken from Shakeel et al. (2021).

3. **Water content:** The engineering perspective on water content evaluation differs. Fluid mud concentrations in dredging range from 50 to 350 kg/m^3 (Teeter, 1992). In natural occurrence, fluid mud lower limit of concentration is 10 kg/m^3 (Kineke et al., 1996), upper limit of 250 kg/m^3 (Allen, 1991).

4. **Particle size distribution (PSD):** In low organic content of fluid mud, 50-70$\%$ solids are of clay sized (McAnally et al., 2007). In fast changing environments, the sand particles (larger size), has tendency to settledown fast and entrain in very less fraction of fluid mud.
5. **Mineralogy:** In fluid mud, platey, which is a cohesive mineral, dominates in mineralogy. In the Gironde estuary, 60-70$\%$ are of clay and mica, 20-25$\%$ are of quartz, and 5- 10$\%$ are of calcite (Granboulan et al., 1989). Studies at Mobile Bay, Alabama, show that dredged mud was dominated by kaolinite and montmorillonite, and the James River, Virginia, was dominated by chlorite and illite (Nichols et al., 1978)
6. **Organic matter:** Fluid mud in a calm environment, such as lakes, with vast amounts of organic matter, substantially affects dewatering and keeps the bed fluid (McAnally et al., 2007). High accumulation of organic content can also found in inland harbors, which creates an intense suspension of fluid mud because of bacterial respiration (Abril et al., 2004; Zander et al., 2020).
7. **Rheological properties:** Fluid mud exhibits viscoelastic, viscoplastic, and/or pseudoplastic flow behaviors. This flow behavior depends on hydrodynamic conditions, mud characteristics, and intermolecular arrangement. Fluid mud rheometry helps us to understand the behavior of fluid mud from flow curve measurement. In rotational rheometry, tests like controlled shear stress (CSS) and controlled shear rates (CSR) variants are performed to obtain flow curves and viscous curves.
8. **Thixotropic properties:** The stress history influences rheological characteristics such as yield stress τ_y, viscosity η, and other fluid mud properties. When constant and sufficient stress or strain is applied on the fluid mud, yield stress and viscosity decrease over time. After a certain resting period, thixotropic strength will be regained. For natural mud to build up to τ_y and associate molecular structure appears to be in the range of 10^4-10^5 seconds (Van Kessel & Blom, 1998).

2.1.2 Fluid mud formation

In the process of sediment erosion in water bodies and on land, the mobile sediments consist of cohesive material (fine-grained) and non-cohesive material (coarse-grained). In shelf waters and tidal embayments, waves and tide action aids the formation of fluid mud (McAnally et al., 2007). In addition, field studies revealed that disposal of dredged materials in open water created fluid mud (Nichols et al., 1978).

As per Mehta et al. (2014), fluid mud is formed by the influence of waves and currents on the muddy sea bed, which entrains the coagulation and settling of the particles. Thus, during the settling of particles, multiple layers of varying concentrations are formed, see Figure 2.2. The top layer (above Lutocline) exhibits Newtonian behavior because of low sediment concentration. Below this layer, fluid mud layer, the sediment particles concentration is increased, creating the larger flocs. However, in the fluid mud later, the insufficient sediment concentration tends to exhibit significant non-Newtonian behavior. As the concentration of the sediments increases over the depth, the material starts exhibiting Newtonian behavior again (Mehta et al., 2014). Finally, the bottom layer has consolidated mud.

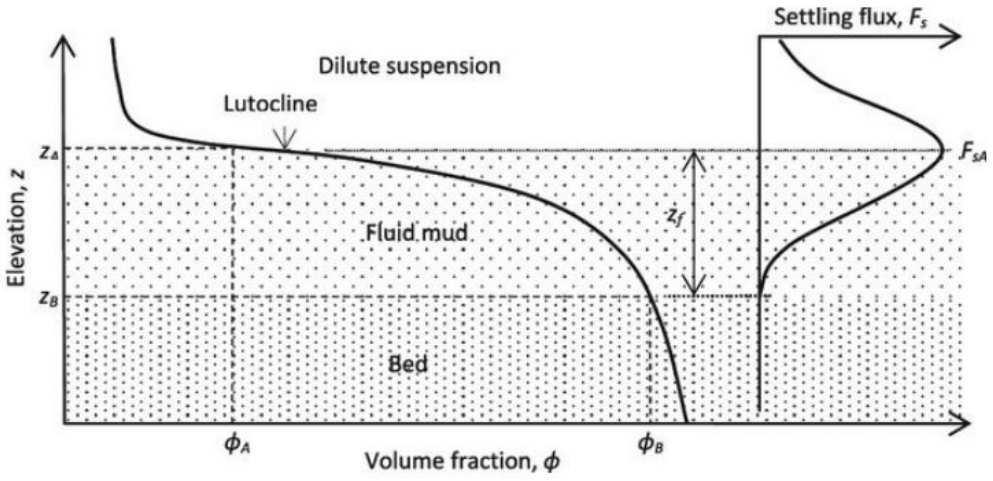

Figure 2.2: The image illustrates different layers of mud at a seaway depth in which the sediment concentration increases over depth and forms different layers. Image taken from Mehta et al. (2014).

2.1.3 In-situ fluid mud testing tools

Nowadays, using t the fluid mud layers, finding undrained shear strength, fluid mud sampler, portable rheometers, and density measurements. Some of the most commonly used in-situ tools are listed below.

1. **Graviprobe:** This measures the undrained shear strength of the fluid mud. Graviprobe is a free fall cone built with accelerometers. The relation of free-fall acceleration and undrained shear strength is mentioned in Bezuijen et al. (2018).

Figure 2.3: The image shows the Graviprobe device. Image taken from (Kirichek et al., 2020).

2. **Rheotune:** This correlates yield stress and density to mechanical tuning fork vibrations in the frequency range of 500 to 800 Hertz (Kirichek et al., 2020).

Figure 2.4: Rheotune. Image taken from (Kirichek et al., 2020)

3. **FANN 286 rheometer:** This device is portable and easy to use on collected mud samples. In this

rheometer configuration, the cup rotates, and the bob geometry is connected to the spring, which records its torque. Thick fluid materials cannot be tested in this rheometer. This rheometer has built-in fixed rotational speeds and also has a variable speed option at low rotational speeds. While performing tests, the shear stress is recorded for different rotational speeds.

Figure 2.5: FANN 286 rheometer

4. **Slib sampler:** Along the vertical direction of this device, the in-situ fluid mud is collected. The samples are taken using the syringe, and density is measured using Anton Paar DMA 35. The procedure is repeated along the axial direction of the slib sampler, and vertical in-situ density profiles are measured (Kirichek et al., 2020).

Figure 2.6: Slib sampler. Image taken from (Kirichek et al., 2020)

2.2 Rheology

Rheology is the science of material's flow and deformation. Some materials exhibits viscoplastic properties, behaves as visco-elastic material upto yielding point and then non-Newtonian fluid. The key link between material flow and deformation behavior is that the shear force creates significant deformations, which causes the material to flow.

2.2.1 Why fluid mud rheology?

Fluid mud exhibits viscoelastic, viscoplastic and/or pseudoplastic flow behaviours (McAnally et al., 2007). Fluid mud rheometry helps us to understand the behaviour of fluid mud from flow/viscous curve measurements.

2.2.2 Glossary of rheology in brief

1. **Rheometry:** The experimental practices followed in rheological tests to define fluid rheological properties.
2. **Flow:** Any material flow can be divided into one of two categories (Liepsch, 2016). The first type of flow is the shear flow, in which the fluid components shear over one another. The second type of flow is extension flow, which occurs when fluid components flow towards or away from each other. The most frequent flow behavior observed in fluids is shear flow, which can be studied with rotational viscometers or rheometers.
3. **Shear stress (τ)**: It is defined as shear force (*F*) acting on a unit area (*A*), see equation 2.1. Let the width of the layer be *h*. On the application of this shear force, the top layer displaces by a distance *x*. The shear strain (γ), also known as the displacement gradient, is given by the ratio of lateral displacement and width, see Eq. 2.2.

$$\tau = \frac{F}{A} \quad [Pa] \tag{2.1}$$

$$\gamma = \frac{x}{h} \tag{2.2}$$

4. **Shear rate:** In solid materials where the flow behavior is not possible, the shear strain is finite for shear stress applied. While in liquids, the shear strain increases over time of shear stress applied. Thus, velocity gradient is created, ($d\gamma/dt$), and often termed as Shear rate ($\dot{\gamma}$).

$$\dot{\gamma} = \frac{d\gamma}{dt} \quad [1/s] \tag{2.3}$$

5. **Dynamic Viscosity:** The shear viscosity, or dynamic viscosity (η), is a proportionality coefficient between shear stress and shear rate. It is also known as apparent viscosity, where it characterizes the tangent to the flow curve.

$$\eta = \frac{\tau}{\dot{\gamma}} \quad [Pa.s] \tag{2.4}$$

6. **Non-Newtonian fluids:** Shear stress or shear rate affects the viscosity of these fluids. Figure 2.7 represents various flow behaviors.

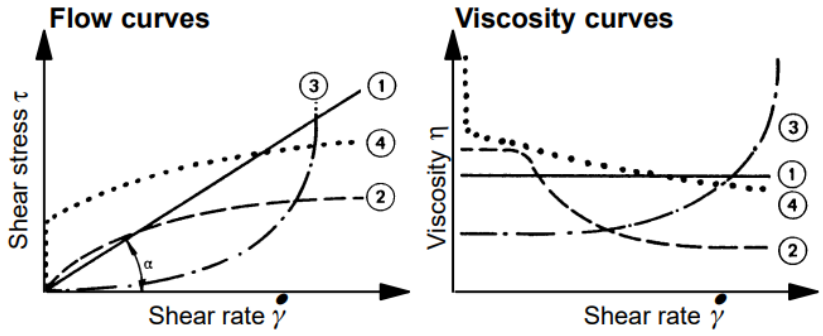

Figure 2.7: Different types of flow behaviour- 1) Newtonian liquid, 2) Pseudo-plastic liquid, 3) Dilatant liquid, and 4) Plastic liquid. Figure adapted from Schramm (1994)

7. **Shear Thinning:** In shear-thinning fluids, the viscosity decreases on the application of shear stress or shear rate (Chandran et al., 2020). The zero shear viscosity (η_0) refers to the viscosity at low shear rates and the Viscous curve plateaus at low shear rate regions. The infinite viscosity (η_∞) refers to the viscosity at high shear rates. The Viscous curve shows a plateau profile. The magnitude of infinite viscosity is several orders smaller than zero viscosity (Liepsch, 2016).

2.2.3 Rheometers

In the world market, there are sophisticated rheometers and viscometers available to test the non-Newtonian fluids. The design of the rheometers is based on input, either controlled stress (CSS) or controlled shear rate (CSR). In advanced rheometers, both of these functional features are available. However, there is two design difference in these rheometers (Schramm, 1994). The outer cylinder (cup) or plate is stationary while the inner geometry (rotor) is driven and vice versa. In both cases, the torque on the inner element is measured.

Controlled shear rate (CSR) in comparison to controlled shear stress (CSS)

The difference between the CSS and CSR should be known in order to perform the tests on visco-elastic fluids and specifically visco-plastic fluids to have a better understanding of some solid and liquid shear responses (Schramm, 1994). Most controlled shear stress (CSS) tests are designed to obtain a higher sensitivity to compare similar fluids at low shear rate values. Gleißle (1993) showed the importance of CSS tests while differentiating the polymer melts of different grades.

Importance of rotational geometry

Based on the viscosity of the sample material ranging from thick to fluidic, the type of rotational geometry chosed for rheology tests (Stieger, 2019). For instance, parallel plate geometry will be used to test high viscous materials like chocolate or honey. For creamy materials, bob-cup, vane-cup geometries can be used. For fluids with low viscosity like water, double gap bob cup geometry can be used (Stieger, 2019). Bob-cup and vane-cup geometry configurations are used in this project to study the rheology of fluid mud samples collected in flume experiments.

Standard rheological protocols

Some of the standard rheological protocols which are often performed on non-Newtonian fluids are described below:

1. **Stress growth:** A constant shear rate is applied in this test, and corresponding shear stress is monitored over time. This test determines the yield points, peak stress, and steady-state stress (Chhabra & Richardson, 2008).
2. **Stress sweep:** Shear stress is increased linearly from zero to a value greater than the yield point in this test, and the corresponding shear rate is recorded. Similar tests can be found in Barnes (1999), Cheng (1986), and Shakeel et al. (2020b) to find the yield stresses of the visco-plastic fluids.
3. **Oscillatory amplitude sweep:** The shear stress or strain is applied in a sinusoidal form at a specific frequency in this test. The storage modulus (G') and loss modulus (G'') are determined from this test (Schramm, 1994). The primary goal of dynamic tests like these is to explore samples rheologically at rest structure, which implies without rupturing the internal structure (Schramm, 1994).

2.2.4 Yield stress of non-Newtonian fluids and its measurement

The behavior of the many fluids can be explained by their rheological properties, like the material yield stresses. The yield stress is a critical stress point below which the viscosity becomes infinite and exhibits solid characteristics. To define this critical phase of this transition, researchers came forwards with their definitions and explanations. Some of the most widely used yield stresses are:

1. **Bingham yield stress:** The word "yield stress" was first coined by Bingham and his coworkers (Steffe, 1967). They stated yield stress as a profound and considerable change in material behavior under a less resistant state. In rotational rheometer experiments, the Bingham yield stress is determined by extrapolating the ramp down controlled shear rate flow curve onto the shear stress axis. Figure 2.8 represents the method to find Bingham yield stress from the flow curve.

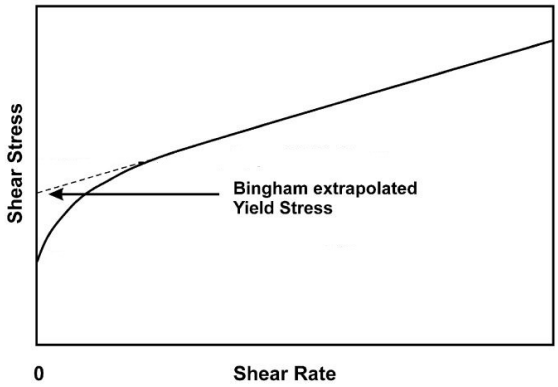

Figure 2.8: Measurement of Yield stresses. Plot taken from Boger (2009)

2. **True Yield Stress:** There are many misconceptions about how the materials yield. The Bingham yield stress should be utilized only to fit the model. However, it has no relation with the actual yield stress (Boger, 2009). The yield stress of the fluid should be determined in low shear rate experiments. However, at such low shear rates, the tests with smooth concentric cylinder geometries, wall-slip may happen.

   Boger (2009) mentioned in his research paper that vane in cup geometry technique eliminates the wall-slip condition. In addition, they performed experiments on paste-like materials and of known properties to analyze the different rheometry techniques. Figure 2.9 illustrates the results obtained from the experiments performed on capillary rheometer, rheometer with conventional couette, and a vane-cup geometry for a paste of true yield stress of 250 Pa. At high shear rates, both Couette and capillary rheometers agree with data points, and below the shear rate of $300 s^{-1}$ shows the significant influence of the slip. On the other hand, the correct yield stress is obtained by extrapolating the vane and cup readings. As a result, vane-cup geometry is recommended for investigations with thick samples.

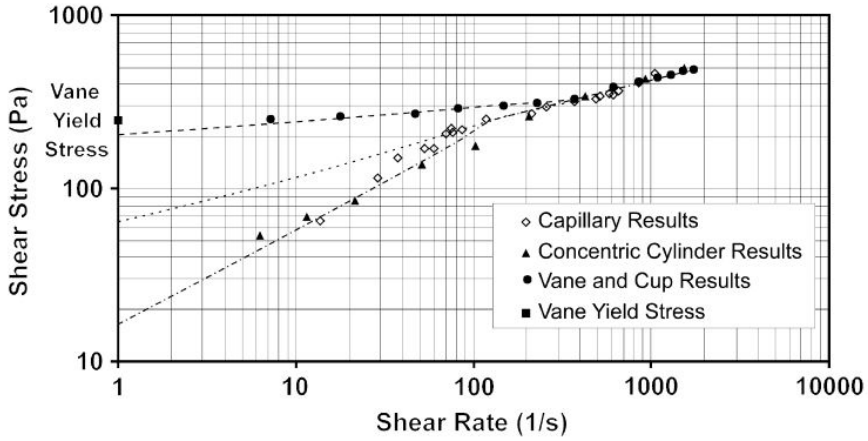

Figure 2.9: The image shows the comparison of different rheometry techniques performed on a paste sample of known yield stress 250Pa. Plot taken from Boger (2009)

Barnes (1999) also observed the condition of wall slip at low shear rates. He defined the wall slip as pseudo yield stress and concluded this artifact as "overlooked by many researchers" see figure 2.10. The leading cause of this condition is still unknown.

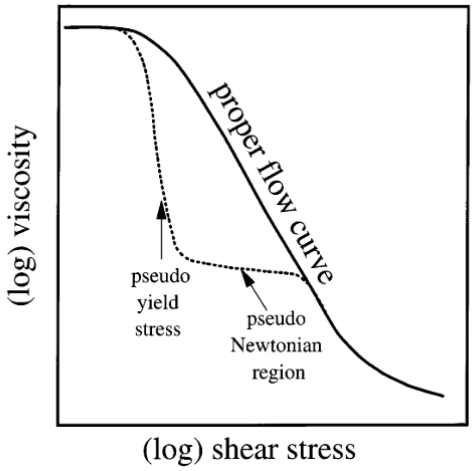

Figure 2.10: Barnes schematized the pseudo yield stress in his research paper, Barnes (1999).

3. **Yield Stresses in thixotropic fluids: Static Yield Stress and Dynamic Yield Stress** The yield stresses in thixotropic fluids are a function of the material's molecular structure. As a result, the recovery period is also a factor. Cheng (1986) reviewed the methods for yield stress in thixotropy fluid. The yield stress obtained for a fully structured fluid material is the same as that of the equilibrium flow curve (EFC).

   EFCs are constant structure curves with constant shear stress and rate across time. When the EFC is exceeded, the structure breaks down, and the shear stress drops. The structure recovers below EFC, and shear stress rises. The yield stress grows as the structure recovers over time. In some materials, the yield stress obtained by extrapolating the EFC is not the same as that produced by prolonged storage materials. The dynamic yield stress is obtained by extrapolating EFC, while the static yield stress is obtained by storing the material for a long time, see figure 2.11.

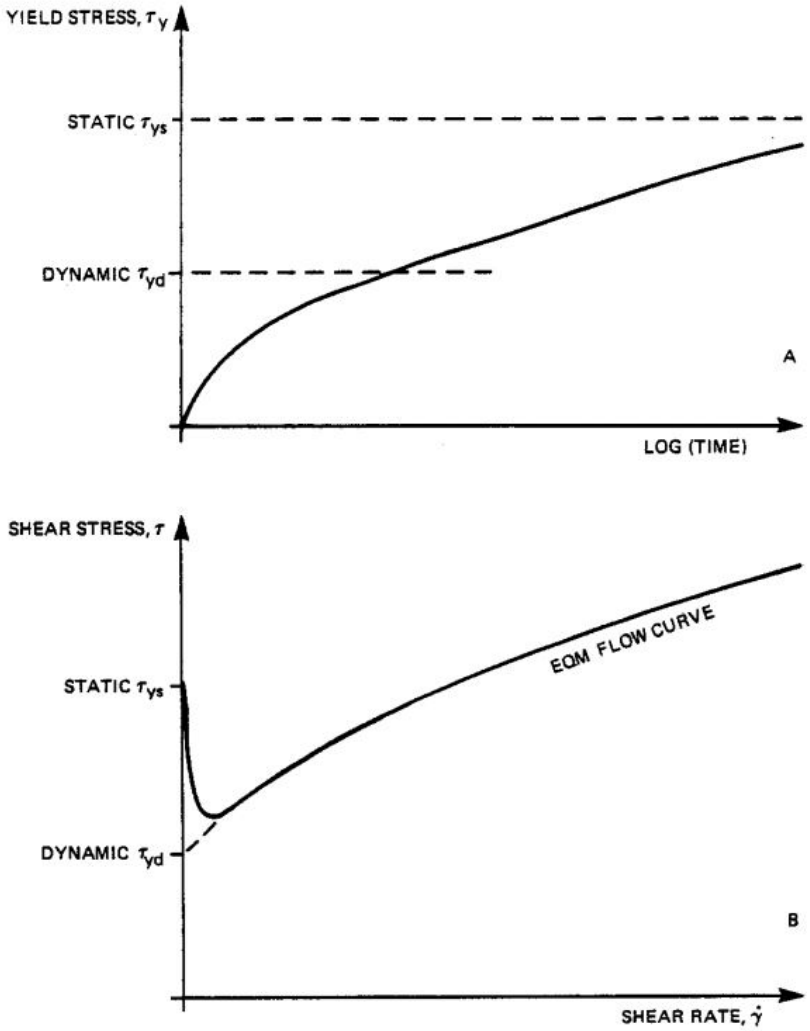

Figure 2.11: Schematic representation of Static and dynamic yield stress defined by Cheng (1986)

Cheng (1986) also developed methods for detecting these stresses. The dynamic yield stress is determined by probing the material at a constant shear rate, while the static yield stress is determined by probing the material at constant shear stress.

In rheometry, the dynamic yield stress is determined from the ramp-down flow curve by performing the controlled shear stress or shear rate experiments using vane geometry. On the other hand, the true static yield stress is determined from the ramp-up flow curve by performing the controlled shear stress experiments using vane geometry, see Figure 2.12.

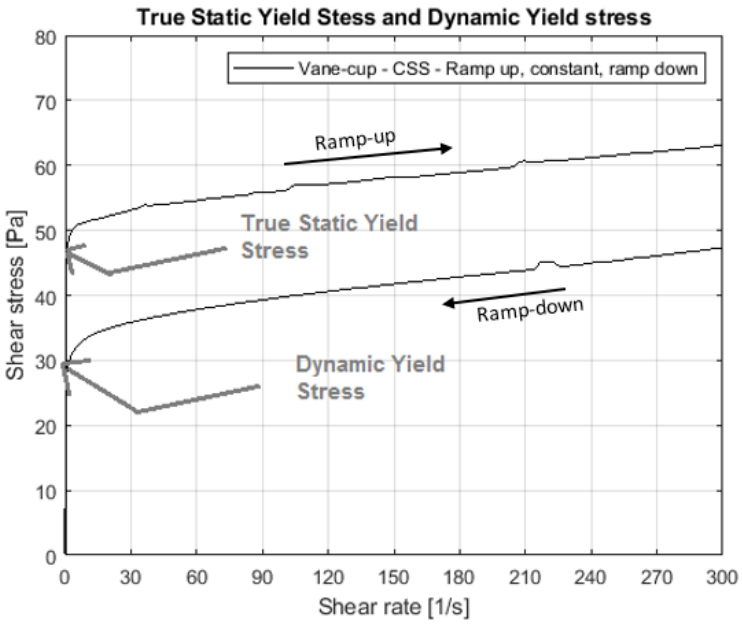

Figure 2.12: Image illustrates the true static and dynamic yield stresses on a flow curve obtained by probing the fluid mud of Beerkanaal in controlled shear stress mode.

4. **Two step yielding processes: Static and Fluidic yield stresses** Ahuja et al. (2020) presented an overview of two-step yielding observed in the available literature. The two-step yielding is distinguished for soft materials based on the microstructures and intermolecular interactions.

   These two-step yielding stresses are referred to as Static and Fluidic yield stresses by Shakeel et al. (2020a). The static yield stress is defined as the lowest stress at which the fluid mud's microstructure begins to distort, but the fluid does not flow. On the other hand, the fluidic yield stress is defined as the yield stress at which the fluid's entire microstructure is destroyed, and the fluid begins to flow. Controlled shear stress ramp-up tests with bob geometry are used to determine the static and fluidic yield stress on the Viscous curve. Shakeel et al. (2020a) observed the two-step yielding in fluid mud employing Couette, parallel plate (PP), and vane geometries with the first step being substantially smaller in case of vane tests.

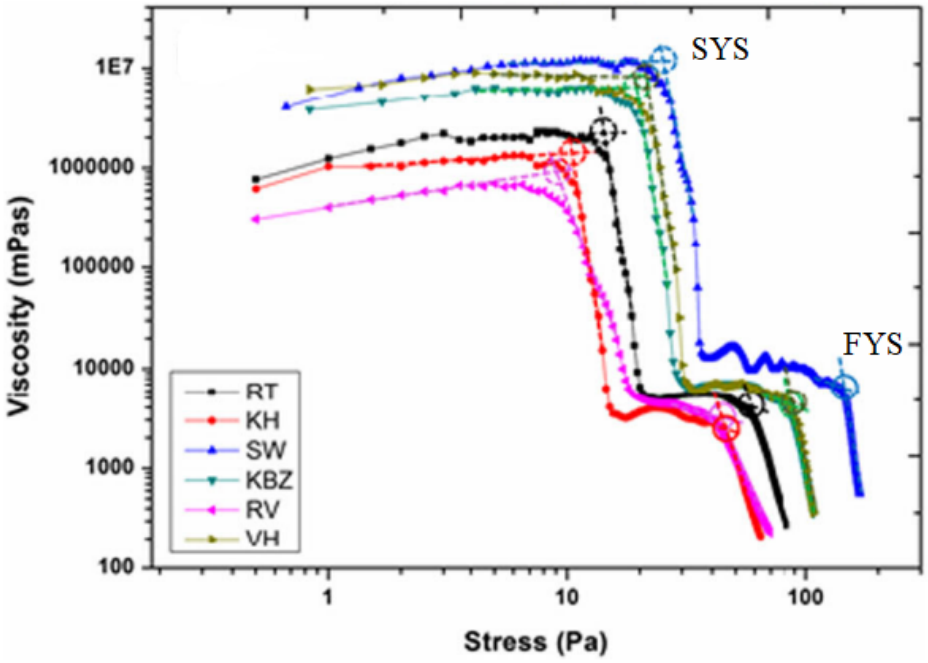

Figure 2.13: The picture legend refers to the different sample locations represents two sharp declines in the Viscous curves obtained from bob-cup geometry (Shakeel et al., 2020a)

.

Shakeel et al. (2021) presented the microstructural study of fluid mud and provided the reason for two-step yielding. Figure 2.14 illustrates two steps yielding with microstructures observed in RheOptiCAD combined with oscillatory sweep tests conducted in roto-viscometer measured with bob-cup elements. In amplitude ramp-up, the first yield point and breakage of the flocs inter-connection were observed. After that, plateau behavior was noticed on further shearing between first and second yield points, attributing to the formation of cylindrical-like structures. On continuous shear, these cylinder-like structures break into small flocs and thus result in a second yield point. The first and second yield points are associated with the two declines in the Viscous curve, see Figure 2.13.

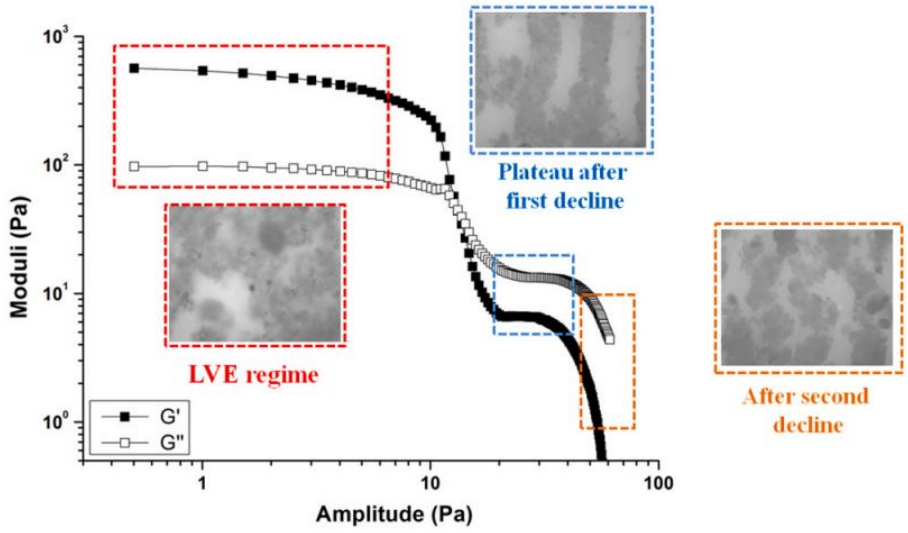

Figure 2.14: Two step yielding in bob-cup oscillatory sweep tests with micro structures. Adapted from Shakeel et al. (2021).

2.2.5 Manifestation of thixotropy effect in non-Newtonian fluids

In the history of thixotropy, there was often confused with the definition of thixotropy (Mewis & Wagner, 2009). For instance, Goodeve (1939), defined thixotropy as "an isothermal reversible decrease of viscosity with an increase of the rate of shear." Presently this is well known as shear thinning. However, the scientific

community currently describes thixotropy as the persistent drop in viscosity with time when a flow is applied to a previously relatively still material and the subsequent recovery of viscosity when the stream is stopped. This description follows IUPAC nomenclature ("The IUPAC Compendium of Chemical Terminology", 2019). The fundamental components of the definition (Mewis & Wagner, 2009) utilized these days are:

1. It depends on the viscosity of fluid because viscosity reduces with the force application.
2. Time-dependent decline of viscosity prompted by the flow.
3. Reversible effect on decline or cease of flow.

Mewis & Wagner (2009), concluded that thixotropy material may or may not be visco-elastic, and step-down shear rate experiments determine this. In addition, they also concluded that measuring thixotropic material is laden with difficulties because particles and their aggregates, time-dependency effects, extreme shear-thinning all can induce errors. Some of the thixotropy quantification methods are described below.

1. **Hysteresis loops**: Green & Weltmann (1946) was the first to use rotational viscometers to determine thixotropy. Experiments were done commencing at zero shear rate and ramping up to maximum shear rate before returning to zero. The measured data is represented as Shear stress vs. Shear rate (Flow curves), and a thixotropic material sample gives the hysteresis loop. Figure 2.15 represents the possible shapes of the hysteresis loop. The shape of the loop is mostly determined by the material and test conditions, such as shear history, test protocols, and shear rate acceleration (Mewis & Wagner, 2009). The linkage of the shear rate and time in the experiment is a disadvantage of this technique. In irreparable softening and visco-elastic materials, hysteresis has also been seen (Bird & Marsh, 2000).

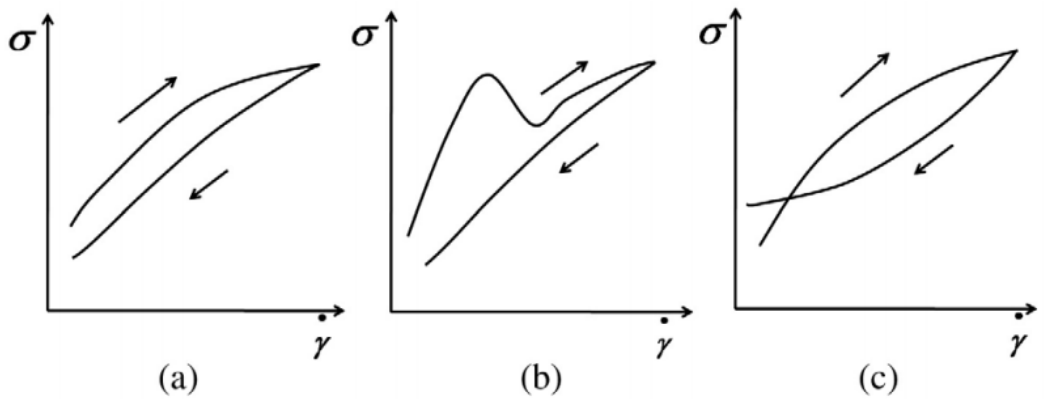

Figure 2.15: Hysteresis loop possible shapes. Figure taken from Mewis & Wagner (2009)

2. **Steps method:** In this approach, the drawbacks of the Hysteresis loop methodology can be avoided (Mewis & Wagner, 2009). The sample is sheared progressively by shear rate or shear stress in this procedure. By running the test in reverse order, the reversibility effect can be determined, see figure 2.16. In this approach, the shear rate and time are uncoupled and help to test the thixotropy models (Mewis & Wagner, 2009).

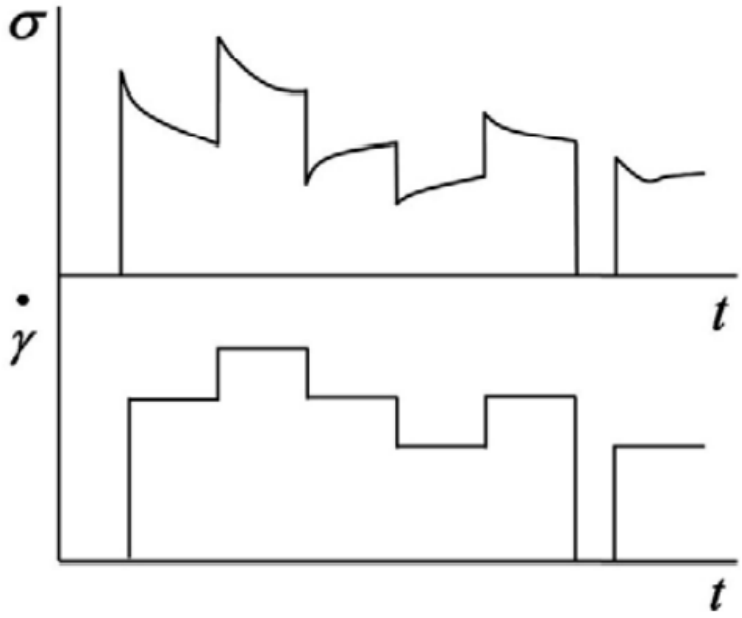

Figure 2.16: Stepwise change shear stress or shear rate. Figure taken from Mewis & Wagner (2009)

3. **Start-up and creep experiments (Mewis & Wagner, 2009):** In the Start-up method, the static sample is suddenly subjected to a constant shear rate (or shear stress). This action causes a stress overshoot, followed by a decay to a steady state. Then, the test is repeated after a short break (similar to the step-wise method). The degree of overshoot stress is determined by the shear history as well as the rest period. Thus, plotting these overshoot stress over the previous rest periods gives information on thixotropic recovery after shear at rest. The main limitation of this technique is, it is a destructive method.

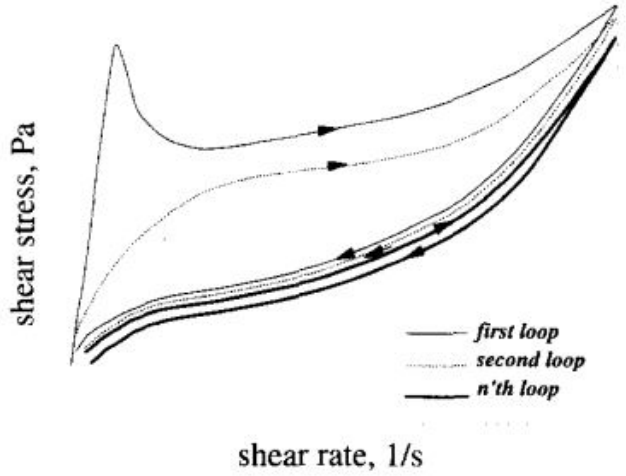

Figure 2.17: Start-up thixotropy test. Figure taken from Barnes (1997)

The Creep method involves applying steady shear stress and measuring the shear rate over time. The problem with this technique is that shear history is essential, and testing near dynamic yield stress is complex due to varying structures based on shear history.

2.2.6 Rheological models

In CFD codes and also in analytical approaches, the rheological models describe the flow behavior of fluids. These rheological models consist of more or less simple mathematical equations. These mathematical equations are constructed using rheological parameters of the fluid, such as viscosity, shear stress, power index, structural parameters, etc.

There are many rheological models available in literature like the Bingham model, Ostwald-de Waele (power-law) model, Herschel-Bulkley model, Houska model, etc. Model selection depends on the curve region required or the range of the data measured to model the curve. Below are the most commonly used rheological models.

1. **Bingham model (Bingham, 1922):** This is one of the most widely used modeling approaches because of a simple equation, see the equation 2.5. It has two parameters, Bingham yield stress, and viscosity. This model's primary goal is to simulate the flow curve for undetermined shear rates.

$$\tau = \tau_y + \eta_B \dot{\gamma} \tag{2.5}$$

   where τ is a shear stress, τ_y is Bingham yield stress, η_B is a Bingham plastic viscosity, and $\dot{\gamma}$ is a shear rate.

2. **Ostwald de Waele (Power law) model:** A straight line defines the relation between shear stress and rate in double logarithmic plots for shear-thinning fluids. For a limited range of shear rate or shear stress, these models are applicable (Chhabra & Richardson, 2008). In the power-law equation, m and n are curve fitting parameters where m is a coefficient of fluid consistency, and n is a flow index, τ is shear stress, and $\dot{\gamma}$ is the shear rate, see equation 2.6.

$$\tau = m(\dot{\gamma})^n \tag{2.6}$$

3. **Herschel–Bulkley model (Herschel & Bulkley, 1926):** This model is a power-law extension and consists of yield stress parameters. The yield stress term represents the shear-thinning after the yield point.

$$\tau = \tau_y + \kappa \dot{\gamma}^n \tag{2.7}$$

   where τ - shear stress, τ_y is yield stress, κ is consistency, $\dot{\gamma}$ is the shear rate, and *n* is the power law index.

4. **Winterwerp & van Kesteren (2004)**: This model incorporates fractal-dimension theory mentioned in Kranenburg (1994).

   According to fractal theory, all physical processes follow a power-law behavior of all sizes. On the other hand, structures are bounded within particular spatial ranges and are not always self-similar at all scales. However, based on several physical studies, it can be established that several mechanisms influencing cohesive sediment, including viscosity, yield strength, and permeability, exhibit similar power-law behavior (Kranenburg, 1994).

   According to this concept, the yield stress for condition without sand is described in Eq2.8

$$\tau_y = A_y \left(\frac{\phi_{clay}}{\phi_{water} + \phi_{clay}} \right)^{\frac{2}{3-n_f}} \tag{2.8}$$

   The fractal dimension (n_f) can be found easily by equating to the slope (n) of the power-law curve in double logarithmic scale, see Eq 2.9.

$$n = \frac{2}{3 - n_f} \tag{2.9}$$

   Winterwerp & van Kesteren (2004) concluded that the fractal dimension of flocs corresponds to the flocs fracture under self-weight consolidation. Typical fractal dimension values in coastal waters range from 1.7 to 2.2, and for sea bed, the range can be 2.6 to 2.8.

5. **Jacobs et al. (2008)** This model is similar to Bingham model in which the viscosity is constant. The model is based on the ratio of water content and plasticity index of the fluid. Jacobs et al. (2008) concluded that the increase in water content in the fluid reduces the rheological properties.

2.2.7 Integration of the time-dependency affect in the rheological models

Thixotropy can be incorporated in rheological models in two different ways (Mewis & Wagner, 2009). First, using phenomenological models to characterize the unknown materials. In this class, principles of continuum mechanics are used, which generally describe the time effects using the memory function. Second, using micromechanical models. In this class, the "structure" parameter is used to define the structure level. The rheological response is associated with the instantaneous structure in these models, and the kinetic equation defines time dependence.

(Šesták et al., 1983):

Houska model is an advanced Herschel-Bulkley model with dynamic parameters used to model thixotropic non-Newtonian fluid flow curves. In the equation, τ is shear stress,τ_0 is yield stress of fully structured fluid, τ_∞ is yield stress of totally destructed fluid, *c* is a structure-dependent contribution to viscosity, λ is the structural parameter, $\dot{\gamma}$ is the shear rate, and *n* is the power-law index.

$$\tau = \tau_\infty + \lambda(\tau_0 - \tau_\infty) + (\mu_\infty + \lambda c)\dot{\gamma}^n \tag{2.10}$$

The structure growth and decay is described by the kinetic equation, see equation 2.11.

$$\frac{\partial \lambda}{\partial t} = a(\lambda_0 - \lambda) - b\lambda\dot{\gamma} \tag{2.11}$$

2.3 Estimation of plate resistance when dragged in non-Newtonian fluids

General forces on ship

Any moving body is subjected to three general forces types- inertia, body and surface forces. When a ship sails at a constant velocity, the inertia force of a ship will be zero. Mass of the ship (gravity) is the only body force that is noticeable (Birk, 2019). Archimedes' principle postulates that the weight of the displaced water by the ship is equal to the weight of the ship.

In the surface forces, the ship's hull interacts with fluids in two ways: normal stresses and tangential stresses (Birk, 2019). The normal stresses are the resultant of the pressure of the fluid over the surface area. In comparison, the tangential stresses are the resultant of the viscosity of the fluid. Therefore, the only force that can be measured directly is the total resistance.

Leijs (2021) conducted single-phase simulations of ship sailing through the fluid mud and concluded that the total resistance of the ship increases with the yield stress of the fluid mud and viscous resistance significantly increases with the yield stress.

Why flat plate experiments?

The ship resistance is dramatically influenced by the roughness of the ship hull, which results in increased fuel utilization and emission of greenhouses gases (Schultz et al., 2011). Numerous research was performed on the roughness effect on ship resistance. Song et al. (2021) research paper showed that the flat plate experiments are in good agreement with the estimation of total resistance by extrapolating it to the ship scale model and validating it to the ship model tests.

Flow of fluid on the flat surface

The fluid velocity at the surface is zero as it flows over a surface. This condition is known as the no-slip boundary condition (Chhabra & Richardson, 2008) The velocity of the liquid gradually increases over the distance from the solid surface. The validity of no-slip conditions for non-Newtonian fluid flow is conflicting. A complete understanding of the boundary layer is essential in application because the flow influences not only the drag force but also the mass and heat transfer when the gradients of temperature/ concentration exist (Chhabra & Richardson, 2008).

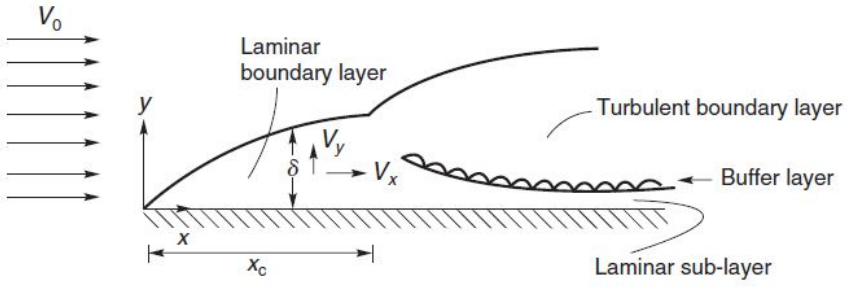

Figure 2.18: Boundary layer development on solid surface. Schematic sketch took from Chhabra & Richardson (2008)

Frictional force of the flat plate dragged in Bingham fluids (Chhabra & Richardson, 2008)

The Reynolds number of the fluid flow describes the flow nature and its maximum value can be found on the trailing edge of a plate .

$$Re_L = \frac{\rho V_0 L}{\mu_B} \tag{2.12}$$

where Re_L is the maximum Reynolds number at distance L from the leading edge (i.e trailing edge of the plate), V_0 is the flow velocity, ρ is the fluid density, and μ_B is the Bingham plastic viscosity

The shear stress acting on an entire plate is

$$\tau_w = \tau_B + 0.646 \left[\frac{\rho V_0^2}{\sqrt{Re_L}} \right] \tag{2.13}$$

where τ_w is the average shear stress and τ_B is the Bingham yield stress.

The drag coefficient C_D is

$$C_D = Bi + \frac{1.292}{\sqrt{Re_L}} \tag{2.14}$$

where Bi is the Bingham number

$$Bi = \frac{2\tau_B}{\rho V_0^2} \tag{2.15}$$

The total frictional force (or drag force) exerted on the plate with plate dimensions L (Length) X W (Width) is

$$F_d = C_D \frac{1}{2} \rho V_0^2 W L \tag{2.16}$$

When the shear stress of the fluid at the surface equals the shear stress in the fluid, them the boundary layer thickness (δ) at distance *x* from the front edge of the plate is given by

$$\delta = 4.64 x Re_x^{-1/2} \tag{2.17}$$

For Bingham fluids flowing over the flat plate, the wall shear rate is given by

$$\dot{\gamma} = \frac{3V_0}{2\delta} \tag{2.18}$$

Frictional force of the flat plate dragged in in Ostwald de Waele (Power law) fluids (Chhabra & Richardson, 2008)

The total frictional force (or drag force) exerted on each side of the plate of dimension L (Length) X W (Width) when dragged in the power law fluid of density ρ at velocity $_0$ is

$$F_d = C_D \frac{1}{2} \rho V_0^2 W L \tag{2.19}$$

where

$$C_D = C(n) Re_L^{\frac{-1}{n+1}} \tag{2.20}$$

where Re_x is the local Reynolds number in function of distance x from the front end of the plate.

$$Re_x = \frac{\rho x^n V_0^{2-n}}{m} \tag{2.21}$$

where

$$C_n = 2(n+1)(3/2F(n))^n \tag{2.22}$$

where

$$F(n) = \left[\frac{280}{39}(n+1) \left(\frac{3}{2} \right)^n \right]^{\frac{1}{(n+1)}} \tag{2.23}$$

The boundary layer thickness(δ) obtained from integral balance approach at distance *x* from the front end is

$$\frac{\delta}{x} = F(n)Re_x^{\frac{-1}{n+1}} \tag{2.24}$$

The wall shear rate when the fluid flows over the flat plate is

$$\dot{\gamma} = \frac{3V_0}{2\delta} \tag{2.25}$$

2.4 Overall summary

The fluid mud is introduced in brief with its characterization, formation and measurement tools. It was observed that the fluid mud rheology is highly affected by the density and organic content of the fluid mud (Shakeel et al., 2021). The relation between the yield stress and volumetric concentration can be found in Winterwerp & van Kesteren (2004). However, the link between density and yield stress using the fractal theory in the literature is not discussed.

The rheology of non-Newtonian fluids is discussed with its measurement of yield stresses, rheometry practices, and the manifestation of the thixotropy effect. In the rheological modeling of flow curves, ramp-down of remolded flow curves are often modeled, which doesn't include the time dependency effect. On the other hand, Houska modeling integrates the time dependency effect, but Houska type modeling for the fluid mud in literature like Toorman (1997) was not considered.

Estimation methods for frictional forces when dragged in Bingham fluids and power-law fluids are available in Chhabra & Richardson (2008). In addition, Leijs (2021) studies were based on CFD simulations and were not validated with experiments.

Thus, this thesis main objectives are:

- rheological study of fluid mud to investigate the link between the density and yield stress,
- quantify the thixotropy and justify its importance in rheological modeling, and
- measure the total resistance of plate dragged in fluid mud comparing its relation with rheology and evaluate available analytical formulas of frictional forces of a plate dragged in non-Newtonian fluids.

Chapter 3

Materials and methods

3.1 Origin of fluid mud

3.1.1 For rheological study of fluid mud from three different canals of Port of Rotterdam

To study the rheology behaviour of fluid mud of three different canals, the fluid mud were brought from Beerkanaal, Calandkanaal and 8e Petroleumhaven in an enclosed container. The dredge locations where the fluid mud samples were collected is shown in the Figure3.1.

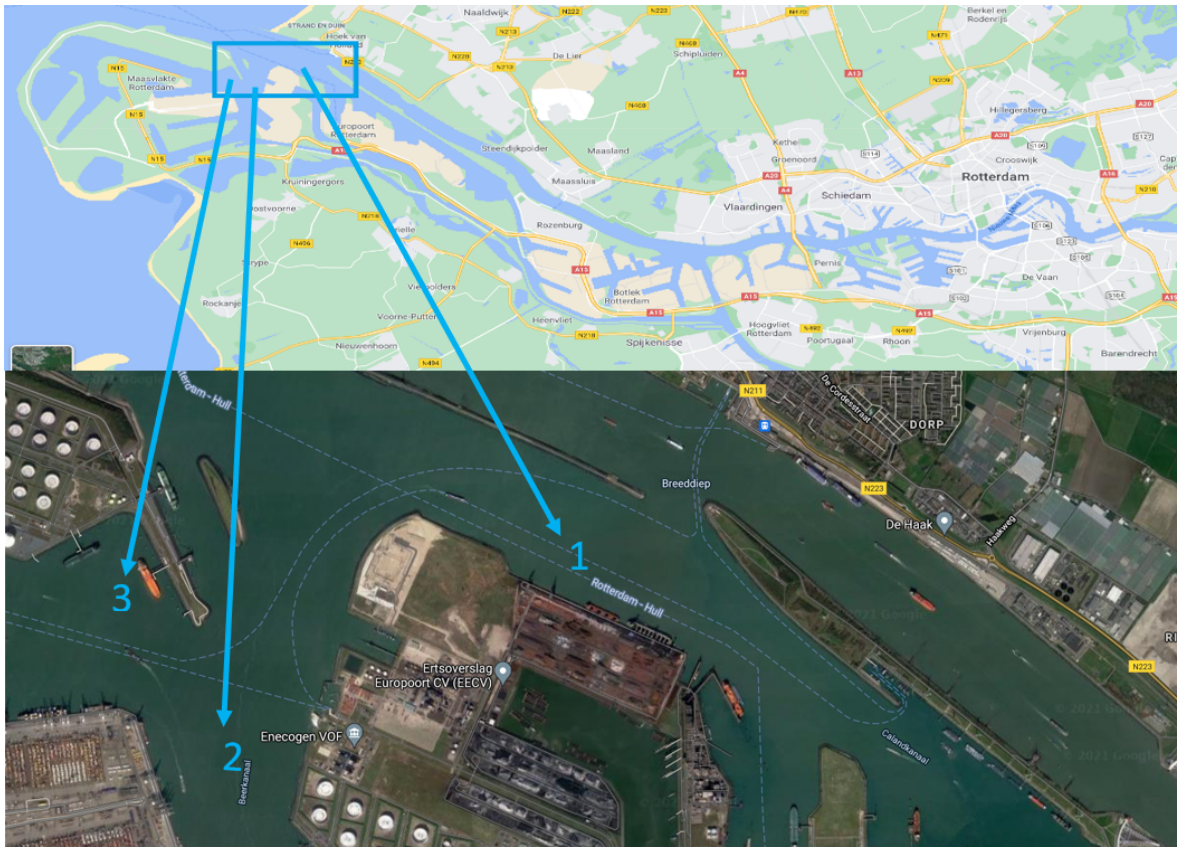

Figure 3.1: 1. Calandkanaal, 2. Beerkanaal, 3. 8e Petroleumhaven *Google Maps* (n.d.)

3.1.2 For towing experiments

The fluid mud for the towing experiments was dredged at Calandkanaal of Port of Rotterdam. Initially, the fluid mud was dredged at four different locations and fluid mud samples were collected for the rheological tests and density measurements. We found that at 100m distance from bay the fluid mud samples Bingham yield strength was more than 120Pa for a density of 1.2g/cc. We observed water injection dredging were performed near to the bay. Since the required fluid mud of Bingham yield strength of 60-70 Pa, we dredged the mud approximately 25m from the bay where the Bingham yield strength of the fluid mud was 70Pa for the density of 1.2g/cc.

3.2 Equipments and facility

The equipment used to perform the experiments is listed below:

1. **Thermo Scientific HAAKE Rheometer:** This is an advanced rotational rheometer with wide range rheology tests capabilities such as different rotating geometries, protocols and temperature control. In this project, all rheology tests perfromed at 20^oC.

Figure 3.2: Thermo Scientific HAAKE Rheometer

2. **Geometries:** In an advanced rotational rheometer, there are wide range of geometries available like Bob, Vane, Groove bob, parallel plate, and double gap bob cup. In this project, bob-cup, and vane-cup geometries are used to perform the rheology tests on fluid mud.

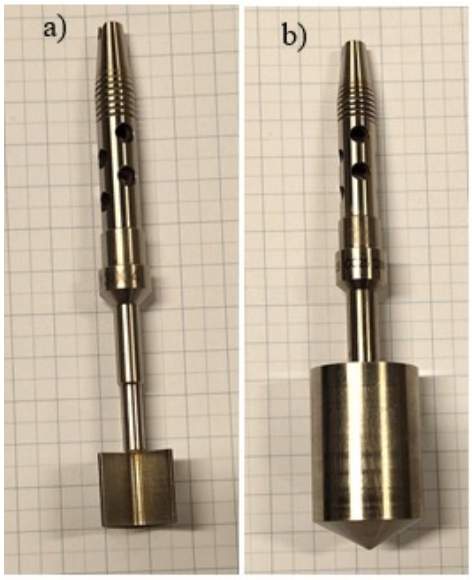

Figure 3.3: a. Vane, b. Bob

3. **FANN 286 rheometer:** This is a portable rheometer which can be operated at 12V or 220V. FANN 286 rheometer is a conventional couette viscometer with controlled rotational speeds of the geometry and viscosity is recorded from the dial gauge, see Figure 3.4. In brief, the cylinder wall rotates, and torque transferred over fluid mud is sensed by the bob and corresponding viscosity is shown in dial gauge.

Figure 3.4: FANN 286 Rheometer

4. **DMA-35:** This is an advanced portable digital density meter manufactured by Anton Paar, see Figure 3.5. In this project, DMA 35 is useful for quick measurement of the fluid mud density. However, because of non homogeneous mixture of fluid mud, DMA 35 show errors for thick mud samples.

Figure 3.5: DMA-35

5. **Oven:** Another method to measure density is by oven test method. In this method, wet weight of the fluid mud sample is measured and kept for drying in oven for 24 hours at 220^oC, see Figure 3.6. The fluid mud densities obtained from the oven test method are represented in Appendix A.

Figure 3.6: Samples kept in oven at temperature of 220^oC

6. **Flume:** The dimensions of the flume are 31m in length, 2.5m in width, and 2.5m in depth, see Figure 3.7. The towing tank is equipped with a carriage, which can be operated up to a maximum speed of 2 m/s.

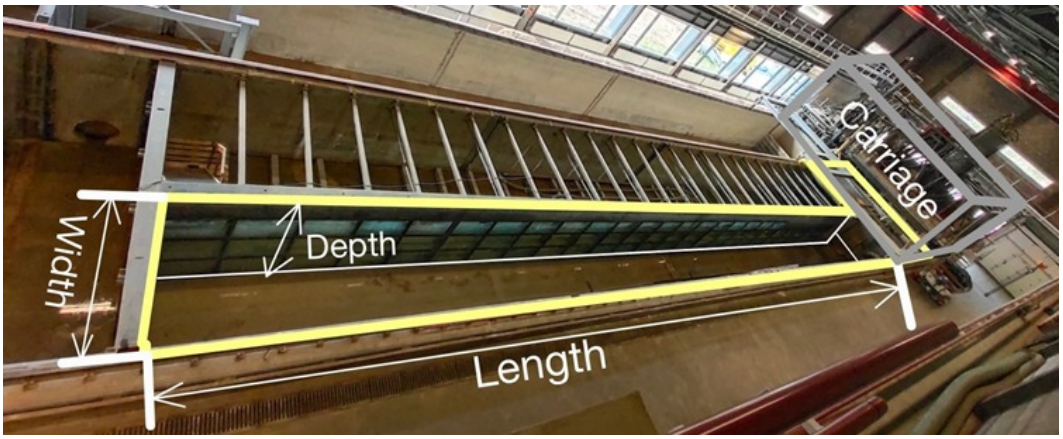

Figure 3.7: Towing tank equipped with towing carriage

7. **Flat plate**

In the flume experiments, a plate was used for which the total resistance was measured in the mud. We assume the thickness of the flat plate is negligible compared to the size of the plate. For the experiments, we had a Cux sampler in which two thin plates are assembled, see Figure 3.8(a). In addition, a flat wooden plate was also designed and built at Deltares was used in the experiments, see Figure 3.8(b).

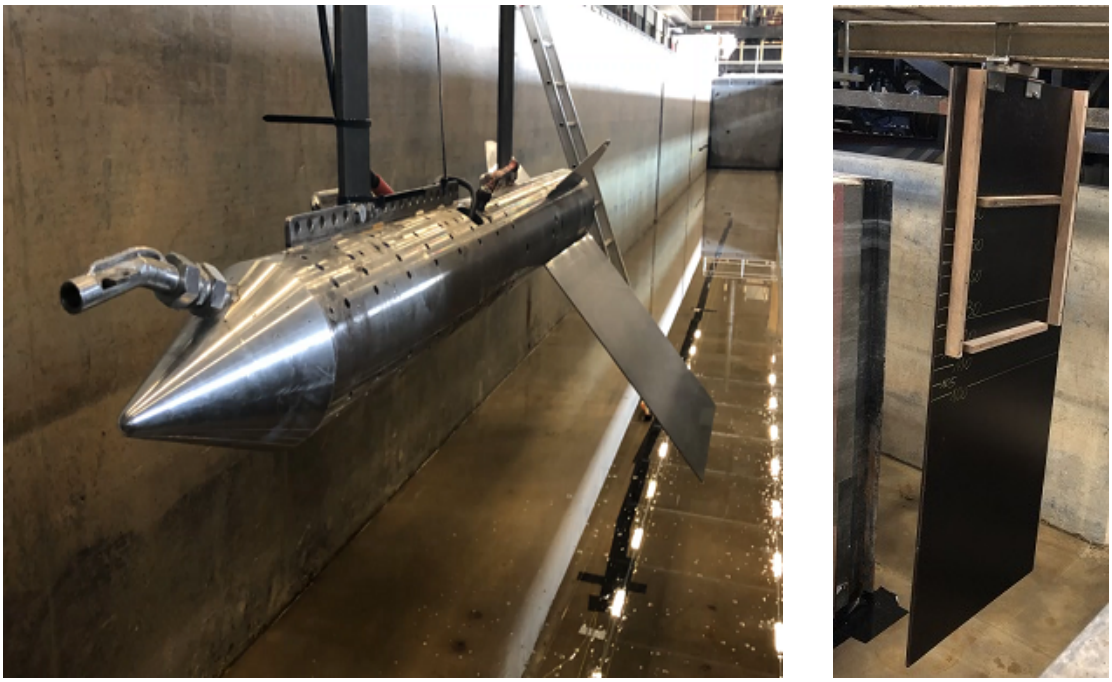

(a) CUX Sampler

(b) Plywood

Figure 3.8: Thin plate towing objects

CUX Sampler looks like small torpedo made of stainless steel equipped with two thin plates assembled with load-cells. The load cells are manufactured by HBM, model S9M with a rated force 500N and an accuracy of $\pm$0.2N. The dimensions of two plates are 50X50 cms and 50X33 cms, see Figure 3.9.

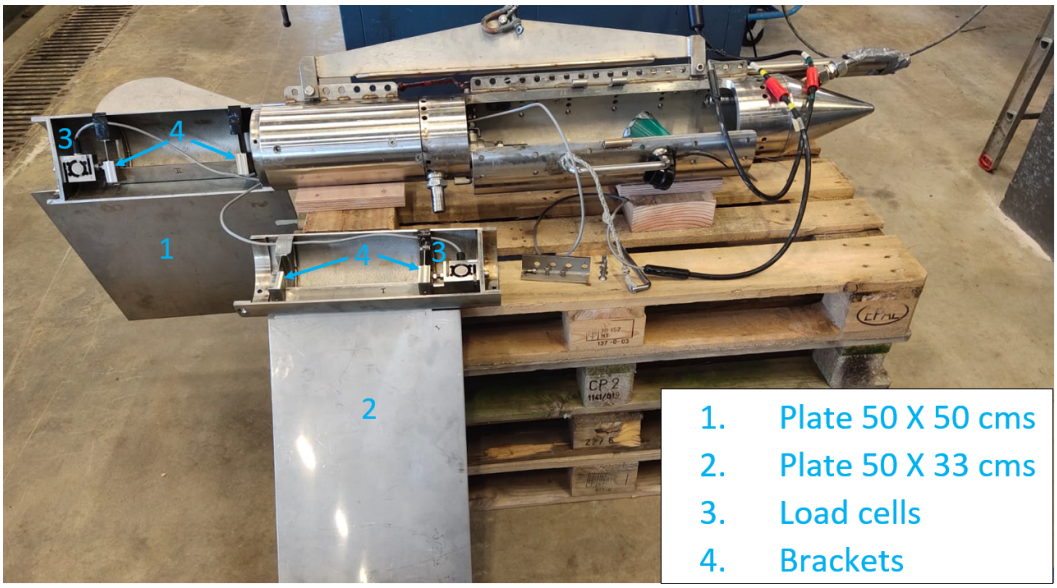

Figure 3.9: Assembly of thin plates in CUX sampler

Wooden plate used in the flume experiments has dimensions of 0.8m in length, 1m depth immersed in fluid mud, and 0.12m thickness. The thickness of the wood plate is assumed to be negligible, and no turbulence near the edges. In order to reduce the bending effect of the plate while towing in a flume, the load cell is connected at $1/3^{rd}$ distance on top of the leading edge, see Figure 3.10.

Figure 3.10: Assembly of load cell to the wood plate

3.3 Dredging and transportation of fluid mud

The fluid mud dredged at Calandkanaal of Port of Rotterdam is collected using a Backhoe dredger, and collected the fluid mud is transferred to a hopper, see Figure 3.11. The fluid mud from the hopper is transferred into trucks and then transported to the flume at Deltares. The volume of the fluid mud required for flume experiments was calculated based on the dimensions of the flume. However, estimating the required volume of fluid mud over the number of truck trips required to transport is not a suitable estimation method. Instead, based on the density of the fluid mud, the mud weight can be calculated using the volume required. Nowadays, trucks have an inbuilt weighing scale to measure the load in a truck.

Figure 3.11: The fluid mud dredged at Calandkanaal (Port of Rotteram) and transported it by truck to the flume at Deltares.

Before dredging, the relation between density and yield strength is studied in the laboratory. In order to meet the test matrix requirements, the strength of the fluid mud is tested using FANN 286 rheometer, and density is measured using DMA 35, see Figure 3.12.

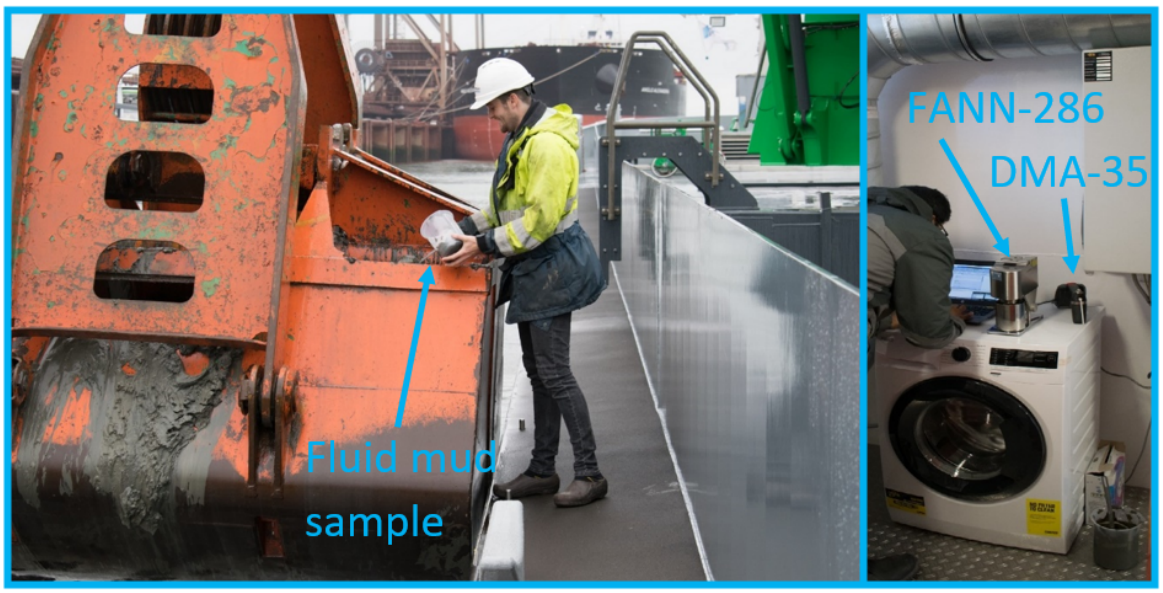

Figure 3.12: Collecting fluid mud and testing the strength of fluid mud and its density

In order to reduce the effort of decreasing the strength of the fluid mud and meet test matrix requirements, the fluid mud is diluted in the hopper by adding sea water, and mixed well with backhoe, see Figure 3.13

Figure 3.13: Mixing the mud with backhoe to make it homogeneous.

Challenges encountered in meeting the test matrix requirements are enumerated below.

1. Mud lumps: Mud lumps makes the mixture non-homogeneous, see Figure 3.14. It was practically impossible to dissolve all the mud lumps inside hopper. However, big lumps can be dissolved.

Figure 3.14: Mud lumps in hopper

2. Sedimentation in hopper: The fluid mud collected in the hopper settled, see Figure 3.15. It was difficult to predict the overall strength of the fluid mud inside the hopper because of the formation of three layers - Water, fluid mud, and thick mud.

Figure 3.15: Water layer on top of hopper

3.3.1 Fluid mud homogenization

After transporting the fluid mud from the hopper to the flume, the challenging task is to maintain a homogeneous mixture of fluid mud inside the flume. Two different approaches are used to tackle this issue. To begin with, fill the flume from the center. Another approach was to use blade and rotor setup, see Figure 3.16. However, the mud strength was too high than required. We added seawater to reduce strength. Because of practical limitations, we could not control the strength of the mud. Thus, the strength was reduced below the requirement. Therefore, the test matrix was revised.

Figure 3.16: Blade rotor setup hanged to the frame to mix the fluid mud in flume.

3.3.2 Experimental setup

The flume experiments and rheology tests are performed at Deltares, in the 'Water-Soil Flume' and 'Physics Lab' respectively.

The towing object hanged from the carriage frame, see in Figure 3.17. The connection between the carriage, the frame and the load cells is rigid, thus we assume no relative motions between them.

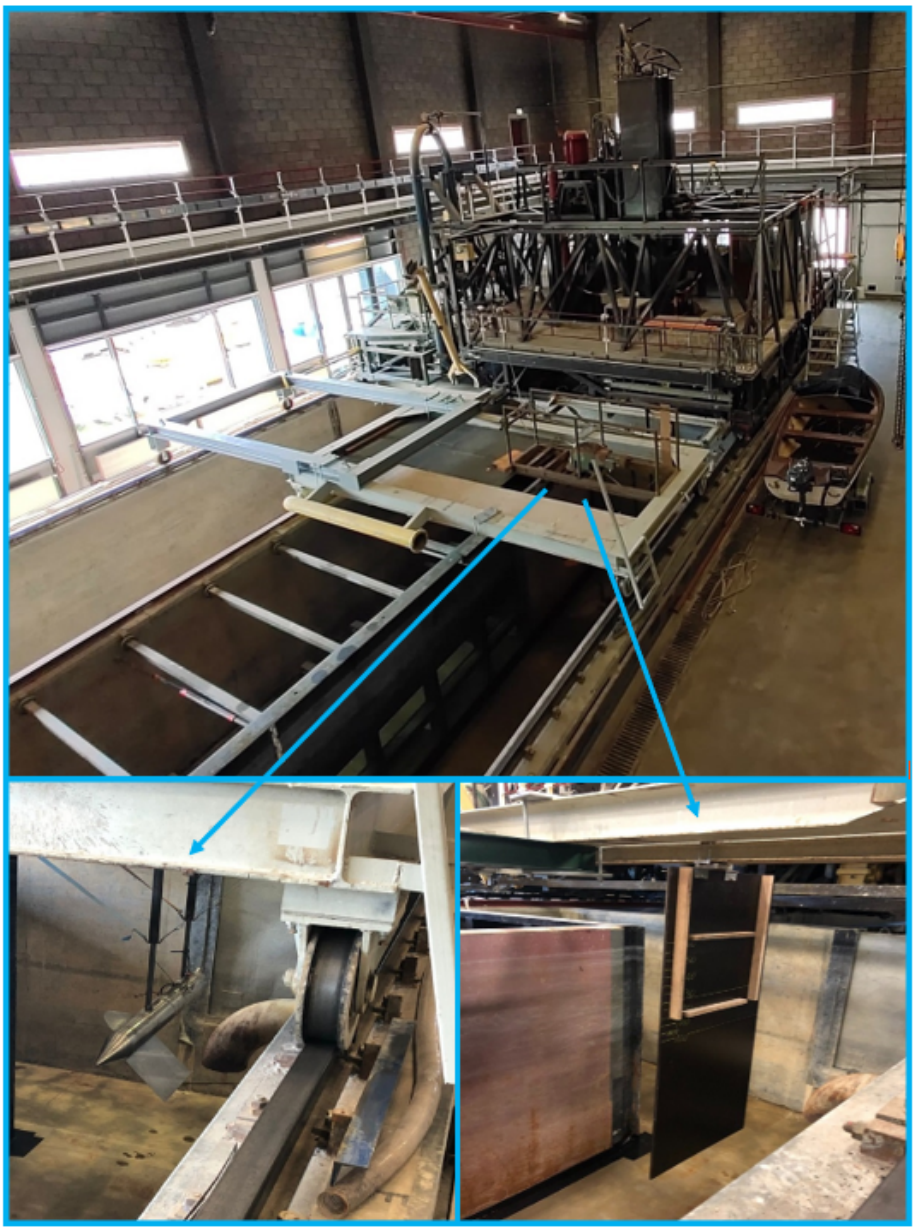

Figure 3.17: Location of the towing object in the test set-up

During the towing experiments, the fluid mud samples are collected at three different fixed positions. One at 10m distance, second at 15m distance, and third at 22.5m distance from one end of the flume, see Figure 3.18. The fluid mud samples are collected with the help of the cup and pole arrangement. We assume the fluid mud is homogeneous after mixing over the depth, and the fluid mud samples are collected at 0.5m depth from fluid mud surface and at the center line of of the flume.

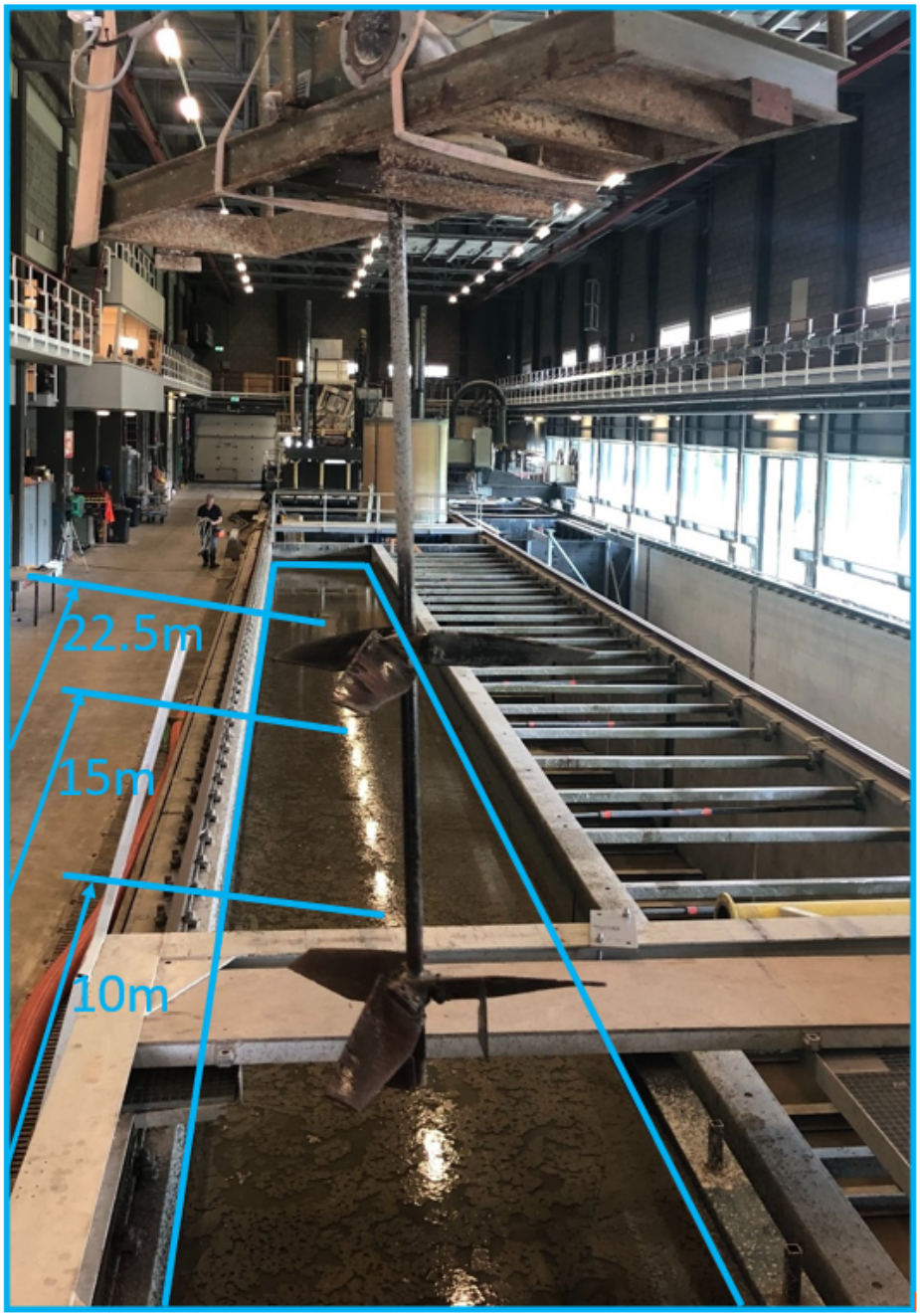

Figure 3.18: Location of fluid mud samples collected while flume experiment

3.3.3 Test matrix

The test matrix for the flume experiments was designed based on the density of fluid mud and towing speeds, see Table 3.1. Because of practical limitations, as discussed in previous sections, the test matrix was revised, see Table 3.2.

Table 3.1: Designed test Matrix for flume experiments

S.No	Fluid mud strength [Pa]	Towing Speeds [m/s]	Repetitions	Total tests
FM1	40-50	0.25, 0.5, 0.75, 1.0	8	32
FM2	20-30	0.25, 0.5, 0.75, 1.0	8	32
FM3	5-10	0.25, 0.5, 0.75, 1.0	8	32

Table 3.2: Revised test Matrix for flume experiments

S.No	Fluid mud strength [Pa]	Towing Speeds [m/s]	Repetitions	Total tests
FM1	20-30	0.25, 0.5, 0.75, 1.0	8	32
FM2	10-20	0.25, 0.5, 0.75, 1.0	8	32
FM3	5-10	0.25, 0.5, 0.75, 1.0	8	32

The test matrix for rheology tests on fluid mud samples were designed on the basis of protocols and geometries. The fluid mud samples were collected at two different periods and from three different location as mentioned in previous discussion, see Figure 3.18. Initially, the protocol for tests with bob was decided up to shear rate of 100 1/s, see Table 3.3. After performing the flume tests on the first mud charge, modification in protocols were done, to get more information on high shear rates from flow curves with bob. Thus, the test matrix was revised for bob geometry for shear rate up to 300 1/s, see Table 3.4.

Table 3.3: Designed test Matrix for rheology experiments

S.No	Objective	Geometery	Protocol	Samples
1	Dynamic Yield Stress and Static Yield Stress	Vane - FL22	CSR 0-20(1/s) 180s up - 60s constant - 180s down	6
2	Flow curve and Bingham Yield Stress	Bob	CSR 0-100(1/s) 180s up - 60s constant - 180s down	6
3	Static Yield Stress and Fluidic Yield Stress	Bob	CSS 0-100(Pa) 150s/20s up	6

Table 3.4: Revised test Matrix for rheology experiments

S.No	Objective	Geometery	Protocol	Samples
1	Dynamic Yield Stress and Static Yield Stress	Vane - FL22	CSR 0-20(1/s) 180s up - 60s constant - 180s down	6
2	Flow curve and Bingham Yield Stress	Bob	CSR 0-300(1/s) 180s up - 60s constant - 180s down	6
3	Static Yield Stress and Fluidic Yield Stress	Bob	CSS 0-100(Pa) 150s/20s up	6

Chapter 4

Experiments on Port of Rotterdam's fluid mud from different locations

The fluid mud from three different canals (Beerkanaal, Calandkanaal, and 8e Petroleumhaven) were brought in an enclosed containers to the Deltares laboratory. First, the particle size distribution was studied and then the rheological experiments were performed by making diluted fluid mud samples.

4.1 Fluid mud particle size distribution (PSD)

The mud samples' PSD was evaluated by diluting the mud samples extensively and using a static light scattering technique (Malvern Mastersizer 2000MU). The d50 of the three canals fluid muds particle size were - 12.5μm for Beerkanaal, 12.2μm for Calandkanaal, and 11.3μm for 8e Petroleumhaven. From Fig 4.1, it seems that all the three canals particle size is similar and hence not varying with location. In addition, the PSD is below 10μm, which means that the fluid mud contains either a high amount of clay or silt, which also means that fluid mud almost contains a negligible amount of sand.

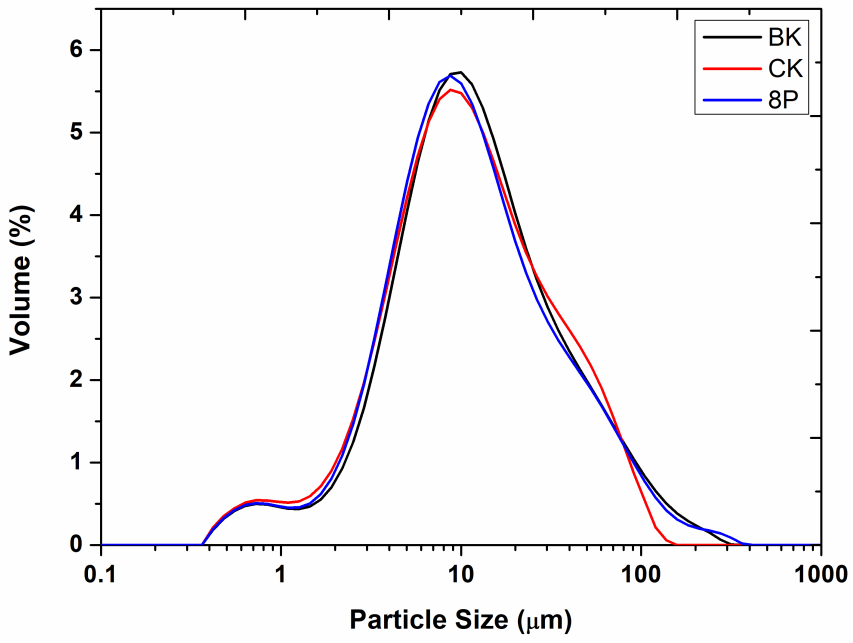

Figure 4.1: Particle size distribution of Beerkanaal(BK), Calandkanaal(CK), and 8e Petroleumhaven(8P) fluid mud

4.2 Preparation of diluted fluid mud samples in the laboratory for rheology tests

The fluid mud samples of varying densities were made in the laboratory by diluting the fluid mud with seawater and freshwater. The density of seawater was 1025 kg/m^3 and freshwater was 1000 kg/m^3 measured using the DMA 35. The density of solids was tested in Helium gas pycnometer at Deltares for Beerkanaal fluid mud and found 2568.3 kg/m^3. These values were considered for fluid mud from different canals in the density calculations of oven test methods. The procedure of making the diluted fluid mud and testing is mentioned below. The oven density calculations are described in the Appendix A.8.

1. The first sample tested was without dilution, and three samples of fluid mud from each canal were kept for consolidation test.
2. The diluted fluid mud samples were made by taking an equal amount of mud in five small beakers, and seawater was added with increasing proportions in cups.
3. The diluted samples with seawater and fluid mud were hand stirred and closed with lids to prevent evaporation.
4. From these samples in a cup, a small portion of fluid mud was collected every time for the rheology test. While performing the rheology test, some fluid mud was collected for density measurement using DMA 35 and the oven test method.
5. For every rheology test, new fluid mud samples were used, and before taking the samples, the fluid mud was homogenized by hand stirring.
6. In rheometer, the fluid mud in a cup was set to a rest period of 10 seconds to maintain the temperature of 20°C, and then the rheometer protocol action was executed.

4.2.1 Rheology tests on fluid mud samples diluted with freshwater

Rheological experiments were performed on the fluid mud samples from Beerkanaal, Calandkanaal and 8e Petroleumhaven diluted with fresh water. The details of fluid mud samples are described in the Appendix A and the yield stress values from these tests are mentioned in the Table 4.2.

Table 4.1: Rheology tests and density details of fluid mud samples diluted with fresh water. Here Conc.= Concentration, Sc= Solid content, Wc= Water content, BYS= Bingham yield stress (at ramp-down, see Figure 2.8), SYS= Static yield stress, FYS= Fluidic yield stress (see Figure 2.13), and DYS= Dynamic yield stress (see Figure 2.12)

Density [g/cc]	Vol. Conc.	Sc [%]	Wc [%]	BYS [Pa]	SYS [Pa]	FYS [Pa]	DYS [Pa]	Test No
Beerkanaal								
1.286	0.16	36	64	43	26.3	96	25.5	62,63,64,65
1.225	0.14	30	70	12	3.3	14.4	7.8	66,67,68,69
1.218	0.13	29	71	10.5	2.5	11.2	6.5	70,71,72,73
1.183	0.11	25	75	4	1.3	4.3	2.7	74,75,76,77
1.155	0.09	22	78	2	0.8	2.5	1.3	78,79,80,81
Calandkanaal								
1.213	0.12	29	71	49	27.59	100.3	32.4	82,83,84,85
1.194	0.12	27	73	27.5	6.7	18.2	16.6	86,87,88,89
1.167	0.10	23	77	12	3.1	12.5	7.4	90,91,92,93
1.155	0.09	22	78	7.5	2.5	8.4	4.6	94,95,96,97
1.129	0.08	19	81	3.5	0.6	3.6	2	98,99,100,101
8e Petroleumhaven								
1.212	0.12	29	71	49.5	29.2	100.4	38.5	102,103,104,105
1.186	0.11	26	74	25	8.1	-	16.5	106,107,108,109
1.176	0.11	24	76	17.5	3.7	-	11.6	110,111,112,113
1.147	0.09	21	79	7.5	1.8	8.9	4.9	114,115,116,117
1.129	0.08	19	81	4	1	5.2	2.8	118,119,120,121

4.2.2 Rheology tests on fluid mud samples diluted with seawater

Rheological experiments were performed on the fluid mud samples from Beerkanaal, Calandkanaal and 8e Petroleumhaven. The details of fluid mud samples are described in the Appendix A and the yield stress values from these tests are mentioned in the Table 4.2.

Table 4.2: Rheology tests and density details of fluid mud samples diluted with seawater. Here Conc.= Concentration, Sc= Solid content, Wc= Water content, BYS= Bingham yield stress, SYS= Static yield stress, FYS= Fluidic yield stress, and DYS= Dynamic yield stress

Density [g/cc]	Vol. Conc.	Sc [%]	Wc [%]	BYS [Pa]	SYS [Pa]	FYS [Pa]	DYS [Pa]	Test No
Beerkanaal								
1.270	0.15	35	65	31.5	45.4	108.6	27.3	1,2,5
1.234	0.13	31	69	15.5	3	17.6	-	6,8
1.214	0.12	29	71	9	1.6	9.5	-	9,11
1.210	0.11	29	71	8	1.4	9.1	5.6	12,13,15
1.158	0.08	23	77	2.3	0.2	2.2	-	16,18
1.134	0.07	20	80	1	0.2	1.2	0.6	19,20,22
1.270	0.15	35	65	26.5	-	-	-	23
1.264	0.15	34	66	32.5	-	-	-	24
1.267	0.15	35	65	28	-	-	-	25
Calandkanaal								
1.197	0.11	27	73	28	9.5	42.6	24.3	26,27,28
1.176	0.09	25	75	16	4	20.1	-	29,30
1.164	0.09	23	77	10.5	3.1	14	-	31,32
1.155	0.08	22	78	7.5	1.6	9.1	5.1	33,34,35
1.138	0.07	20	80	4.5	0.6	4.6	-	36,37
1.119	0.06	18	82	2.5	0.4	2.2	1.3	38,39,40
1.209	0.11	28	72	43.5	-	-	-	41
1.210	0.11	28	72	43	-	-	-	42
1.208	0.11	28	72	44.5	-	-	-	43
8e Petroleumhaven								
1.192	0.10	26	74	29	25.8	53	23.9	44,45,46
1.171	0.09	24	76	15	3.4	17	-	47,48
1.149	0.08	21	79	7.5	1.2	8.1	-	49,50
1.131	0.07	19	81	4	0.2	3.6	2.7	51,52,53
1.128	0.06	19	81	3	0.2	3.6	-	54,55
1.112	0.05	17	83	2	0.2	1.8	1.3	56,57,58
1.204	0.11	28	72	44.5	-	-	-	59
1.207	0.11	28	72	47	-	-	-	60
1.205	0.11	28	72	43.5	-	-	-	61

4.2.3 Discussion

Relation between the density and the yield stress

From the Table 4.2 and 4.1, the yield stress like Bingham yield stress, static yield stress, fluidic yield stress, and dynamic yield stress are plotted against the density measured using oven test, see Figure 4.2, 4.3, 4.4, and 4.5.

The plots suggest that the yield stress grows exponentially and the rheology of fluid mud changes with the location. In addition, some fluid mud samples were kept for consolidation for 10, 13, and 18 days in rheometer cups (see test numbers 23-25, 41-43, and 59-61 in Appendix A) to observe the influence of the consolidation. The rheology tests of these consolidated mud suggest that there is neither a significant increase in density nor Bingham yield stress (see Figure A.5, A.10, and A.14 in Appendix A.

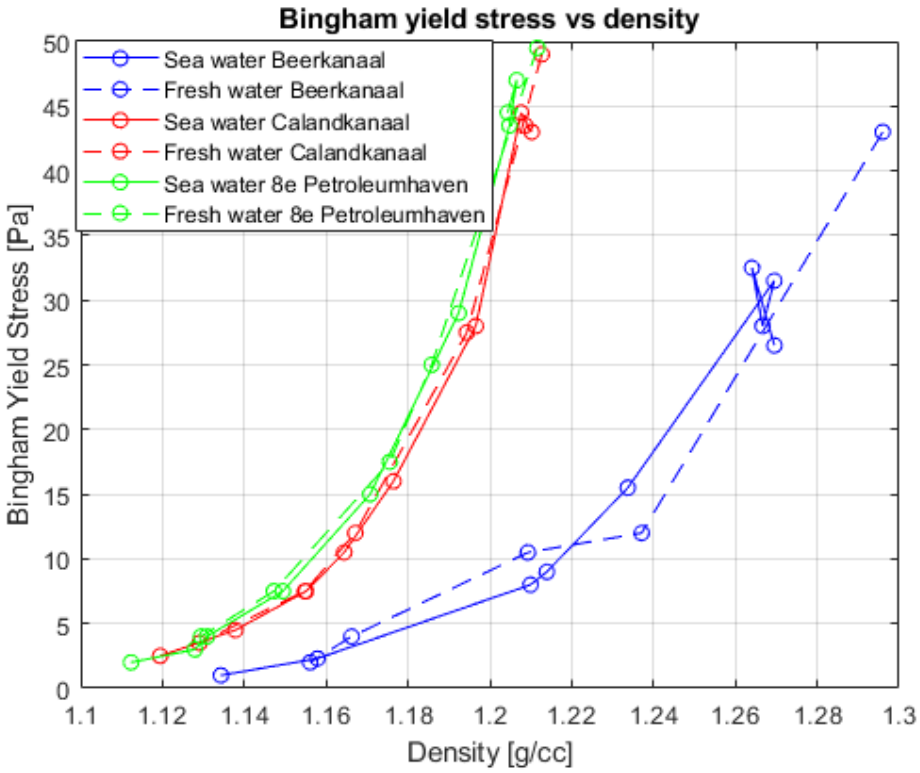

Figure 4.2: Bingham yield stress vs density of the fluid mud samples diluted with sea water and fresh water.

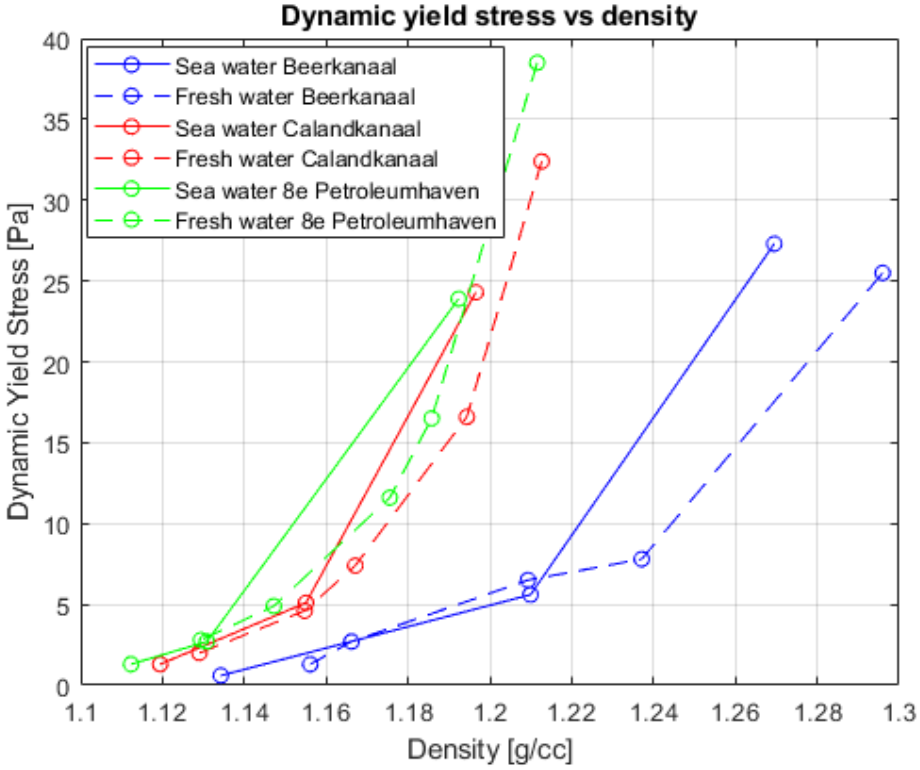

Figure 4.3: Dynamic yield stress vs density of the fluid mud samples diluted with sea water and fresh water.

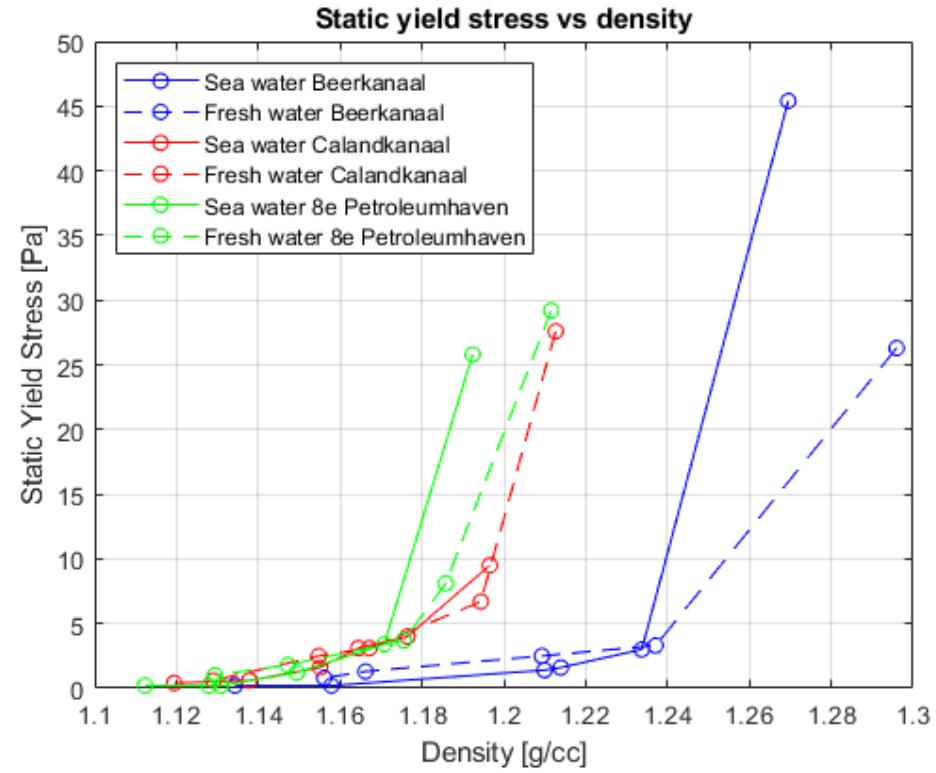

Figure 4.4: Static yield stress vs density of the fluid mud samples diluted with sea water and fresh water.

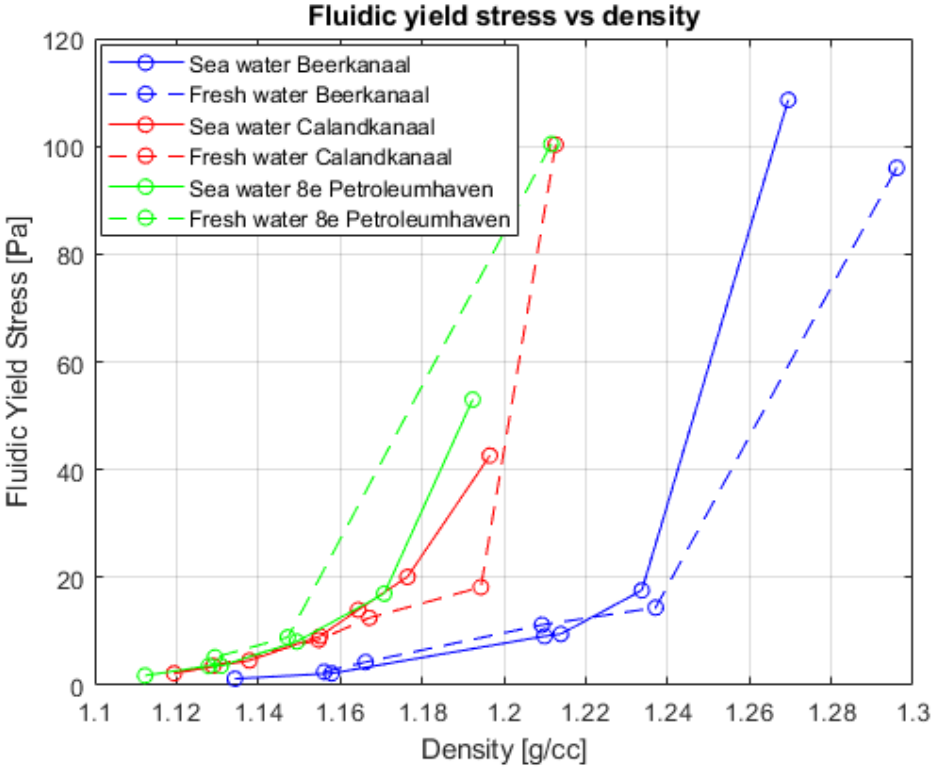

Figure 4.5: Fluidic yield stress vs density of the fluid mud samples diluted with sea water and fresh water.

Influence of salt content on the rheology of fluid mud

In order to check the influence of salt in the fluid mud on the rheological properties of fluid mud, normalized Bingham yield stress of the seawater dilution samples and the freshwater dilution samples are plotted against its added water mass ratio (see Figure 4.6). The added water mass ratio is given by the Eq.4.1.

$$\text{added water mass ratio} = (\text{added water volumetric ratio}) X \frac{\rho_{water}}{\rho_{undiluted}} \tag{4.1}$$

where

$$\text{added water volumetric ratio} = \frac{\rho_{undiluted} - \rho_{diluted}}{\rho_{diluted} - \rho_{water}} \tag{4.2}$$

where $\rho_{undiluted}$ is the density of undiluted fluid mud, $\rho_{diluted}$ is the density of fluid mud, and ρ_{water} is the density of water. The values of added water mass ratio and the corresponding Bingham yield stress are mentioned in the Table 4.3

Table 4.3: Table represents the added water mass ratio of the fluid mud samples.

Seawater dilution			**Freshwater dilution**		
Test no	**BYS**	**added water mass ratio**	**Test no**	**BYS**	**added water mass ratio**
Beerkanaal					
1 to 5	31.5	0.00	62 to 65	43	0
6 to 8	15.5	0.14	66 to 69	12	0.22
9 to 11	9	0.25	70 to 73	10.5	0.26
12 to 15	8	0.27	74 to 77	4	0.47
16 to 18	2.3	0.74	78 to 81	2	0.73
19 to 22	1	1.12	-	-	-
Calandkanaal					
26 to 28	28	0.00	82 to 85	49	0
29 to 30	16	0.12	86 to 89	27.5	0.08
31 to 32	10.5	0.20	90 to 93	12	0.23
33 to 35	7.5	0.28	94 to 97	7.5	0.32
36 to 37	4.5	0.47	98 to 101	3.5	0.57
38 to 40	2.5	0.75	-	-	-
8e Petroleumhaven					
44 to 46	29	0.00	102 to 105	49.5	0
47 to 48	15	0.13	106 to 109	25	0.12
49 to 50	7.5	0.31	110 to 113	17.5	0.17
51 to 53	4	0.53	114 to 117	7.5	0.38
54 to 55	3	0.57	118 to 121	4	0.56
56 to 58	2	0.85	-	-	-

The Figure 4.6 suggests that the salt in the fluid mud which was increased by diluting the samples with seawater has little or insignificant influence on the fluid mud on the Bingham yield stress. However, the little deviation can be seen as the added water mass ratio increasing, see Figure 4.6, solid-line and dashed-line curves are close.

Similar results were obtained by Ten Brummelhuis (2021), who is peer master student in PRISMA project at Port of Rotterdam.

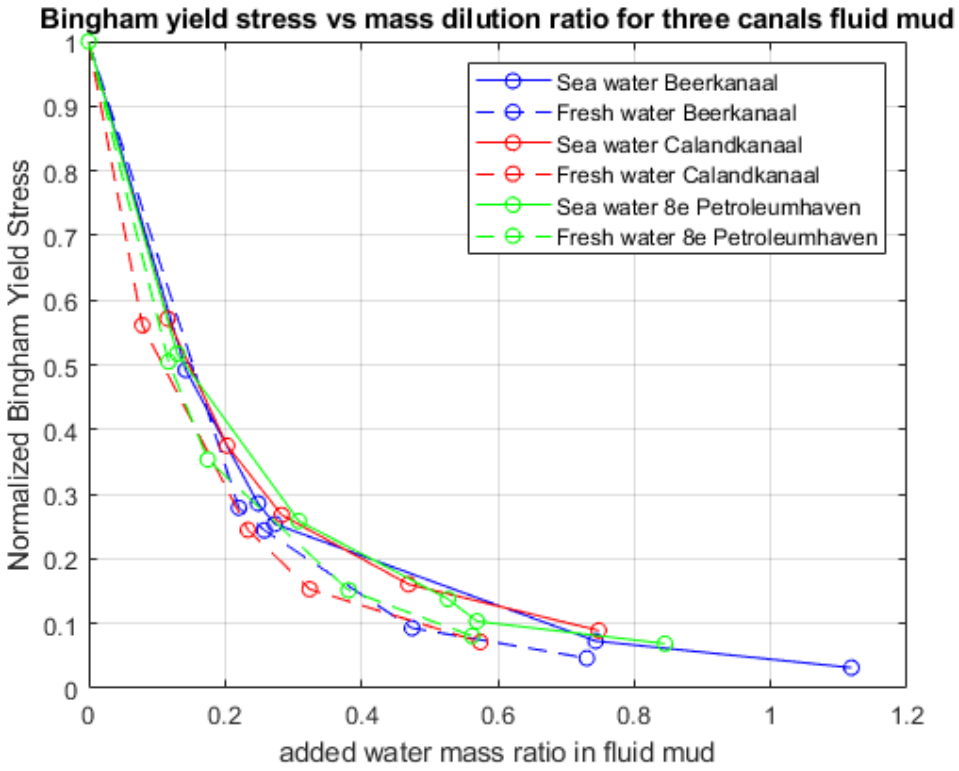

Figure 4.6: Influence of salt content in the rheology behaviour of fluid mud. Dashed line indicates dilution with freshwater, and solid line indicates dilution with seawater.

Relation between the volumetric concentration of solids and yield stresses

Generally, the salt is dissolved in rheological conditions, in the bed, or any flow. Thus, the volumetric concentration of solids has to be calculated from solids density and seawater density (V/V) (see Eq. A.16). Similar relations on mining sediments are discussed in Winterwerp & van Kesteren (2004).

Figure 4.7,4.8 and 4.9 represents the relation between the volumetric concentration of solids to the yield stresses, which suggest that the fluid mud rheological property follows the power-law, and the rheological property increases with the volumetric concentration of solids. Thus, the fractal theory applies to the thick to high diluted fluid mud, and power-law curves can estimate the rheological properties of fluid mud of different dilutions.

The fractal dimension for all the canals fluid mud found in the range of 2.5-2.7 (see Table 4.4) which suggests that fluid mud flocs get fractured by its self-weight during the consolidation on the bed.

Table 4.4: Fractal dimension values obtained from the Figure 4.7,4.8 and 4.9

	BYS	**SYS**	**FYS**	**DYS**
Beerkanaal	2.53	2.68	2.62	2.57
Calandkanaal	2.51	2.64	2.60	2.59
8e Petroleumhaven	2.62	2.75	2.61	2.56

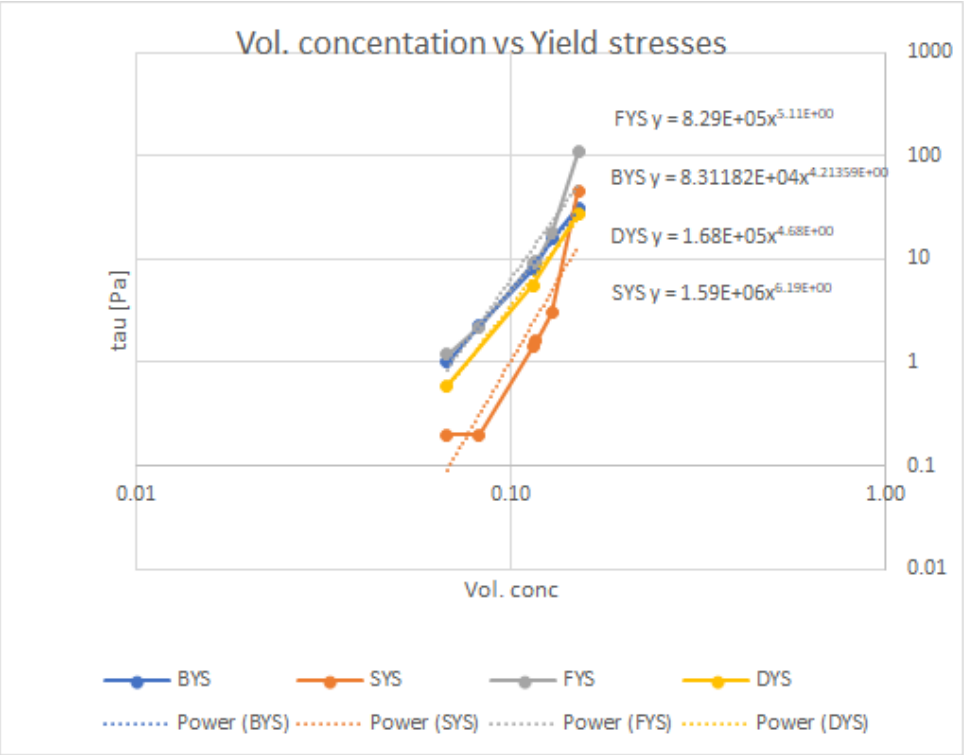

Figure 4.7: Plots represents the increase of yield stresses with the increase of volumetric concentration of solids in double logarithmic scale for the Beerkanaal fluid mud.

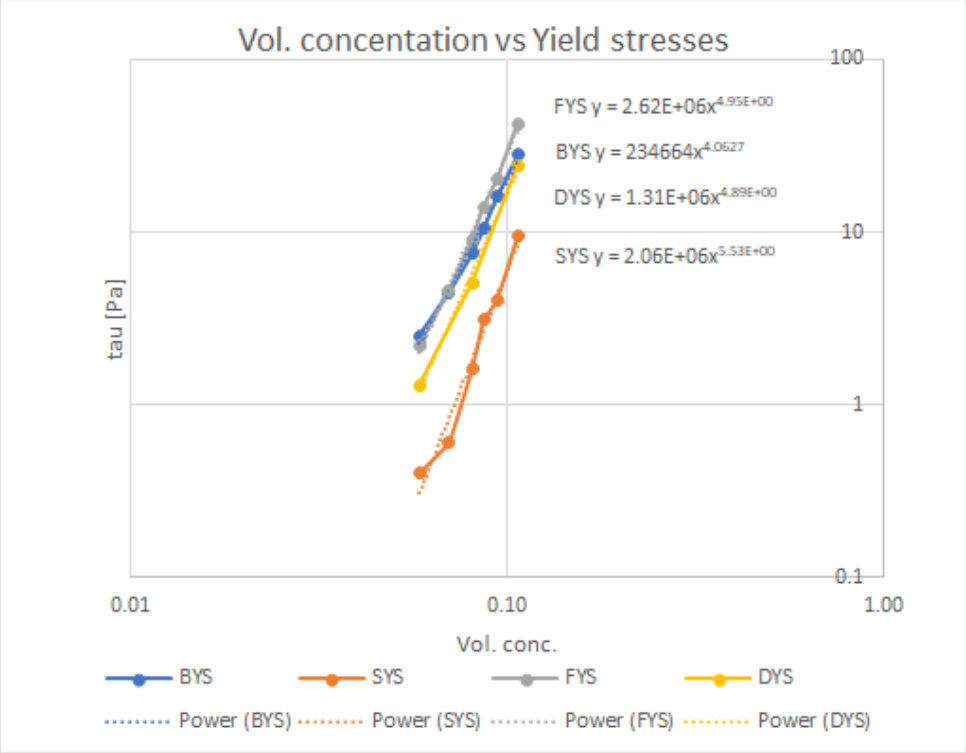

Figure 4.8: Plots represents the increase of yield stresses with the increase of volumetric concentration of solids in double logarithmic scale for the Calandkanaal fluid mud.

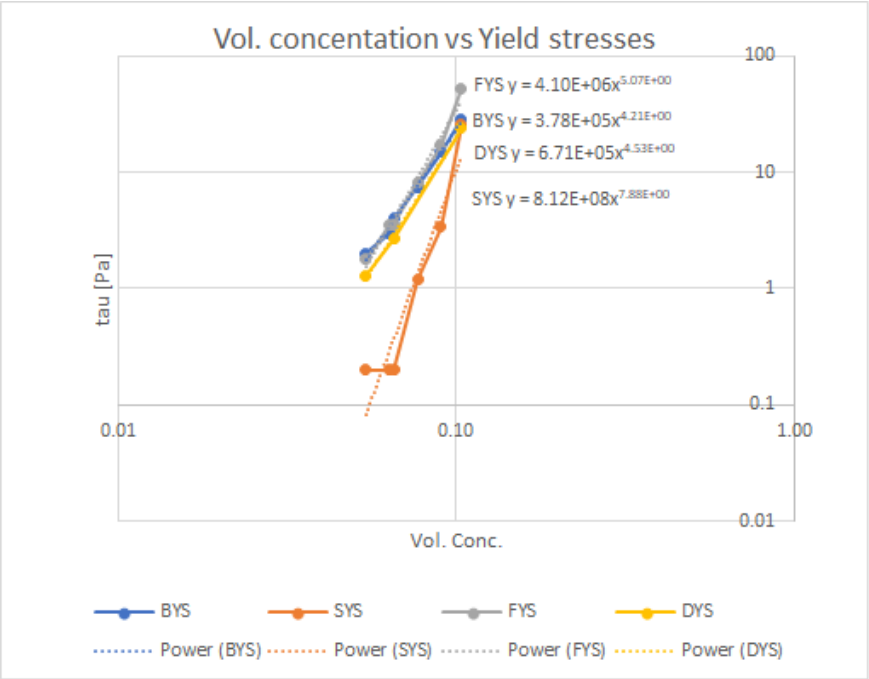

Figure 4.9: Plots represents the increase of yield stresses with the increase of volumetric concentration of solids in double logarithmic scale for the 8e Petroleumhaven fluid mud.

Relation between the geo-technical water content and yield stresses

Based on the Atterberg-Limits, the Geo-technical water content is defined as the ratio of the mass of water content to the mass of the solid content in the fluid mud.

Figures 4.10,4.11 and 4.12 represents the relation between the Geotechnical water content of the fluid mud to the yield stresses. The rheological properties decrease with an increase of Geotechnical water content in the fluid mud. This relation helps estimate the amount of water required to reduce the strength of the fluid mud for flume experiments.

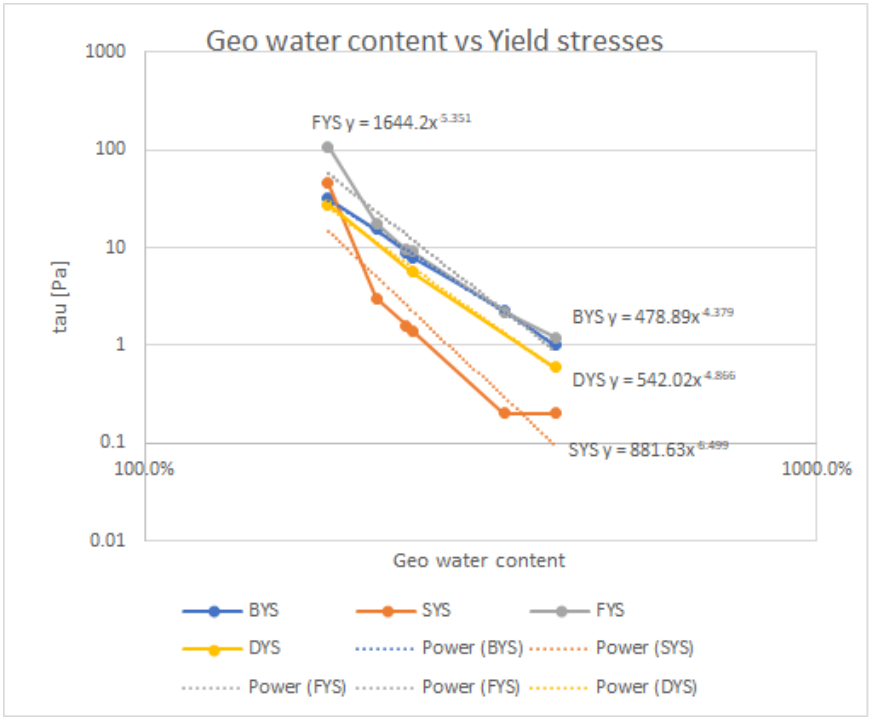

Figure 4.10: Plots represents the decrease of yield stresses with the increase of geo-technical water content in double logarithmic scale for the Beerkanaal fluid mud.

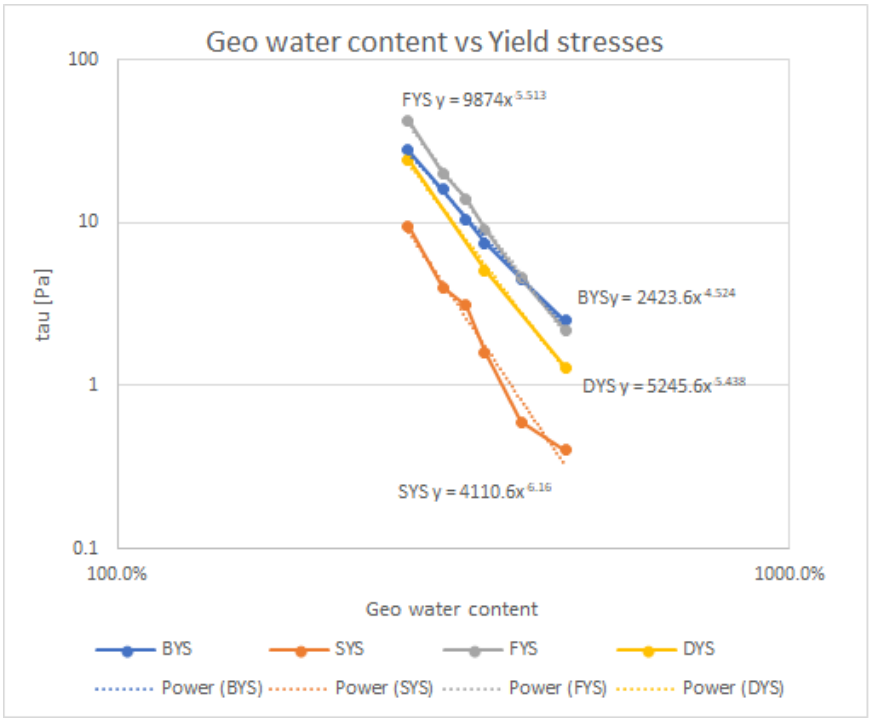

Figure 4.11: Plots represents the decrease of yield stresses with the increase of geo-technical water content in double logarithmic scale for the Calandkanaal fluid mud.

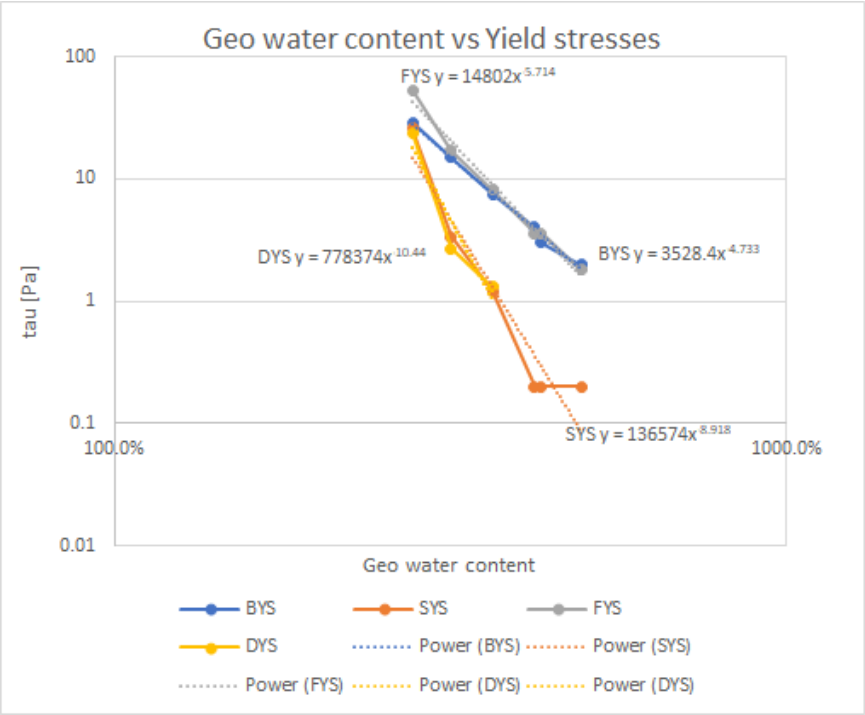

Figure 4.12: Plots represents the decrease of yield stresses with the increase of geo-technical water content in double logarithmic scale for the 8e Petroleumhaven fluid mud.

4.3 Rheometry practice tests

For the rheometry practice tests Beerkanaal fluid mud is used and the rheological measurements were performed on a Thermo Scientific HAAKE MARS I rheometer, see figure 3.2. This rheometer can be operated in three modes: stress controlled, shear rate controlled, or deformation controlled. Creep tests are performed using the rheometer's controlled shear stress (CSS) mode, whereas stress growth studies are performed using the controlled shear rate (CSR) mode. Table 4.5 represents the list of rheological protocols performed on Beerkanaal fluid mud to study the rheometry practice and compare with different geometry configurations.

The tests in CSR protocols were easy to perform because we are controlling the rotation speed of geometry in the CSR test. In contrast, the tests in CSS were challenging to obtain a ramp-down flow curve because in CSS tests, torque is controlled, and the shear stress shoots up drastically when fluid mud reaches yield point and becomes difficult to control. The details of fluid mud and rheometry protocols are described in A.7

During these tests, the fluid mud was not diluted, and for each rheometer test, a fresh fluid mud sample was used. The procedure of testing the fluid mud in the rheometer is similar as mentioned in the previous section 4.2.

Table 4.5: List of rheological experiments performed on Beerkanaal fluid mud to assess the rheometry. Here CSS = Controlled shear stress, CSR = Controlled shear rate.

Test No	Configuration	Mode	Protocol
130	Vane(FL16)-cup	CSR	0-100(1/s) 180s up - 60s constant - 180s down
131	Vane(FL16)-cup	CSS	0-120Pa 180s up - 60s constant - 180s down
132	Vane(FL22)-cup	CSR	0-20(1/s) 180s up - 60s constant - 180s down
133	Vane(FL22)-cup	CSS	0-120Pa 180s up - 60s constant - 180s down
134	Bob-cup	CSR	0-100(1/s) 180s up - 60s constant - 180s down
135	Bob-cup	CSS	0-120Pa 180s up - 60s constant - 180s down
136	Bob-cup	CSS	0-85Pa 180s up - 60s constant - 180s down
137	Groove bob-cup	CSR	0-100(1/s) 180s up - 60s constant - 180s down
138	Groove bob-cup	CSS	0-90Pa 180s up - 60s constant - 180s down

4.3.1 Details of geometry configuration

The concentric cylinders geometries(CC DIN 25), also known as bob-cup geometry, have an inner diameter of the cup 27mm and the outer diameter of the bob 25mm. The gap between the bottom of the cup and the bob end was 5.3mm.

In the vane(FL22)-cup geometry configuration, the inner diameter of the cup was 27mm, and the outer diameter of the vane geometry was 22mm. The gap between the bottom of the cup and vane was maintained at a gap of 1mm (as per Shakeel et al. (2020b), but manual advices gap of 11mm).

The vane (FL16) has an outer diameter of 16mm and the cup's inner diameter of 27mm. The gap between the wall of the cup and the rotor is 11mm.

4.3.2 Shear rate conversion theory for vane(FL22)-cup configuration rheometry

The Thermo Scientific HAAKE MARS rheometer is advanced and computerized. From the instruction manual, 006-1422, Version 2.6, Eq. 4.3 and 4.4 are used to calculate A and M, which are the geometry factors for coaxial cylinder geometries with recessed ends.

$$A = \frac{1}{2\pi R_i^2 L} \tag{4.3}$$

$$M = \frac{2\delta^2}{\delta^2 - 1}; \delta = \frac{R_a}{R_i} \tag{4.4}$$

where R_a is the rotor outer radius, R_i is the cup inner radius, and L is the height of the cylindrical rotor.

The manual states that there is no flow field defined for the sample around the vane. Thus shear rate in the sample cannot be calculated, and geometry factor M by default is set to 1.0. Dzuy & Boger (1983) calculated geometry factor A (see Eq. 4.5) for vane geometry.

$$A = \frac{1}{4\pi R_i^3 (\frac{L}{2R_i} - \frac{1}{3})} \tag{4.5}$$

Since we know the dimensions of the vane-cup configuration, replacing the vane(FL22) with an imaginary cylindrical bob of the same rotor diameter, the value of δ=13.6/11= 1.24. Substituting this value in Eq. 4.4 gives M = 5.8.

Thus, the results from the HAAKE rheometer vane(FL22) tests must be corrected by multiplying the shear rate with a factor of 5.8 and dividing the viscosity by 5.8 to compare with the bob-cup measurements.

4.3.3 Discussion

Wall-slip artefact in bob-cup configuration fluid mud rheometry

Comparing the CSS and CSR tests of bob-cup geometry configuration seems that a wall-slip artifact influences the fluid mud in the bob-cup rheometry, see Figure 4.13. This artifact is confirmed by performing the rheology tests using vane (FL22)-cup configuration where the two-steps in flow curve at similar shear rate range 0-15 (1/s) is not present, see Figure 4.14. Besides, the comparison of the viscous curves obtained from CSS tests of bob and vane (FL22) geometries, also suggests the wall-slip artifact, see Figure 4.15.

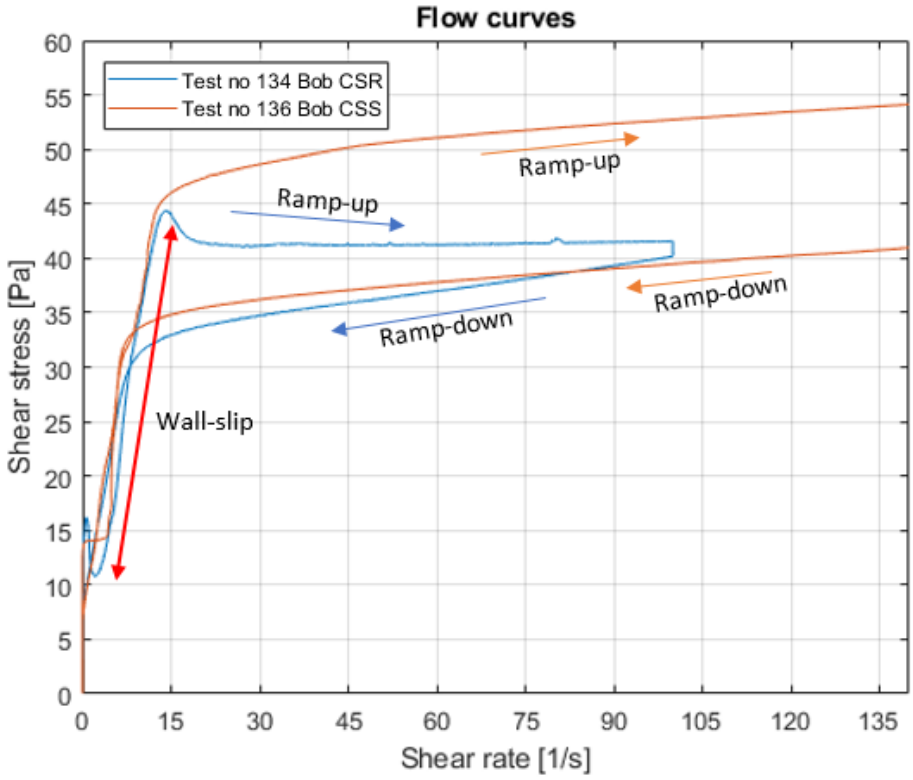

Figure 4.13: Illustration of the wall-slip artefact in bob-cup rheometry on Beerkanaal fluid mud. In the legend, the test numbers are represented and the corresponding details of the flow curve are mentioned in Table 4.5.

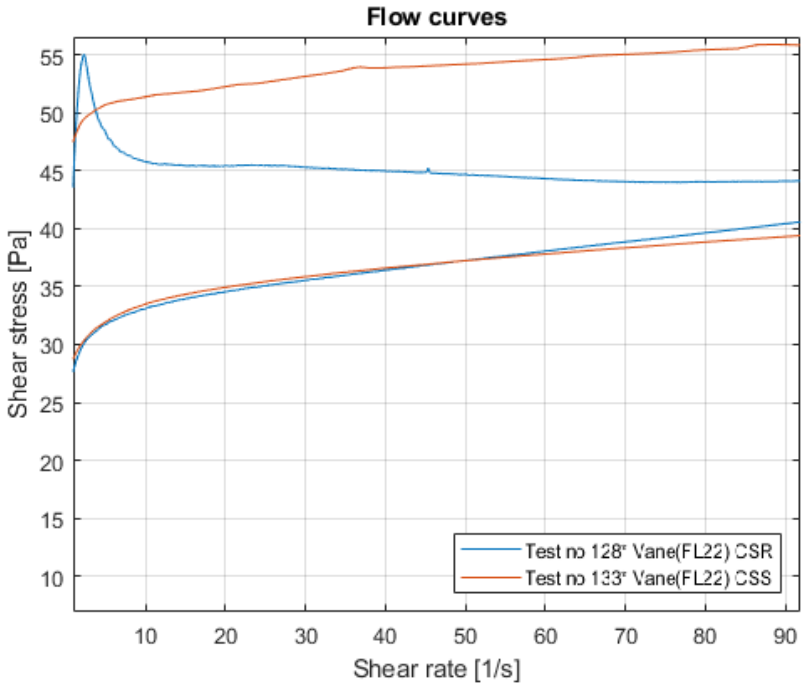

Figure 4.14: Comparison of CSS and CSR with vane geometry. In the legend, the test numbers are represented and the corresponding details of the flow curve are mentioned in Table 4.5.

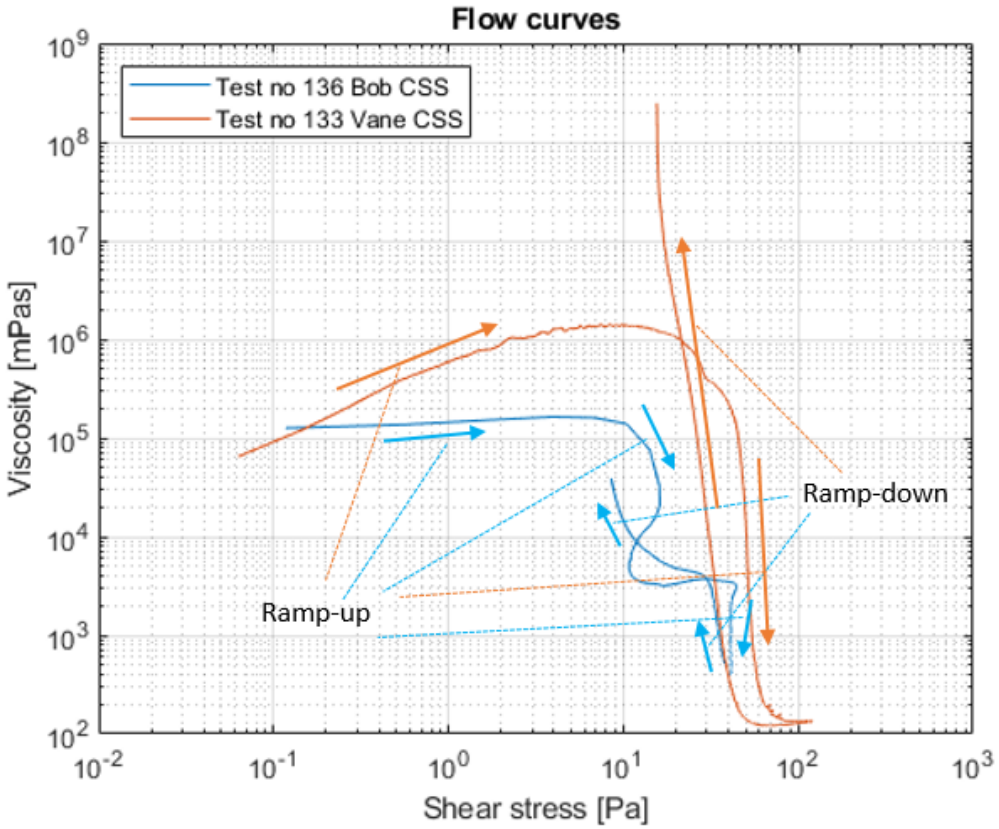

Figure 4.15: Comparison of the viscous curves obtained from CSS ramp tests of bob and vane(FL22) geometry. For tests with vane, correction factor was applied. In the legend, the test numbers are represented and the corresponding details of the flow curve are mentioned in Table 4.5.

Comparison of CSR tests of different geometries

Comparing the CSR tests of bob-cup, vane-cup (FL22), groove bob-cup, and vane-cup(FL16) rheometry on Beerkanaal fluid mud of density 1.272g/cc seems to be agreeing to produce approximately same flow curve except for vane(FL16)-cup geometry. Table 4.6 represents the Bingham yield stress obtained by extrapolating the ramp-down flow curves onto the shear stress axis of respective tests.

Table 4.6: Comparison of Bingham yield stress obtained from different geometry configuration flow curve

Geometry	Bingham yield stress [Pa]	Test No
Bob-cup	32.5	134
vane(FL22)-cup	33.5	128
Groove bob-cup	31.5	137
vane(FL16)-cup	46	130

From figure 4.16, the geometries bob, vane (FL22), and groove bob represent nearly similar flow curves, but the vane (FL16) shows a much larger Bingham yield stress value. The reason can be because of geometry factor value M in Eq. 4.4 which also requires the correction factor. Another possible reason can be the influence of turbulence in the gap between the cup and rotor.

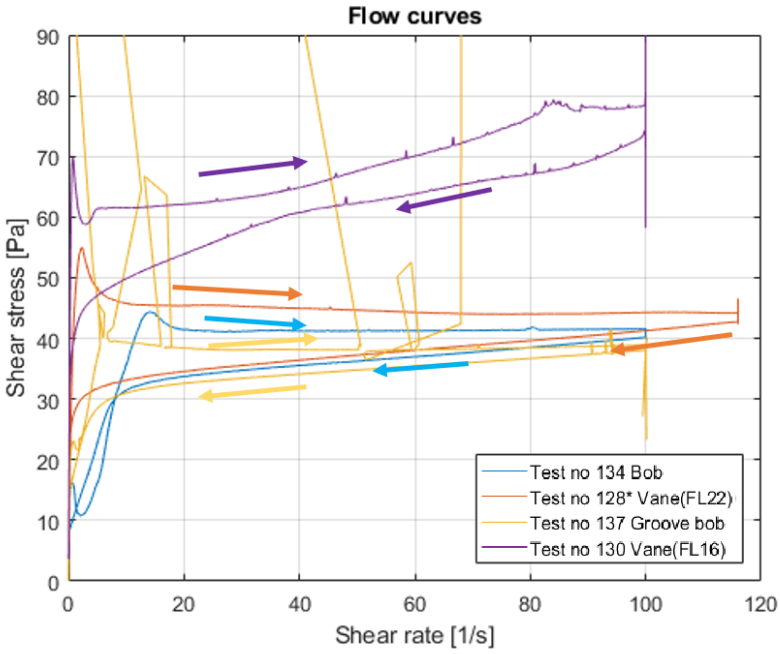

Figure 4.16: comparison of CSR tests with different geometries

Comparison of CSS tests of different geometries

The flow curves from CSS tests of different geometries suggest that the vane(FL22) and vane(FL16) induce the secondary flow at a shear rate of approximately 250(1/s) and 50(1/s), respectively, see Figure 4.17. On the other hand, the CSS tests with bob-cup and groove bob-cup configuration show no secondary flows.

It seems that the groove bob is very sensitive to sand or solid particles in the mud. When solid particles strike in the grooves of the groove bob, excursions are developed in the flow curves, see figure 4.16 and 4.17.

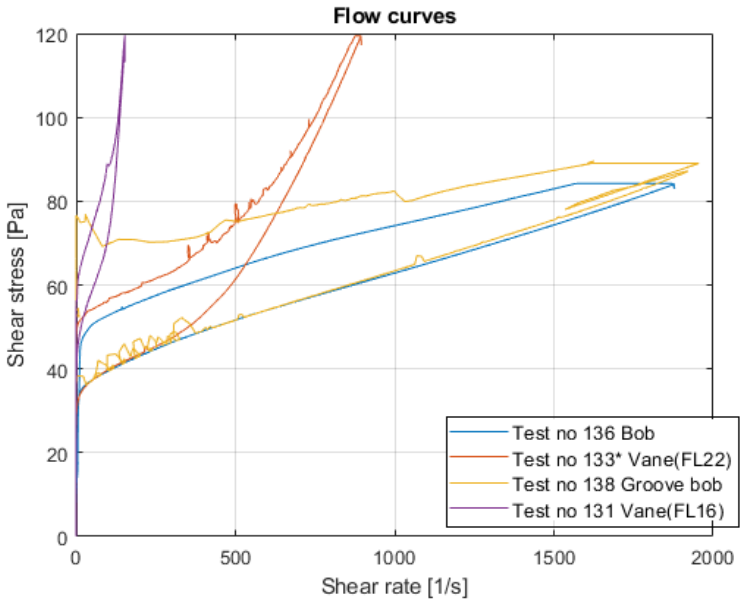

Figure 4.17: Comparison of CSR tests with different geometries. In the legend, the number with 'T' represents the test number. The details of the flow curve are mentioned in Table 4.5.

Determination of true static yield stress from bob-cup CSR tests

Comparing the flow curves obtained from the bob-cup CSR test (Test no 134) and vane(FL22)-cup CSS test (Test no 133) of the same fluid mud sample suggests that the peak stress (Peak stress=44.34Pa) in the bob-cup flow curves is very near to true static yield stress (tSYS=44.06Pa) of the fluid mud (using protocols of Cheng (1986)), see Figure 4.18. In conclusion, the static yield stress (43.1Pa) obtained from Cheng (1986) protocols found very close to the fluidic yield stress (44.1Pa) obtained from Shakeel et al. (2020a) protocols.

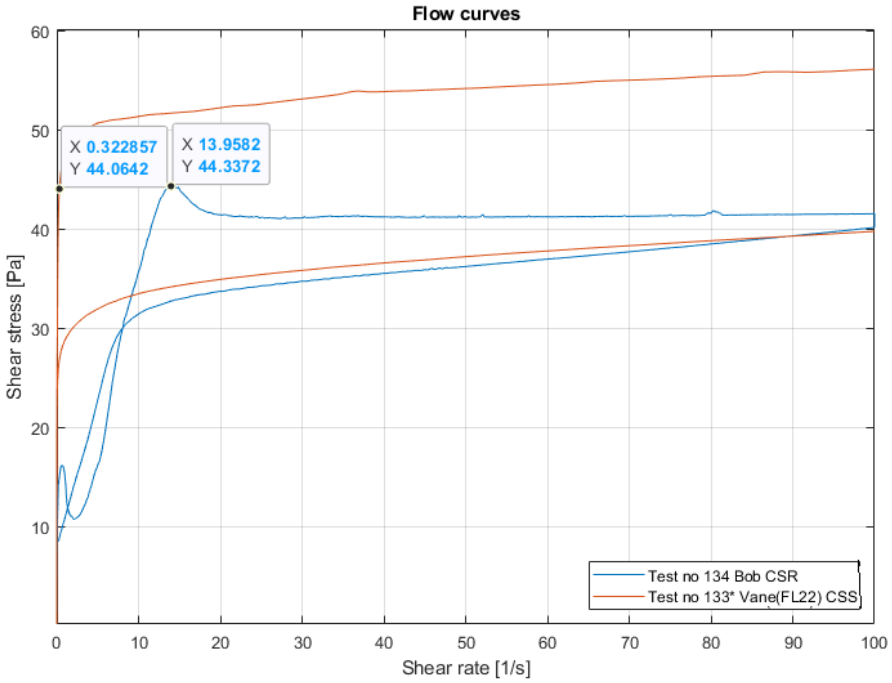

Figure 4.18: Comparison of bob-cup CSR test and vane(FL22)-cup CSS test

Comparison of HAAKE rheometer and FANN 286 rheometer

In order to test the fluid mud on-site while dredging at Port of Rotterdam for flume experiments, a portable rheometer FANN 286 was used. However, the FANN 286 rheometer is an old technology viscometer that does not assure the accuracy of the flow curves. Therefore, before using FANN 286 rheometer, the flow curves obtained from the FANN 286 rheometer and HAAKE rheometer are compared.

Figure 4.19 represents the entire flow curve obtained from bob-cup in CSR mode (test no 134), only ramp-down flow curve obtained from bob-cup in CSS mode (test no 136), and FANN 286 ramp down the curve. The difference between the Bingham yield stress obtained from the HAAKE rheometer and FANN 286 rheometer is approximately 12 Pa. This suggests that using FANN 286 rheometer, a correction of 12Pa should be added.

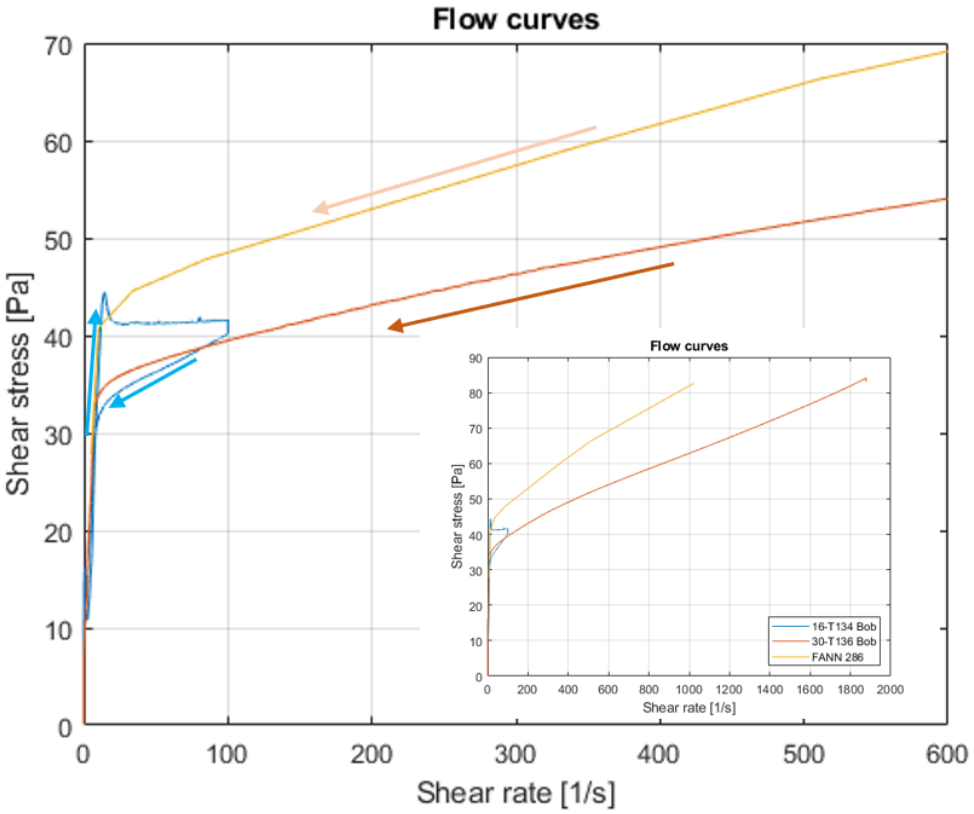

Figure 4.19: Comparison of HAAKE rheometer (Test no 134 & 136) and FANN 286 rheometer

Chapter 5

Thixotropy effect of fluid mud

The main aim of the thixotropy quantification is to justify the importance of thixotropy property in fluid mud modeling and check the curve fitting of flow curve with the Houska thixotropy model.

In the flume experiments, three different fluid mud strengths were proposed. The high strength fluid mud in the test matrix is named Fluid mud 1, medium-strength fluid mud as Fluid mud 2, and weak fluid mud strength as Fluid mud 3.

5.1 Quantification of thixotropy effect of fluid mud

5.1.1 Hysteresis loop method

This method is applied to the rheology tests of fluid mud samples collected during the flume experiments. The comparison of the thixotropic effect is made by measuring the area under the flow curve. Table 5.1 represents the values of the area under the flow curve of the fluid mud. The area under the flow curve of un-remolded fluid mud collected during the dredging at Calandkanaal is 3595Pa/s.

Table 5.1: Hysteresis loop or area under the flow curve of the fluid mud used in flume experiments. The values in red colour were omitted in the average calculations.

Sample No	1	2	3	4	5	6	Average	Test No
Fluid mud 1	85.51	78.05	89.52	109.8	87.57	129.6	85.16	139;140;141; 142;143;144
Fluid mud 2	58.69	40.58	52.27	52.23	52.55	45.79	53.94	145;146;147; 148;149;150
Fluid mud 3	33.05	44.95	28.57	47.09	35.69	52.02	44.28	151;152;153; 154;155;156

Figure 5.1 suggests that the thixotropy is significantly influenced by remolding in the flume experiments. This also suggests that in-situ mud exhibits higher thixotropy than the fluid mud used in the flume experiments. Thus, the rheological modeling must account for the thixotropy effect for thick or high viscous fluid mud.

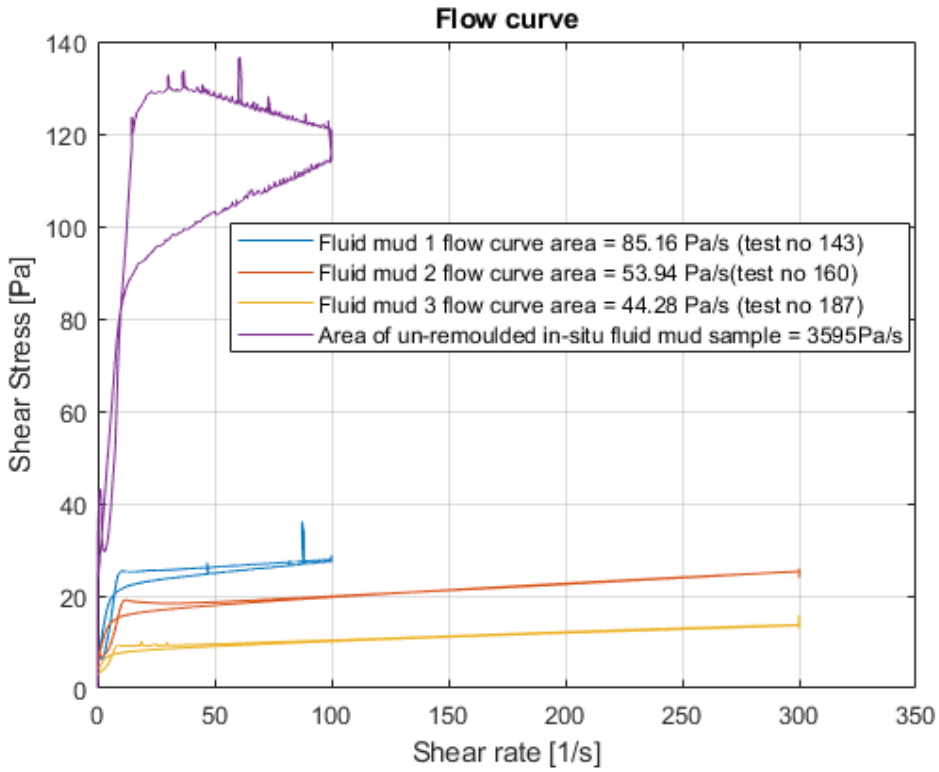

Figure 5.1: Flow curves with hysteresis area of the fluid mud samples of different strengths collected during flume experiments.

In conclusion, this method was highly uncertain because the area depends on the flow curve's shear stress and shear rate. Any uncertainty in the flow curve drastically changes the value of hysteresis area, see red labeled values in Table 5.1.

5.1.2 Sensitivity method

Another approach to quantify the thixotropy effect is the method of sensitivity. The sensitivity is defined as the ratio of true static yield stress and Bingham yield stress. As discussed in the section 4.3.3, the true static yield stress can be approximated from the bob-cup CSR tests.

Table 5.2 represents the sensitivity of the fluid mud used in the flume experiments. It seems that un-remolded fluid mud has high thixotropy with a sensitivity of 40%, which means that 40% structure strength can regrow from destructed structure strength.

The sensitivity of remolded and diluted fluid mud showed negligible thixotropy. Table 5.2 also suggests that sensitivity decreases with the dilution of fluid mud.

In conclusion, the sensitivity method suggests that thixotropy is significant in in-situ fluid mud and should be considered in the rheological modeling of thick/ high viscous fluid mud.

Table 5.2: Sensitivity of the fluid mud used in the flume experiments

Fluid mud	True static yield stress [Pa]	Bingham yield stress [Pa]	Sensitivity	Reference
Un-remoulded fluid mud	129.7	90	1.4	-
Fluid mud 1	24.3	21.2	1.1	Table 6.2
Fluid mud 2	16.3	16.5	1.0	Table 6.4
Fluid mud 3	9.3	9.3	1.0	Table 6.6

5.2 Houska rheological model

The rheological flow curves of the fluid mud collected during the flume experiments, see Figures 5.3,5.4 and 5.5. The main aim of the modeling is to integrate the time dependency into the flow curve using the Houska equation, see Eq. 2.10. The parameter used in the Houska equation is represented in the Table 5.3. The challenging part in the Houska modeling is to find structure growth and decay parameters.

Figure 5.2 represents the Houska curve fitting to the flow curve of unremolded fluid mud, which suggests that the significant thixotropy effect of the fluid mud can be well curve fitted with the Houska equation except at low shear rates.

Table 5.3: Houska equation variables value

Fluid mud	**At $\lambda = 0$**			**dτ difference of SYS and DYS**	**dK**	**a [1/s]**	**b**	**Curve fitting to the flow curve test number**
	τ_y [Pa]	**K [Pa.s^n]**	**n**					
Unremolded fluid mud	79	1.5	0.655	35	0.9	0.001	0.0002	-
FM1	17	0.4	0.645	4	0.3	0.02	0.0005	143
FM2	12	0.28	0.65	3	0.1	0.045	0.0005	160
FM3	5.5	0.45	0.505	1.5	0.05	0.0095	0.001	187

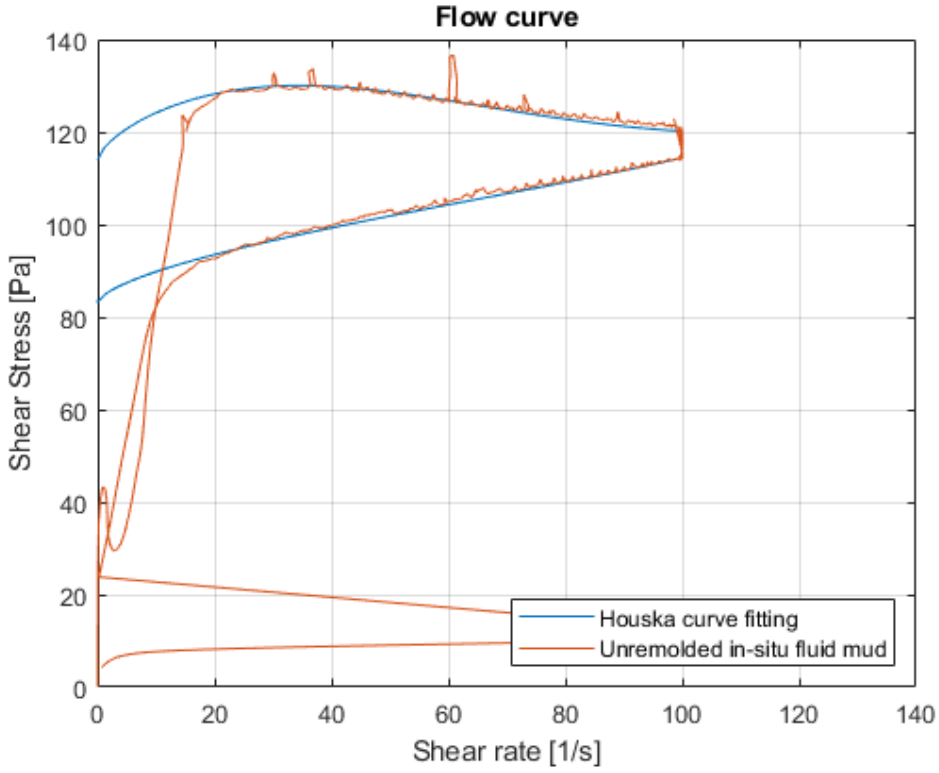

Figure 5.2: Houska flow curve modelling to the flow curve of unremolded fluid mud

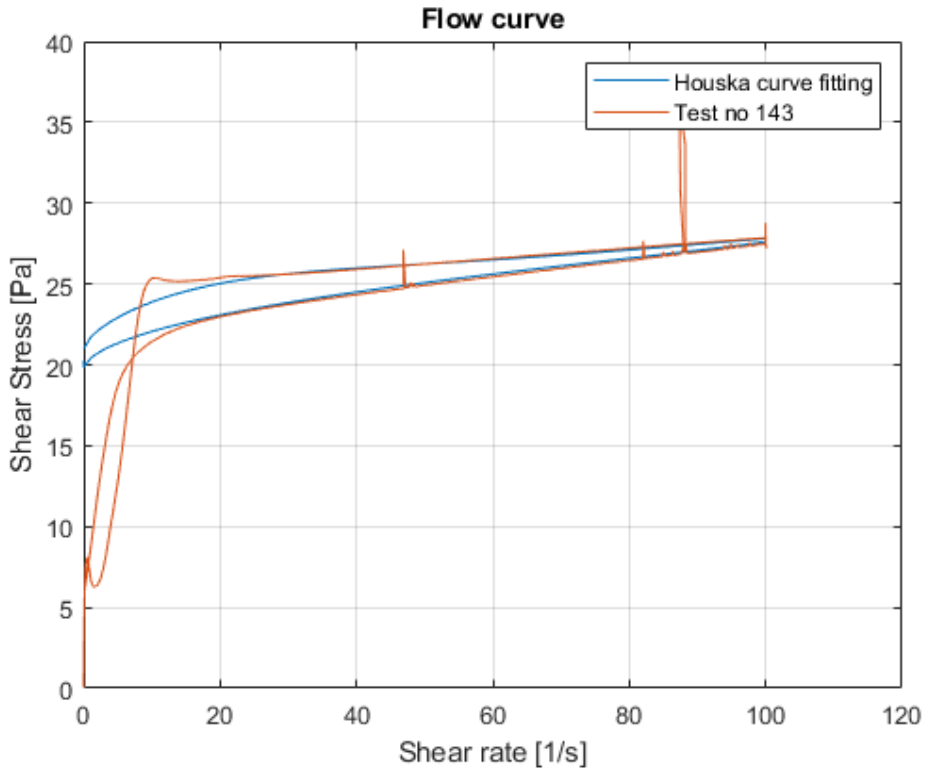

Figure 5.3: Houska flow curve modelling to the flow curve of fluid mud-1 sample collected during the flume experiments, see test number 143

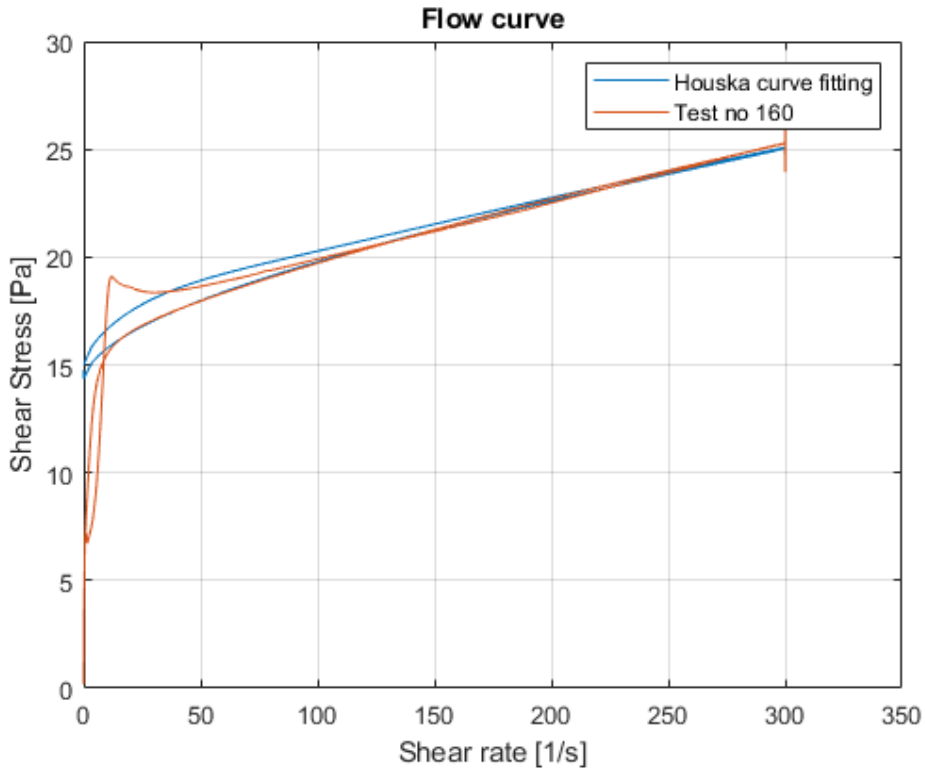

Figure 5.4: Houska flow curve modelling to the flow curve of fluid mud-2 sample collected during the flume experiments, see test number 160

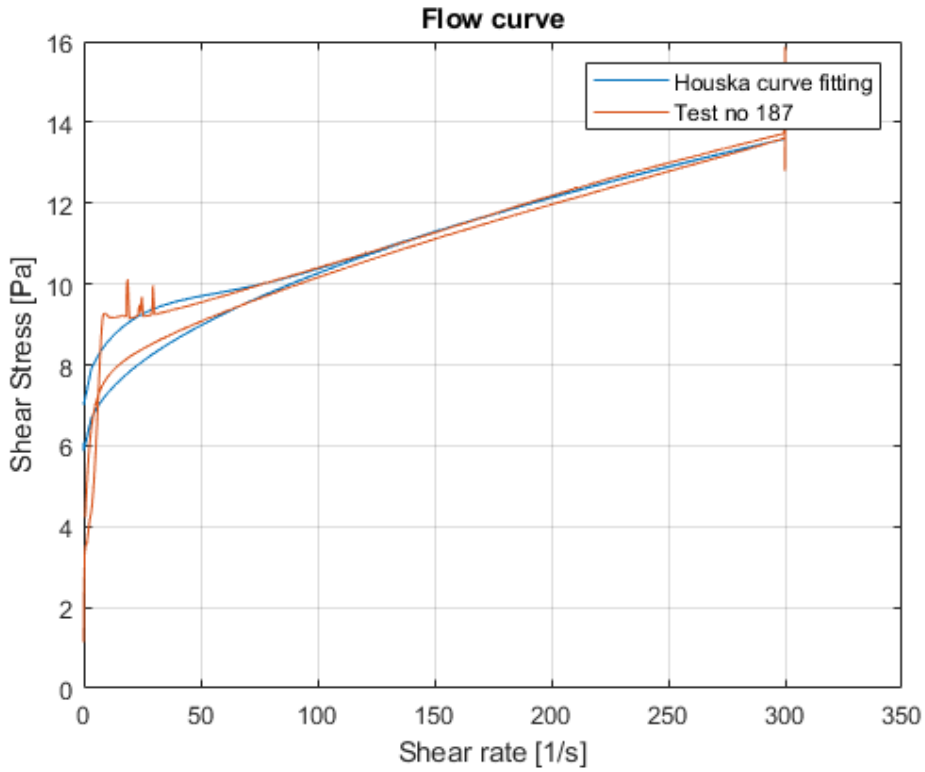

Figure 5.5: Houska flow curve modelling to the flow curve of fluid mud-3 sample collected during the flume experiments, see test number 187

Chapter 6

Flume experiments of a plate dragged in fluid mud

6.1 Experimental procedure and results

Over time, the density measurement of the fluid mud kept changing. Initially, the densitometer (DMA 35) was used to measure the density of fluid mud. But deviations were found comparing these measurements to pycnometer and oven test methods. After that, the oven test method was adapted to find the density of the fluid mud (see Appendix A.8). In the oven test method, the density of fluid mud was calculated using the dry weight of solids, water content, seawater density, and solid's density. However, we found a significant deviation when these densities (for seawater and freshwater samples) plotted against the yield stress of the fluid mud samples. Because of this reason, it was decided to use seawater to dilute the fluid mud in the flume. However, over time the importance of density of solids studied and corrected the formulas in the oven test calculations (see Appendix A.8.3).

Initially, the research committee chose the Cux sampler for the flume experiments to measure the resistance on thin plates when dragged in fluid mud. But, the calibration tests of the Cux sampler showed unreliable force measurements. Thus, a new plate assembled with load-cell was designed and built at Deltares used in the flume experiments. The design details of these plates are discussed in 3.2.

After the calibration of the load cell, the flat wooden plate was hanged to the frame of towing carriage, see Figure 3.17. The original mud of fluidic yield strength 130Pa and Bingham yield stress 85Pa was diluted to 25Pa Bingham yield stress (approximately). The flat plate was immersed at 0.95m, and trial tests were performed at 0.5m/s. The force measured during the test went from 70N to 50N. Rheological tests confirmed that the fluid mud in the flume is non-homogeneous. In the tests, the Bingham yield stress was about 27Pa in the region of 70N and 18Pa in the region of 50N.

Various attempts were made to homogenize the fluid mud, like using the concrete block. The concrete block hanged to a crane and then moved fluid mud from one side of the flume to the other side. However, only some improvements were made, but the force measured was still unsteady and unacceptable. The propeller (blade-rotor set-up) effectively homogenized the fluid mud locally but not the whole tank.

After waiting the whole night, the fluid mud showed the same behavior both rheologically, and the force measured the previous day. In order to homogenize the fluid mud over the whole tank, a truck with a pump was called. Fluid mud was pumped to this truck, mixed well, and then pumped back to the tank. In this process, the fluid mud was pumped from one side of the tank to the other side.

In the flume experiments, the flat plate was dragged in the fluid mud at four different speeds. Three different fluid mud strengths were proposed for the flume experiments, and each test run was repeated eight times. Thus, high strength fluid mud in the test matrix is named Fluid mud 1, medium-strength fluid mud as Fluid mud 2, and weak fluid mud strength as Fluid mud 3.

6.1.1 Experiments of flat plate moved in fluid mud-1

In the flume experiment, the fluid mud in the flume was mixed using a propeller set-up. The propeller set-up was hanged to the carriage and run over the flume back and forth three times. After the mixing process, the fluid mud samples (FM1S1, FM1S2, and FM1S3) were collected after 15 minutes (approximately) of rest for rheology tests. The location of fluid mud samples taken in the flume is shown in Figure 3.18.

The plate moved in mud at different velocities and they are 0.25m/s, 0.5m/s, 0.75m/s, and 1.0m/s. For each velocity configuration, eight repetitions of tests were performed, see table 6.1. During the tests with a velocity above 1m/s, the detected force was unacceptably unsteady. Thus, the maximum speed in the test matrix was set to 1m/s.

Table 6.1: Measurement of total resistance of plate moved in fluid mud-1. The total resistance signal for each velocity configuration is shown in Appendix B.1.

Towing Velocities [m/s] / Test Repetitions	0.25	0.5	0.75	1.0
1	-39.28	-47.43	-48.74	-56.19
2	-38.95	-45.77	-48.84	-55.46
3	-38.57	-45.31	-50.03	-54.32
4	-38.41	-43.58	-51.51	-55.4
5	-38.64	-44.25	-49.37	-53.89
6	-39.18	-42.95	-49.10	-53.17
7	-41.23	-42.83	-48.98	-55.17
8	-39.45	-42.84	-48.91	-53.75
Average in [N]	**-39.21**	**-44.37**	**-49.44**	**-54.67**

At the end of the flume experiments, the fluid mud samples FM1S4, FM1S5, and FM1S6 were collected for rheology tests. Table 6.2 represents the details of fluid mud-1 rheology. The measurement of Bingham yield stress by the Bingham curve fitting method is shown in Appendix B.2

Table 6.2: Details of fluid mud-1 rheology. The tests details are described in the Appendix B.2. Here BYS is the Bingham yield stress, SYS is static yield stress, DYS is the dynmaic yield stress, FYS is the fluidic yield stress

Samples	**Density [g/cc]**	**BYS [Pa]**	**true SYS [Pa]**	**DYS [Pa]**	**SYS [Pa]**	**FYS [Pa]**	**Bingham viscosity [Pas]**	**Test No**
FM1S1	1.200	20.7	22.1	13.6	5.5	23.21	0.05141	139,142,145
FM1S2	1.203	22.0	24.1	14.5	5.9	25.11	0.05529	140,143,146
FM1S3	1.203	22.0	26.4	13.9	6.1	25.11	0.05529	141,144,147
FM1S4	1.201	20.8	23.5	13.2	5.6	23.32	0.04954	148,151,154
FM1S5	1.200	19.8	23.6	14.0	5.6	22.56	0.04777	149,152,155
FM1S6	1.203	21.9	26.0	13.9	5.9	23.79	0.05288	150,153,156
Average	**1.202**	**21.2**	**24.3**	**13.8**	**5.8**	**23.85**	**0.05203**	

6.1.2 Experiments of flat plate moved in fluid mud-2

In order to reduce the strength of the fluid mud and meet the test matrix requirements (see section 3.3.3), the fluid mud was mixed with seawater. The seawater was brought from Port of Rotterdam in a truck. The amount of water required to mix in the fluid mud was estimated using the density of the existing fluid mud, the density of the seawater, and tank volume.

Without removing the existing fluid mud in the flume, approximately $4m^3$ of water was added and mixed with the propeller. The average Bingham yield strength of the fluid mud over the tank found was nearly 17Pa. In the towing tank, the level of the fluid mud was increased by 5cm, and so for the flat plate (the flat plate now immersed by 1m).

The flume experiments were performed the next day of the fluid mud-2 arrangement in the flume. Before commencing the flume experiments, the fluid mud was mixed with a propeller (a similar procedure used in fluid mud-1 experiments). After 15 minutes (approximately) of rest, the fluid mud samples FM2S1, FM2S2, and FM2S3 were collected for rheology tests.

Few trial runs were performed at towing velocity of 0.5m/s. We observed a reduction of measured force compared to the previous day's average force. The rheology of fluid mud also shows a reduction of Bingham yield stress. Therefore, this suggests that the degradation of fluid mud influences the total resistance in mud.

The flume experiments were performed by moving the plate in mud with velocities 0.25m/s, 0.5m/s, 0.75m/s, and 1.0m/s. Similarly, like the tests for fluid mus-1, eight repetitions of tests were performed for each velocity, see table 6.3.

Table 6.3: Measurement of total resistance of plate moved in fluid mud-2. The total resistance signal for each velocity configuration is shown in Appendix B.1.

Towing Velocities [m/s] / Test Repetitions	0.25	0.5	0.75	1.0
1	-28.66	-33.28	-37.90	-43.98
2	-30.82	-33.67	-39.22	-45.48
3	-30.77	-34.63	-39.10	-45.85
4	-30.88	-33.57	-37.18	-45.80
5	-29.31	-34.72	-39.32	-45.58
6	-30.54	-34.93	-39.08	-45.64
7	-31.21	-35.00	-38.67	-44.72
8	-30.15	-34.35	-38.76	-43.51
Average in [N]	**-30.29**	**-34.27**	**-38.65**	**-45.07**

After completion of flume experiments, fluid mud samples FM2S4, FM2S5, and FM2S6 were collected for rheology tests. Table 6.4 represents the rheology details of fluid mud-2. The Bingham yield stress was measured by fitting the Bingham model to the flow curve (see Appendix B.2.2).

Table 6.4: Details of fluid mud-2 rheology. The tests details are described in the Appendix B.2.2. Here BYS is the Bingham yield stress, SYS is static yield stress, DYS is the dynmaic yield stress, FYS is the fluidic yield stress

Samples	**Density [g/cc]**	**BYS [Pa]**	**true SYS [Pa]**	**DYS [Pa]**	**SYS [Pa]**	**FYS [Pa]**	**Bingham viscosity [Pas]**	**Test No**
FM2S1	1.192	16.7	16.5	9.7	4.2	16.9	0.02860	157,160,163
FM2S2	1.192	16.4	16.6	9.6	4.3	16.5	0.02812	158,161,164
FM2S3	1.191	16.0	16.9	9.5	3.9	16.3	0.02771	159,162,165
FM2S4	1.192	17.0	16.1	9.5	4.3	16.6	0.02627	166,169,172
FM2S5	1.192	16.7	16.1	9.3	4.1	16.9	0.02863	167,170,173
FM2S6	1.190	16.0	15.7	9.2	4.2	16.5	0.02762	168,171,174
Average	**1.191**	**16.5**	**16.3**	**9.5**	**4.2**	**16.6**	**0.02782**	

6.1.3 Experiments of flat plate moving in fluid mud-3

A similar approach used in reducing the strength of the fluid mud-2 was used here. The plate immersed in fluid mud-3 was 1m in depth. The fluid mud mixture was mixed well with the propeller, and trial runs were performed to check homogeneity.

On the day of flume experiments in fluid mud-3, the flat plate was moved at velocities 0.25m/s, 0.5m/s, 0.75m/s, and 1.0m/s. For each velocity, eight repetitions of tests were conducted (see table 6.5). Prior to the tests, the fluid mud was mixed with the propeller, and fluid mud samples FM3S1, FM3S2, and FM3S3 were collected for rheology tests.

The tests at 1.0m/s seemed unsteady throughout the experiments. So, after completing tests with velocities below 1.0m/s, slight design modifications to the plate were done. A steel wire was introduced from one side of the plate to counter the lift created by the fluid mud flow. In order to confirm that the addition of the steel wire does not affect the test results, some tests at low velocities were done to check the repeatability with the new design. The steel wire setup seems to make the tests steady at 1.0m/s.

Table 6.5: Measurement of total resistance of plate moved in fluid mud-3. The total resistance signal for each velocity configuration is shown in Appendix B.1.

Towing Velocities [m/s] / Test Repetitions	0.25	0.5	0.75	1.0
1	-17.37	-19.9	-23.65	-25.99
2	-17.51	-20.16	-23.63	-28.35
3	17.83	-20.96	-34.14	-27.23
4	-18.50	-20.75	-24.05	-26.75
5	-17.40	-20.27	-23.44	-29.54
6	-17.73	-20.53	-23.65	-28.27
7	-18.29	-20.64	-23.81	-28.20
8	-17.73	-20.52	-23.66	-27.68
Average	**-13.34**	**-20.47**	**-25.01**	**-27.75**

After completing tests in the flume, the fluid mud samples FM3S4, FM3S5, and FM3S6 were collected for rheology tests. Table 6.6 represents the rheology tests details of fluid mud-3. The Bingham yield stress was measured by fitting the Bingham model to the flow curve (see Appendix B.2.3)

Table 6.6: Details of fluid mud-3 rheology. The tests details are described in the Appendix B.2.3. Here BYS is the Bingham yield stress, SYS is static yield stress, DYS is the dynmaic yield stress, FYS is the fluidic yield stress

Samples	**Density [g/cc]**	**BYS [Pa]**	**true SYS [Pa]**	**DYS [Pa]**	**SYS [Pa]**	**FYS [Pa]**	**Bingham viscosity [Pas]**	**Test No**
FM3S1	1.174	9.5	9.4	5.4	2.8	9.7	0.01925	175,178,181
FM3S2	1.174	9.5	9.5	5.4	2.9	9.9	0.01878	176,179,182
FM3S3	1.173	9.5	9.7	5.3	2.9	9.4	0.01878	177,180,183
FM3S4	1.168	8.3	8.4	4.7	2.7	8.6	0.01760	184,187,190
FM3S5	1.169	9.3	9.1	5.1	2.7	9.0	0.01839	185,188,191
FM3S6	1.187	9.5	9.9	5.5	2.9	9.6	0.01925	186,189,192
Average	**1.174**	**9.3**	**9.3**	**5.2**	**2.8**	**9.4**	**0.01868**	

6.2 Discussion

6.2.1 Comparison of plate's resistance in mud to the plate's frictional force dragged in Bingham and Power-law fluids calculated analytically

The analytical formulas for finding the frictional forces on a plate when dragged in Bingham fluids and power-law fluids are given in Eq. 2.16 and Eq. 2.19 respectively, and the calculations are mentioned in the Appendix B.3.

Table 6.7 represents the details of the total resistance of plate measured in flume experiments and the calculated frictional force using analytical formulas.

Table 6.7: Details of plate's resistance in mud measured in flume experiments and plate's frictional force calculated analytically.

Tests in	Velocity [m/s]	Area of plate [m^2]	Total drag force obtained from the towing experiments [N]	Frictional force calculated using Bingham model [N]	Frictional force calculated using Power law model [N]
Fluid mud 1	0.25	1.52	39.0	35.3	21.0
	0.5	1.52	44.3	37.3	27.2
	0.75	1.52	49.1	39.9	31.7
	1	1.52	54.5	43.0	35.3
Fluid mud 2	0.25	1.6	30.3	27.7	15.4
	0.5	1.6	34.3	29.2	20.8
	0.75	1.6	38.7	31.2	24.8
	1	1.6	45.1	33.6	28.1
Fluid mud 3	0.25	1.6	17.8	15.9	9.0
	0.5	1.6	20.5	17.1	12.6
	0.75	1.6	23.8	18.7	15.3
	1	1.6	27.8	20.6	17.6

Figures 6.1, 6.2 and 6.3 illustrates the resistance of a plate moved in fluid mud at different velocities. It seems that at low velocities, the total resistance of a plate is closer to the frictional force of a plate in Bingham fluids. As the velocity increased, the total resistance of a plate increased significantly.

The reason for a significant increase in the total resistance might be because of stagnation pressure. The stagnation pressure in the flow of Newtonian fluids is 1/2$\rho\ V^2$ where ρ is the density of the fluid, and V is the velocity of flow. When the velocity increases in a flow, the stagnation pressure increases by an order 2. Thus, the stagnation pressure seems to increase significantly with speed.

The frictional force of a plate moved in power-law fluids is far compared to the total resistance at low velocities. However, as the velocity increases, the frictional force estimations in power-law fluids and Bingham fluids gets closer.

In Figure 6.4 and 6.5, the shear rate of the Power-law fluids and Bingham fluids are calculated using the Eq. 2.25 and Eq. 2.18. These figures also suggests that the range of applied shear stress in the rheometry CSR tests was suitable for this application.

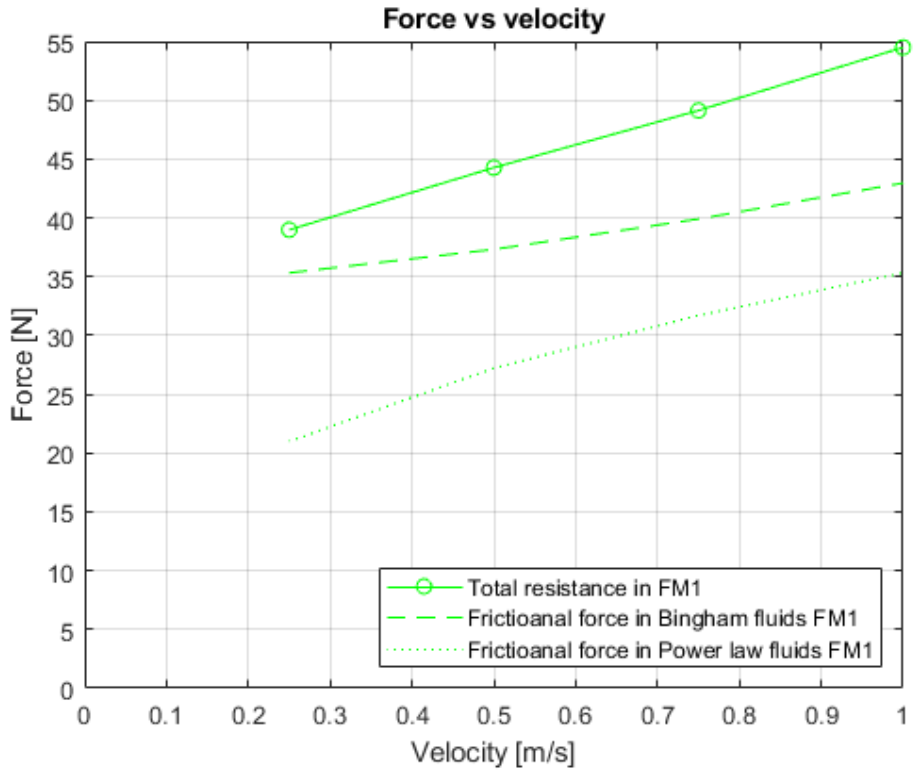

Figure 6.1: Comparison of total resistance of plate moved in fluid mud-1 to the frictional resistance calculated using the analytical formulas.

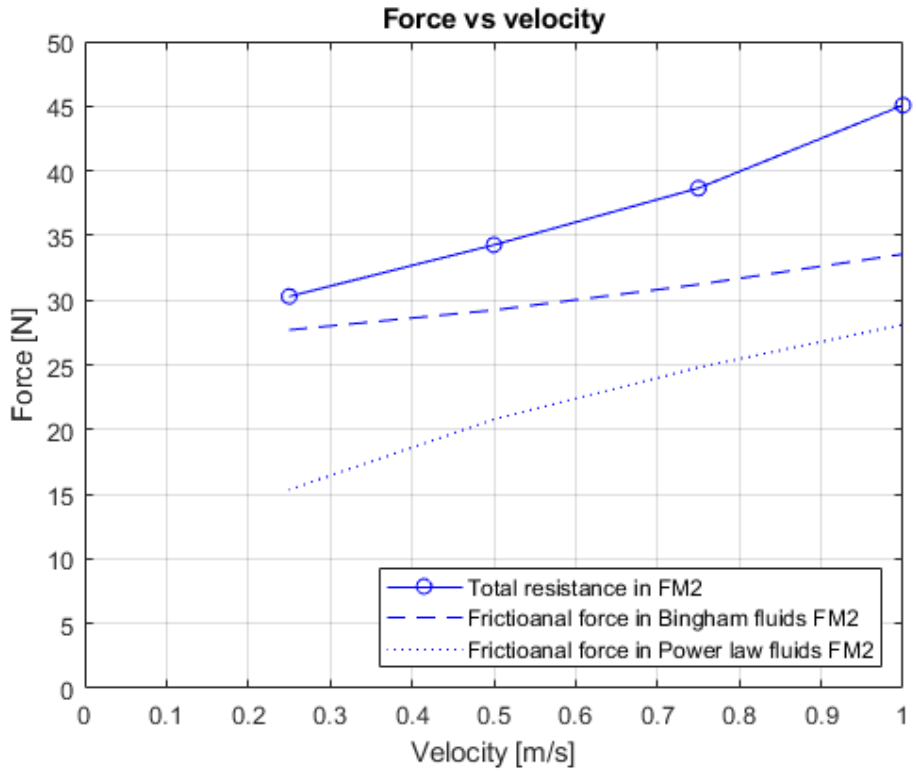

Figure 6.2: Comparison of total resistance of plate moved in fluid mud-2 to the frictional resistance calculated using the analytical formulas.

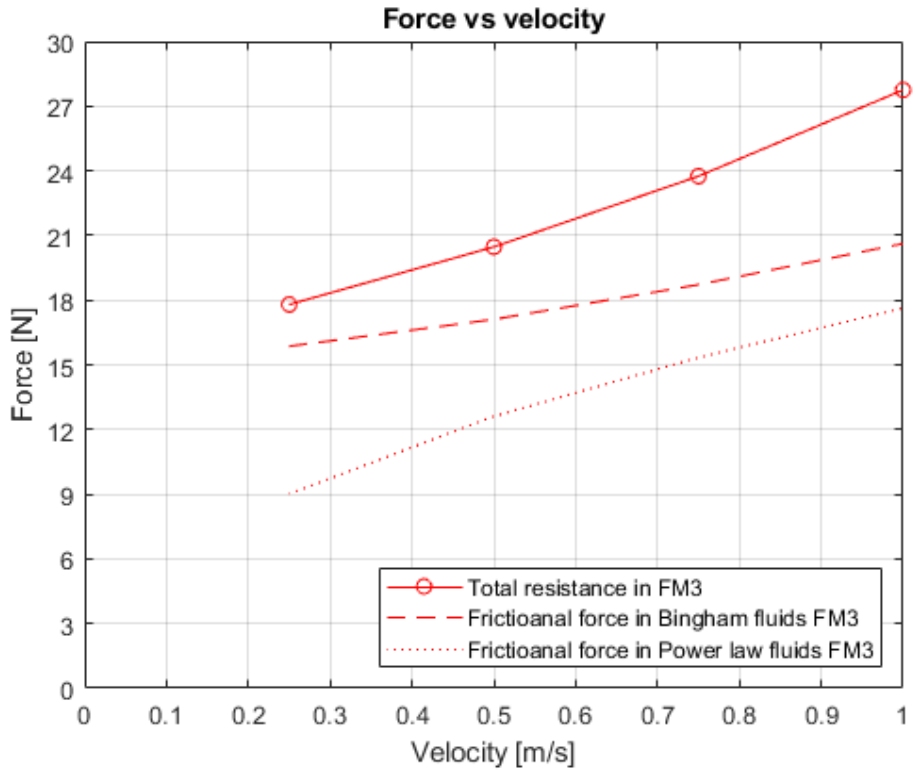

Figure 6.3: Comparison of total resistance of plate moved in fluid mud-3 to the frictional resistance calculated using the analytical formulas.

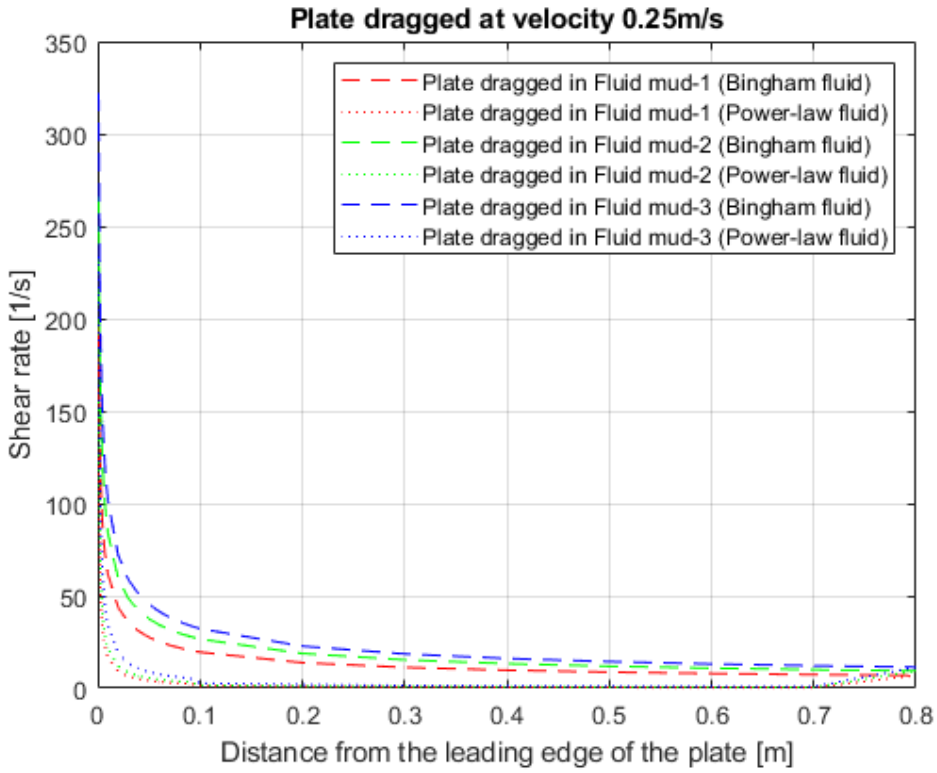

Figure 6.4: Comparison of shear rate of Bingham fluid and power-law fluids flowing over the plate at 0.25m/s

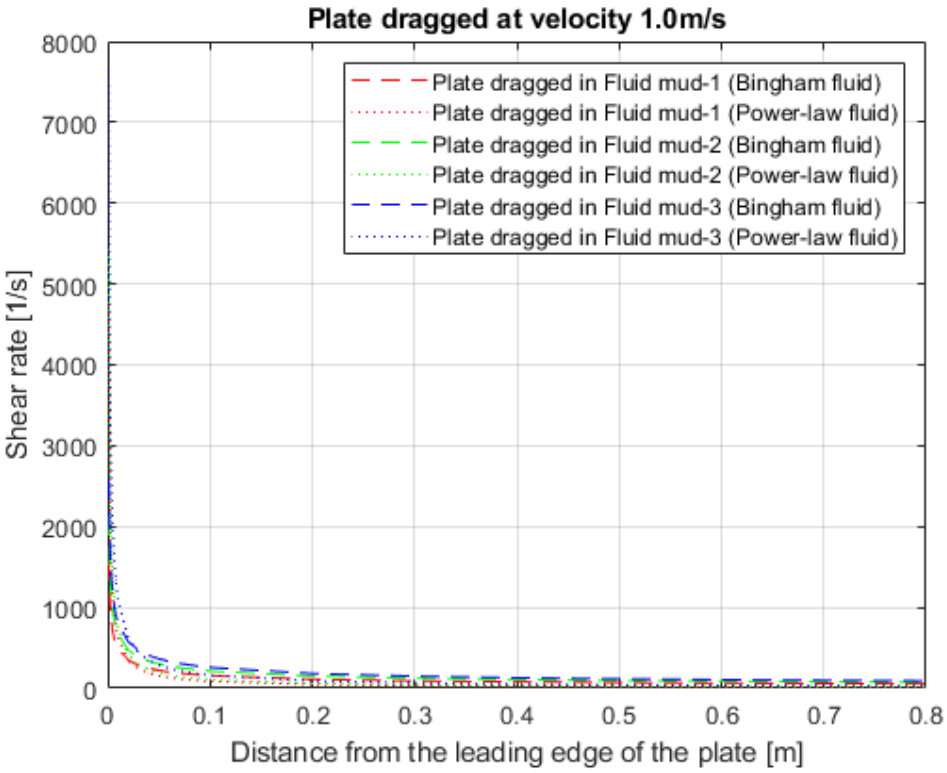

Figure 6.5: Comparison of shear rate of Bingham fluid and power-law fluids flowing over the plate at 1.0m/s

Figure 6.6 represents the relation between the total resistance of a plate moving in fluid mud and velocity. Extrapolating the curves linearly onto the force axis at velocity 0m/s seems to be related to the fluid mud's yield stress.

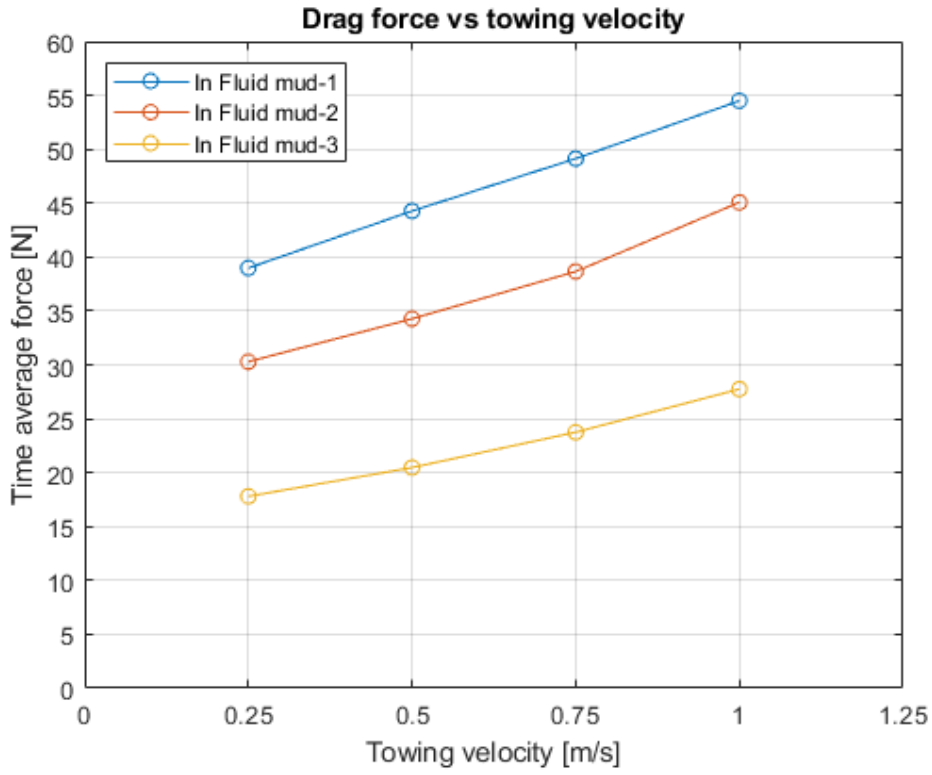

Figure 6.6: Total resistance of a plate moved in fluid mud measured in the flume experiments.

When the extrapolated force is divided by the wetted surface area of the plate, the value obtained seems close to the Bingham yield stress of the fluid mud, see Table 6.8. Thus, it suggests that when the plate comes to rest, the stress caused by the fluid mud is approximately the yield stress.

Table 6.8: Stress values obtained from the extrapolated force and wetted surface area seems closer to the the Bingham yield stress.

Towing in fluid mud	**Extrapolated force(EF) at velocity=0 [N]**	**Wetted surface area(WSA) [m^2]**	**Stress = EF/WSA [Pa]**	**Bingham yield stress of the fluid mud [Pa]**
FM-1	33.87	1.52	22.28	21.2
FM-2	24.89	1.6	15.56	16.5
FM-3	14.15	1.6	8.84	9.3

Chapter 7

Conclusions and recommendations

7.1 Conclusions

The main conclusions of this thesis assignment are grouped according to research questions:

1. What is the link between the presence of clay and rheological properties of mud? And how it can link to the density and the yield stress of mud?
    - The relationship between the volumetric concentration, geotechnical water content with the yield stresses of fluid mud was found.
    - Choosing the right elements and protocols to measure the yield stresses of fluid mud were investigated and the wall slip problem in the rheometry was bypassed.
    - Power law relations were found for the relation with volumetric concentration, for yield stress in agreement with fractal dimension theory.
    - It was confirmed that the yield stress increases with the density of the fluid mud grow exponentially (Power-law) and the relation between the yield stress and density of thick mud found sensitive.
    - The influence of seawater dilution or freshwater dilution is negligible on the Bingham yield stress of fluid mud.
2. How thixotropy of fluid mud can be quantified and taken into account in the non-Newtonian rheological modeling?
    - The time-dependency effect (thixotropy) was found in the flow curves of fluid mud from different locations of Port of Rotterdam.
    - In this study, the thixotropy effect of the fluid mud was quantified in two methods: Hysteresis loop method and sensitivity method.
        (a) It was found that the Hysteresis loop method is very sensitive and inaccurate because it depends on the protocol's shear stress and shear rate limits. However, it was found that an increase in water content in the fluid mud decreases the hysteresis area.
        (b) In the sensitivity method, it was found that the un-remolded mud has a sensitivity of 40$\%$, which indicates that the remolded mud can build up 40$\%$ strength. Thus, the thixotropy effect is significant in thick unremolded mud.
    - Rheological flow curve of mud are modelled using the Houska equation given in the Eq 2.10 which integrates the time-dependency effect. It was found that at high shear rates Houska thixotropy model fits good to the flow curve of fluid mud and poor curve fit at low shear rates.
3. What existing analytical formulas for non-Newtonian fluids can be used for estimating the plate resistance measured in the flume experiments?
    - In this work, the analytical formulas for the frictional forces acting on a flat plate in either power-law or Bingham fluids are considered. Overall, the formulas for Bingham fluids give a better estimation. However, the average error for three fluid muds at low speed is 11$\%$ whereas at high speed is 32$\%$. The reason for the larger error at higher speed is most likely because of the neglected pressure contribution, which increases with the velocity square (V^2).

- Despite the remolding of the mixture in the flume, thixotropy was measured by rheometer. Extrapolating the total resistance of a plate found the stress acting on a plate is very near to Bingham yield stress suggesting the thixotropy was sheared away in the towing of the plate.

7.2 Recommendations

Based on the findings of this research, the following recommendations are made:

1. The un-remolded mud and remolded mud have significant differences in rheological behaviour suggesting the influence of thixotropy is worth investigating in the future. In addition, integrating the thixotropy effect in fractal theory can be considered worth exploring.
2. With the fractal dimension, one may embark on a combination of in-situ density measurements and in-situ rheology (to verify the relation density-rheology regularly). This also helps investigate the rheological behavior difference between the laboratory prepared fluid mud samples and in-situ natural fluid mud samples of the same density values.
3. In the rheometry practices, the bob-cup geometry seems to prone wall-slip. Investigating the reason of wall-slip is worth to cross check the possibility of wall-slip on a plate moved in mud.
4. In the flume experiments, the fluid mud was remolded many times by the mixing process. Therefore, it is important to investigate the fluid mud time dependency property and perform the tests when the mud rebuilds its structure. This could help integrate the thixotropy effect in measuring the total resistance of plate dragged in fluid mud.

Appendices

Appendix A

Rheology and density measurements of three canals fluid mud

A.1 Beerkanaal fluid mud samples diluted with seawater

Beerkanaal fluid mud samples diluted with seawater of density 1025kg/m^3 were made in the laboratory. The fluid mud samples of different dilutions were made in the morning and stored in cups with a closed lid. Before using the fluid mud from the cup, it was hand-stirred for a homogenized mixture. The density of the fluid mud is measured using the oven test method. The details of rheometry, density, and properties of fluid mud are represented in Table A.1

Some fluid mud samples with no dilution were kept for consolidation on December 21, 2020. The first consolidated sample (Test no 23) 10 days tested on January 5, 2021, the second consolidated sample (Test no 24) 13 days tested on January 8, 2021, and the third consolidated sample (Test no 25) 18 days tested on January 13, 2021.

Table A.1: Details of rheometry and oven test results for Beerkanaal fluid mud samples diluted with seawater. All the tests were performed on December 21, 2020. (excluding the test no 23 to 25.

Test no	Time	From oven test method					Rheometry	
		Density [g/cc]	Vol. Concen-tration	Geo water content [%]	Hydro water content [%]	Solid content [%]	Geometry	Protocols
1	14:24	1.270	0.15	162	65	35	Bob	CSR 0-100 180s up - 60s constant - 180s down
2	13:12	1.270	0.15	162	65	35	Vane	CSR 0-100 240s up - 90s constant - 240s down
3	13:37	1.270	0.15	162	65	35	Groove bob	CSR 0-100 240s up - 60s constant - 240s down
4	14:42	1.270	0.15	162	65	35	Bob	CSR 0-100 50s up - 50s constant - 50s down
5	14:49	1.270	0.15	162	65	35	Bob	CSS 0-150 150s up
6	15:00	1.234	0.13	184	69	31	Bob	CSR 0-100 180s up - 60s constant - 180s down
7	15:09	1.234	0.13	184	69	31	Bob	CSR 0-100 50s up - 50s constant - 50s down
8	15:15	1.234	0.13	184	69	31	Bob	CSS 0-150 150s up
9	15:28	1.214	0.12	202	71	29	Bob	CSR 0-100 180s up - 60s constant - 180s down
10	15:40	1.214	0.12	202	71	29	Bob	CSR 0-100 50s up - 50s constant - 50s down
11	15:24	1.214	0.12	202	71	29	Bob	CSS 0-20 100s up
12	15:52	1.210	0.11	208	71	29	Bob	CSR 0-100 180s up - 60s constant - 180s down
13	16:32	1.210	0.11	208	71	29	Vane	CSR 0-100 180s up - 60s constant - 180s down
14	15:46	1.210	0.11	208	71	29	Bob	CSR 0-100 50s up - 50s constant - 50s down
15	16:05	1.210	0.11	208	71	29	Bob	CSS 0-20 100s up
16	16:09	1.158	0.08	282	77	23	Bob	CSR 0-100 180s up - 60s constant - 180s down
17	16:18	1.158	0.08	282	77	23	Bob	CSR 0-100 50s up - 50s constant - 50s down
18	16:24	1.158	0.08	282	77	23	Bob	CSS 0-20 100s up
19	16:33	1.134	0.07	317	80	20	Bob	CSR 0-100 180s up - 60s constant - 180s down
20	16:20	1.134	0.07	317	80	20	Vane	CSR 0-100 180s up - 60s constant - 180s down
21	16:48	1.134	0.07	317	80	20	Bob	CSR 0-100 50s up - 50s constant - 50s down
22	16:57	1.134	0.07	317	80	20	Bob	CSS 0-20 100s up
23	14:18	1.270	0.15	84	65	35	Bob	CSR 0-100 180s up - 60s constant - 180s down
24	15:27	1.264	0.15	105	66	34	Bob	CSR 0-100 180s up - 60s constant - 180s down
25	13:22	1.267	0.15	96	65	35	Bob	CSR 0-100 180s up - 60s constant - 180s down

The flow curves obtained in CSR tests with bob-cup geometry are represented in the Figure A.1 and A.2. The CSR tests with vane(FL22)-cup geometry are represented in Figure A.3. The CSR test with groove bob is represented in Figure A.4. Some of the undiluted fluid mud samples were kept for consolidation (21, 24, and 29 days) in the rheometry cup. On the day of rheology tests, the water layer in the rheometry cup with consolidated mud was removed carefully. The flow curves of the consolidated mud are represented in Figure A.5. The Bingham yield stress of these flow curves are represented in Table 4.2.

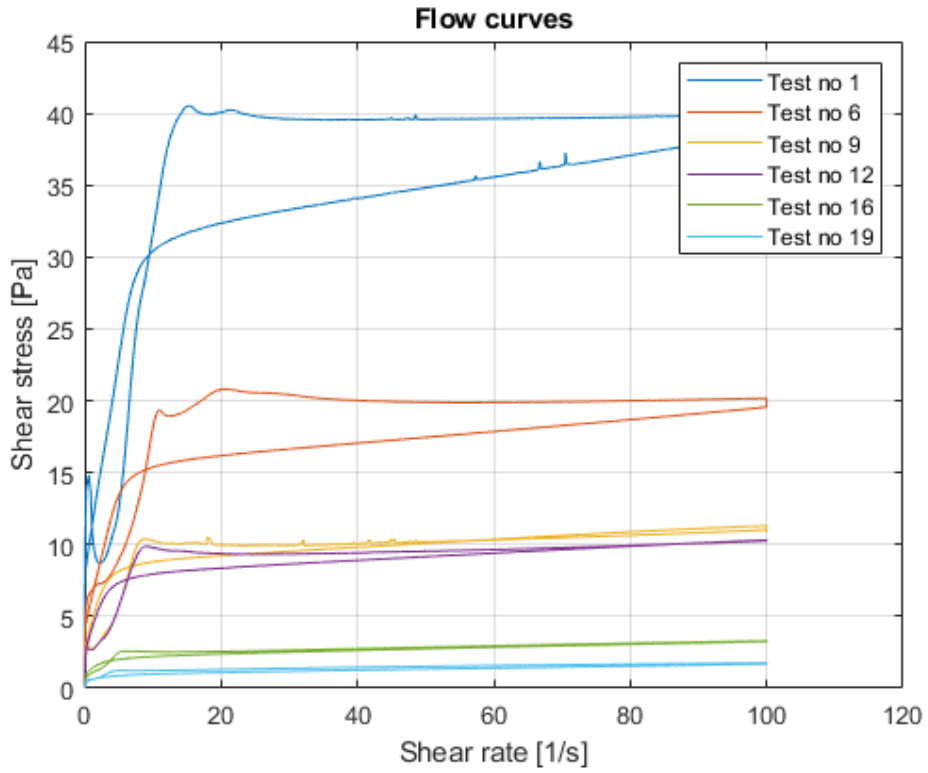

Figure A.1: Beerkanaal fluid mud samples diluted with seawater tested in CSR mode with bob-cup geometry to obtain flow curves.

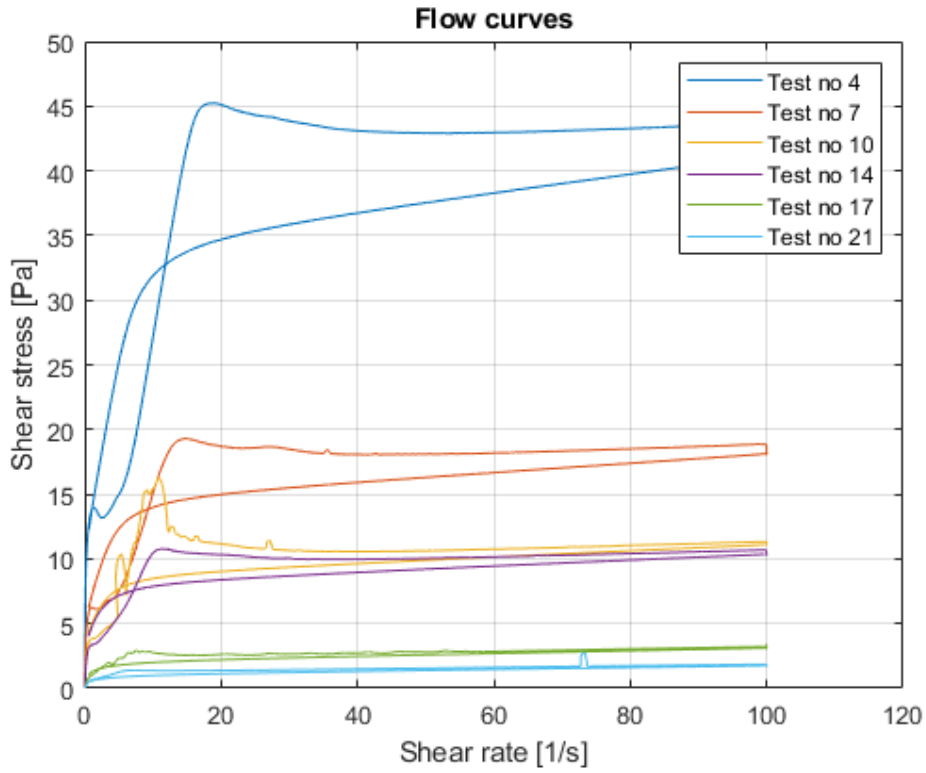

Figure A.2: Beerkanaal fluid mud samples diluted with seawater tested in CSR mode (0-50(1/s) ramp up and down) with bob-cup geometry to obtain flow curves.

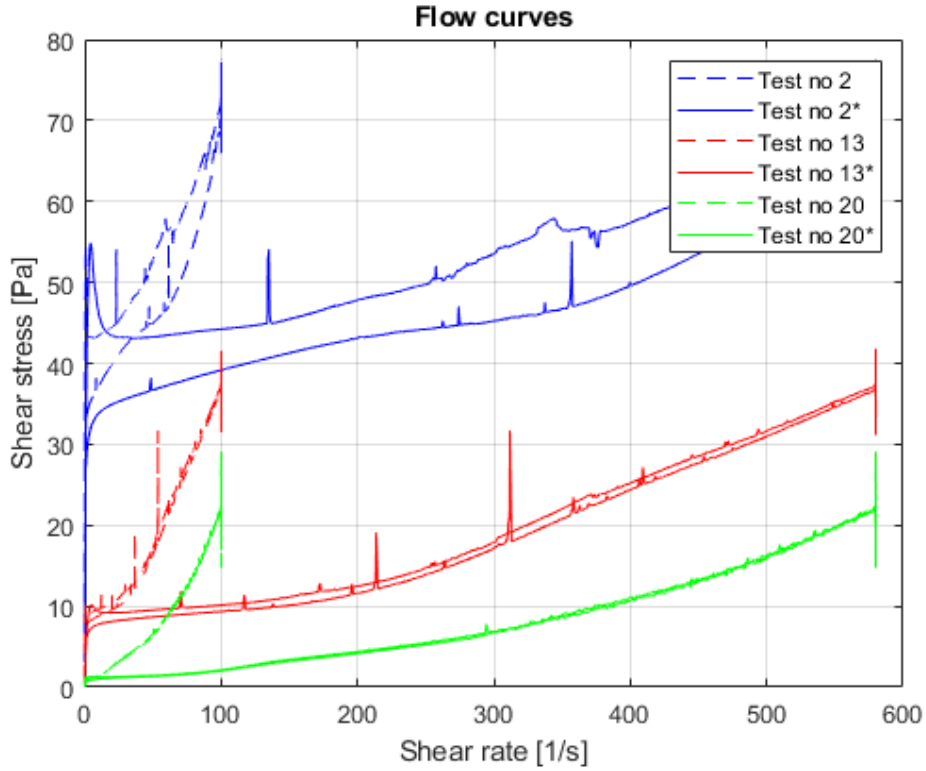

Figure A.3: Beerkanaal fluid mud samples diluted with seawater tested in CSR mode with vane(FL22)-cup geometry. The dashed-line curve is without correction factor and solid line is with correction factor.

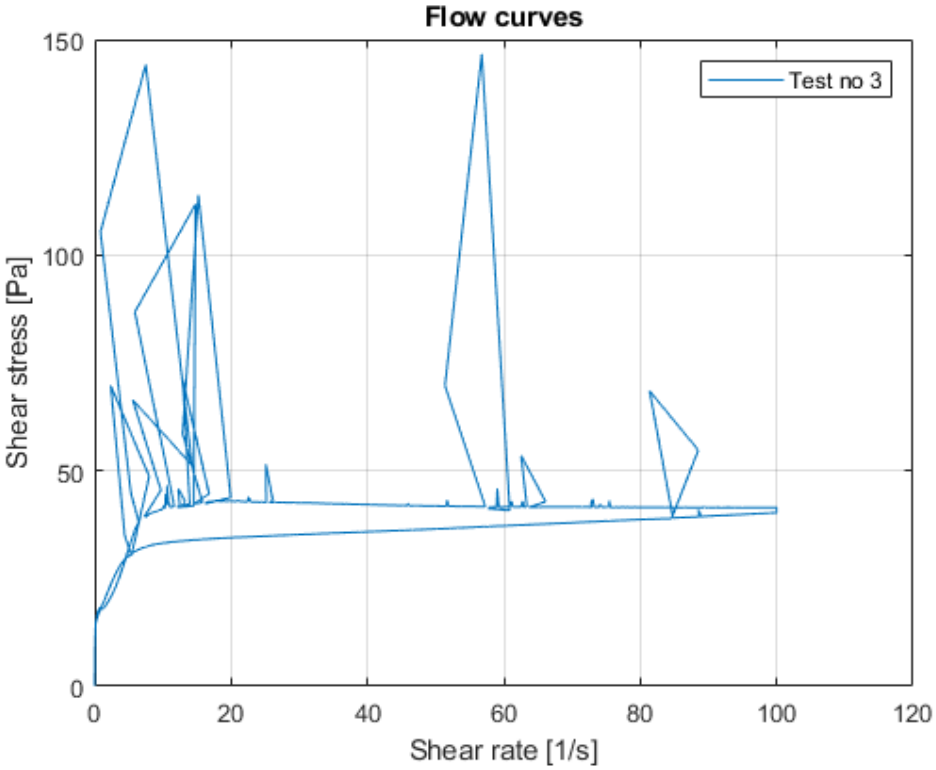

Figure A.4: Beerkanaal fluid mud sample without dilution tested in CSR mode with groove bob-cup geometry to obtain flow curve of undiluted fluid mud.

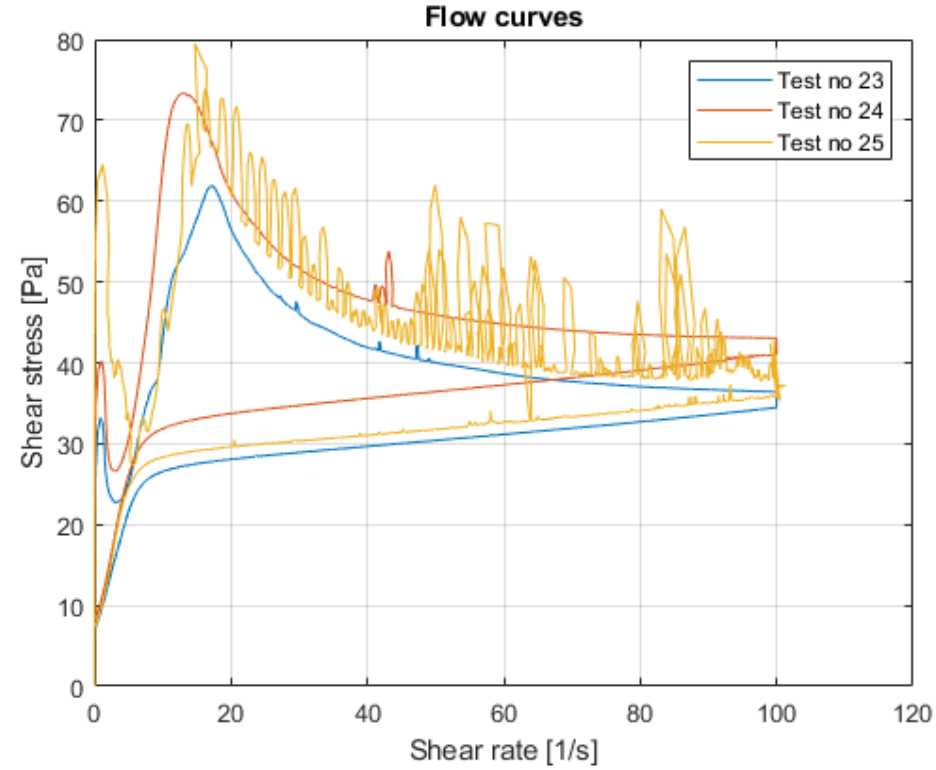

Figure A.5: Beerkanaal consolidated fluid mud sample tested in CSR mode with bob-cup geometry to obtain flow curve.

The Beerkanaal fluid mud samples with seawater dilution were tested in CSS mode with bob-cup geometry

to obtain the viscous curves, see Figure A.6.

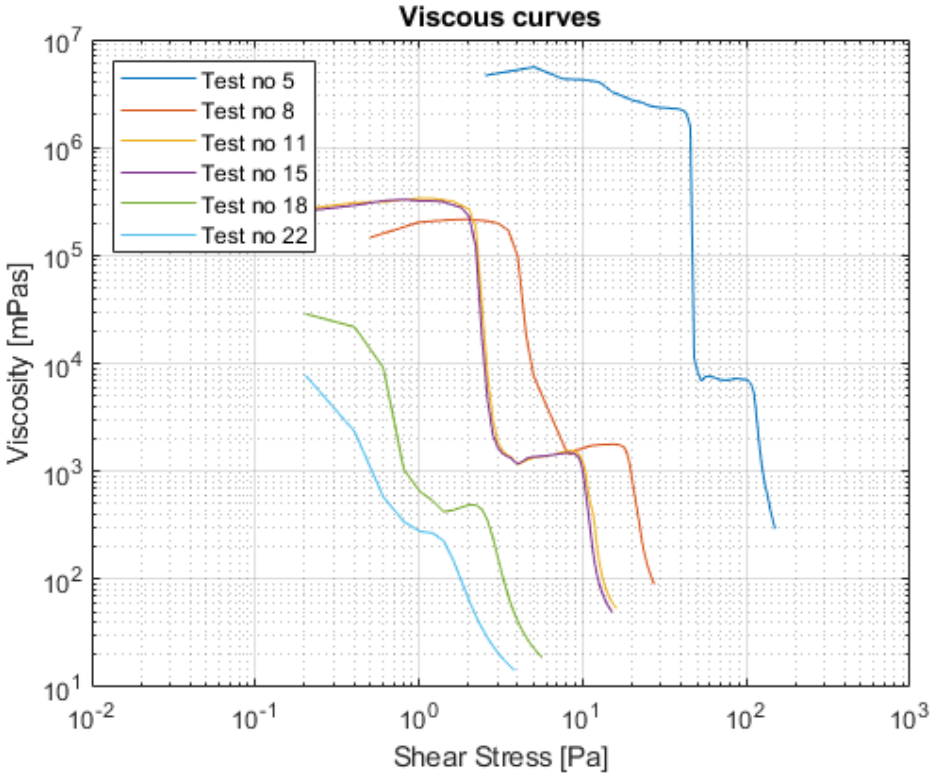

Figure A.6: Viscous curves of Beerkanaal fluid mud with sea water dilutions plotted on logarithmic scale

A.2 Calandkanaal fluid mud samples diluted with seawater

Calandkanaal fluid mud samples diluted with seawater of density 1025kg/m^3 were made in the laboratory. The fluid mud samples of different dilutions were made in the morning and stored in cups with a closed lid. Before using the fluid mud from the cup, it was hand-stirred for a homogenized mixture. The density of the fluid mud is measured using the oven test method. The details of rheometry, density, and properties of fluid mud are represented in Table A.2.

Some fluid mud samples with no dilution were kept for consolidation on December 21, 2020. The first consolidated sample (Test no 41) 10 days tested on January 5, 2021, the second consolidated sample (Test no 42) 13 days tested on January 8, 2021, and the third consolidated sample (Test no 43) 18 days tested on January 13, 2021.

Table A.2: Details of rheometry and oven test results for Calandkanaal fluid mud samples diluted with seawater. All the tests were performed on December 23, 2020. (excluding the test no 41 to 43.

Test no	Time	From oven test method					Rheometry	
		Density [g/cc]	Vol. Concen-tration	Geo water content [%]	Hydro water content [%]	Solid content [%]	Geometry	Protocols
26	14:29	1.197	0.11	213	73	27	Bob	CSR 0-100 180s up - 60s constant - 180s down
27	16:08	1.197	0.11	213	73	27	Vane	CSR 0-100 180s up - 60s constant - 180s down
28	14:53	1.197	0.11	213	73	27	Bob	CSS 0-150 150s up
29	15:16	1.176	0.09	242	75	25	Bob	CSR 0-100 180s up - 60s constant - 180s down
30	15:27	1.176	0.09	242	75	25	Bob	CSS 0-150 150s up
31	15:44	1.164	0.09	253	77	23	Bob	CSR 0-100 180s up - 60s constant - 180s down
32	16:09	1.164	0.09	253	77	23	Bob	CSS 0-150 150s up
33	16:19	1.155	0.08	274	78	22	Bob	CSR 0-100 180s up - 60s constant - 180s down
34	15:55	1.155	0.08	274	78	22	Vane	CSR 0-100 180s up - 60s constant - 180s down
35	16:45	1.155	0.08	274	78	22	Bob	CSS 0-20 100s up
36	17:05	1.138	0.07	315	80	20	Bob	CSR 0-100 180s up - 60s constant - 180s down
37	17:23	1.138	0.07	315	80	20	Bob	CSS 0-20 100s up
38	17:31	1.119	0.06	342	82	18	Bob	CSR 0-100 180s up - 60s constant - 180s down
39	15:44	1.119	0.06	342	82	18	Vane	CSR 0-100 180s up - 60s constant - 180s down
40	17:40	1.119	0.06	342	82	18	Bob	CSS 0-20 100s up
41	14:47	1.209	0.11	136	72	28	Bob	CSR 0-100 180s up - 60s constant - 180s down
42	15:45	1.210	0.11	130	72	28	Bob	CSR 0-100 180s up - 60s constant - 180s down
43	16:46	1.208	0.11	134	72	28	Bob	CSR 0-100 180s up - 60s constant - 180s down

The flow curves obtained in CSR tests with bob-cup geometry are represented in Figure A.7 and viscous curves from CSS tests are shown in Figure A.8. The tests in vane(FL22)-cup geometry are represented in Figure A.9. Some of the undiluted fluid mud samples were kept for consolidation (21, 24, and 29 days) in the rheometry cup. On the day of rheology tests, the water layer in the rheometry cup with consolidated mud was removed carefully. The flow curves of the consolidated mud are represented in Figure A.10. The yield stresses from these flow curves are represented in Table 4.2.

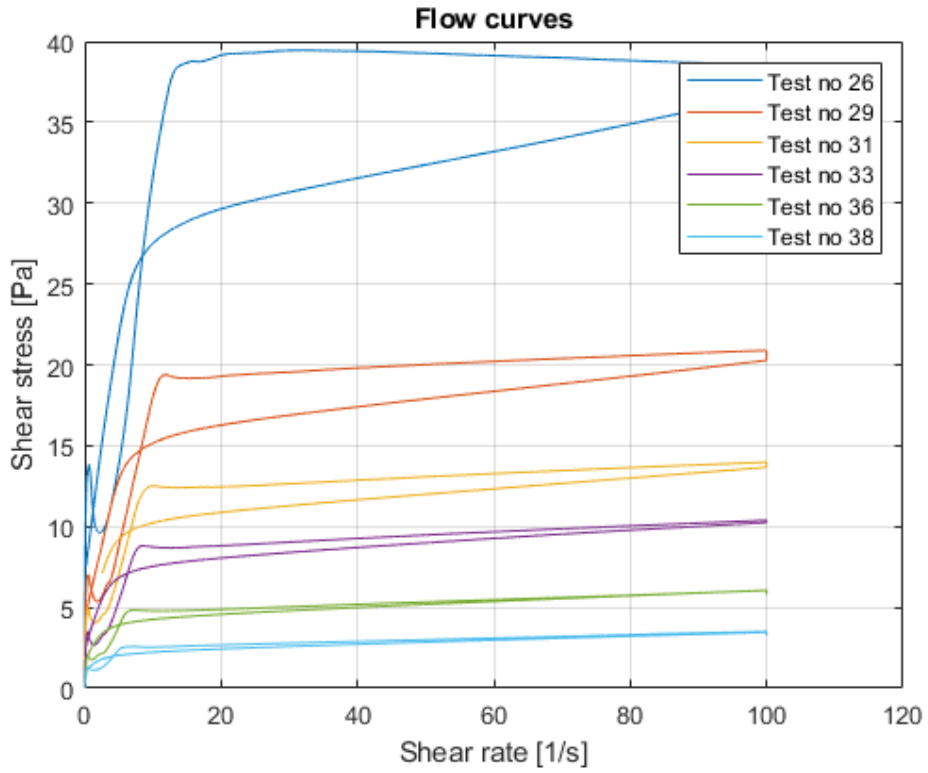

Figure A.7: Calandkanaal fluid mud samples diluted with seawater tested in CSR mode with bob-cup geometry to obtain flow curves.

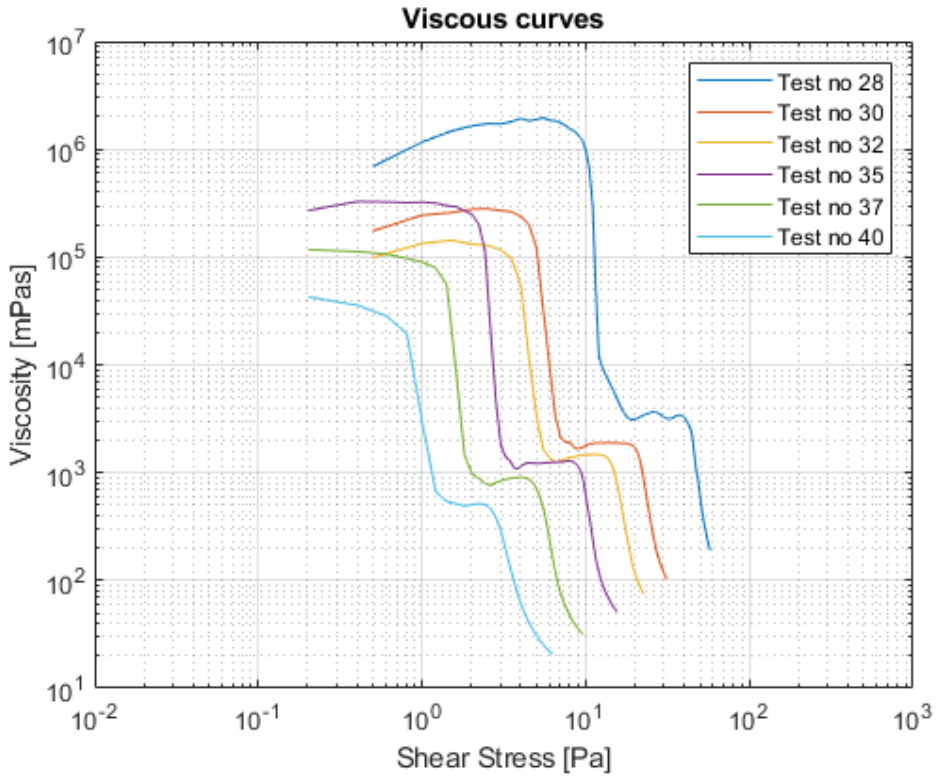

Figure A.8: Calandkanaal fluid mud samples diluted with seawater tested in CSS mode with bob-cup geometry to obtain viscous curves.

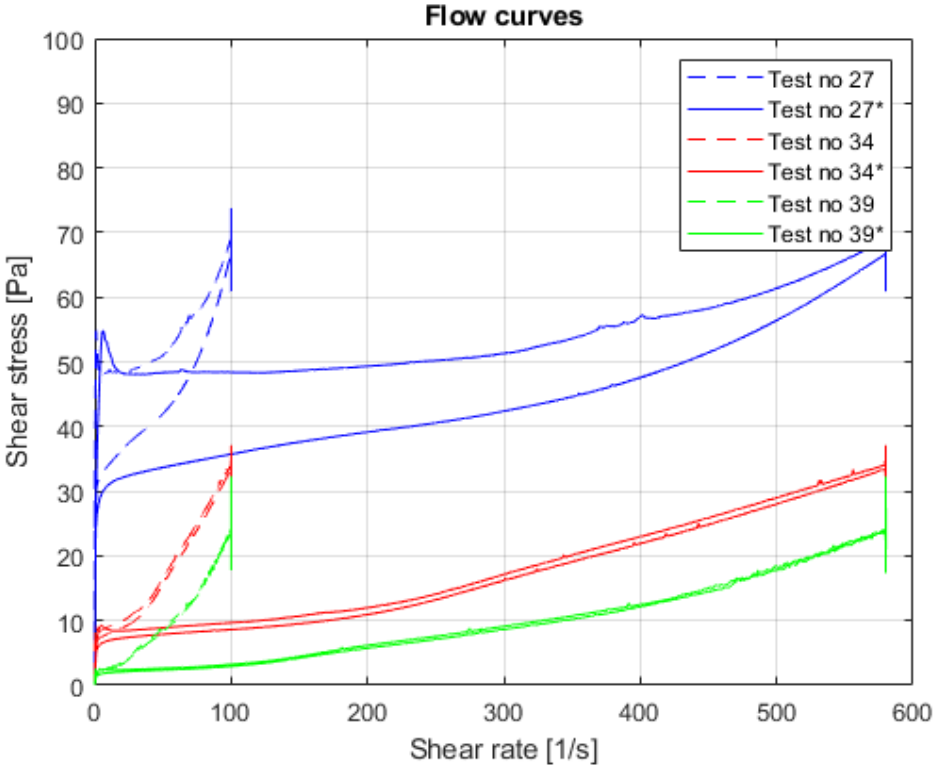

Figure A.9: Calandkanaal fluid mud samples diluted with seawater tested in CSR mode with vane(FL22)-cup geometry to obtain flow curves. The dashed-line curve is without correction factor and solid line is with correction factor.

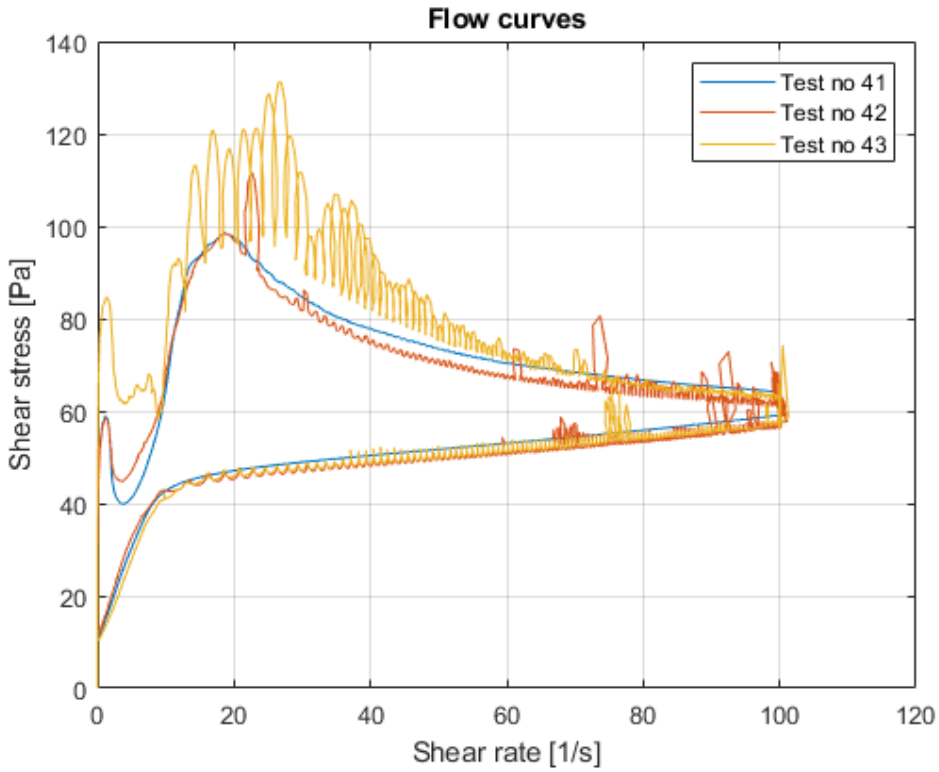

Figure A.10: Calandkanaal consolidated fluid mud samples tested in CSR mode with bob-cup geometry to obtain flow curve.

A.3 8e Petroleumhaven fluid mud samples diluted with seawater

8e Petroleumhaven fluid mud samples diluted with seawater of density 1025kg/m^3 were made in the laboratory. The fluid mud samples of different dilutions were made in the morning and stored in cups with a closed lid. Before using the fluid mud from the cup, it was hand-stirred for a homogenized mixture. The density of the fluid mud is measured using the oven test method. The details of rheometry, density, and properties of fluid mud are represented in Table A.3

Some fluid mud samples with no dilution were kept for consolidation on December 21, 2020. The first consolidated sample (Test no 59) 10 days tested on January 5, 2021, the second consolidated sample (Test no 60) 13 days tested on January 8, 2021, and the third consolidated sample (Test no 61) 18 days tested on January 13, 2021

Table A.3: Details of rheometry and oven test results for 8e Petroleumhaven fluid mud samples diluted with seawater. All the tests were performed on December 24, 2020 (excluding the test no 59 to 61.

Test no	Time	From oven test method					Rheometry	
		Density [g/cc]	Vol. Concen-tration	Geo water content [%]	Hydro water content [%]	Solid content [%]	Geometry	Protocols
44	13:14	1.0.05	0.10	231	74	26	Bob	CSR 0-100 180s up - 60s constant - 180s down
45	15:32	1.0.05	0.10	231	74	26	Vane	CSR 0-100 180s up - 60s constant - 180s down
46	13:23	1.0.05	0.10	231	74	26	Bob	CSS 0-20 100s up
47	13:32	1.171	0.09	232	76	24	Bob	CSR 0-100 180s up - 60s constant - 180s down
48	13:44	1.171	0.09	232	76	24	Bob	CSS 0-20 100s up
49	13:51	1.149	0.08	0.09	79	21	Bob	CSR 0-100 180s up - 60s constant - 180s down
50	14:02	1.149	0.08	0.09	79	21	Bob	CSS 0-20 100s up
51	14:11	1.131	0.07	314	81	19	Bob	CSR 0-100 180s up - 60s constant - 180s down
52	15:20	1.131	0.07	314	81	19	Vane	CSR 0-100 180s up - 60s constant - 180s down
53	14:21	1.131	0.07	314	81	19	Bob	CSS 0-20 100s up
54	14:28	1.128	0.06	334	81	19	Bob	CSR 0-100 180s up - 60s constant - 180s down
55	14:38	1.128	0.06	334	81	19	Bob	CSS 0-20 100s up
56	14:46	1.112	0.05	388	83	17	Bob	CSR 0-100 180s up - 60s constant - 180s down
57	15:08	1.112	0.05	388	83	17	Vane	CSR 0-100 180s up - 60s constant - 180s down
58	14:56	1.112	0.05	388	83	17	Bob	CSS 0-20 100s up
59	15:05	1.204	0.11	136	72	28	Bob	CSR 0-100 180s up - 60s constant - 180s down
60	16:02	1.207	0.11	152	72	28	Bob	CSR 0-100 180s up - 60s constant - 180s down
61	14:05	1.204	0.11	137	72	28	Bob	CSR 0-100 180s up - 60s constant - 180s down

The flow curves obtained in CSR tests with bob-cup geometry are represented in Figure A.11, and viscous curves from CSS tests are shown in Figure A.12. The tests in vane(FL22)-cup geometry are represented in Figure A.25. Some of the undiluted fluid mud samples were kept for consolidation (21, 24, and 29 days) in the rheometry cup. On the day of rheology tests, the water layer in the rheometry cup with consolidated mud was removed carefully. The flow curves of the consolidated mud are represented in Figure A.14. The yield stresses from these flow curves are represented in Table 4.2.

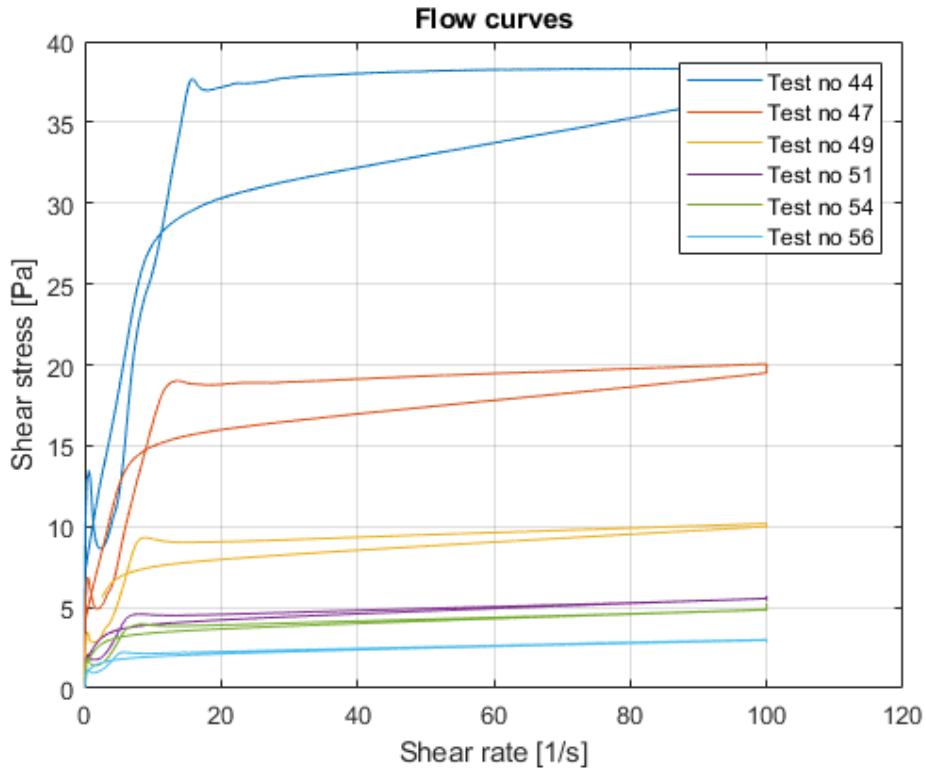

Figure A.11: 8e Petroleumhaven fluid mud samples diluted with seawater tested in CSR mode with bob-cup geometry to obtain flow curves.

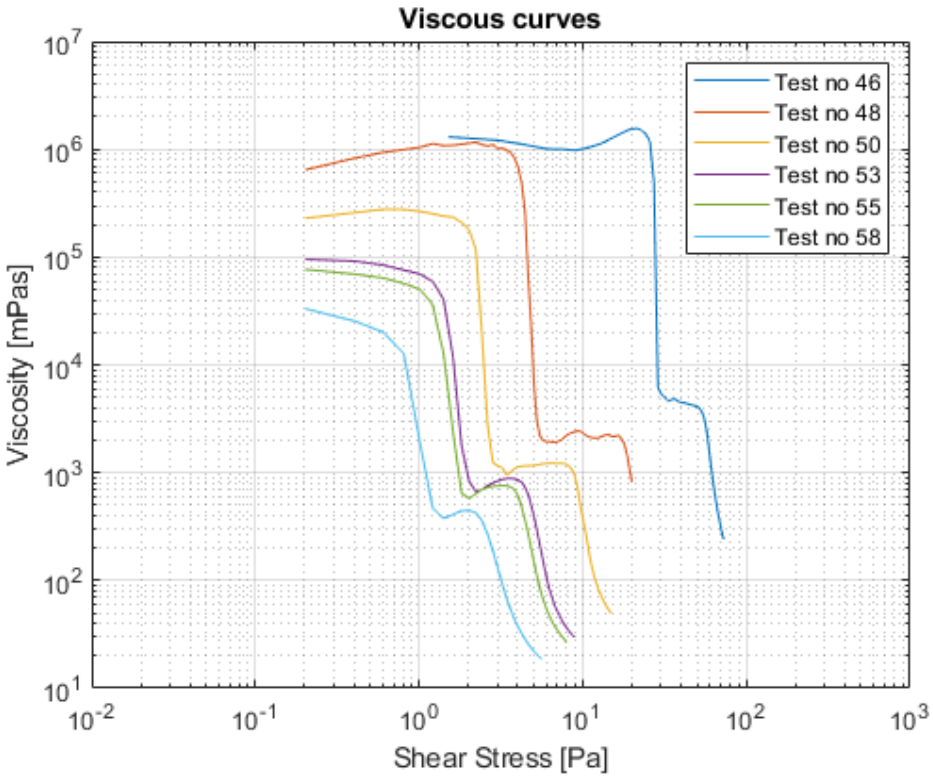

Figure A.12: 8e Petroleumhaven fluid mud samples diluted with seawater tested in CSS mode with bob-cup geometry to obtain viscous curves.

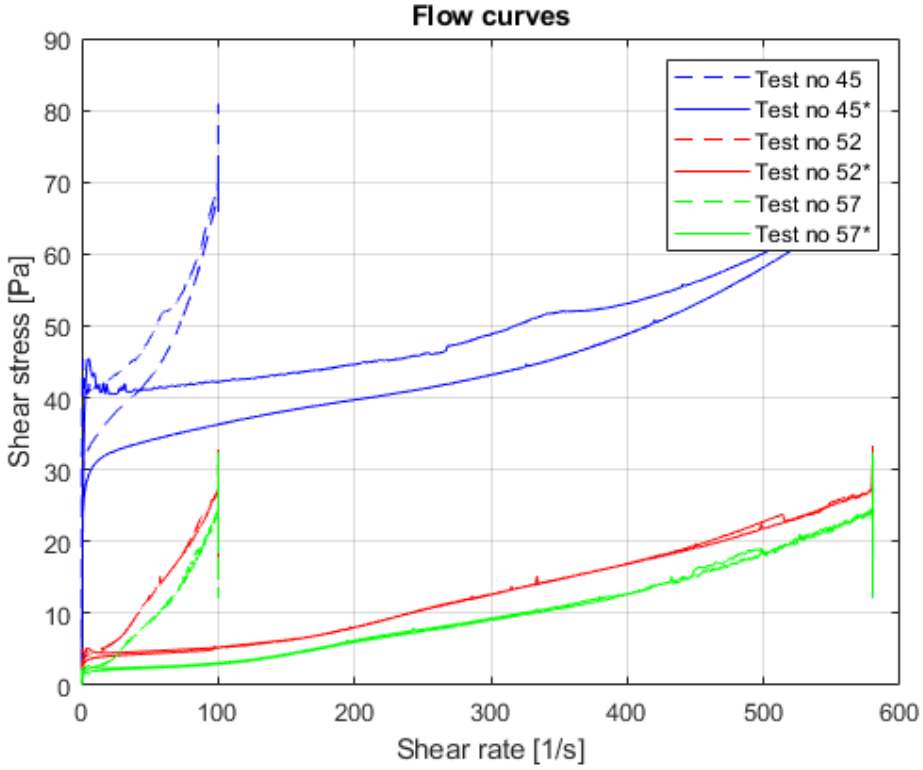

Figure A.13: 8e Petroleumhaven fluid mud samples diluted with seawater tested in CSR mode with vane(FL22)-cup geometry to obtain flow curves. The dashed-line curve is without correction factor and solid line is with correction factor.

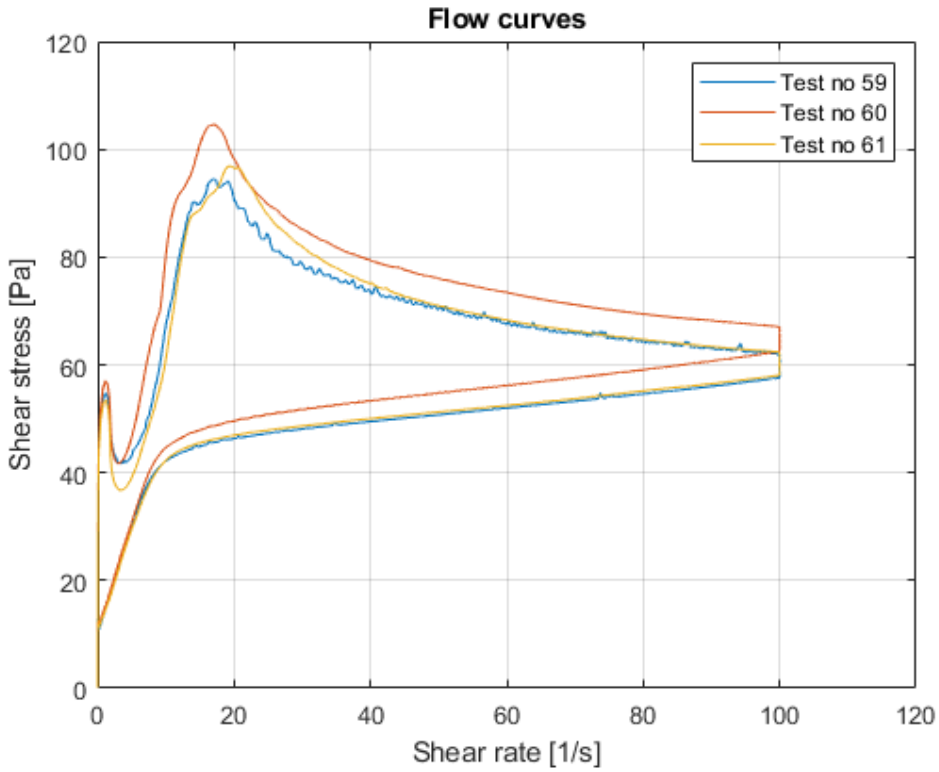

Figure A.14: 8e Petroleumhaven consolidated fluid mud samples tested in CSR mode with bob-cup geometry to obtain flow curve.

A.4 Beerkanaal fluid mud samples diluted with freshwater

Beerkanaal fluid mud samples diluted with freshwater of density 1000kg/m^3 were made in the laboratory. The fluid mud samples of different dilutions were made in the morning and stored in cups with a closed lid. Before using the fluid mud from the cup, it was hand-stirred for a homogenized mixture. The density of the fluid mud is measured using the oven test method. The details of rheometry, density, and properties of fluid mud are represented in Table A.4. In this table, the test numbers from 62 to 65 are the fluid mud samples without dilution, and in density calculations, the density of pore water used is 1025kg/m^3.

Table A.4: Details of rheometry and oven test results for Beerkanaal fluid mud samples diluted with freshwater. All the tests were performed on January 20, 2021.

Test no	Time	From oven test method					Rheometry	
		Density [g/cc]	Vol. Concen-tration	Geo water content [%]	Hydro water content [%]	Solid content [%]	Geometry	Protocols
62	13:28	1.286	0.16	155	64	36	Bob	CSS 0-150 Pa 150s up
63	13:37	1.286	0.16	155	64	36	Bob	CSR 0-100 180s up - 60s constant - 180s down
64	14:05	1.286	0.16	155	64	36	vane	CSR 0-20 180s up - 60s constant - 180s down
65	14:19	1.286	0.16	155	64	36	Groove bob	CSR 0-100 180s up - 60s constant - 180s down
66	14:55	1.225	0.14	201	70	30	Bob	CSS 0-20 Pa 100s up
67	15:00	1.225	0.14	201	70	30	Bob	CSR 0-100 180s up - 60s constant - 180s down
68	15:17	1.225	0.14	201	70	30	vane	CSR 0-20 180s up - 60s constant - 180s down
69	15:29	1.225	0.14	201	70	30	Groove bob	CSR 0-100 180s up - 60s constant - 180s down
70	15:52	1.218	0.13	211	71	29	Bob	CSS 0-20 Pa 100s up
71	15:59	1.218	0.13	211	71	29	Bob	CSR 0-100 180s up - 60s constant - 180s down
72	16:13	1.218	0.13	211	71	29	vane	CSR 0-20 180s up - 60s constant - 180s down
73	16:27	1.218	0.13	211	71	29	Groove bob	CSR 0-100 180s up - 60s constant - 180s down
74	16:47	1.183	0.11	251	75	25	Bob	CSS 0-20 Pa 100s up
75	16:54	1.183	0.11	251	75	25	Bob	CSR 0-100 180s up - 60s constant - 180s down
76	17:07	1.183	0.11	251	75	25	vane	CSR 0-20 180s up - 60s constant - 180s down
77	17:18	1.183	0.11	251	75	25	Groove bob	CSR 0-100 180s up - 60s constant - 180s down
78	17:29	1.155	0.09	307	78	22	Bob	CSS 0-20 Pa 100s up
79	17:32	1.155	0.09	307	78	22	Bob	CSR 0-100 180s up - 60s constant - 180s down
80	17:43	1.155	0.09	307	78	22	vane	CSR 0-20 180s up - 60s constant - 180s down
81	17:53	1.155	0.09	307	78	22	Groove bob	CSR 0-100 180s up - 60s constant - 180s down

In order to compare the freshwater and seawater dilutions of fluid mud rheology, Beerkanaal fluid mud samples with freshwater dilutions were made. The fluid mud samples were then tested in CSR mode with bob-cup, vane-cup, groove bob-cup geometry, and CSS mode with bob-cup. The tests in CSR mode with bob-cup geometry are represented in the Figure A.15, with vane-cup geometry see Figure A.16, and with groove bob-cup geometry see Figure A.17. The yield stresses obtained from these tests were represented in Table 4.1.

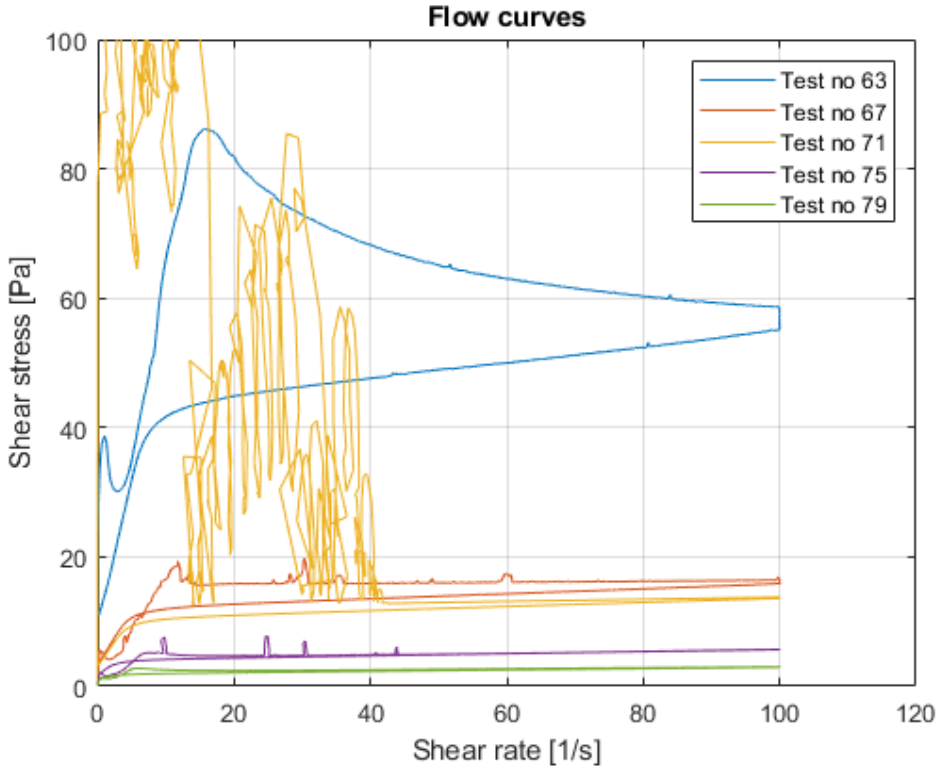

Figure A.15: Beerkanaal fluid mud diluted with freshwater tested in CSR mode with bob-cup geometry to obtain flow curve.

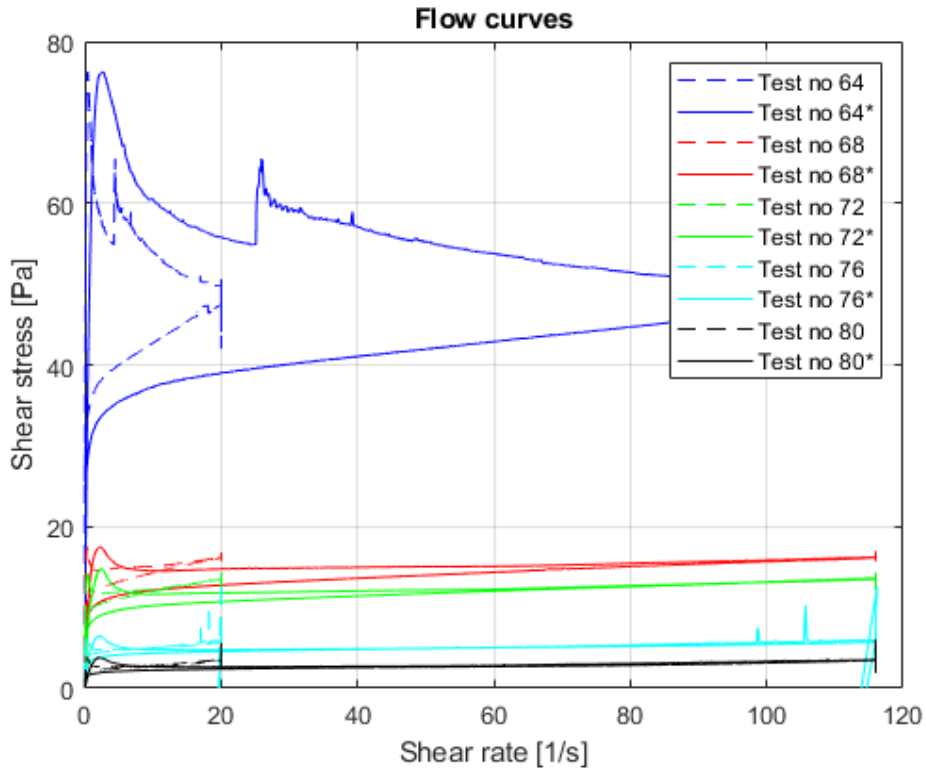

Figure A.16: Beerkanaal fluid mud diluted with freshwater tested in CSR mode with vane(FL22)-cup geometry to obtain flow curve. The dashed-line curve is without correction factor and solid line is with correction factor.

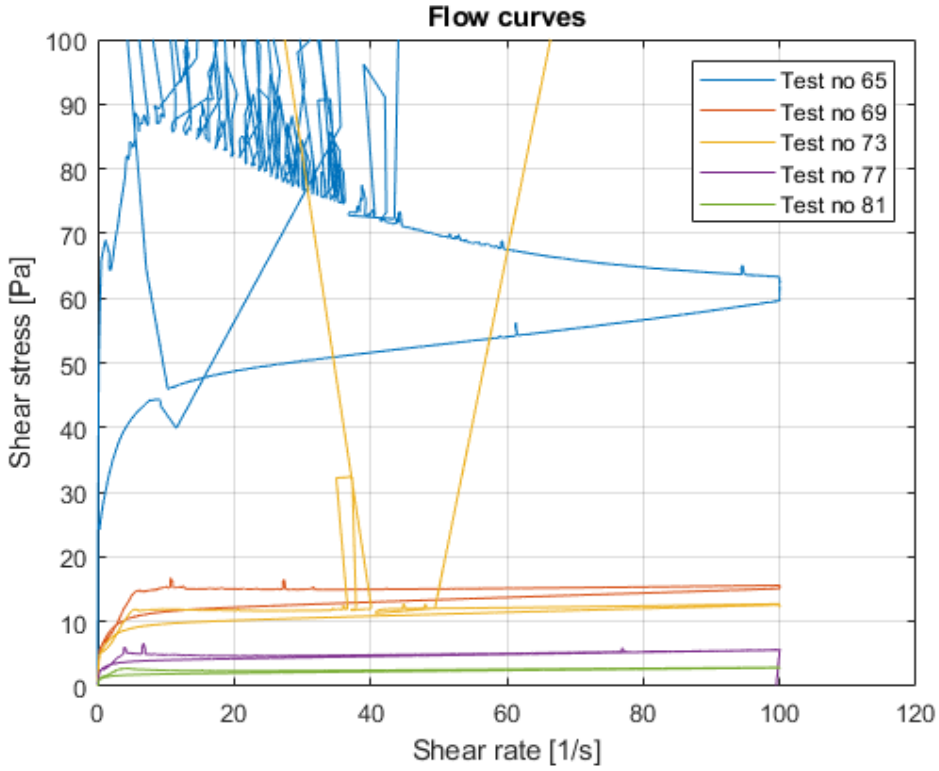

Figure A.17: Beerkanaal fluid mud samples diluted with freshwater tested in CSR mode with groove bob-cup geometry.

The CSS tests on Beerkanaal fluid mud samples with freshwater dilution with bob-cup geometry are shown

in Figure A.18.

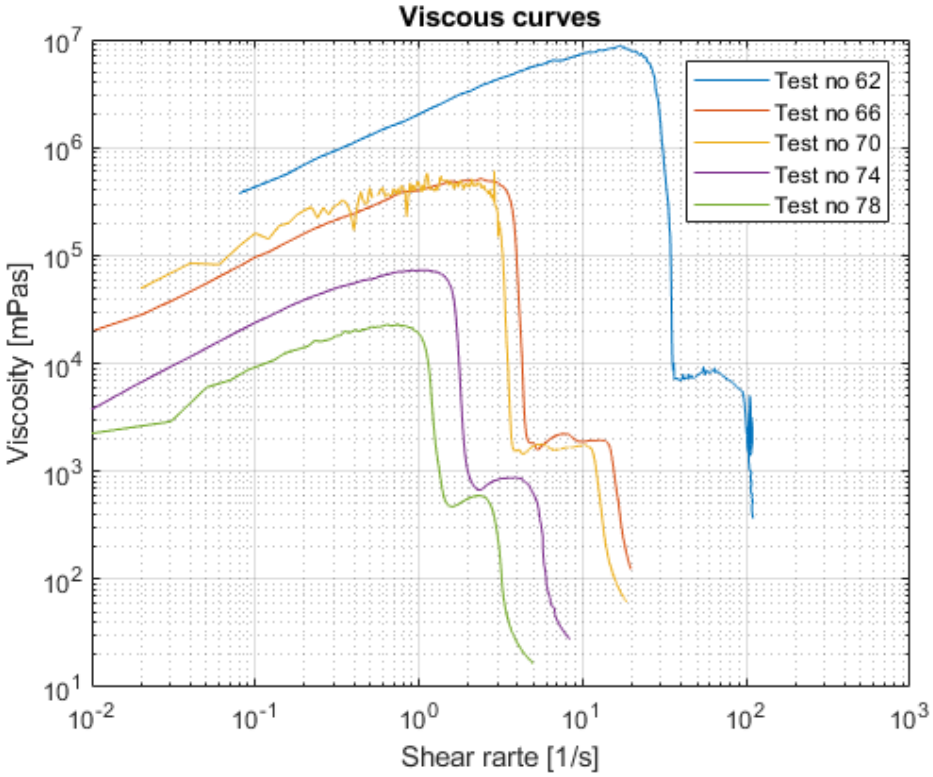

Figure A.18: Beerkanaal fluid mud diluted with freshwater tested in CSS mode with bob-cup geometry to obtain viscous curves in logarithmic scale.

A.5 Calandkanaal fluid mud samples diluted with freshwater

Calandkanaal fluid mud samples diluted with freshwater of density 1000kg/m^3 were made in the laboratory. The fluid mud samples of different dilutions were made in the morning and stored in cups with a closed lid. Before using the fluid mud from the cup, it was hand-stirred for a homogenized mixture. The density of the fluid mud is measured using the oven test method. The details of rheometry, density, and properties of fluid mud are represented in Table A.5. In this table, the test numbers from 82 to 85 are the fluid mud samples without dilution, and in density calculations, the density of pore water used is 1025kg/m^3.

Table A.5: Details of rheometry and oven test results for Calandkanaal fluid mud samples diluted with freshwater. All the tests were performed on January 21, 2021.

Test no	Time	From oven test method					Rheometry	
		Density [g/cc]	Vol. Concen-tration	Geo water content [%]	Hydro water content [%]	Solid content [%]	Geometry	Protocols
82	12:53	1.213	0.12	213	71	29	Bob	CSS 0-150 Pa 150s up
83	12:59	1.213	0.12	213	71	29	Bob	CSR 0-100 180s up - 60s constant - 180s down
84	13:14	1.213	0.12	213	71	29	vane	CSR 0-20 180s up - 60s constant - 180s down
85	13:25	1.213	0.12	213	71	29	Groove bob	CSR 0-100 180s up - 60s constant - 180s down
86	13:41	1.194	0.12	238	73	27	Bob	CSS 0-20 Pa 100s up
87	13:43	1.194	0.12	238	73	27	Bob	CSR 0-100 180s up - 60s constant - 180s down
88	14:03	1.194	0.12	238	73	27	vane	CSR 0-20 180s up - 60s constant - 180s down
89	14:13	1.194	0.12	238	73	27	Groove bob	CSR 0-100 180s up - 60s constant - 180s down
90	14:28	1.167	0.10	267	77	23	Bob	CSS 0-20 Pa 100s up
91	14:37	1.167	0.10	267	77	23	Bob	CSR 0-100 180s up - 60s constant - 180s down
92	14:53	1.167	0.10	267	77	23	vane	CSR 0-20 180s up - 60s constant - 180s down
93	15:22	1.167	0.10	267	77	23	Groove bob	CSR 0-100 180s up - 60s constant - 180s down
94	15:36	1.155	0.09	256	78	22	Bob	CSS 0-20 Pa 100s up
95	15:42	1.155	0.09	256	78	22	Bob	CSR 0-100 180s up - 60s constant - 180s down
96	16:00	1.155	0.09	256	78	22	vane	CSR 0-20 180s up - 60s constant - 180s down
97	16:11	1.155	0.09	256	78	22	Groove bob	CSR 0-100 180s up - 60s constant - 180s down
98	16:22	1.129	0.08	357	81	19	Bob	CSS 0-20 Pa 100s up
99	16:27	1.129	0.08	357	81	19	Bob	CSR 0-100 180s up - 60s constant - 180s down
100	16:41	1.129	0.08	357	81	19	vane	CSR 0-20 180s up - 60s constant - 180s down
101	16:51	1.129	0.08	357	81	19	Groove bob	CSR 0-100 180s up - 60s constant - 180s down

In order to compare the freshwater and seawater dilutions of fluid mud rheology, Calandkanaal fluid mud samples with freshwater dilutions were made. The fluid mud samples were then tested in CSR mode with bob-cup, vane-cup, groove bob-cup geometry, and CSS mode with bob-cup. The tests in CSR mode with bob-cup geometry are represented in the Figure A.19, with vane-cup geometry see Figure A.20, and with groove bob-cup geometry see Figure A.21. The yield stresses obtained from these tests were represented in Table 4.1.

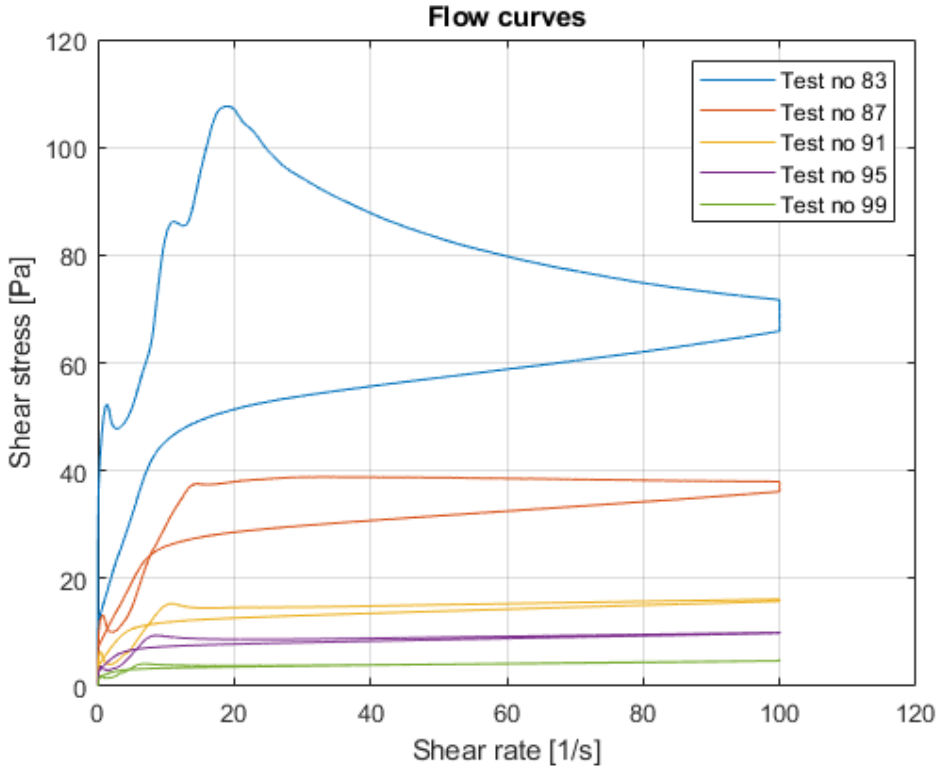

Figure A.19: Calandkanaal fluid mud diluted with freshwater tested in CSR mode with bob-cup geometry to obtain flow curves.

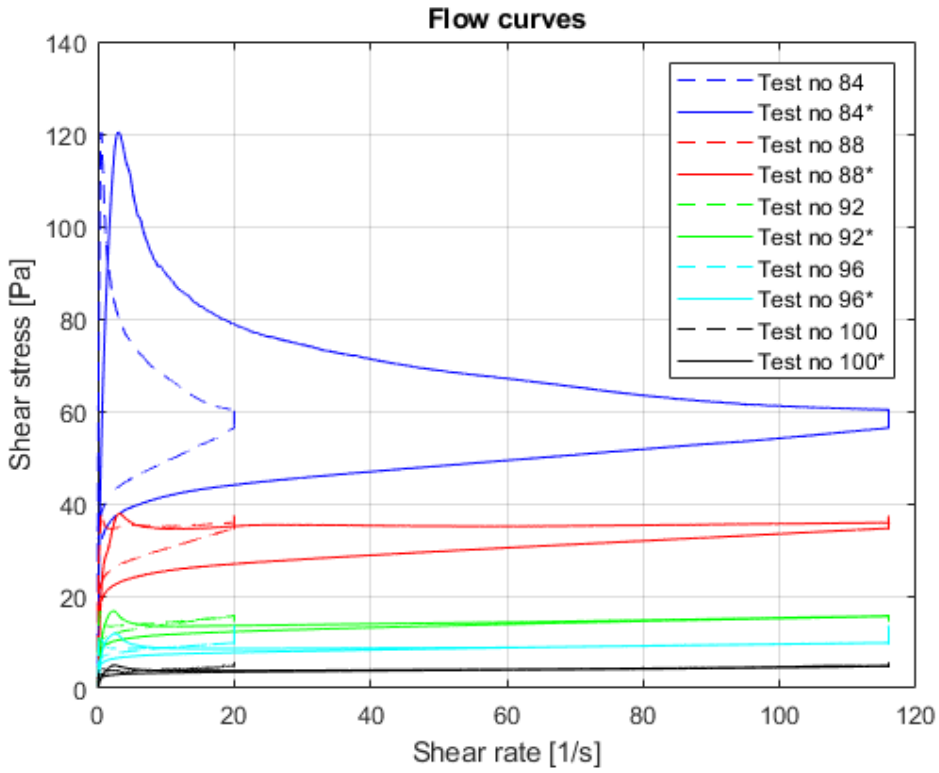

Figure A.20: Calandkanaal fluid mud diluted with freshwater tested in CSR mode with vane(FL22)-cup geometry to obtain flow curves. The dashed-line curve is without correction factor and solid line is with correction factor.

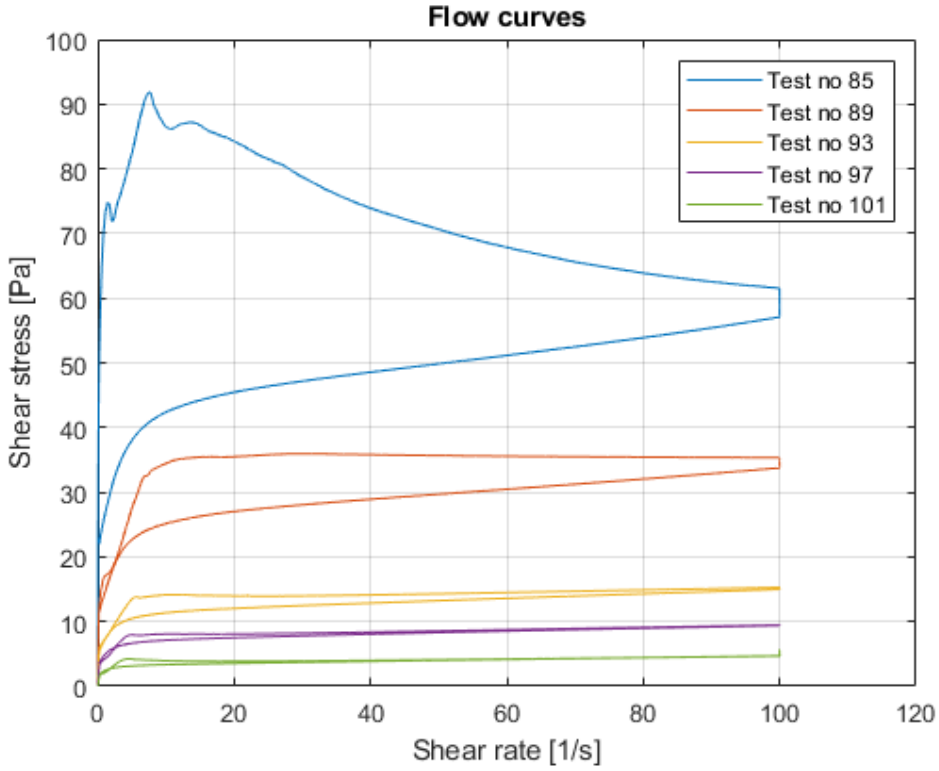

Figure A.21: Calandkanaal fluid mud diluted with freshwater tested in CSR mode with groove bob-cup geometry to obtain flow curves.

The CSS tests on Calandkanaal fluid mud samples with freshwater dilution with bob-cup geometry are

shown in Figure A.22.

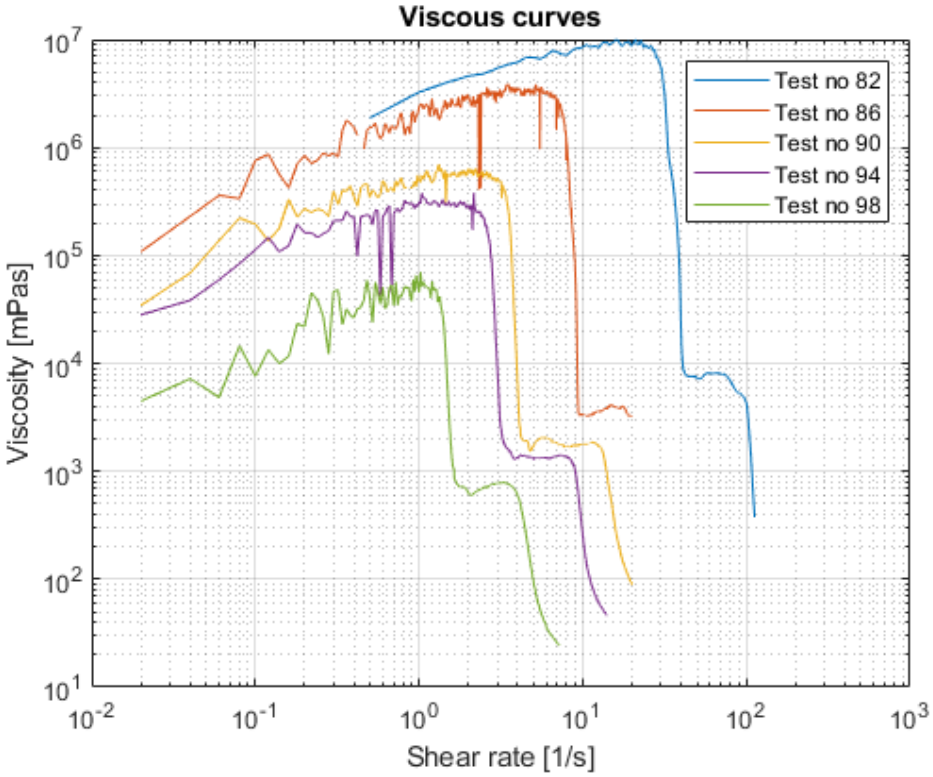

Figure A.22: Calandkanaal fluid mud diluted with freshwater tested in CSS mode with bob-cup geometry to obtain viscous curves.

A.6 8e Petroleumhaven fluid mud samples diluted with freshwater

8e Petroleumhaven fluid mud samples diluted with freshwater of density 1000kg/m^3 were made in the laboratory. The fluid mud samples of different dilutions were made in the morning and stored in cups with a closed lid. Before using the fluid mud from the cup, it was hand-stirred for a homogenized mixture. The density of the fluid mud is measured using the oven test method. The details of rheometry, density, and properties of fluid mud are represented in Table A.6. In this table, the test numbers from 102 to 105 are the fluid mud samples without dilution, and in density calculations, the density of pore water used is 1025kg/m^3.

Table A.6: Details of rheometry and oven test results for 8e Petroleumhaven fluid mud samples diluted with freshwater. All the tests were performed on January 22, 2021.

Test no	Time	From oven test method					Rheometry	
		Density [g/cc]	Vol. Concen-tration	Geo water content [%]	Hydro water content [%]	Solid content [%]	Geometry	Protocols
102	10:57	1.0.08	0.12	187	71	29	Bob	CSS 0-150 Pa 150s up
103	11:02	1.0.08	0.12	187	71	29	Bob	CSR 0-100 180s up - 60s constant - 180s down
104	13:06	1.0.08	0.12	187	71	29	vane	CSR 0-20 180s up - 60s constant - 180s down
105	13:57	1.0.08	0.12	187	71	29	Groove bob	CSR 0-100 180s up - 60s constant - 180s down
106	11:15	1.186	0.11	218	74	26	Bob	CSS 0-20 Pa 100s up
107	11:21	1.186	0.11	218	74	26	Bob	CSR 0-100 180s up - 60s constant - 180s down
108	13:16	1.186	0.11	218	74	26	vane	CSR 0-20 180s up - 60s constant - 180s down
109	14:06	1.186	0.11	218	74	26	Groove bob	CSR 0-100 180s up - 60s constant - 180s down
110	11:33	1.176	0.11	247	76	24	Bob	CSS 0-20 Pa 100s up
111	11:38	1.176	0.11	247	76	24	Bob	CSR 0-100 180s up - 60s constant - 180s down
112	13:26	1.176	0.11	247	76	24	vane	CSR 0-20 180s up - 60s constant - 180s down
113	14:16	1.176	0.11	247	76	24	Groove bob	CSR 0-100 180s up - 60s constant - 180s down
114	11:49	1.147	0.09	296	79	21	Bob	CSS 0-20 Pa 100s up
115	11:54	1.147	0.09	296	79	21	Bob	CSR 0-100 180s up - 60s constant - 180s down
116	13:36	1.147	0.09	296	79	21	vane	CSR 0-20 180s up - 60s constant - 180s down
117	14:26	1.147	0.09	296	79	21	Groove bob	CSR 0-100 180s up - 60s constant - 180s down
118	12:07	1.129	0.08	356	81	19	Bob	CSS 0-20 Pa 100s up
119	12:11	1.129	0.08	356	81	19	Bob	CSR 0-100 180s up - 60s constant - 180s down
120	13:47	1.129	0.08	356	81	19	vane	CSR 0-20 180s up - 60s constant - 180s down
121	14:36	1.129	0.08	356	81	19	Groove bob	CSR 0-100 180s up - 60s constant - 180s down

In order to compare the freshwater and seawater dilutions of fluid mud rheology, 8e Petroleumhaven fluid mud samples with freshwater dilutions were made. The fluid mud samples were then tested in CSR mode with bob-cup, vane-cup, groove bob-cup geometry, and CSS mode with bob-cup. The tests in CSR mode with bob-cup geometry are represented in the Figure A.23, with vane-cup geometry see Figure A.24, and with groove bob-cup geometry see Figure A.25. The yield stresses obtained from these tests were represented in Table 4.1.

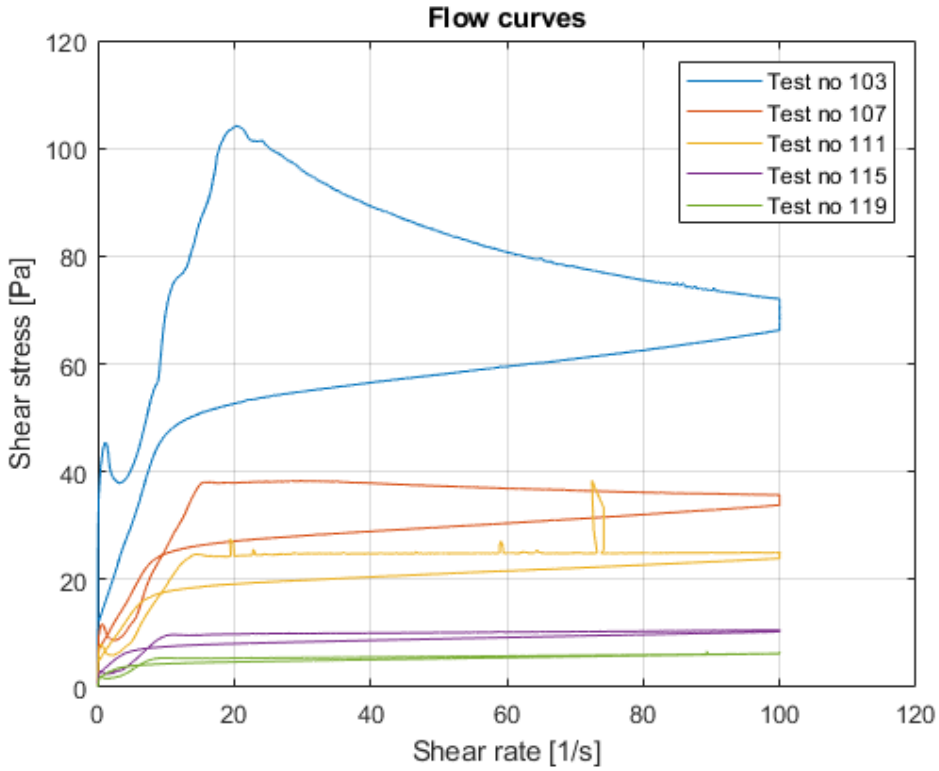

Figure A.23: 8e Petroleumhaven fluid mud diluted with freshwater tested in CSR mode with bob-cup geometry to obtain flow curves.

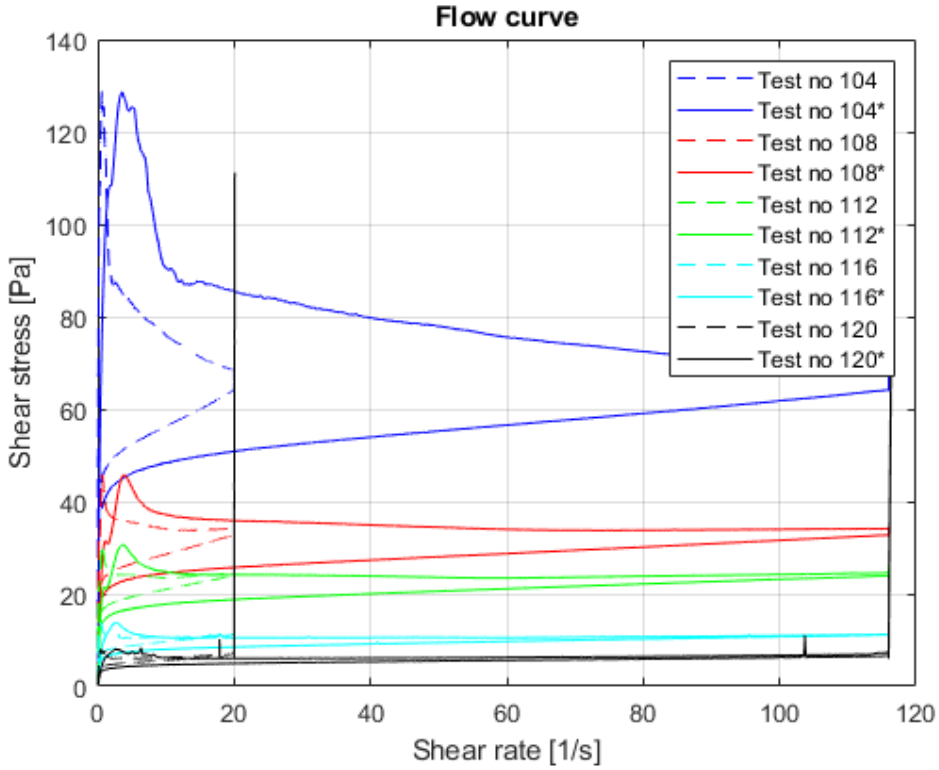

Figure A.24: 8e Petroleumhaven fluid mud diluted with freshwater tested in CSR mode with vane(FL22)-cup geometry to obtain flow curves. The dashed-line curve is without correction factor and solid line is with correction factor.

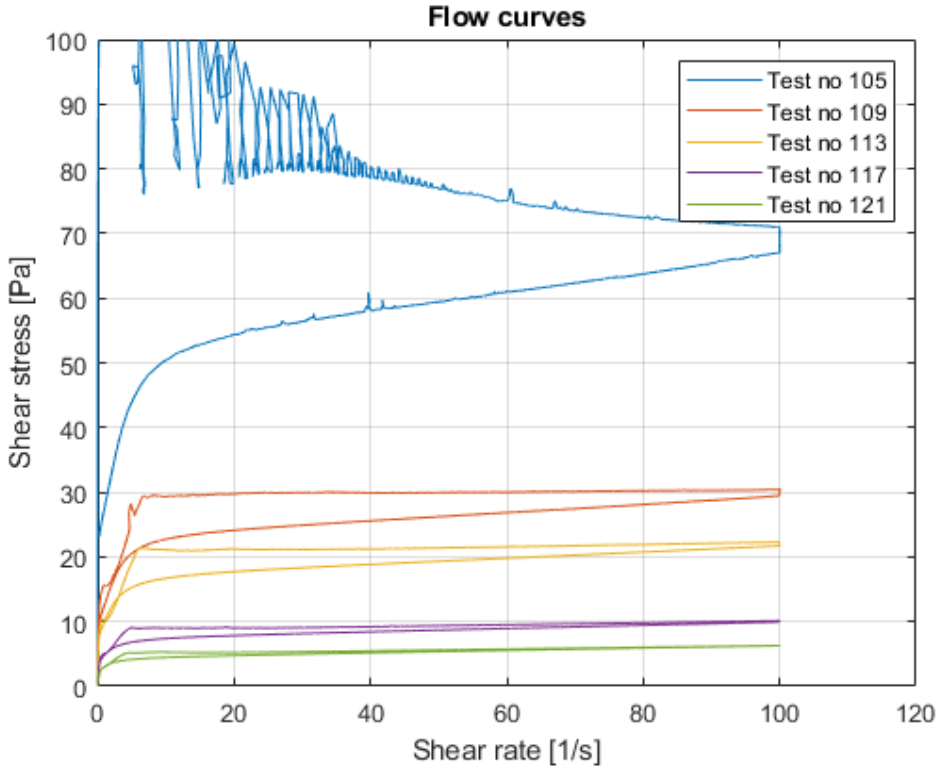

Figure A.25: 8e Petroleumhaven fluid mud diluted with freshwater tested in CSR mode with groove bob-cup geometry to obtain flow curves.

The CSS tests on 8e Petroleumhaven fluid mud samples with freshwater dilution with bob-cup geometry

are shown in the Figure A.26.

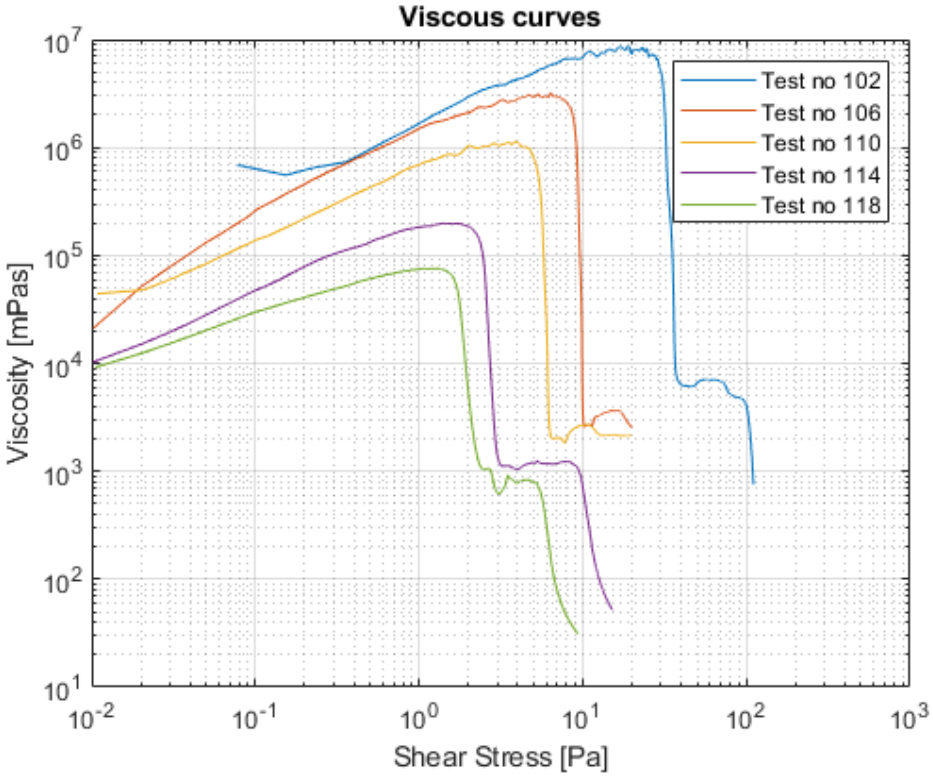

Figure A.26: 8e Petroleumhaven fluid mud diluted with freshwater tested in CSS mode with bob-cup geometry to obtain viscous curves.

A.7 Rheometry study using Beerkanaal fluid mud

Rheometry practices were studied using the undiluted Beerkanaal fluid mud and tested in CSS and CSR mode with bob-cup, vane-cup, and groove bob cup geometry. Table A.7 represents the details of rheometry and oven test results of fluid mud samples used in the experiments.

Table A.7: Details of rheometry and oven test results of undiluted Beerkanaal fluid mud samples used in the rheometry practice experiments.

Test no	Time	From oven test method					Rheometry	
		Density [g/cc]	Vol. Concen-tration	Geo water content [%]	Hydro water content [%]	Solid content [%]	Geometry	Protocols
122	11:16	1.294	0.17	154	63	37	Bob	CSR 0-100 180s up - 60s constant - 180s down
123	11:30	1.294	0.17	154	63	37	Bob	CSS 0-240Pa 180s up - 60s constant - 180s down
124	11:59	1.294	0.17	154	63	37	vane	CSR 0-20 180s up - 60s constant - 180s down
125	11:53	1.294	0.17	154	63	37	vane	CSS 0-240Pa 180s up - 60s constant - 180s down
126	12:10	1.294	0.17	154	63	37	Groove bob	CSR 0-100 180s up - 60s constant - 180s down
127	12:22	1.294	0.17	154	63	37	Groove bob	CSS 0-240Pa 180s up - 60s constant - 180s down
128	10:26	1.271	0.15	171	65	35	vane FL22	CSR 0-20 180s up - 60s constant - 180s down
129	10:37	1.271	0.15	171	65	35	vane FL22	CSS 0-240Pa 180s up - 60s constant - 180s down
130	11:06	1.271	0.15	171	65	35	vane FL16	CSR 0-100 180s up - 60s constant - 180s down
131	11:16	1.271	0.15	171	65	35	vane FL16	CSS 0-120Pa 180s up - 60s constant - 180s down
132	11:27	1.271	0.15	171	65	35	vane FL22	CSR 0-20 180s up - 60s constant - 180s down
133	11:37	1.271	0.15	171	65	35	vane FL22	CSS 0-120Pa 180s up - 60s constant - 180s down
134	12:22	1.271	0.15	171	65	35	Bob	CSR 0-100 180s up - 60s constant - 180s down
135	12:34	1.271	0.15	171	65	35	Bob	CSS 0-120Pa 180s up - 60s constant - 180s down
136	13:05	1.271	0.15	171	65	35	Bob	CSS 0-85Pa 180s up - 60s constant - 180s down
137	12:42	1.271	0.15	171	65	35	Groove bob	CSR 0-100 180s up - 60s constant - 180s down
138	12:52	1.271	0.15	171	65	35	Groove bob	CSS 0-90Pa 180s up - 60s constant - 180s down

Figure A.27 and A.28 shows the tests in CSR and CSS mode with bob-cup geometry respectively. Figure A.29 and A.30 shows the tests in CSR and CSS mode with vane(FL22)-cup geometry respectively. A.31 and A.32 shows the tests in CSR and CSS mode with vane-cup geometry respectively. Figure A.33 shows the tests in CSS and CSR with vane(FL16)-cup geometry.

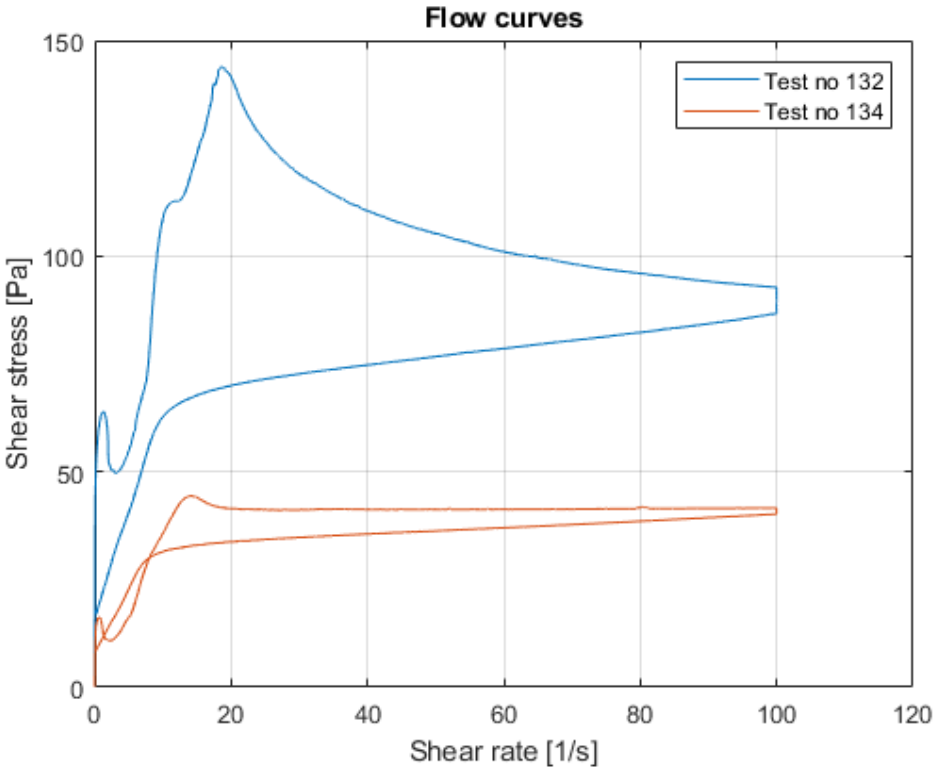

Figure A.27: Beerkanaal fluid mud tested in CSR mode with bob-cup geometry.

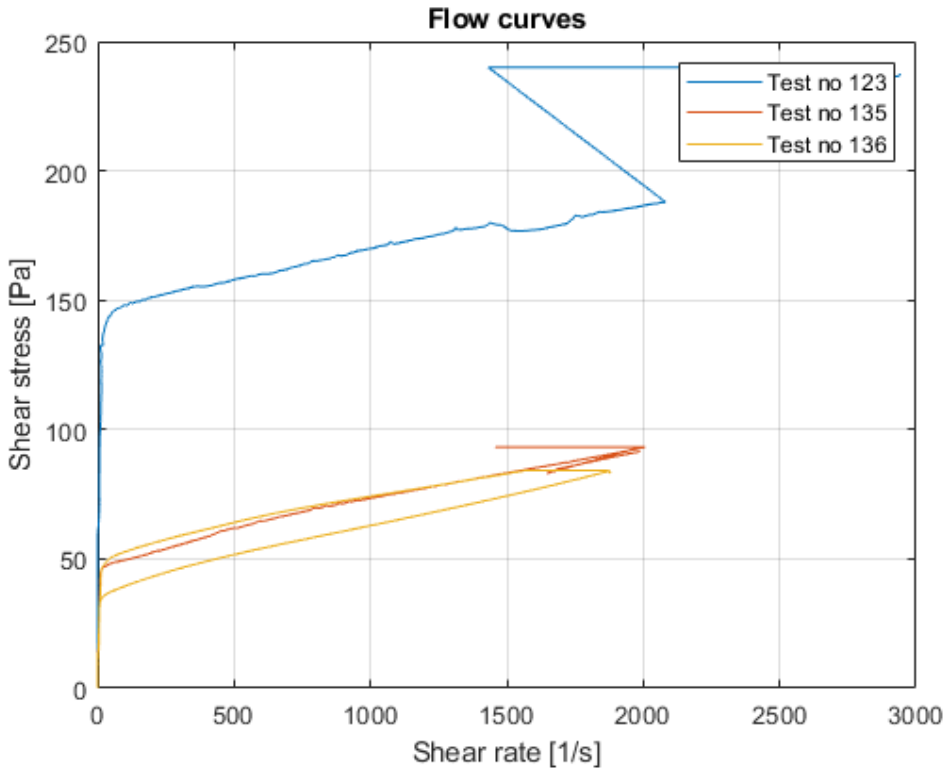

Figure A.28: Beerkanaal fluid mud tested in CSS mode with bob-cup geometry.

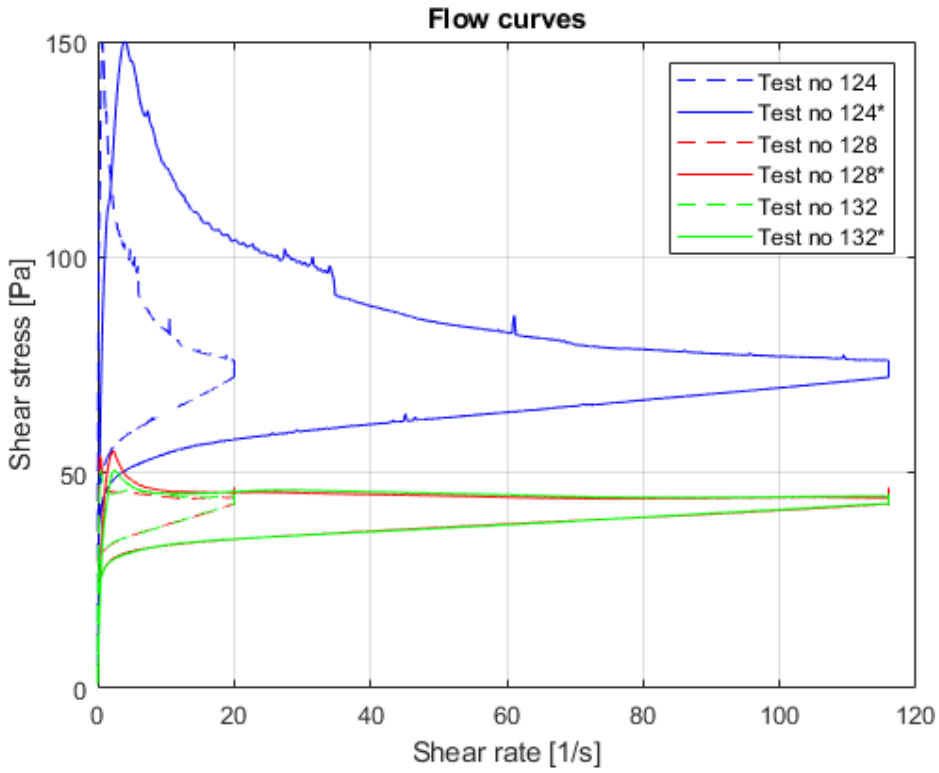

Figure A.29: Beerkanaal fluid mud tested in CSR mode with vane(FL22)-cup geometry.

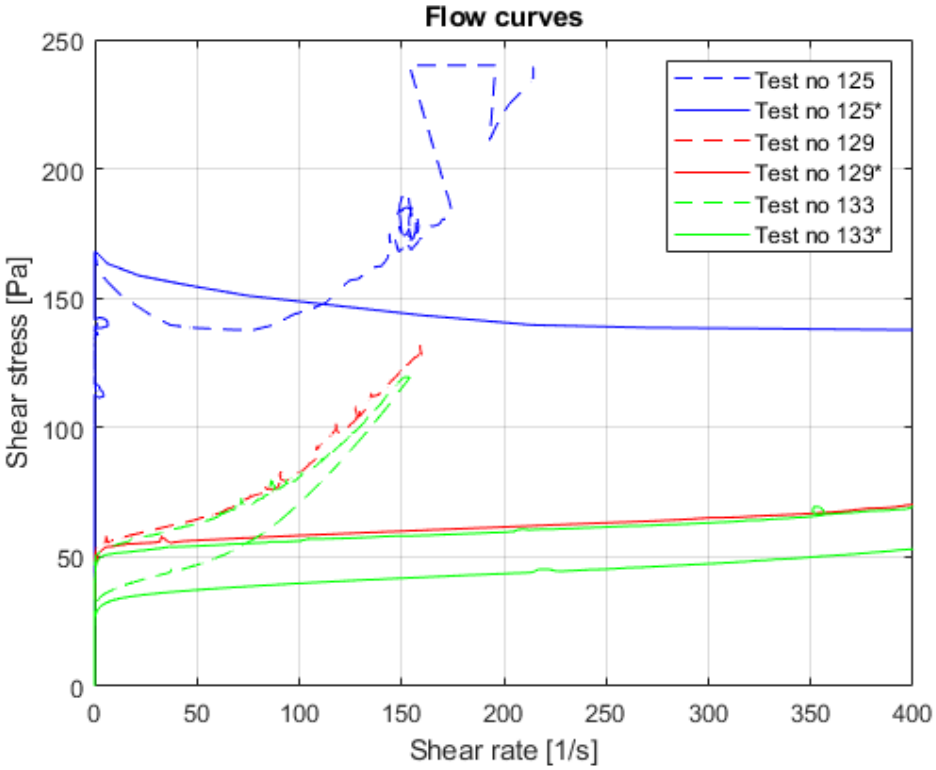

Figure A.30: Beerkanaal fluid mud tested in CSS mode with vane(FL22)-cup geometry.

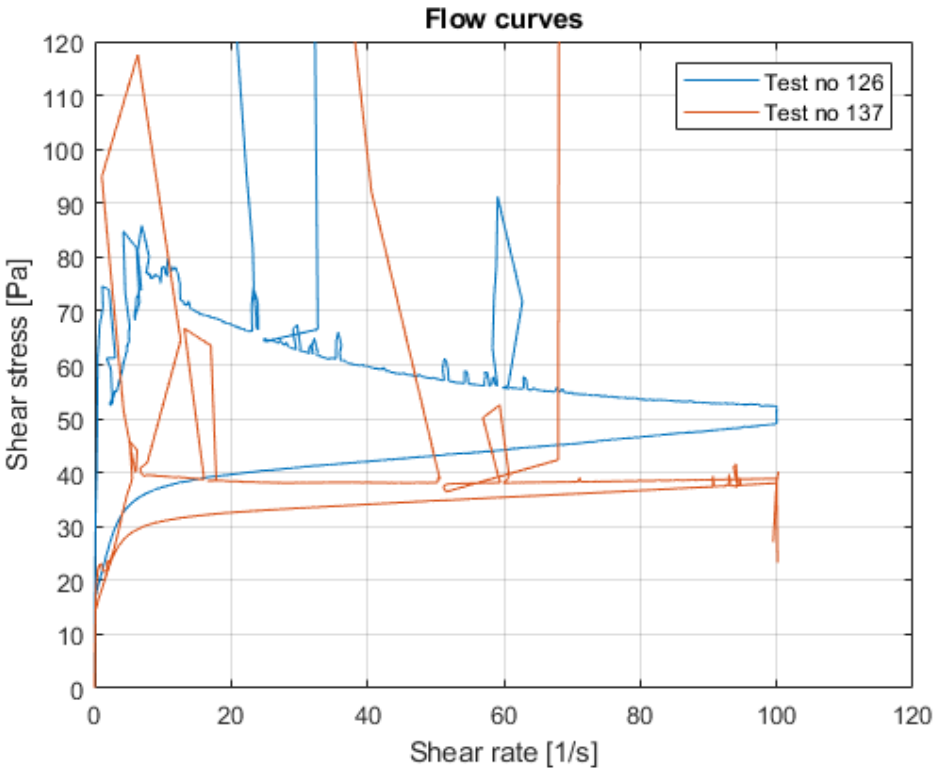

Figure A.31: Beerkanaal fluid mud tested in CSR mode with groove bob-cup geometry.

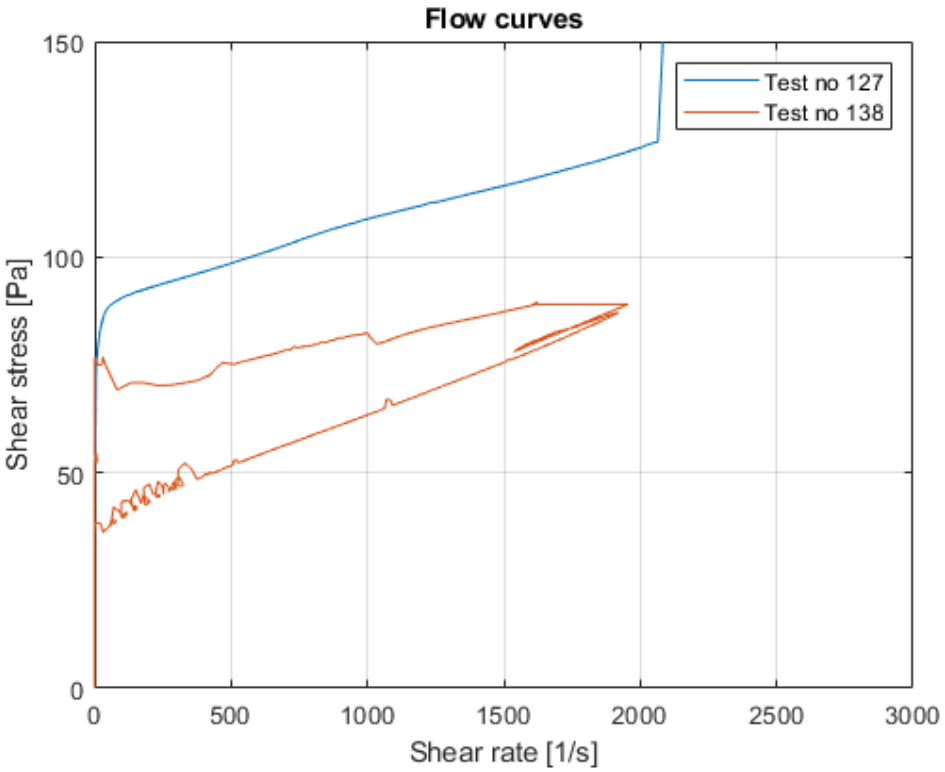

Figure A.32: Beerkanaal fluid mud tested in CSS mode with groove bob-cup geometry.

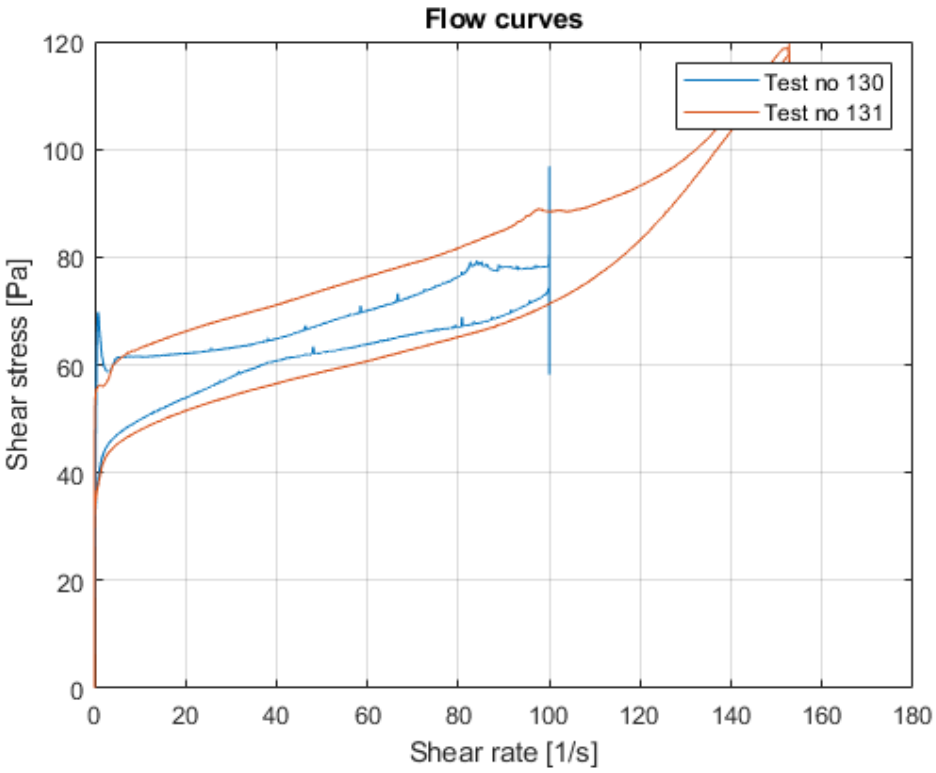

Figure A.33: Beerkanaal fluid mud tested in CSR and CSS mode with small vane(FL16)-cup geometry.

A.8 Oven test density measurements and corrections

A.8.1 Procedure

The oven test method for measuring the density of the fluid mud is described below:

1. Weigh the empty cup (W_{cup}) in which the fluid mud sample will be kept.
2. Put the fluid mud in the cup and weigh it again ($W_{cup+wetmud}$).
3. Keep the sample in the Oven which is maintained at a temperature of 105°C for 24 hours.
4. After 24 hours, weigh the cup with dry fluid mud ($W_{cup+drymud}$).

A.8.2 Calculations

Let the density of water in the fluid mud represented as ρ_{water}, density of solids in the fluid mud represented as ρ_{solids}.

The density of fluid mud (ρ_{fm}) sample is given by

$$\rho_{fm} = 1000 * \frac{1 + \frac{W_w}{W_s}}{\frac{\rho_{water}}{\rho_{solids}} + \frac{W_w}{W_s}} \tag{A.1}$$

where W_w is the weight of water (see Eq.A.2), W_s is the weight of dry solids (see Eq.A.3) in the fluid mud.

$$W_w = W_{cup+wetmud} - W_{cup+drymud} \tag{A.2}$$

$$W_s = W_{cup+drymud} - W_{cup} \tag{A.3}$$

The ratio of the Weight of water (W_w) to the weight of solids (W_s) is also known as Geo-technical water content. In the oven test of seawater dilution samples, the salt deposits in the fluid mud.

$$\text{Geo-technical water content} = \frac{W_w}{W_s} \tag{A.4}$$

The ratio of the weight of water (W_w) to the weight of fluid mud before drying (W_t) is known as Hydro water content.

$$\text{Hydro water content} = \frac{W_w}{W_t} \tag{A.5}$$

The ratio of the dry weight of fluid mud (W_s) to the weight of the fluid mud before drying (W_t) is known solids content in fluid mud. In the oven tests for seawater dilution fluid mud samples, the dry weight of the fluid mud contains the salt residuals.

$$\text{Solid content} = \frac{W_w}{W_t} \tag{A.6}$$

The volumetric concentration of solids ($V.Conc._{solids}$ in the fluid mud is given by

$$V.Conc._{solids} = \frac{1}{\frac{W_w}{W_s} + \frac{\rho_{water}}{\rho_{solids}}} \tag{A.7}$$

A.8.3 Corrections in density of solids for sea water dilution tests

The density of solids measured using Helium Pycnometer for the undiluted Beerkanaal fluid mud (fluid mud of Test numbers 62-65) is 2568.3kg/m^3 . This test was done by the lab technician at Deltares and the report given by them is shown in FigureA.34.

AccuPyc 1330 V3.03
Serial Number: 973
Density and Volume Report

Sample ID: 2
Sample Weight: 11.4080 g
Temperature: 25.9 C
Number of Purges: 3
Cell Volume: 12.0439 cm3

Started: 18/02/21 10:44:58
Completed: 18/02/21 10:59:21

Equilibration Rate: 0.0050 psig/min
Expansion Volume: 8.2878 cm3

Run#	Volume cm3	Deviation cm3	Density g/cm3	Deviation g/cm3	Elapsed Time (h:m:s)
1	4.4327	-0.0091	2.5736	0.0053	0:08:52
2	4.4445	0.0027	2.5668	-0.0016	0:11:23
3	4.4482	0.0064	2.5646	-0.0037	0:14:15

Average Volume: 4.4418 cm3
Average Density: 2.5683 g/cm3

Standard Deviation: 0.0081 cm3
Standard Deviation: 0.0047 g/cm3

Figure A.34: Report of density of solids for Beerkanaal fluid mud

In the Helium Pycnometer test, the salt is not evaporated in oven drying and the value of the density of solids contains salt. Thus density of solids must be corrected in the fluid mud density calculations for the seawater dilution tests because the seawater which was added contains salt.

The density of seawater is 1025kg/m^3 and at a salt density is 2160kg/m^3, the volumetric concentration of salt (C_{salt} in such seawater is 0.0216[-]. This corresponds to 0.0475g salt per gram of water.

$$C_{salt} = \frac{\rho_{water} - 1000}{\rho_{salt} - 1000} \tag{A.8}$$

$$\frac{salt[g]}{water_{fresh}[g]} = \frac{C_{salt}}{1 - C_{salt}} \frac{\rho_{salt}}{1000} = 0.047 \tag{A.9}$$

In the oven test, only water evaporates and the salt deposits in the solid mass. In addition, we measure how much water evaporates (W_w). If we know the density of pore water of the fluid mud, we can calculate the amount of salt deposited in the oven test.

With the Helium pycnometer we know the mass of dry solids and also we know the ratio of salt to solids. We deduct the mass of salt (*s*) from the total mass (*M*), and using the density of salt, we deduct the volume taken by the salt from the volume of the mud (*V*). Thus, the solids density is the ratio of corrected mass and corrected volume.

$$\rho_{solids} = \frac{M - s}{V - \frac{s}{\rho_{salt}}} \tag{A.10}$$

The solid density with salt is given by the Helium gas Pycnometer test (Eberli et al., 1997)

$$\rho_{solids+salt} = \frac{M}{V} \tag{A.11}$$

Thus, we can calculate the actual solids density from

$$\frac{\rho_{solids}}{\rho_{solids+salt}} = \frac{1 - \frac{s}{M}}{1 - \frac{s}{M}\frac{M}{V\rho_{salt}}} \tag{A.12}$$

In the salt dilution tests, we are adding salt to the system. From the oven test, we know the mass of water (and hence the dry mass of salt, if salt content in water is known) and we know the total dry mass. Thus, the ratio s/M is known per sample.

$$\frac{s}{M} = \frac{(1-x)\rho_{salt}}{(1-x)\rho_{salt} + x\rho_{solids}} \tag{A.13}$$

where *x* is the volumetric concentration of solids in the dry material

Rearranging the Eq.A.13, we get

$$\frac{x}{1-x} = \frac{\rho_{salt}}{\rho_{solids}} \left(\frac{M}{s} - 1 \right) \tag{A.14}$$

$$\rho_{solids+salt} = (1-x)\rho_{salt} + x\rho_{solids} \tag{A.15}$$

The salt is dissolved in the rheological conditions, in the bed and in any flow. Thus, the volumetric concentration of solids has to be calculated from solids density and seawater density (V/V).

$$Vol.Conc._{solids} = \frac{\rho_{fluidmud} - \rho_{seawater}}{\rho_{solids} - \rho_{seawater}} \tag{A.16}$$

A.8.4 Difference between seawater dilution samples and freshwater dilution samples

In the freshwater dilution fluid mud samples, the salt is tied to the solids, so the mixture density can be calculated on basis of freshwater density and with uncorrected density from pycnometer.

With the salt water dilution fluid mud samples, the density of solids and salt needs to be calculated for each sample, on the basis of individual sample salt/mass total ratio.

Appendix B

Flume experiments of a plate dragged in fluid mud

B.1 Load-cell signal of the plate dragged in the fluid mud

In the flume experiments, the flat plate was dragged in the fluid mud at four different speeds. Three different fluid mud strengths were proposed for the flume experiments, and each test run was repeated eight times. Thus, high strength fluid mud in the test matrix is named Fluid mud 1, medium-strength fluid mud as Fluid mud 2, and weak fluid mud strength as Fluid mud 3.

B.1.1 Wooden plate dragged in the fluid mud 1

Figure B.1,B.2,B.3, and B.4 represents the load-cell signal of total resistance of plate when moved in the Fluid mud 1 at speeds 0.25m/s,0.5m/s,0.75m/s, and 1.0m/s respectively.

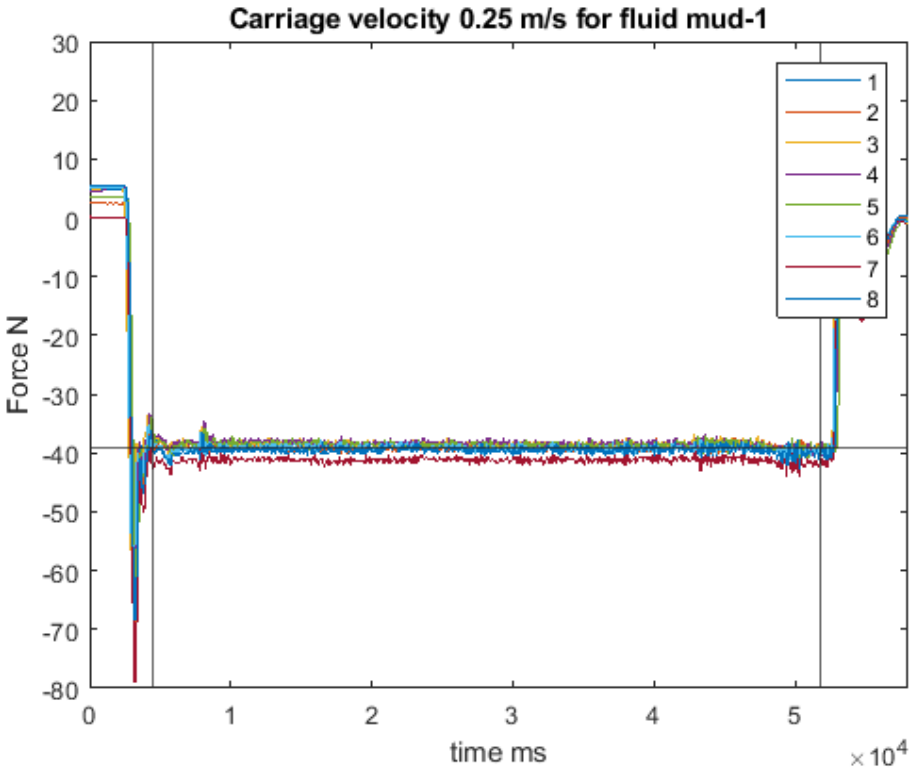

Figure B.1: Total resistance of the plate moved at speed 0.25m/s in fluid mud 1

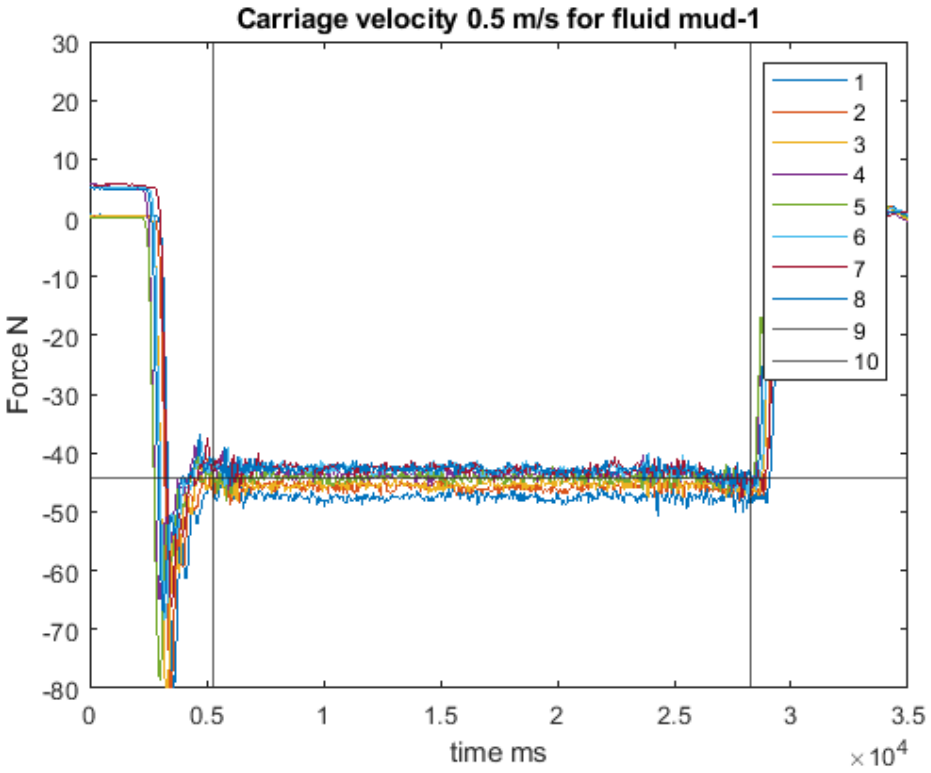

Figure B.2: Total resistance of the plate moved at speed 0.5m/s in fluid mud 1

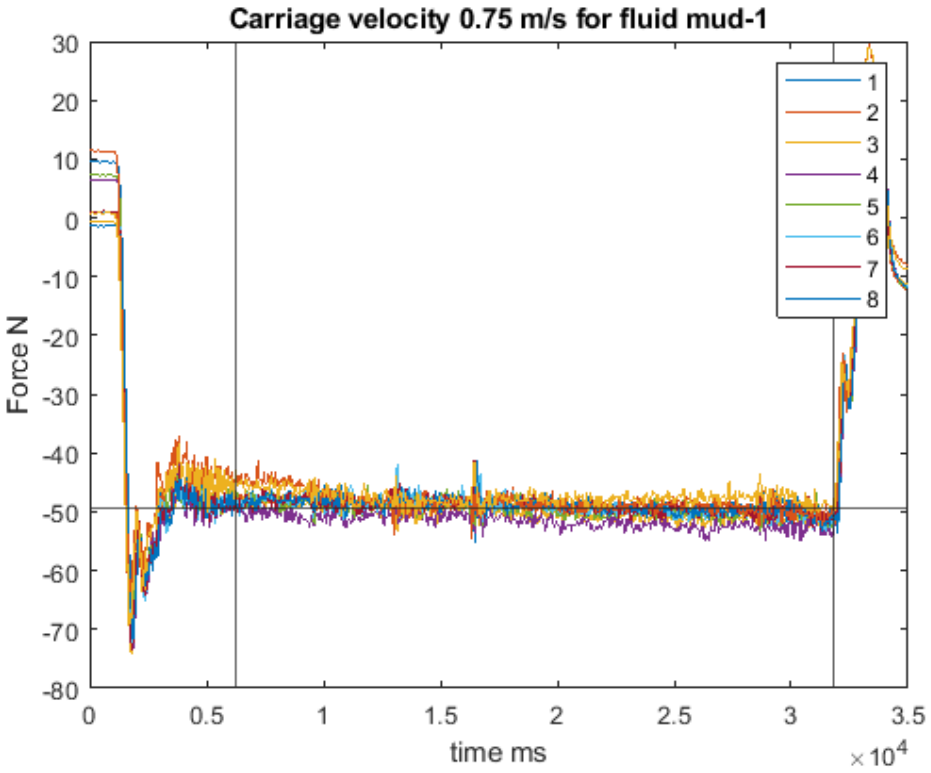

Figure B.3: Total resistance of the plate moved at speed 0.75m/s in fluid mud 1

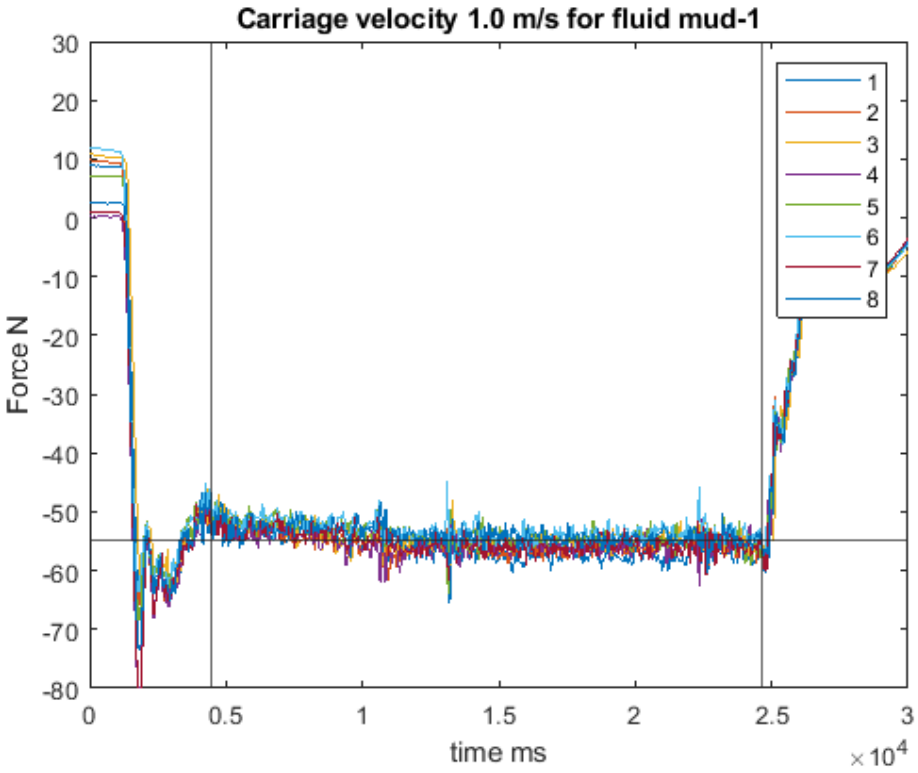

Figure B.4: Total resistance of the plate moved at speed 1.0m/s in fluid mud 1

B.1.2 Wooden plate dragged in the Fluid mud 2

Figure B.5,B.6,B.7, and B.8 represents the load-cell signal of total resistance of plate when moved in the Fluid mud 2 at speeds 0.25m/s,0.5m/s,0.75m/s, and 1.0m/s respectively.

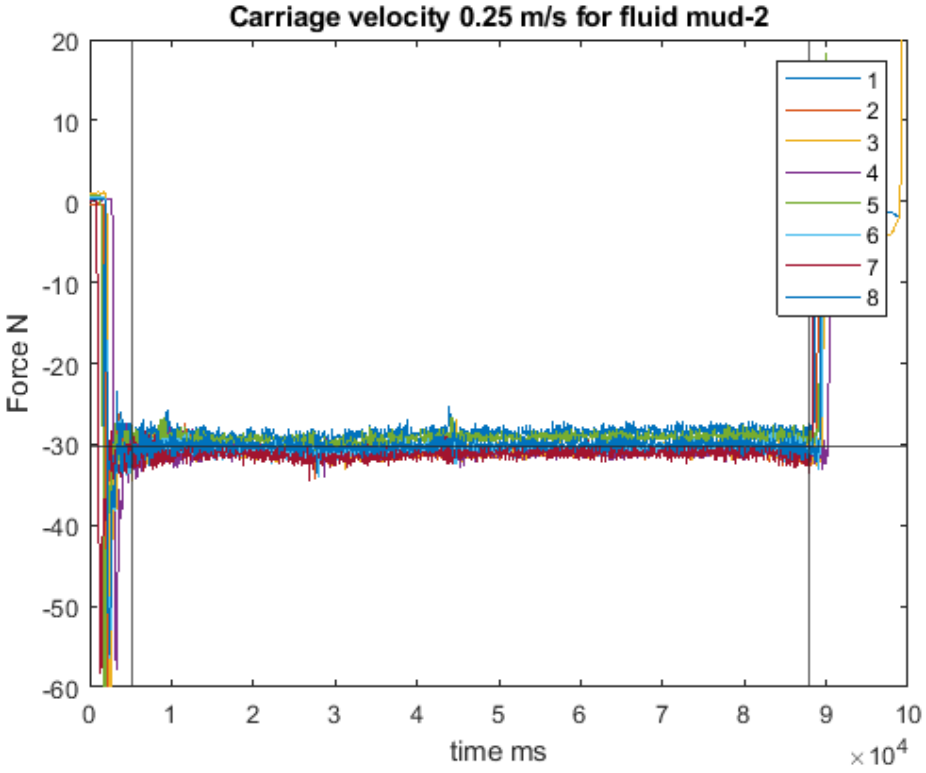

Figure B.5: Total resistance of the plate moved at speed 0.25m/s in fluid mud 2

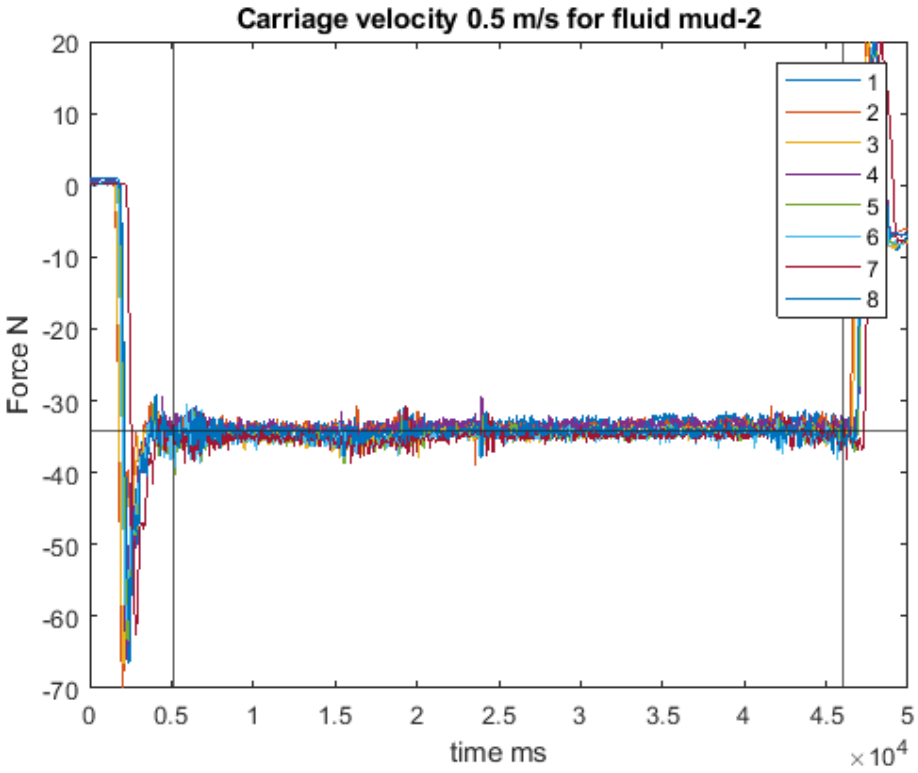

Figure B.6: Total resistance of the plate moved at speed 0.5m/s in fluid mud 2

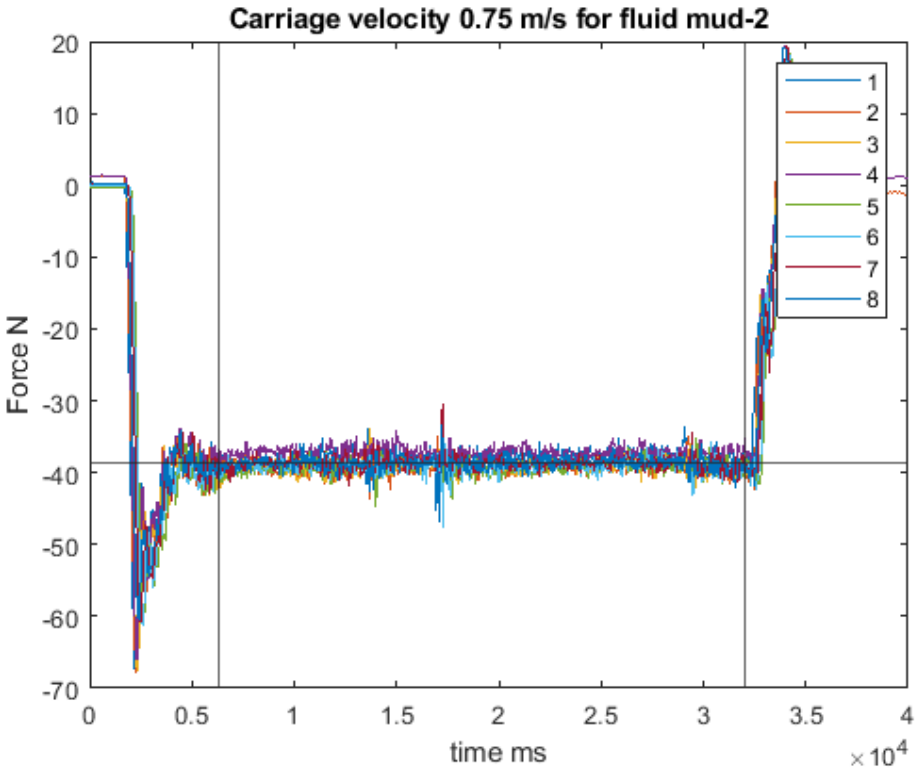

Figure B.7: Total resistance of the plate moved at speed 0.75m/s in fluid mud 2

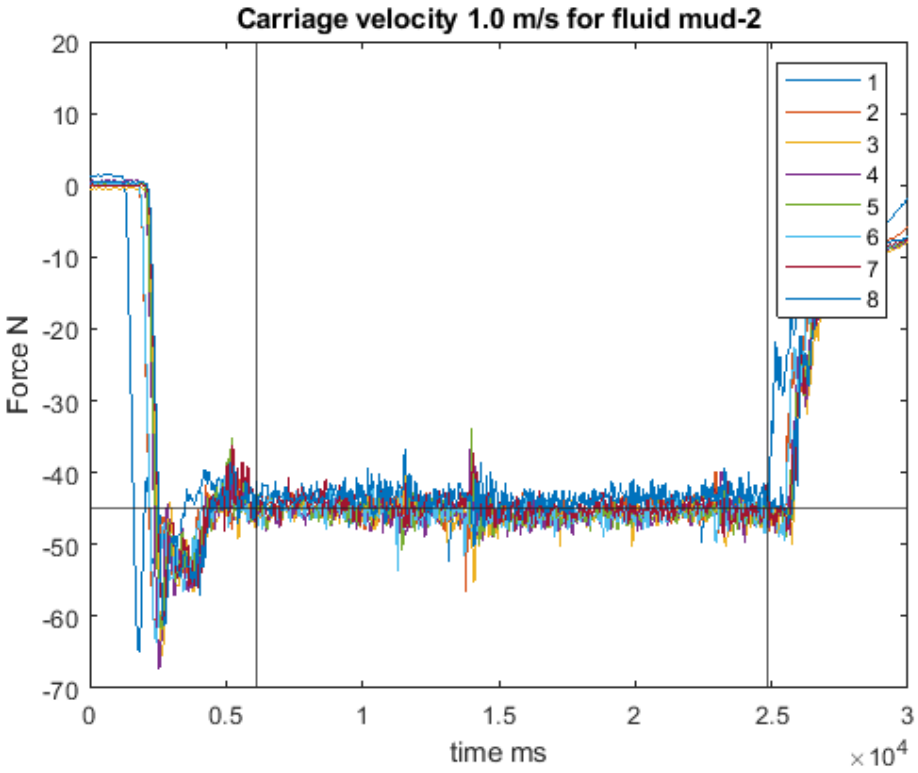

Figure B.8: Total resistance of the plate moved at speed 1.0m/s in fluid mud 2

B.1.3 Wooden plate dragged in the Fluid mud 3

Figure B.9,B.10,B.11, and B.12 represents the load-cell signal of total resistance of plate when moved in the Fluid mud 3 at speeds 0.25m/s,0.5m/s,0.75m/s, and 1.0m/s respectively.

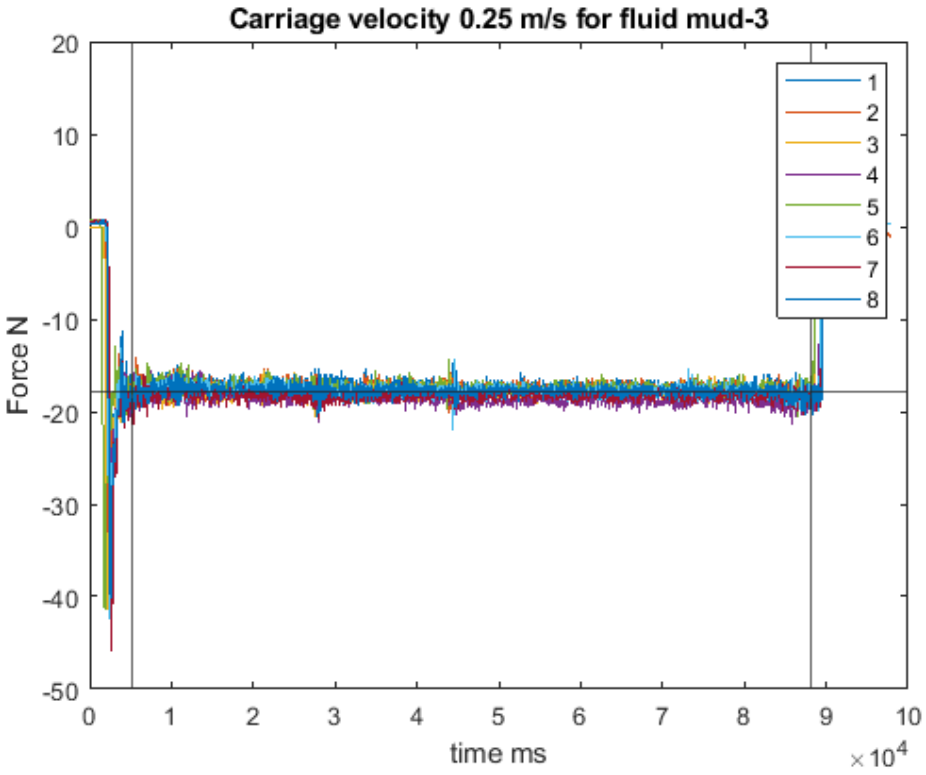

Figure B.9: Total resistance of the plate moved at speed 0.25m/s in fluid mud 3

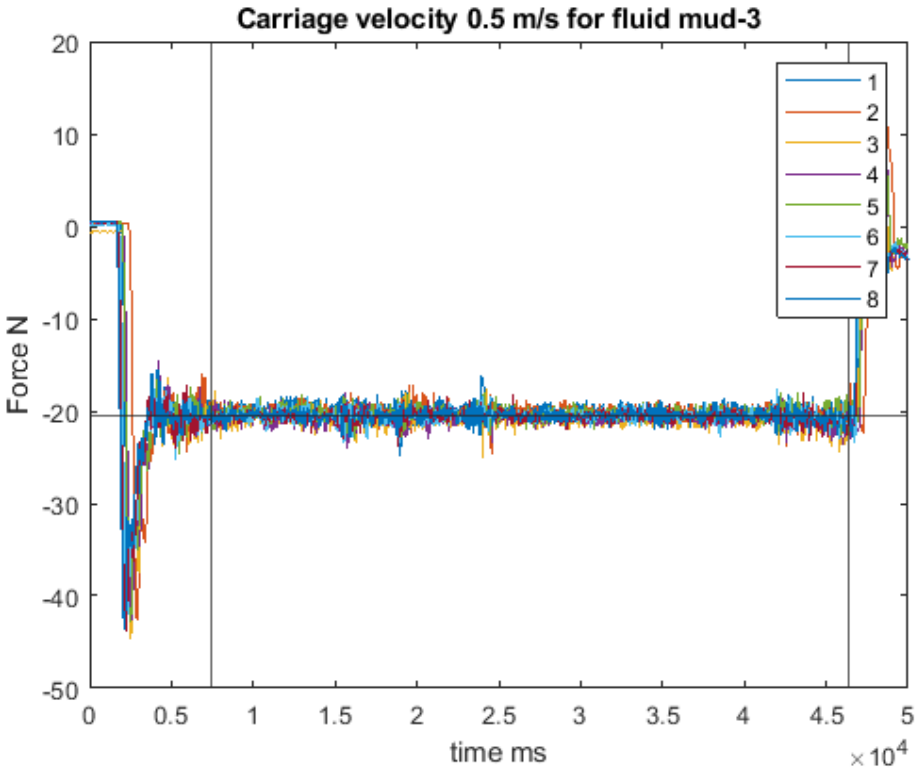

Figure B.10: Total resistance of the plate moved at speed 0.5m/s in fluid mud 3

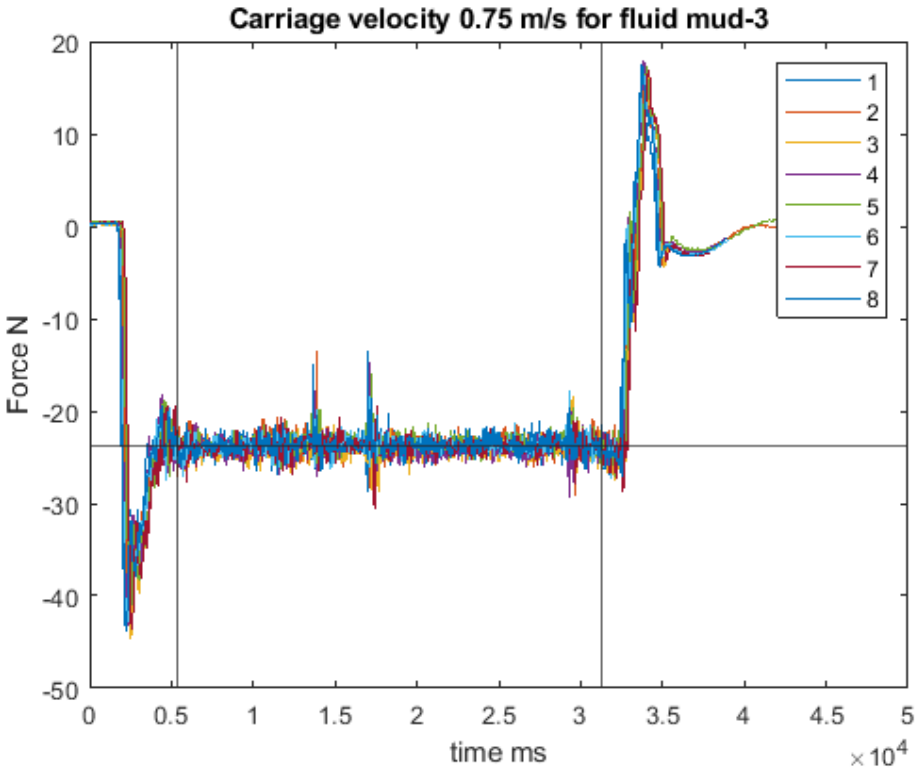

Figure B.11: Total resistance of the plate moved at speed 0.75m/s in fluid mud 3

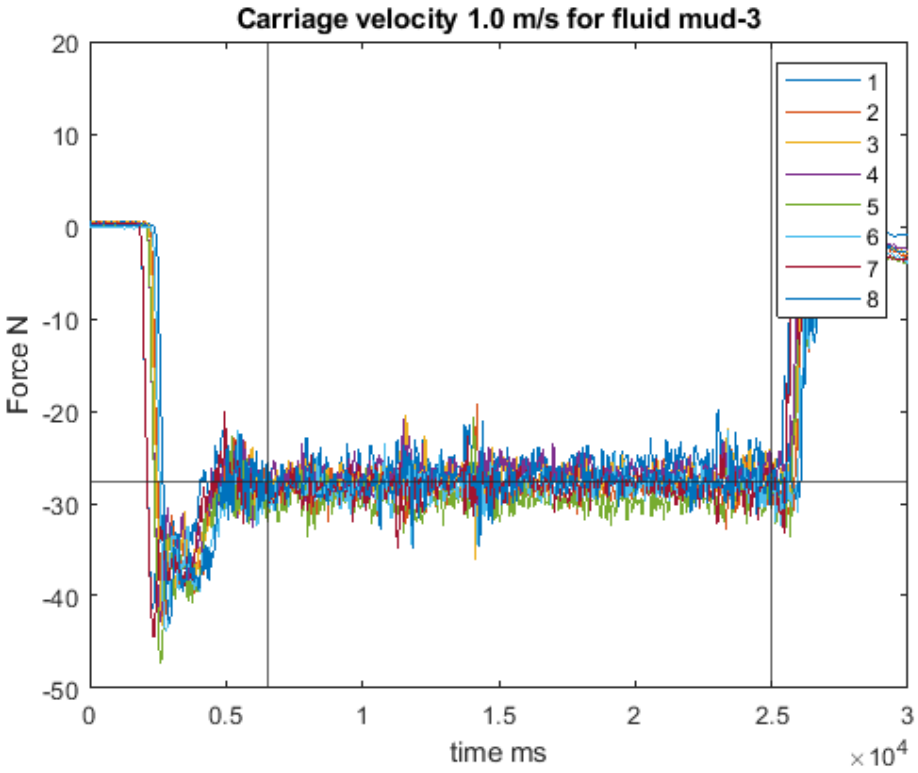

Figure B.12: Total resistance of the plate moved at speed 1.0m/s in fluid mud 3

B.1.4 Cux sampler plates dragged in the Fluid mud 3

Two thin plates of dimensions 0.5m X 0.33m and 0.5m X 0.5m. were assembled to the Cux sampler and flume experiments were carried out by dragging it at speeds 0.25m/s,0.5m/s,0.75m/s,1.0m/s,1.25m/s, and 1.5m/s.

Load-cell signal of total resistance of thin plate of dimensions 0.5m X 0.33m dragged in the Fluid mud 3

Figure B.13,B.14,B.15,B.16,B.17, and B.18 represents the load-cell signal of total resistance of plate when moved in the Fluid mud 3 at speeds 0.25m/s,0.5m/s,0.75m/s,1.0m/s,1.25m/s, and 1.5m/s respectively.

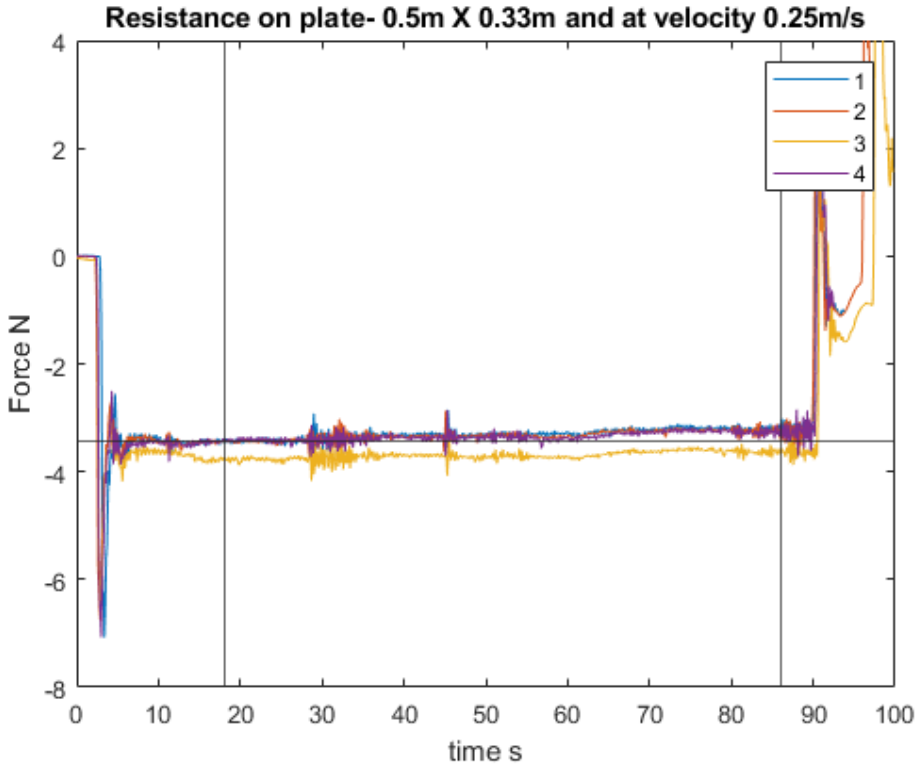

Figure B.13: Total resistance of 0.5m X 0.33m size plate moved at speed 0.25m/s in fluid mud 3

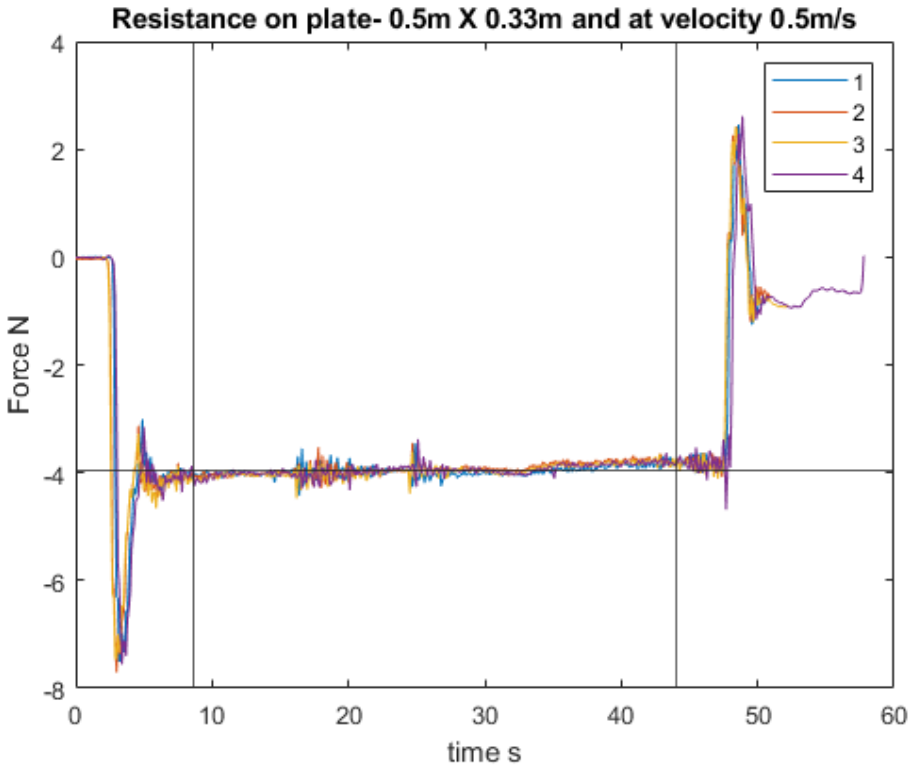

Figure B.14: Total resistance of 0.5m X 0.33m size plate moved at speed 0.5m/s in fluid mud 3

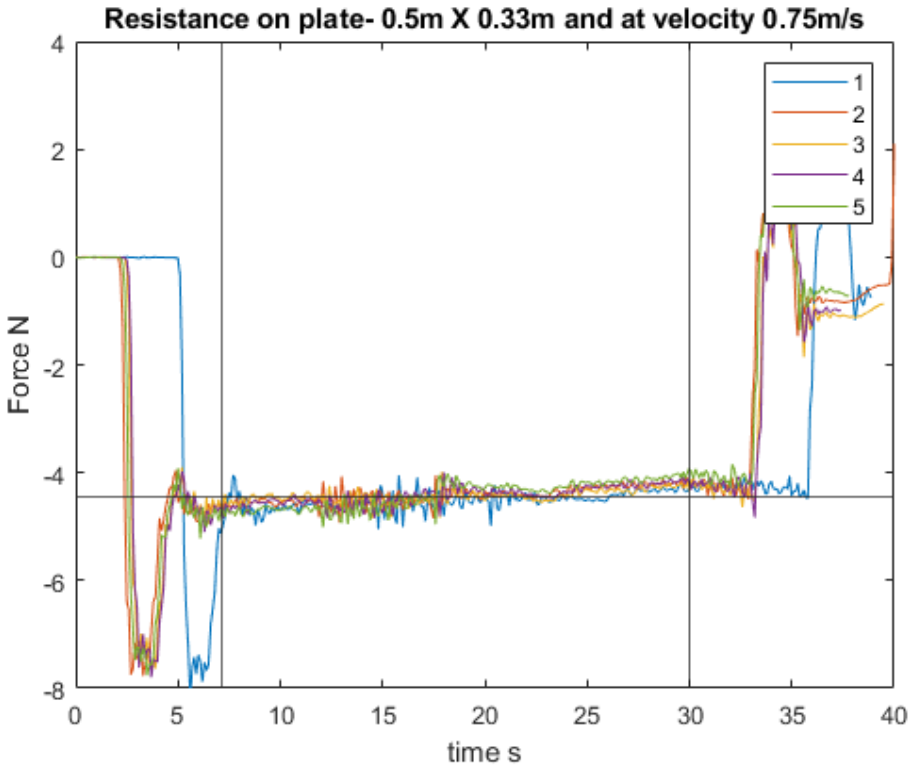

Figure B.15: Total resistance of 0.5m X 0.33m size plate moved at speed 0.75m/s in fluid mud 3

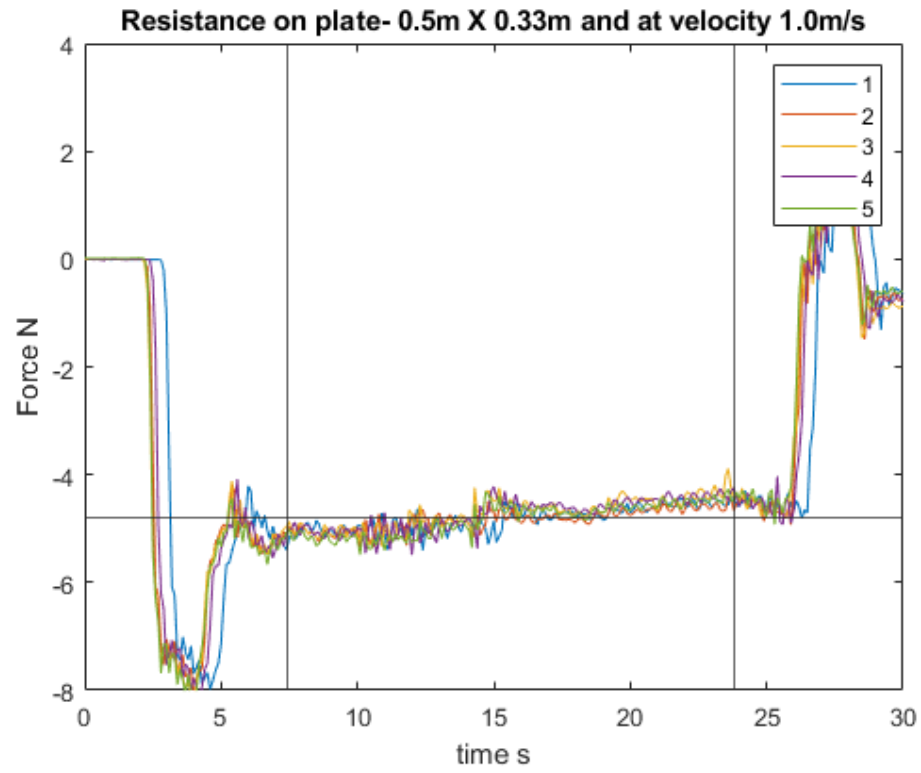

Figure B.16: Total resistance of 0.5m X 0.33m size plate moved at speed 1.0m/s in fluid mud 3

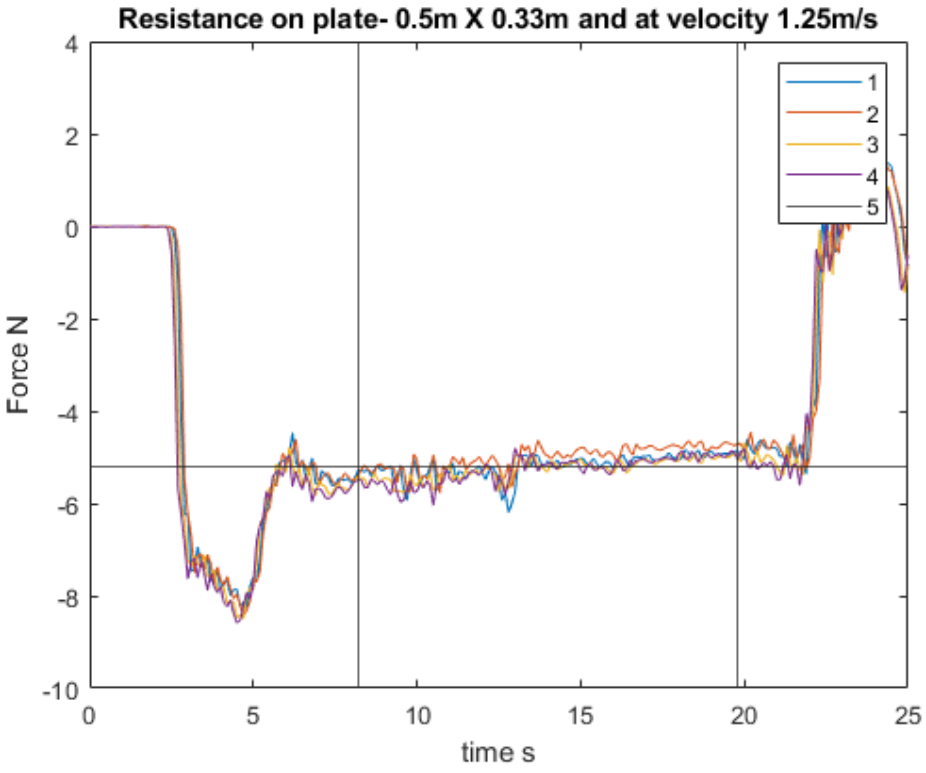

Figure B.17: Total resistance of 0.5m X 0.33m size plate moved at speed 1.25m/s in fluid mud 3

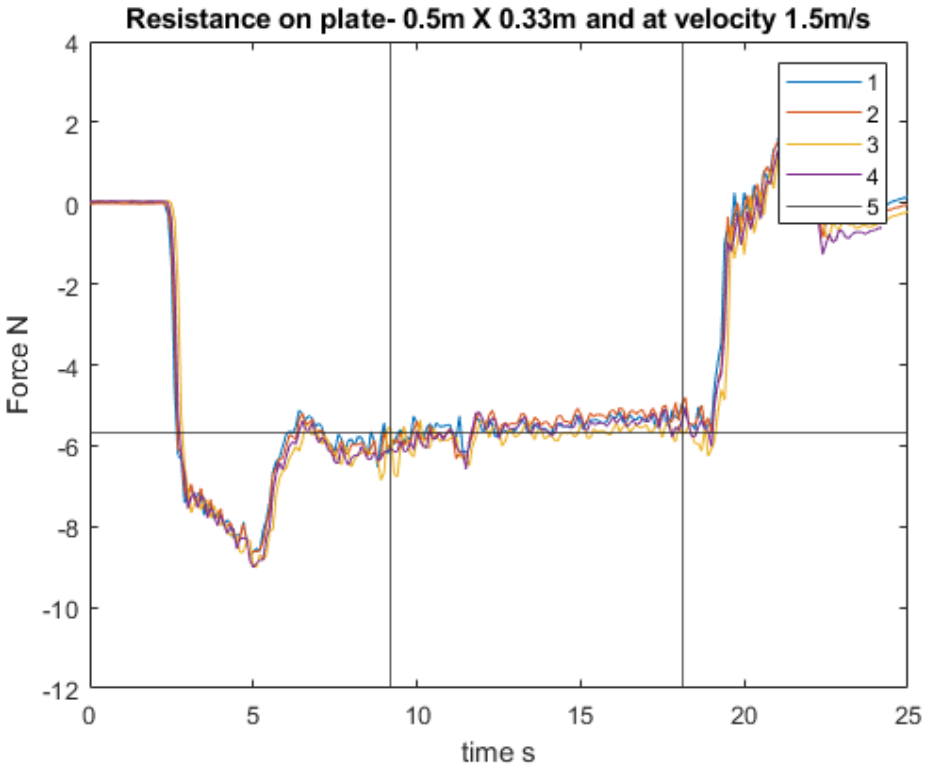

Figure B.18: Total resistance of 0.5m X 0.33m size plate moved at speed 1.5m/s in fluid mud 3

Load-cell signal of total resistance of thin plate of dimensions 0.5m X 0.5m dragged in the Fluid mud 3

Figure B.19,B.20,B.21,B.22,B.23, and B.24 represents the load-cell signal of total resistance of plate when moved in the Fluid mud 3 at speeds 0.25m/s,0.5m/s,0.75m/s,1.0m/s,1.25m/s, and 1.5m/s respectively.

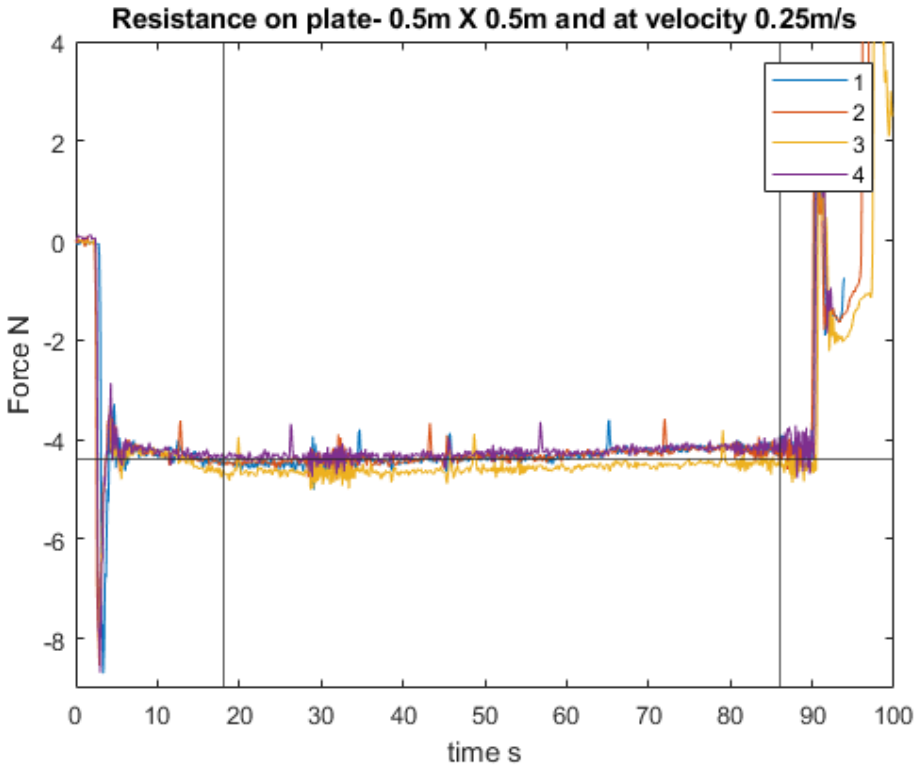

Figure B.19: Total resistance of 0.5m X 0.5m size plate moved at speed 0.25m/s and in fluid mud 3

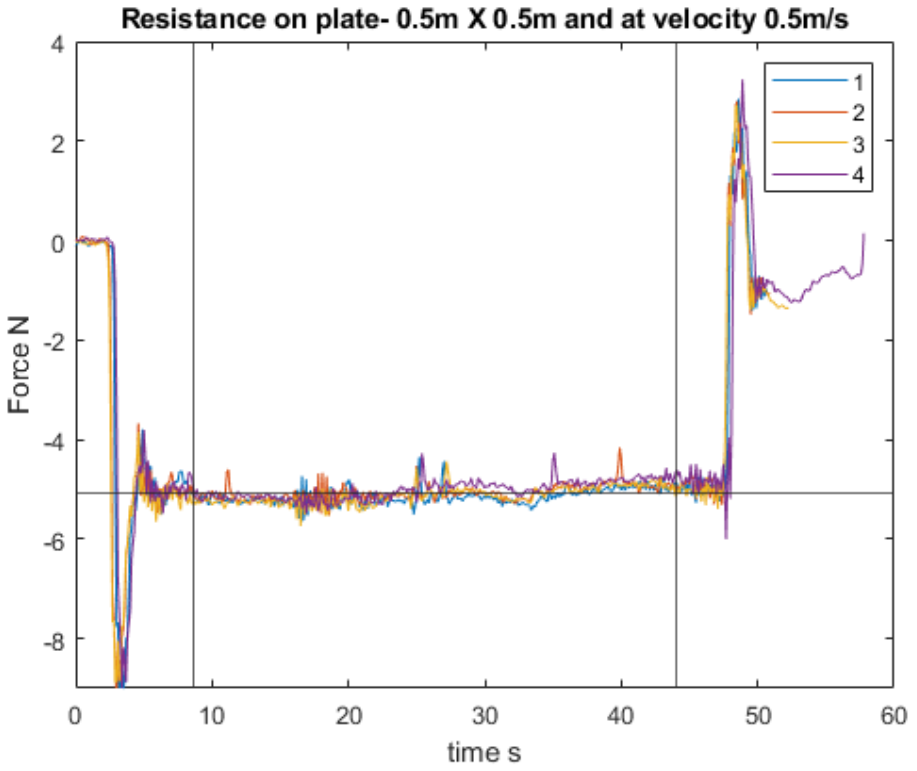

Figure B.20: Total resistance of 0.5m X 0.5m size plate moved at speed 0.5m/s in fluid mud 3

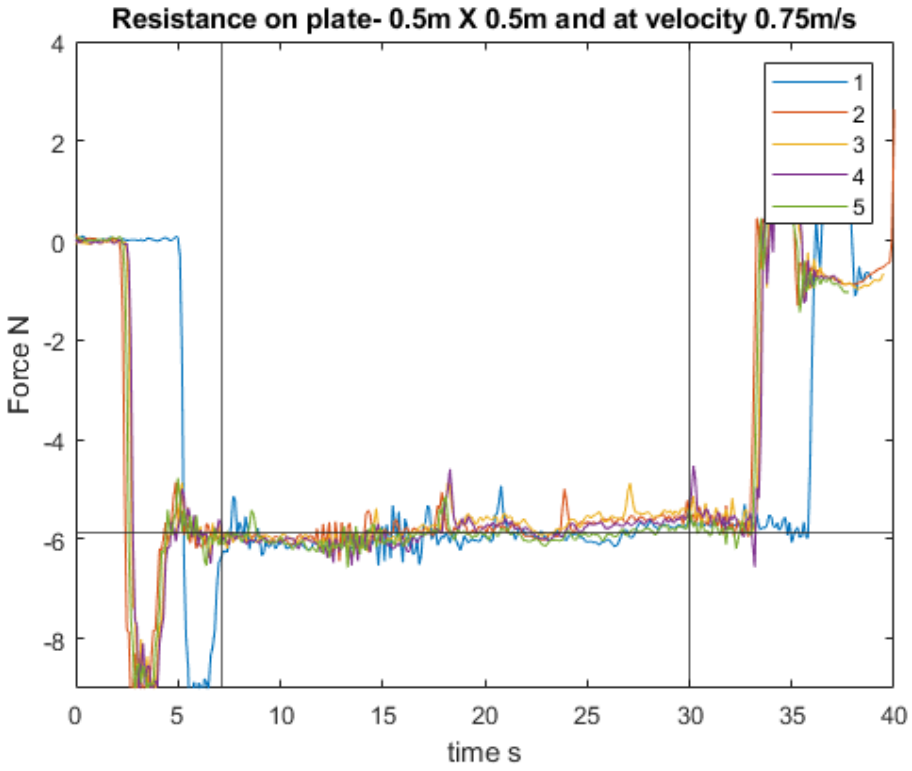

Figure B.21: Total resistance of 0.5m X 0.5m size plate moved at speed 0.75m/s in fluid mud 3

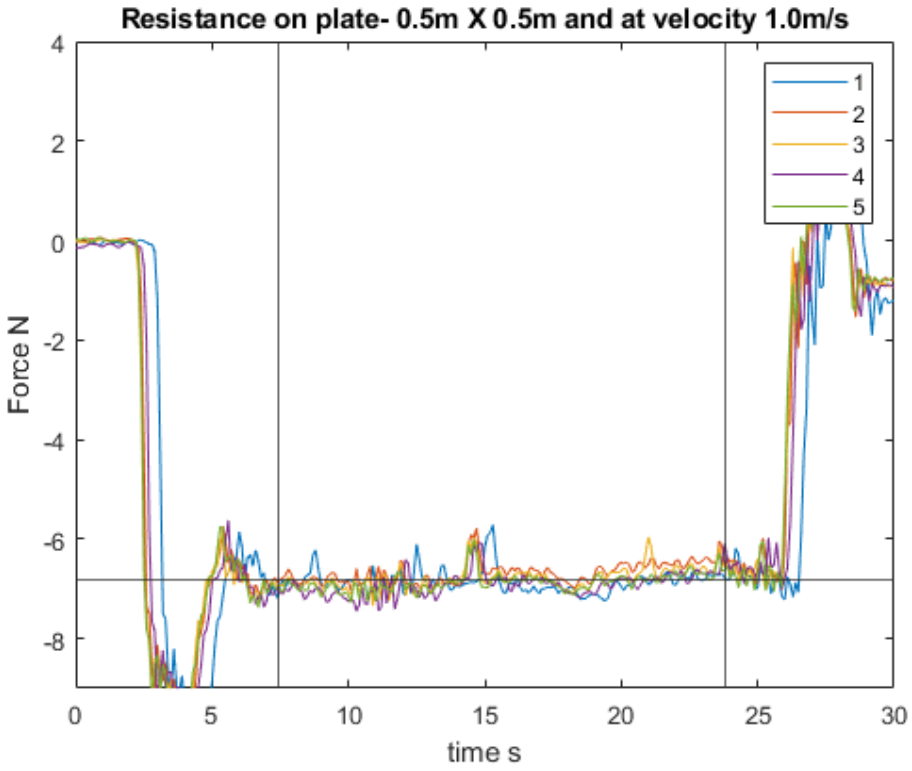

Figure B.22: Total resistance of 0.5m X 0.5m size plate moved at speed 1.0m/s in fluid mud 3

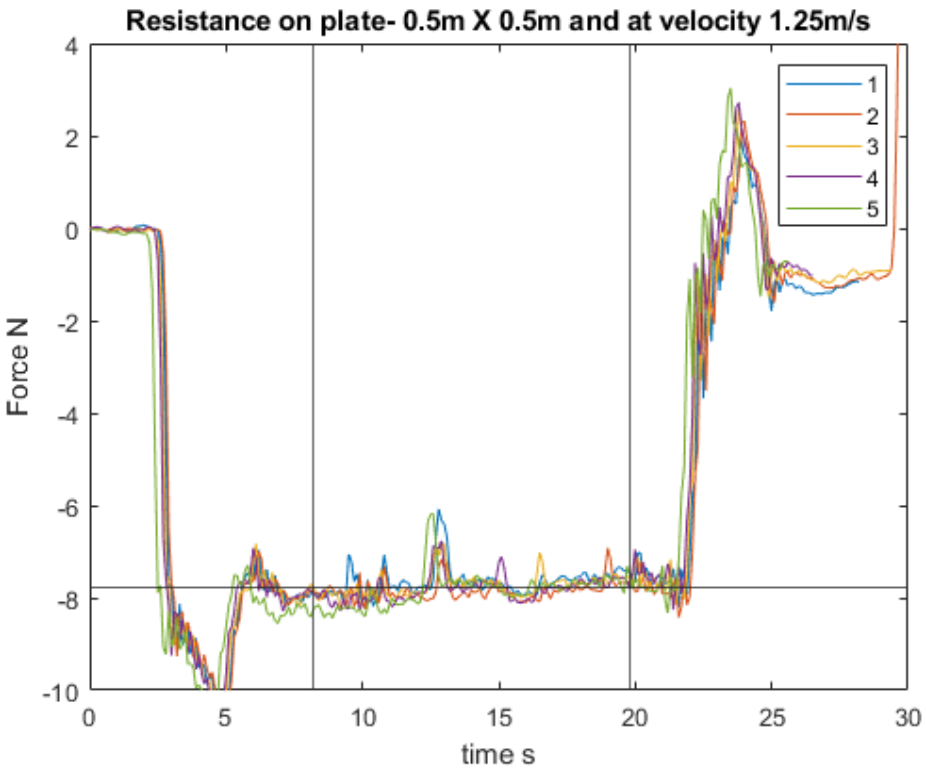

Figure B.23: Total resistance of 0.5m X 0.5m size plate moved at speed 1.25m/s in fluid mud 3

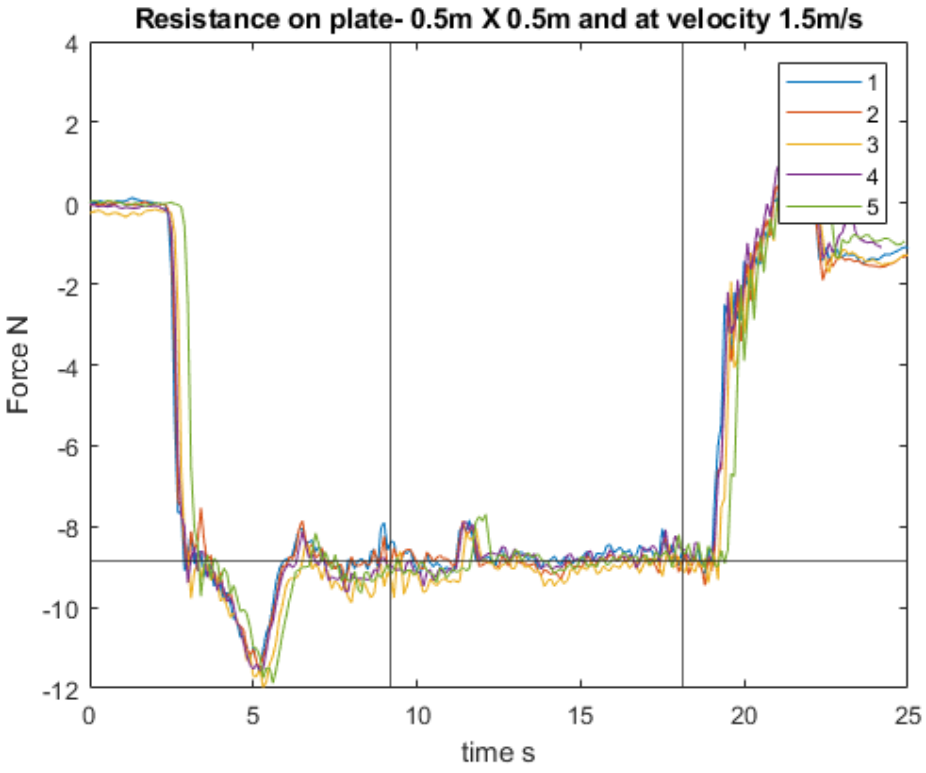

Figure B.24: Total resistance of 0.5m X 0.5m size plate moved at speed 1.5m/s in fluid mud 3

B.2 Rheology and oven test results of fluid mud

In the flume experiments, the fluid mud dredged at Calandkanaal was diluted to meet the test matrix requirements. In the test matrix, three different strengths of the fluid mud were proposed, and thus for simple identification of fluid mud condition used in the test matrix, numbers were given to the fluid mud. In brief, Fluid mud 1 means the fluid mud used in the first flume experiments, Fluid mud 2 means the fluid mud used in the second flume experiments, and Fluid mud 3 means the fluid mud used in the third flume experiments.

B.2.1 Fluid mud 1: Fluid mud used in first set of flume experiments

The fluid mud was homogenized with rotor and blade set up in the first flume experiments. After the mixing process and the rest of approximately fifteen minutes, three fluid mud samples were collected (10:40 AM), and after the completion of flume experiments, three fluid mud samples were collected (03:50 PM). The collected fluid mud samples were labeled with acronyms. For instance, the label FM1S1 means Fluid mud 1 and sample number 1. The sample numbers are fixed to the location points, which are discussed in Chapter 3. Table B.1 represents the details of rheometry and oven test results of the fluid mud samples.

Table B.1: Details of rheometry and oven test results for Calandkanaal fluid mud samples collected during the first flume experiments. All the tests were performed on May 19, 2021.

Test no	Sample Id	From oven test method					Rheometry	
		Density [g/cc]	Vol. Concen-tration	Geo water content [%]	Hydro water content [%]	Solid content [%]	Geometry	Protocols
139	FM1S1	1.200	0.11	201	73	27	Vane	CSR 0-20 180s up - 60s constant - 180s down
140	FM1S2	1.203	0.11	195	72	28	Vane	CSR 0-20 180s up - 60s constant - 180s down
141	FM1S3	1.203	0.11	205	72	28	Vane	CSR 0-20 180s up - 60s constant - 180s down
142	FM1S1	1.200	0.11	201	73	27	Bob	CSR 0-100 180s up - 60s constant - 180s down
143	FM1S2	1.203	0.11	195	72	28	Bob	CSR 0-100 180s up - 60s constant - 180s down
144	FM1S3	1.203	0.11	205	72	28	Bob	CSR 0-100 180s up - 60s constant - 180s down
145	FM1S1	1.200	0.11	201	73	27	Bob	CSS 0-100 150s up
146	FM1S2	1.203	0.11	195	72	28	Bob	CSS 0-100 150s up
147	FM1S3	1.203	0.11	205	72	28	Bob	CSS 0-100 150s up
148	FM1S4	1.201	0.11	201	73	27	Vane	CSR 0-20 180s up - 60s constant - 180s down
149	FM1S5	1.200	0.11	206	73	27	Vane	CSR 0-20 180s up - 60s constant - 180s down
150	FM1S6	1.203	0.11	195	72	28	Vane	CSR 0-20 180s up - 60s constant - 180s down
151	FM1S4	1.201	0.11	201	73	27	Bob	CSR 0-100 180s up - 60s constant - 180s down
152	FM1S5	1.200	0.11	206	73	27	Bob	CSR 0-100 180s up - 60s constant - 180s down
153	FM1S6	1.203	0.11	195	72	28	Bob	CSR 0-100 180s up - 60s constant - 180s down
154	FM1S4	1.201	0.11	201	73	27	Bob	CSS 0-100 150s up
155	FM1S5	1.200	0.11	206	73	27	Bob	CSS 0-100 150s up
156	FM1S6	1.203	0.11	195	72	28	Bob	CSS 0-100 150s up

The flow curves obtained in CSR tests with bob-cup geometry are represented in the Figure B.25 and B.26. The CSR tests with vane(FL22)-cup geometry are represented in Figure B.29 and B.30. The fluid

mud samples were also tested in CSS mode with bob-cup geometry to obtain the viscous curves, see Figure B.27 and B.28.

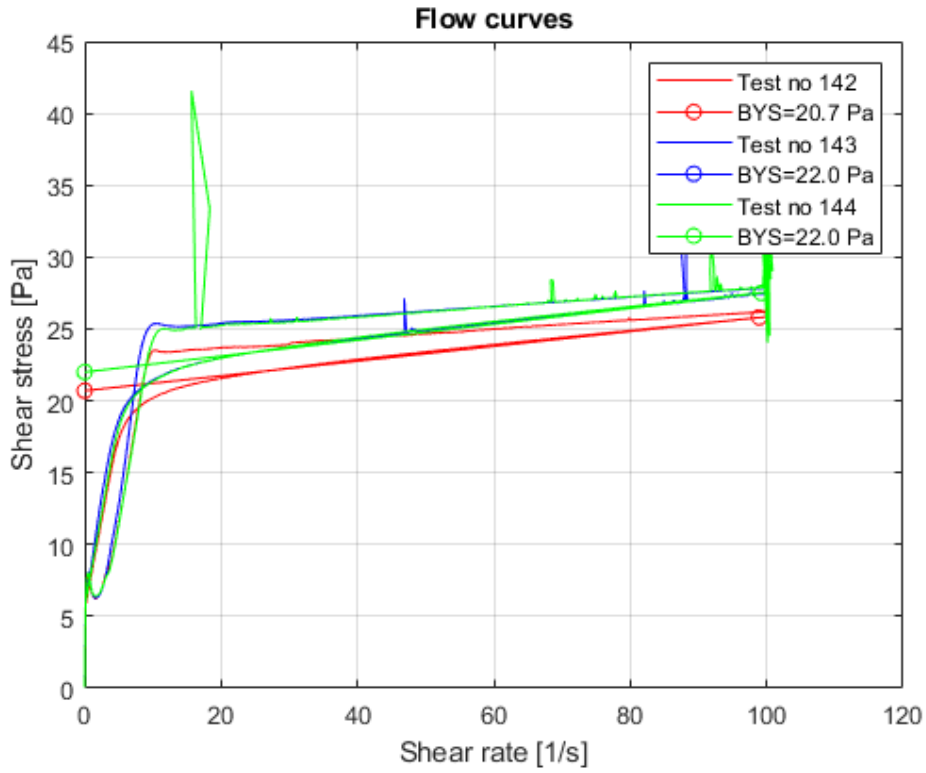

Figure B.25: Fluid mud-1 samples were collected before the flume tests were tested in CSR mode using bob-cup geometry to obtain flow curves.

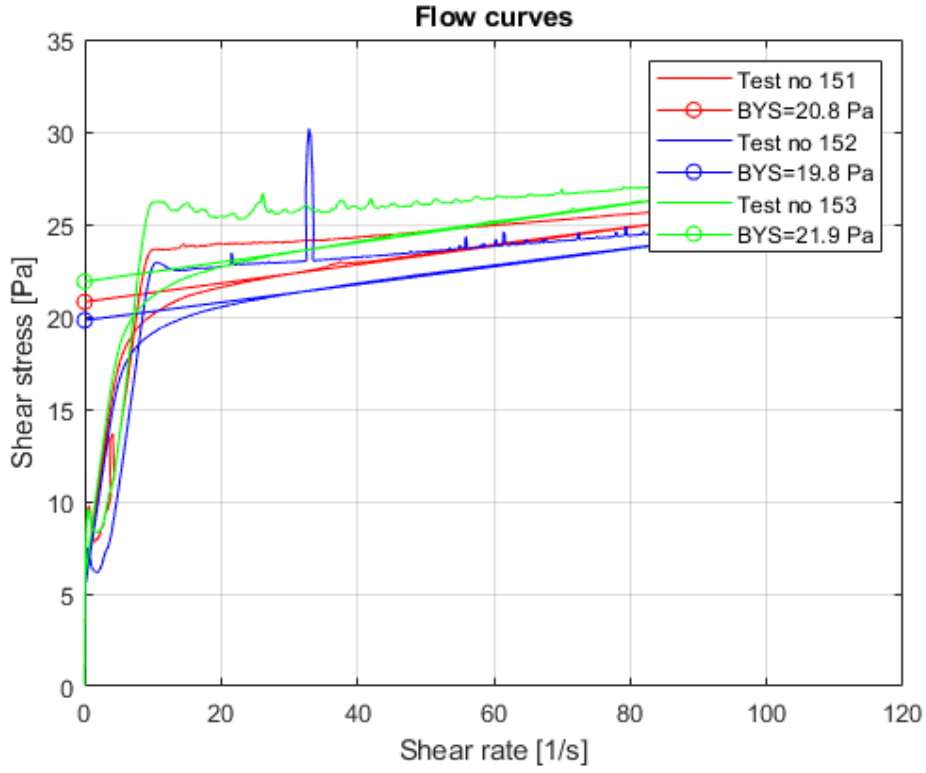

Figure B.26: Fluid mud-1 samples were collected after the flume tests were tested in CSR mode using bob-cup geometry to obtain flow curves.

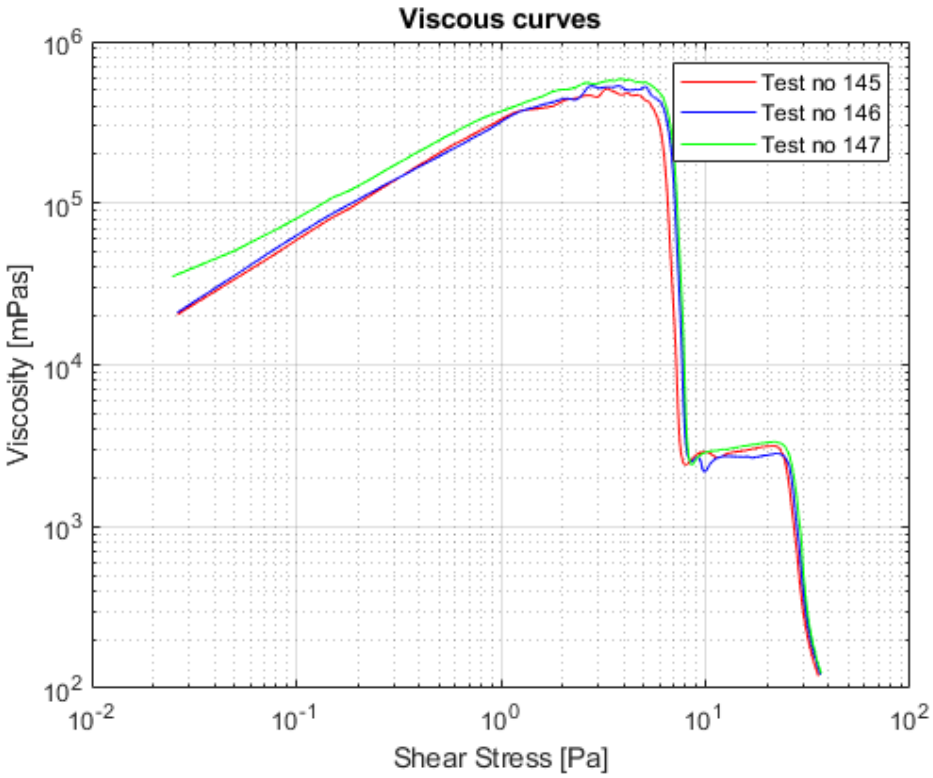

Figure B.27: Fluid mud-1 samples were collected before the flume tests were tested in CSS mode using bob-cup geometry to obtain viscous curves.

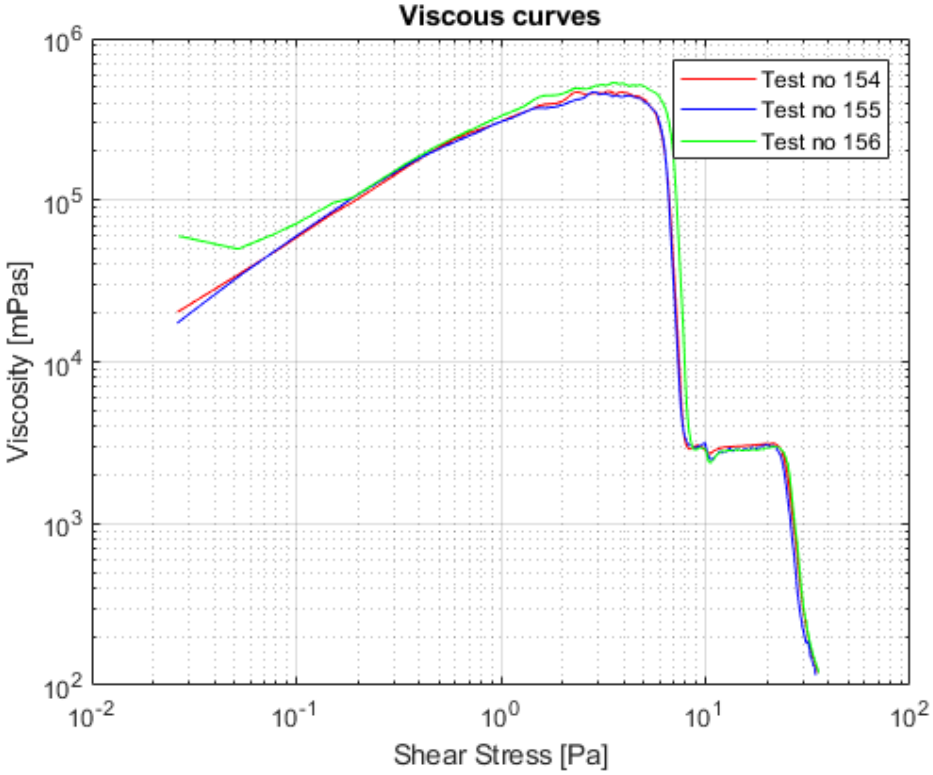

Figure B.28: Fluid mud-1 samples were collected after the flume tests were tested in CSS mode using bob-cup geometry to obtain viscous curves.

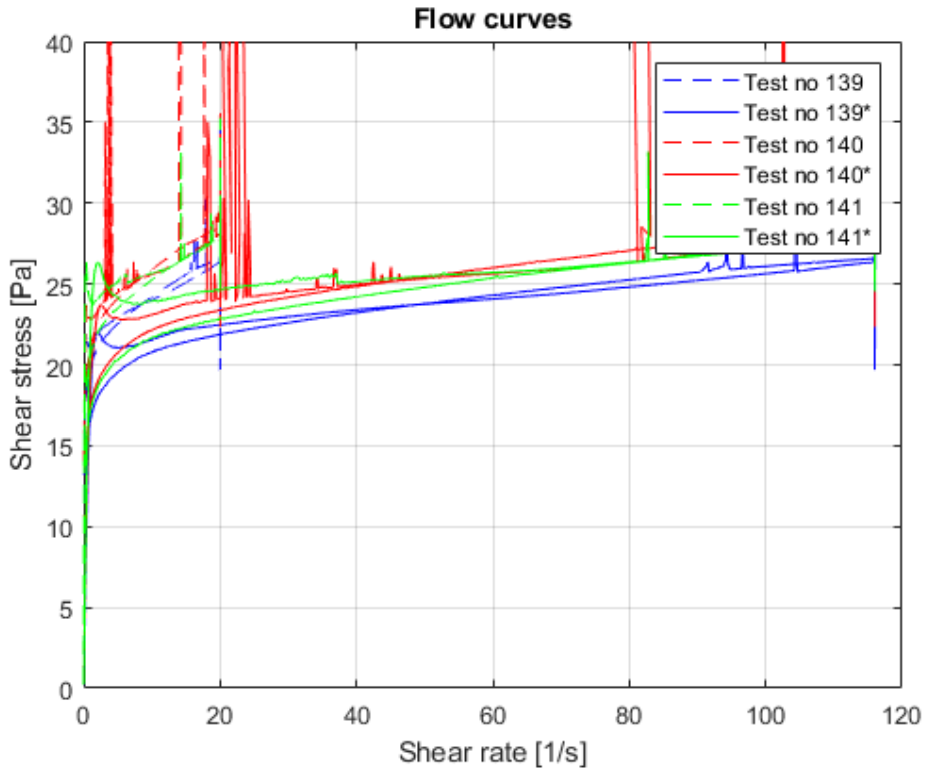

Figure B.29: Fluid mud-1 samples were collected before the flume tests were tested in CSR mode using vane(FL22)-cup geometry to obtain flow curves.

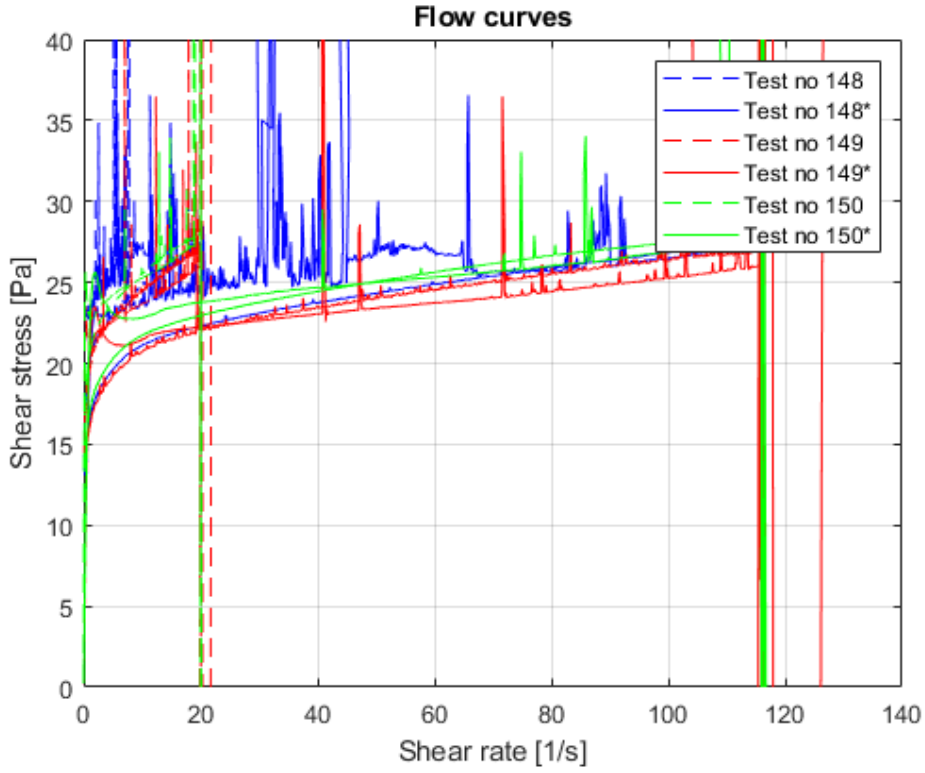

Figure B.30: Fluid mud-1 samples were collected after the flume tests were tested in CSR mode using vane(FL22)-cup geometry to obtain flow curves.

B.2.2 Fluid mud 2: Fluid mud used in second set of flume experiments

The fluid mud was homogenized with rotor and blade set up in the second flume experiments. After the mixing process and the rest of approximately fifteen minutes, three fluid mud samples were collected (09:45 AM), and after the completion of flume experiments, three fluid mud samples were collected (01:00 PM). The collected fluid mud samples were labeled with acronyms. For instance, the label FM1S1 means Fluid mud 2 and sample number 1. The sample numbers are fixed to the location points, which are discussed in Chapter 3. Table B.2 represents the details of rheometry and oven test results of the fluid mud samples.

Table B.2: Details of rheometry and oven test results for Calandkanaal fluid mud samples collected during the second flume experiments. All the tests were performed on May 25, 2021.

Test no	Sample Id	From oven test method					Rheometry	
		Density [g/cc]	Vol. Concen-tration	Geo water content [%]	Hydro water content [%]	Solid content [%]	Geometry	Protocols
157	FM2S1	1.192	0.10	213	74	26	Vane	CSR 0-20 180s up - 60s constant - 180s down
158	FM2S2	1.192	0.10	217	74	26	Vane	CSR 0-20 180s up - 60s constant - 180s down
159	FM2S3	1.191	0.10	229	74	26	Vane	CSR 0-20 180s up - 60s constant - 180s down
160	FM2S1	1.192	0.10	213	74	26	Bob	CSR 0-300 180s up - 60s constant - 180s down
161	FM2S2	1.192	0.10	217	74	26	Bob	CSR 0-300 180s up - 60s constant - 180s down
162	FM2S3	1.191	0.10	229	74	26	Bob	CSR 0-300 180s up - 60s constant - 180s down
163	FM2S1	1.192	0.10	213	74	26	Bob	CSS 0-100 150s up
164	FM2S2	1.192	0.10	217	74	26	Bob	CSS 0-100 150s up
165	FM2S3	1.191	0.10	229	74	26	Bob	CSS 0-100 150s up
166	FM2S4	1.192	0.10	199	74	26	Vane	CSR 0-20 180s up - 60s constant - 180s down
167	FM2S5	1.192	0.10	213	74	26	Vane	CSR 0-20 180s up - 60s constant - 180s down
168	FM2S6	1.191	0.10	214	74	26	Vane	CSR 0-20 180s up - 60s constant - 180s down
169	FM2S4	1.192	0.10	199	74	26	Bob	CSR 0-100 180s up - 60s constant - 180s down
170	FM2S5	1.192	0.10	213	74	26	Bob	CSR 0-100 180s up - 60s constant - 180s down
171	FM2S6	1.191	0.10	214	74	26	Bob	CSR 0-100 180s up - 60s constant - 180s down
172	FM2S4	1.192	0.10	199	74	26	Bob	CSS 0-100 150s up
173	FM2S5	1.192	0.10	213	74	26	Bob	CSS 0-100 150s up
174	FM2S6	1.191	0.10	214	74	26	Bob	CSS 0-100 150s up

The flow curves obtained in CSR tests with bob-cup geometry are represented in the Figure B.31 and B.32. The CSR tests with vane(FL22)-cup geometry are represented in Figure B.35 and B.36. The fluid mud samples were also tested in CSS mode with bob-cup geometry to obtain the viscous curves, see Figure B.33 and B.34.

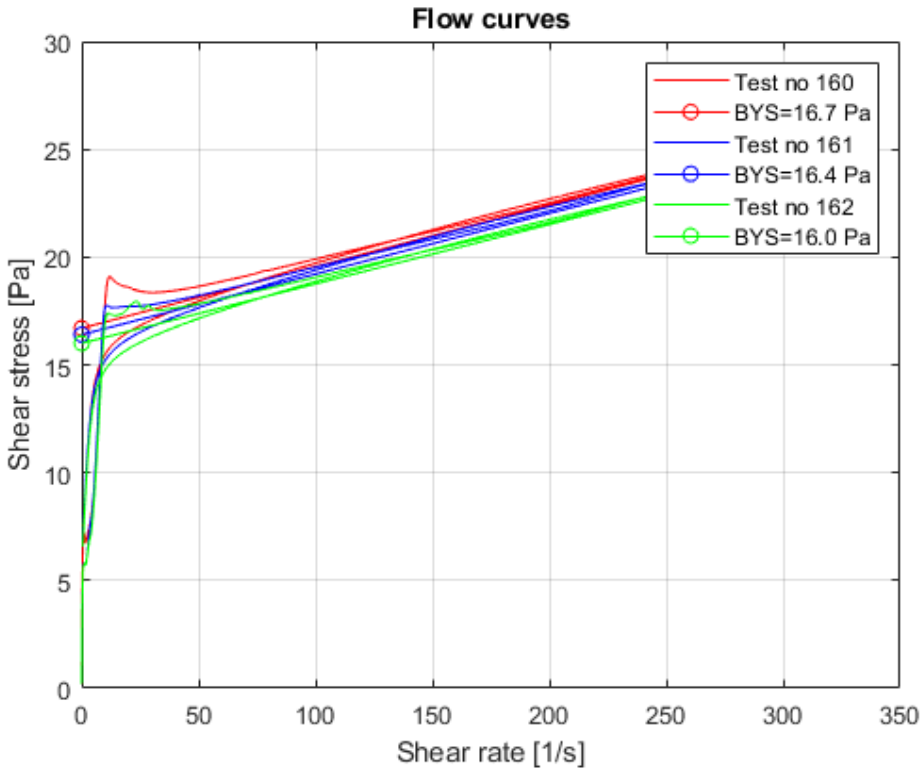

Figure B.31: Fluid mud-2 samples were collected before the flume tests were tested in CSR mode using bob-cup geometry to obtain flow curves.

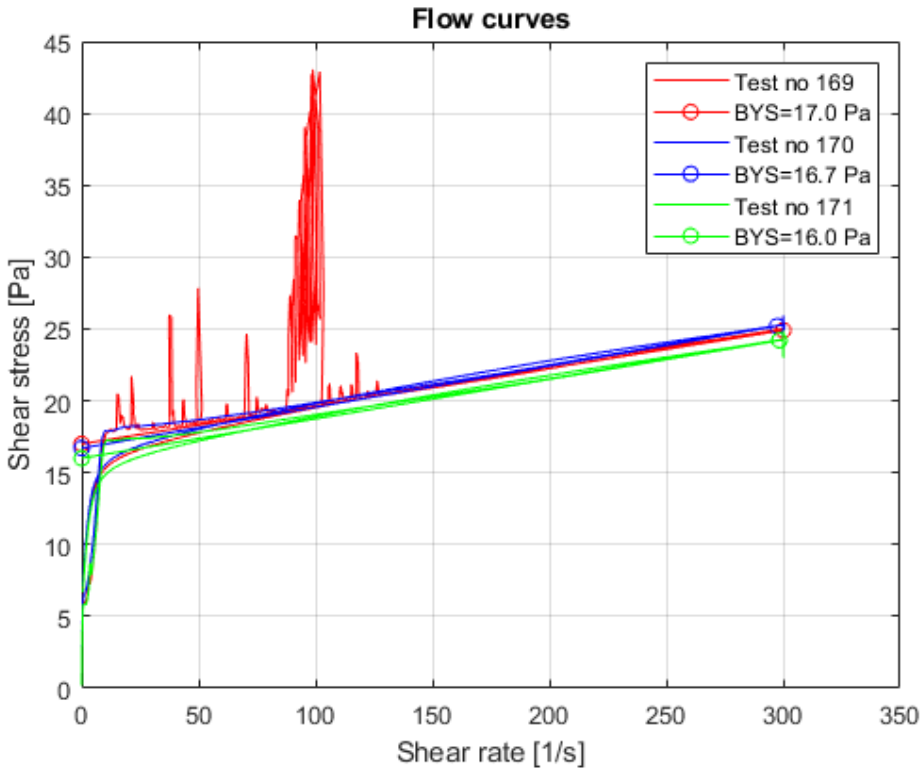

Figure B.32: Fluid mud-2 samples were collected after the flume tests were tested in CSR mode using bob-cup geometry to obtain flow curves.

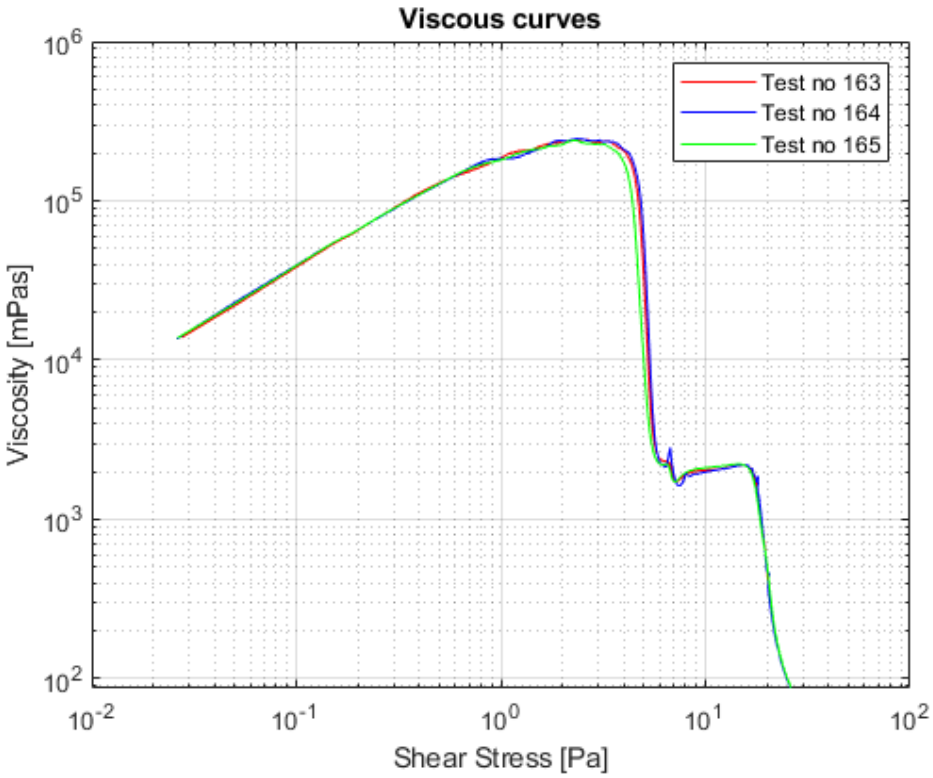

Figure B.33: Fluid mud-2 samples were collected before the flume tests were tested in CSS mode using bob-cup geometry to obtain viscous curves.

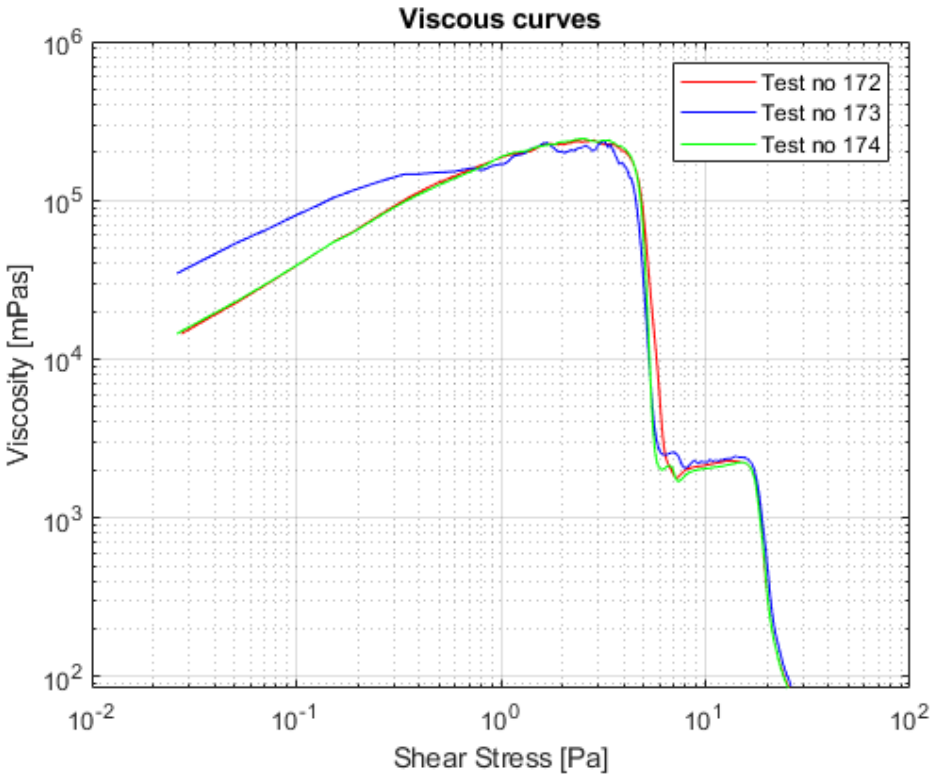

Figure B.34: Fluid mud-2 samples were collected after the flume tests were tested in CSS mode using bob-cup geometry to obtain viscous curves.

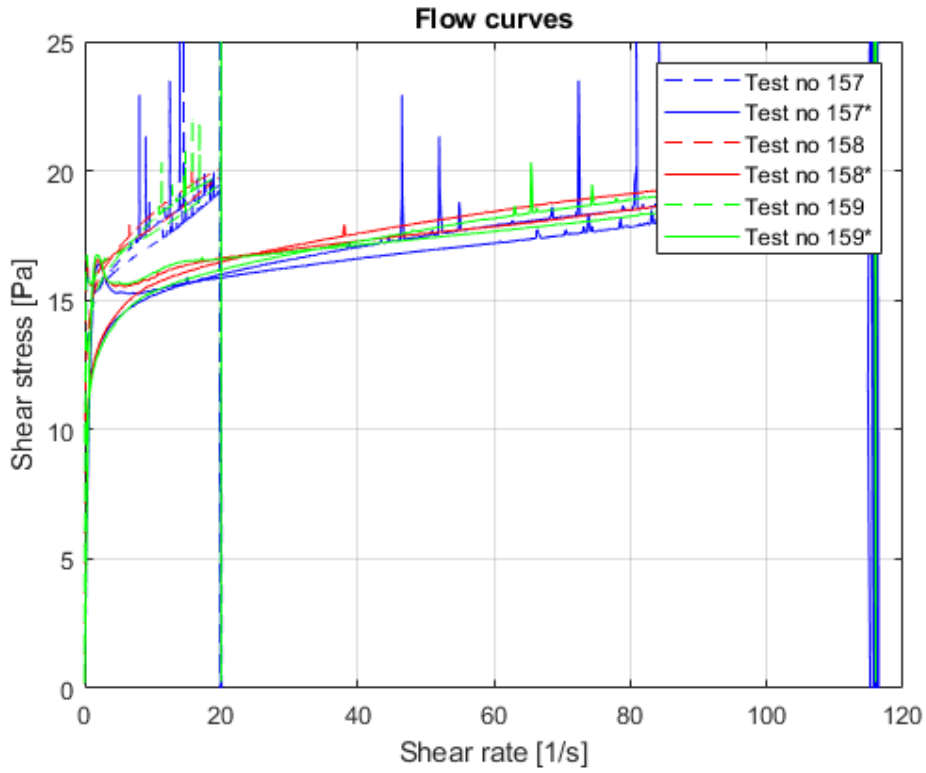

Figure B.35: Fluid mud-2 samples were collected before the flume tests were tested in CSR mode using vane(FL22)-cup geometry to obtain flow curves.

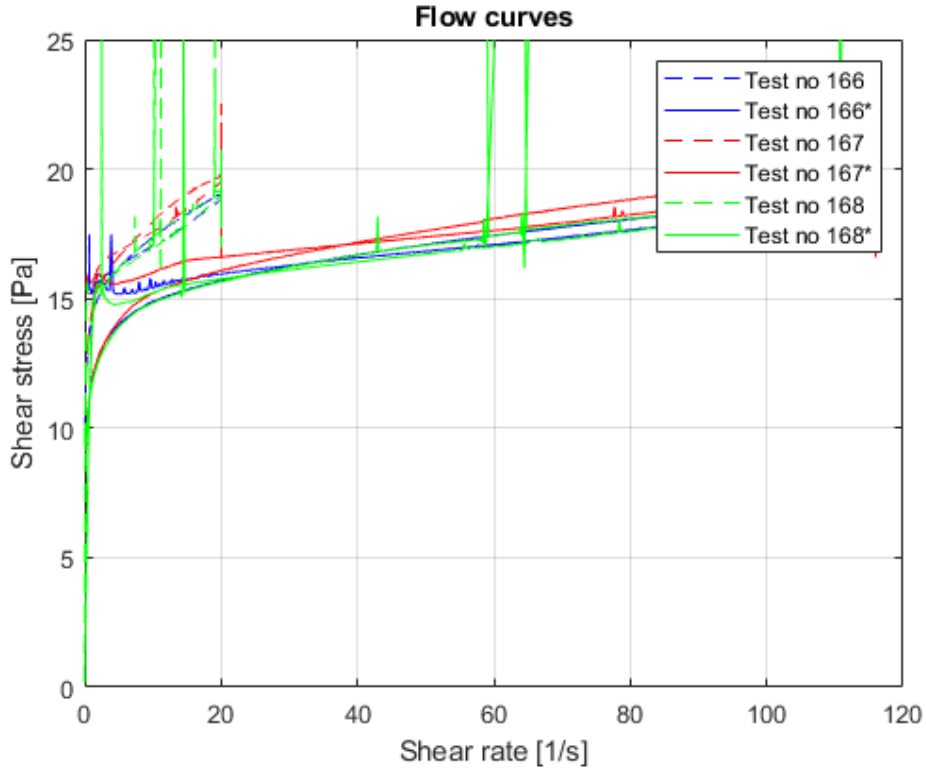

Figure B.36: Fluid mud-2 samples were collected after the flume tests were tested in CSR mode using vane(FL22)-cup geometry to obtain flow curves.

B.2.3 Fluid mud 3: Fluid mud used in third set of flume experiments

The fluid mud was homogenized with rotor and blade set up in the third flume experiments. After the mixing process and the rest of approximately fifteen minutes, three fluid mud samples were collected (09:45 AM), and after the completion of flume experiments, three fluid mud samples were collected (04:00 PM). The collected fluid mud samples were labeled with acronyms. For instance, the label FM1S1 means Fluid mud 3 and sample number 1. The sample numbers are fixed to the location points, which are discussed in Chapter 3. Table B.3 represents the details of rheometry and oven test results of the fluid mud samples.

Table B.3: Details of rheometry and oven test results for Calandkanaal fluid mud samples collected during the third flume experiments. All the tests were performed on May 27, 2021.

Test no	Sample Id	From oven test method					Rheometry	
		Density [g/cc]	Vol. Concen-tration	Geo water content [%]	Hydro water content [%]	Solid content [%]	Geometry	Protocols
175	FM3S1	1.174	0.09	253	76	24	Vane	CSR 0-20 180s up - 60s constant - 180s down
176	FM3S2	1.174	0.09	173	76	24	Vane	CSR 0-20 180s up - 60s constant - 180s down
177	FM3S3	1.173	0.09	239	76	24	Vane	CSR 0-20 180s up - 60s constant - 180s down
178	FM3S1	1.174	0.09	253	76	24	Bob	CSR 0-300 180s up - 60s constant - 180s down
179	FM3S2	1.174	0.09	173	76	24	Bob	CSR 0-300 180s up - 60s constant - 180s down
180	FM3S3	1.173	0.09	239	76	24	Bob	CSR 0-300 180s up - 60s constant - 180s down
181	FM3S1	1.174	0.09	253	76	24	Bob	CSS 0-100 150s up
182	FM3S2	1.174	0.09	173	76	24	Bob	CSS 0-100 150s up
183	FM3S3	1.173	0.09	239	76	24	Bob	CSS 0-100 150s up
184	FM3S4	1.168	0.09	245	76	24	Vane	CSR 0-20 180s up - 60s constant - 180s down
185	FM3S5	1.169	0.09	251	76	24	Vane	CSR 0-20 180s up - 60s constant - 180s down
186	FM3S6	1.187	0.10	241	76	24	Vane	CSR 0-20 180s up - 60s constant - 180s down
187	FM3S4	1.168	0.09	245	76	24	Bob	CSR 0-100 180s up - 60s constant - 180s down
188	FM3S5	1.169	0.09	251	76	24	Bob	CSR 0-100 180s up - 60s constant - 180s down
189	FM3S6	1.187	0.10	241	76	24	Bob	CSR 0-100 180s up - 60s constant - 180s down
190	FM3S4	1.168	0.09	245	76	24	Bob	CSS 0-100 150s up
191	FM3S5	1.169	0.09	251	76	24	Bob	CSS 0-100 150s up
192	FM3S6	1.187	0.10	241	76	24	Bob	CSS 0-100 150s up

The flow curves obtained in CSR tests with bob-cup geometry are represented in the Figure B.37 and B.38. The CSR tests with vane(FL22)-cup geometry are represented in Figure B.41 and B.42. The fluid mud samples were also tested in CSS mode with bob-cup geometry to obtain the viscous curves, see Figure B.39 and B.40.

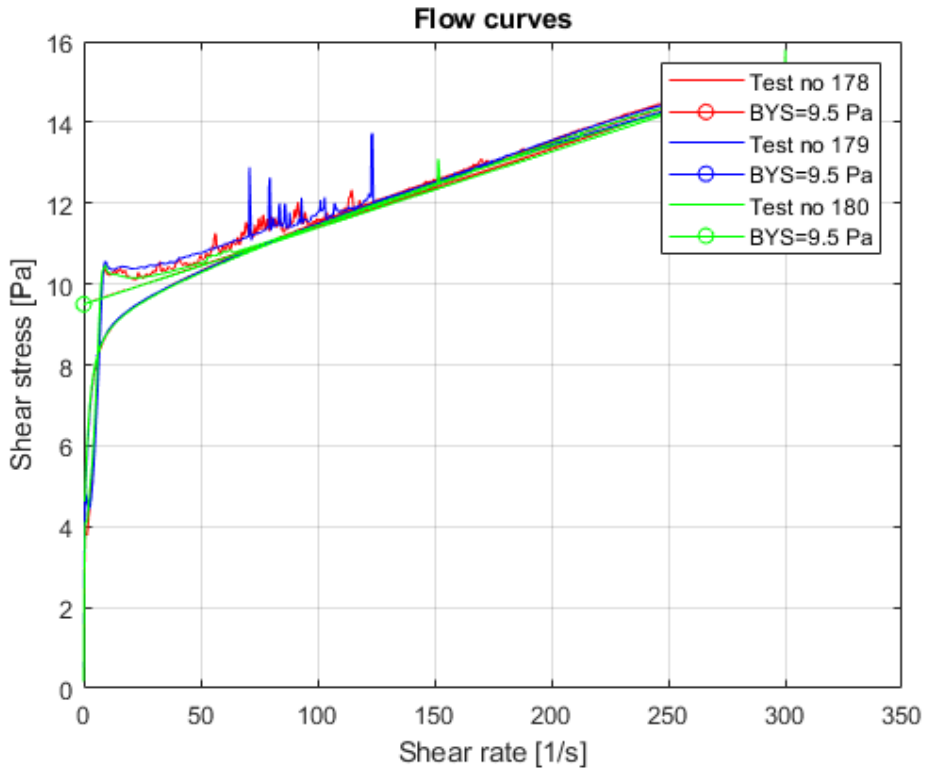

Figure B.37: Fluid mud-3 samples were collected before the flume tests were tested in CSR mode using bob-cup geometry to obtain flow curves.

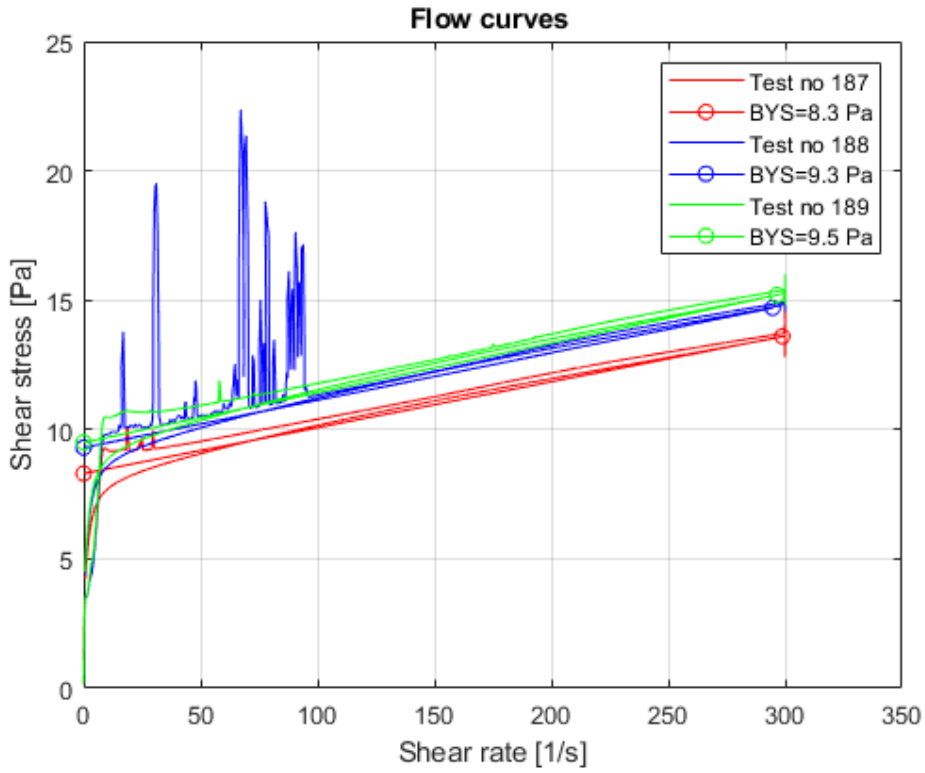

Figure B.38: Fluid mud-3 samples were collected after the flume tests were tested in CSR mode using bob-cup geometry to obtain flow curves.

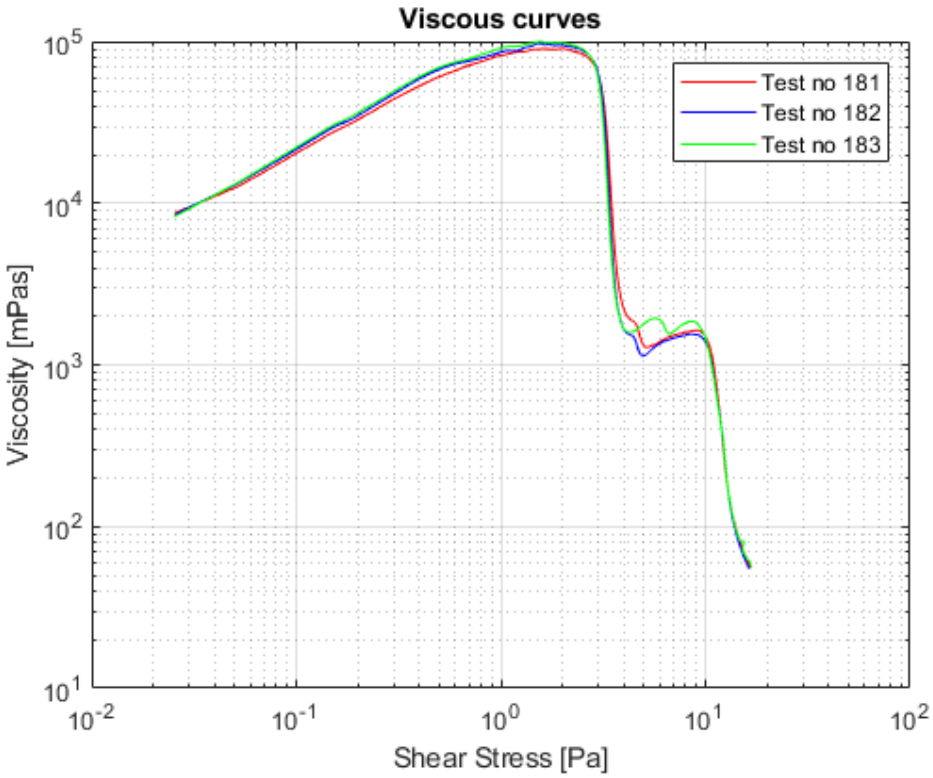

Figure B.39: Fluid mud-3 samples were collected before the flume tests were tested in CSS mode using bob-cup geometry to obtain viscous curves.

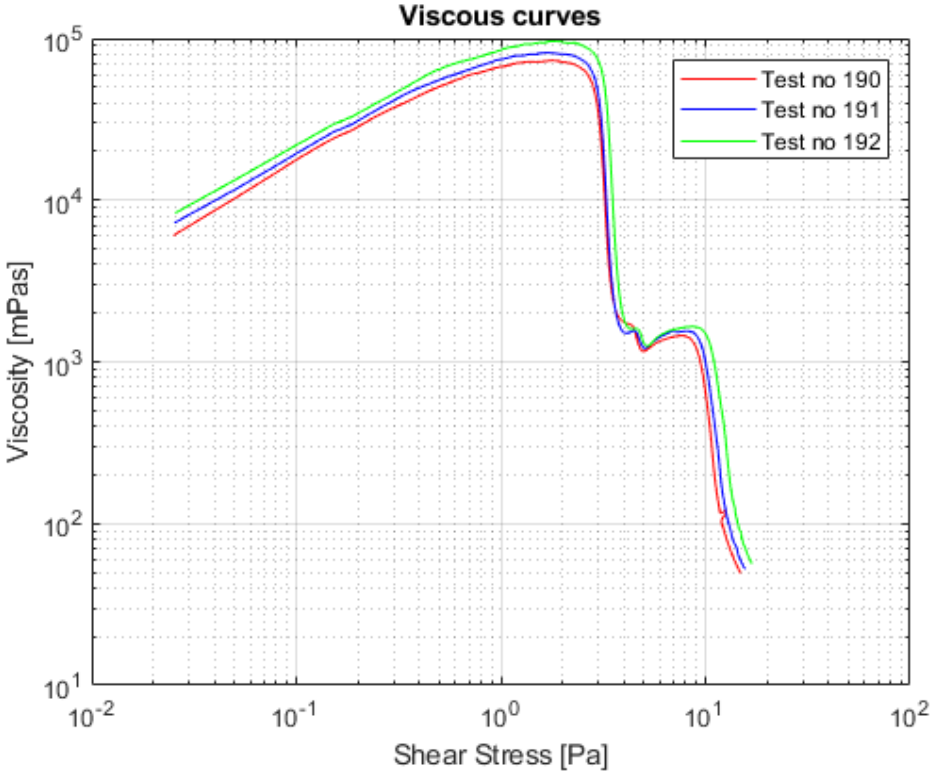

Figure B.40: Fluid mud-3 samples were collected after the flume tests were tested in CSS mode using bob-cup geometry to obtain viscous curves.

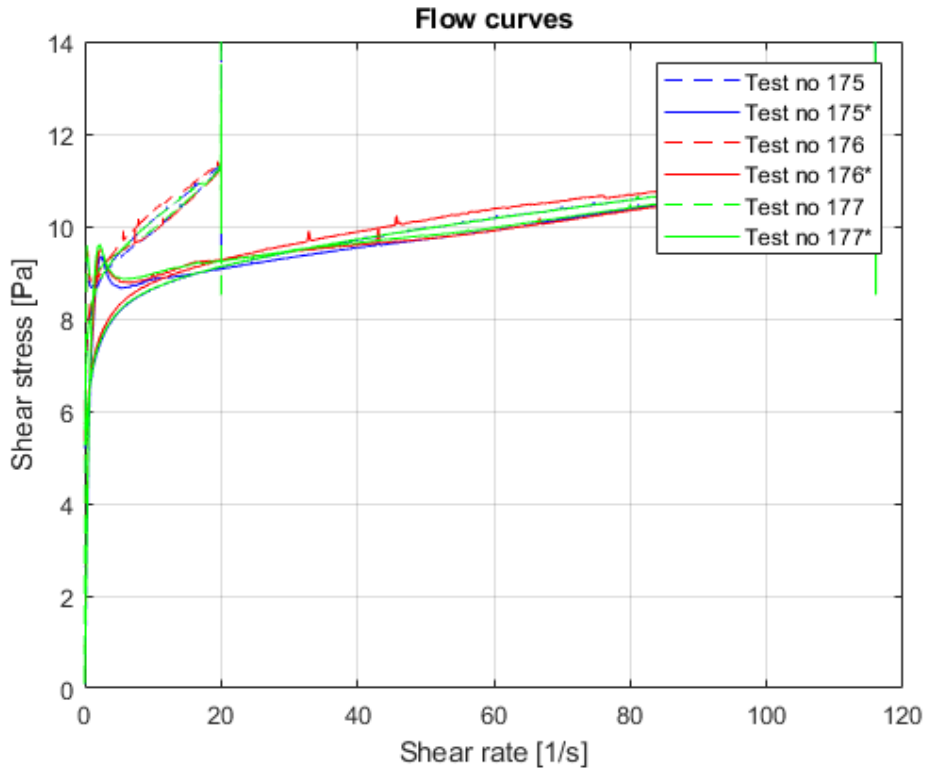

Figure B.41: Fluid mud-3 samples were collected before the flume tests were tested in CSR mode using vane(FL22)-cup geometry to obtain flow curves.

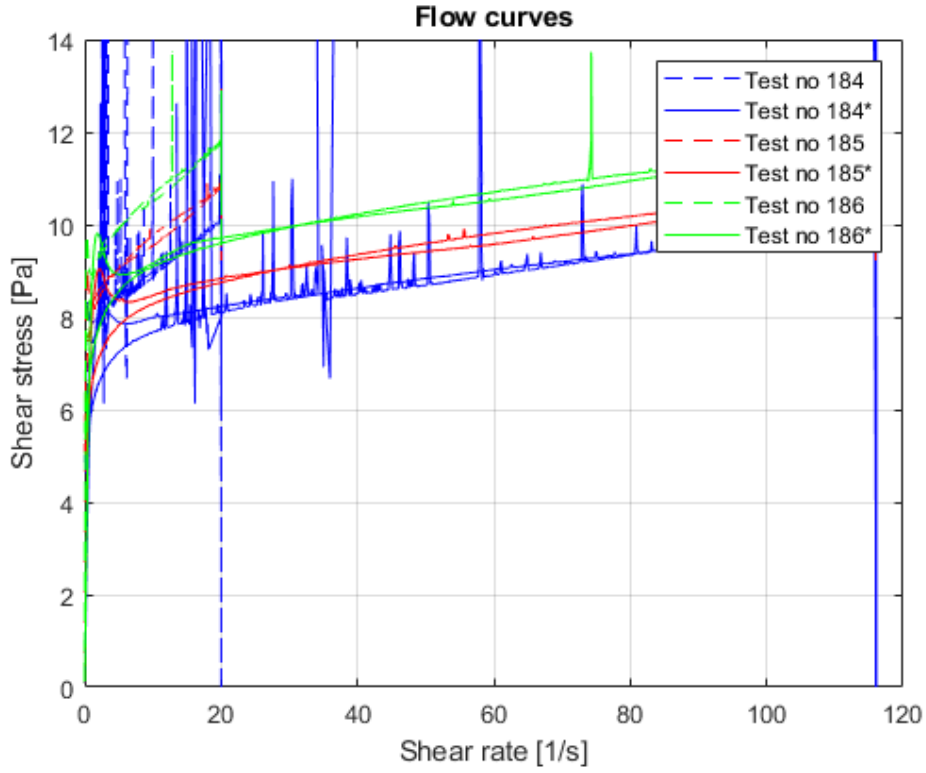

Figure B.42: Fluid mud-3 samples were collected after the flume tests were tested in CSR mode using vane(FL22)-cup geometry to obtain flow curves.

B.2.4 Fluid mud 3: Fluid mud used in the flume experiments with CUX sampler

The fluid mud was homogenized with rotor and blade set up in the flume experiments with CUX sampler. During the flume experiments, three fluid mud samples were collected (01:30 PM). The collected fluid mud samples were labeled with acronyms. For instance, the label CUXFM3S1 means Fluid mud 3 in the flume experiments with CUX sampler and sample number 1. Table B.4 represents the details of rheometry and oven test results of the fluid mud samples.

Table B.4: Details of rheometry and oven test results for Calandkanaal fluid mud samples collected during the third flume experiments. All the tests were performed on May 27, 2021.

Test no	Sample Id	From oven test method					Rheometry	
		Density [g/cc]	Vol. Concen-tration	Geo water content [%]	Hydro water content [%]	Solid content [%]	Geometry	Protocols
193	CUXFM3S1	1.172	0.09	231	76	24	Bob	CSR 0-100 180s up - 60s constant - 180s down
194	CUXFM3S2	1.170	0.09	233	76	24	Bob	CSR 0-100 180s up - 60s constant - 180s down
195	CUXFM3S1	1.172	0.09	231	76	24	Bob	CSS 0-100 150s up
196	CUXFM3S2	1.170	0.09	233	76	24	Bob	CSS 0-100 150s up
197	CUXFM3S1	1.172	0.09	231	76	24	Vane	CSR 0-20 180s up - 60s constant - 180s down
198	CUXFM3S2	1.170	0.09	233	76	24	Vane	CSR 0-20 180s up - 60s constant - 180s down

The flow curves obtained in CSR tests with bob-cup geometry are represented in the Figure B.43. The CSR tests with vane(FL22)-cup geometry are represented in Figure B.45. The fluid mud samples were also tested in CSS mode with bob-cup geometry to obtain the viscous curves, see Figure B.44.

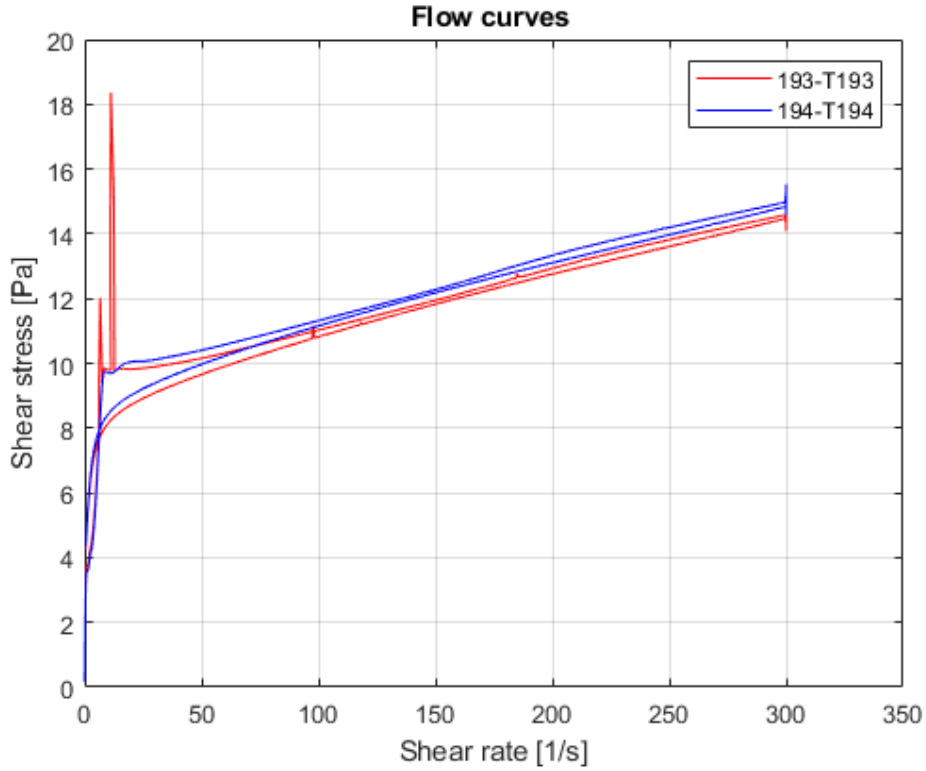

Figure B.43: Fluid mud-3 samples were collected during the flume tests with the Cux sampler were tested in CSR mode using bob-cup geometry to obtain flow curves.

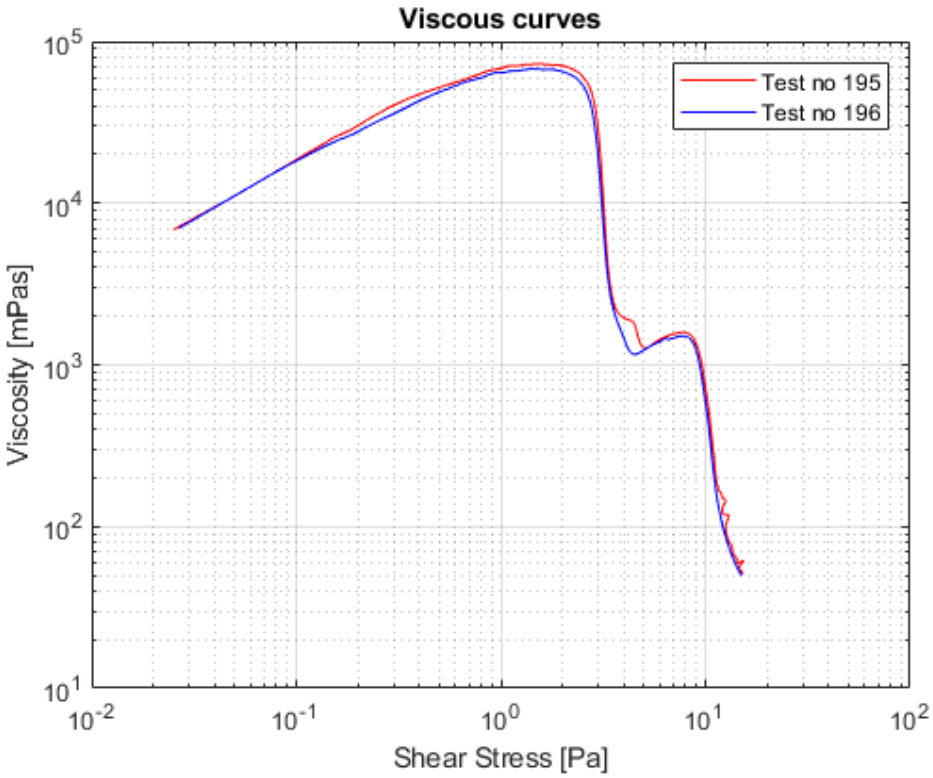

Figure B.44: Fluid mud-3 samples were collected during the flume tests with the Cux sampler were tested in CSS mode using bob-cup geometry to obtain viscous curves.

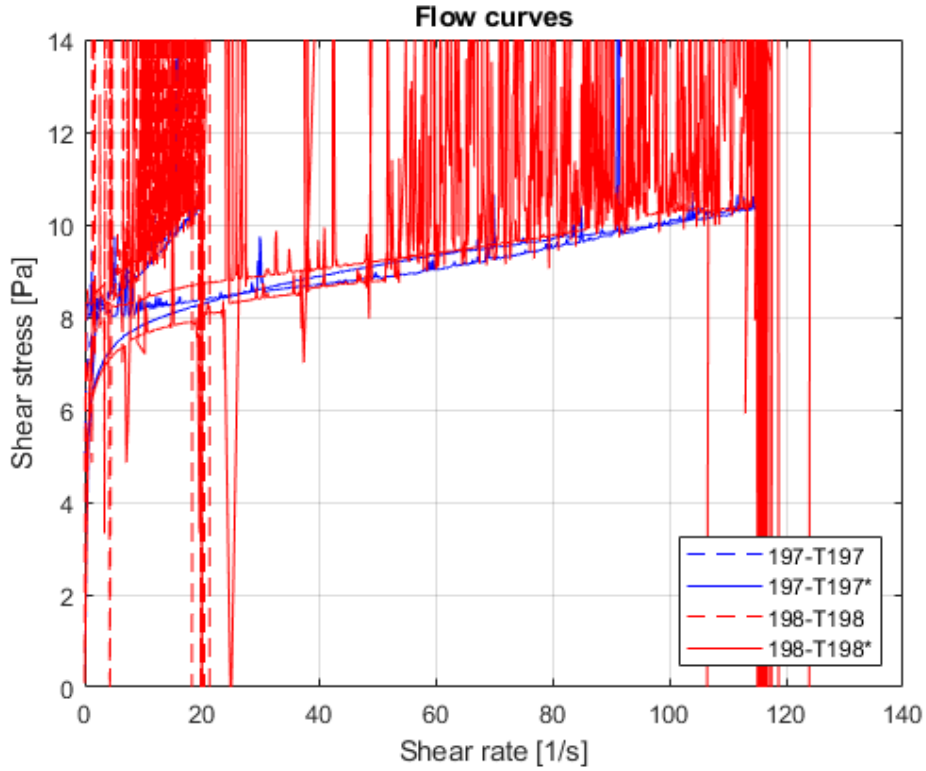

Figure B.45: Fluid mud-3 samples were collected during the flume tests with the Cux sampler were tested in CSR mode using vane(FL22)-cup geometry to obtain flow curves.

B.3 Analytical calculations of frictional force on a plate dragged in Power law fluids and Bingham fluids

The flow curves of the fluid mud samples collected during the flume experiments were fitted with Ostwald-de Waele (Power-law) model using the Thermo scientific HAAKE rheometer job manager software, see Figure B.46, B.47, B.48,B.49,B.50, and B.51. From these curve fittings, the values of fluid consistency (m) and flow index (n) were found, see Table B.5. The calculations of frictional force on a plate when dragged in power-law fluids are represented in Table B.6.

Table B.5: Details of power law curve fitting parameters and calculation of frictional force on a plate

	Sample number	**Fluid mud 1**		**Fluid mud 2**		**Fluid mud 3**	
		m	n	m	n	m	n
m and n	1	13.52	0.1456	9.443	0.1684	4.811	0.1987
	2	14.66	0.1412	9.114	0.1721	5.107	0.1869
	3	14	0.1528	8.888	0.172	5.008	0.1895
constant values	4	14.04	0.1367	9.165	0.172	4.277	0.1993
	5	12.87	0.1459	9.548	0.1665	4.849	0.1922
	6	14.81	0.136	8.968	0.1702	5.152	0.1865
	Average	**13.98**	**0.14**	**9.19**	**0.17**	**4.87**	**0.19**
F(n) (Eq. 2.23)		6.6343		6.5392		6.4642	
Cn (Eq. 2.22)		1.848		1.822		1.801	

Table B.6: Calculations of frictional force on a plate dragged in power-law fluids.

Fluid mud	**Velocity [m/s]**	**Reynolds number (Eq. 2.21)**	**Drag coefficient (Eq. 2.20)**	**Frictional force [N] (Eq. 2.19)**
Fluid mud-1	0.25	6	0.36	21.0
	0.5	23	0.12	27.2
	0.75	49	0.06	31.7
	1.0	84	0.04	35.3
Fluid mud-2	0.25	10	0.25	15.4
	0.5	36	0.09	20.8
	0.75	75	0.05	24.8
	1.0	126	0.03	28.1
Fluid mud-3	0.25	19	0.15	9.0
	0.5	67	0.05	12.6
	0.75	139	0.03	15.3
	1.0	234	0.02	17.6

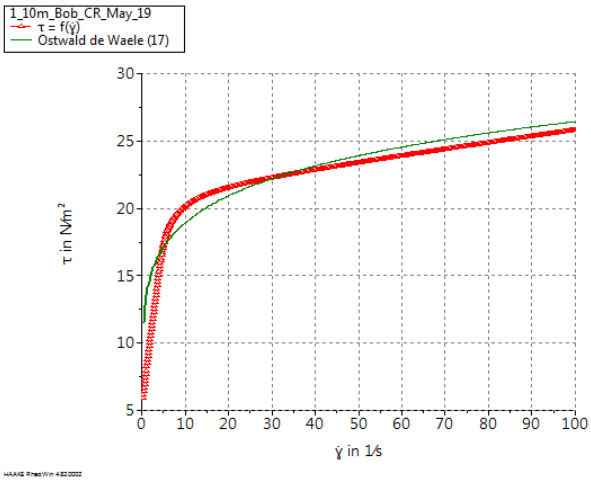

(a) Power law curve fitting to the ramp-down flow curve of Fluid mud-1 and sample no 1 (Test no 142)

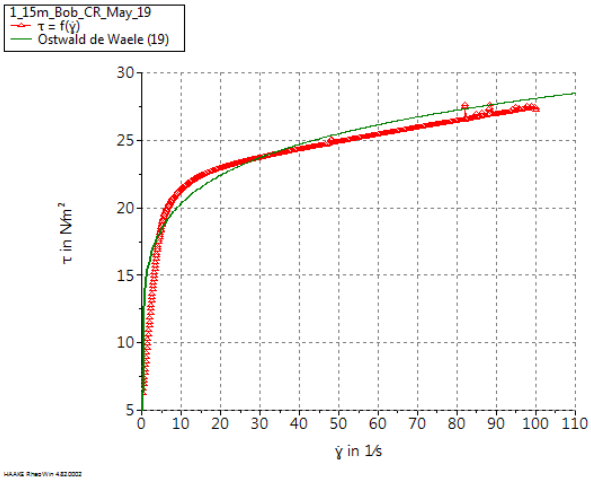

(b) Power law curve fitting to the ramp-down flow curve of Fluid mud-1 and sample no 2 (Test number 143)

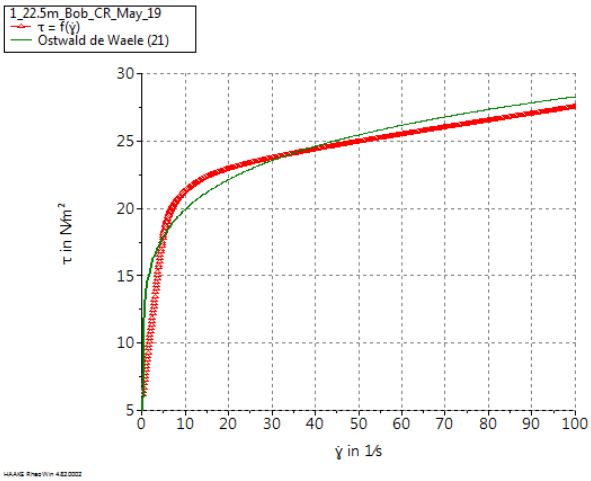

(c) Power law curve fitting to the ramp-down flow curve of Fluid mud-1 and sample no 3 (Test number 144)

Figure B.46: Ostwald-de Waele (Power-law) model curve fitting to the ramp-down flow curves of the fluid mud collected before the first set of flume experiments.

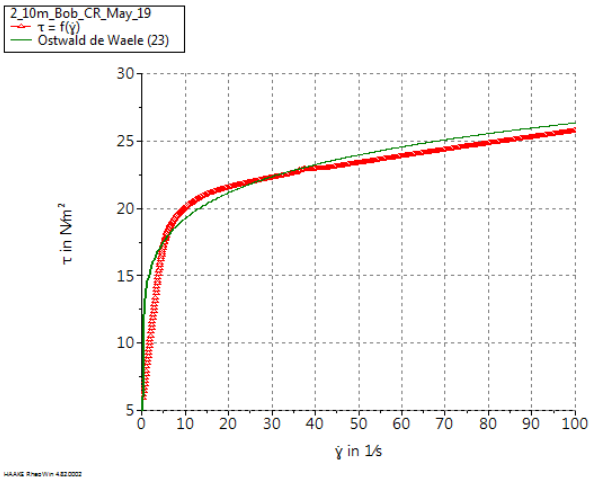

(a) Power law curve fitting to the ramp-down flow curve of Fluid mud-1 and sample no 4 (Test number 151)

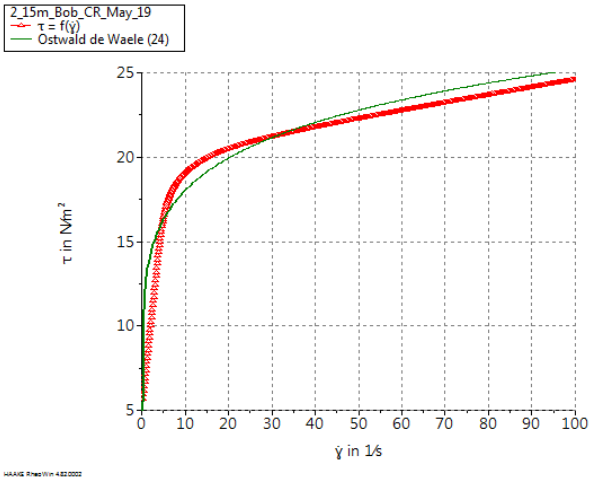

(b) Power law curve fitting to the ramp-down flow curve of Fluid mud-1 and sample no 5 (Test number 152)

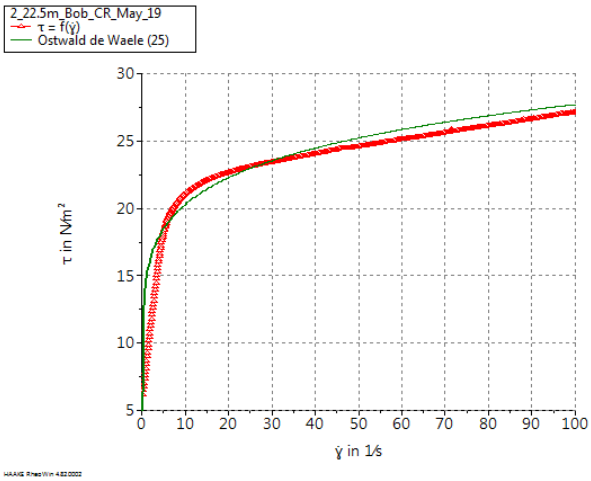

(c) Power law curve fitting to the ramp-down flow curve of Fluid mud-1 and sample no 6 (Test number 153)

Figure B.47: Ostwald-de Waele (Power-law) model curve fitting to the ramp-down flow curves of the fluid mud collected after the first set of flume experiments.

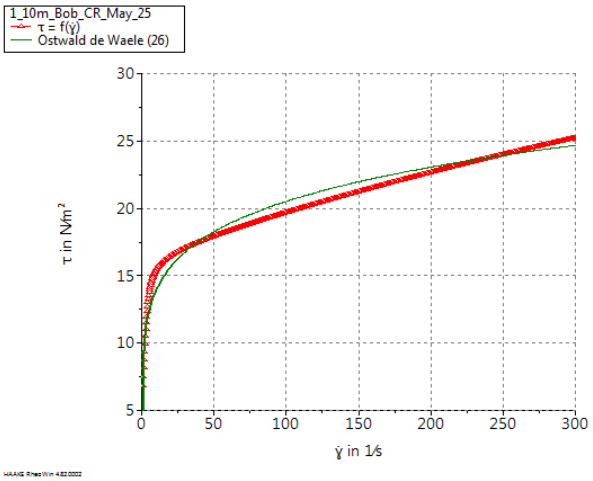

(a) Power law curve fitting to the ramp-down flow curve of Fluid mud-2 and sample no 1 (Test no 160)

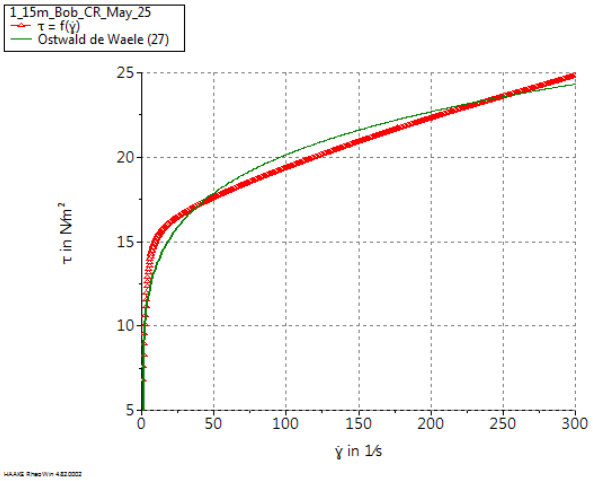

(b) Power law curve fitting to the ramp-down flow curve of Fluid mud-2 and sample no 2 (Test number 161)

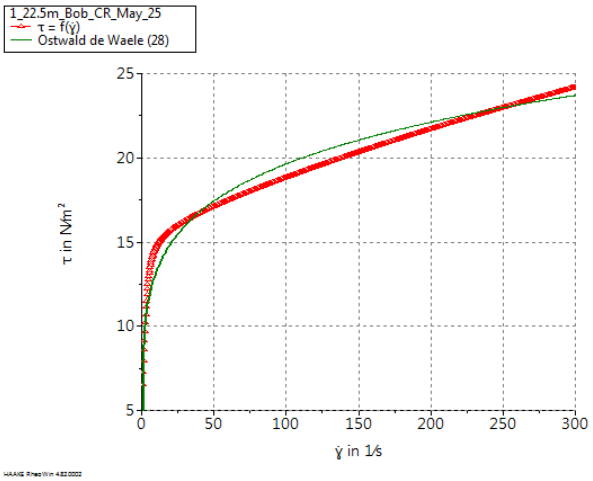

(c) Power law curve fitting to the ramp-down flow curve of Fluid mud-2 and sample no 3 (Test number 162)

Figure B.48: Ostwald-de Waele (Power-law) model curve fitting to the ramp-down flow curves of the fluid mud collected before the second set of flume experiments.

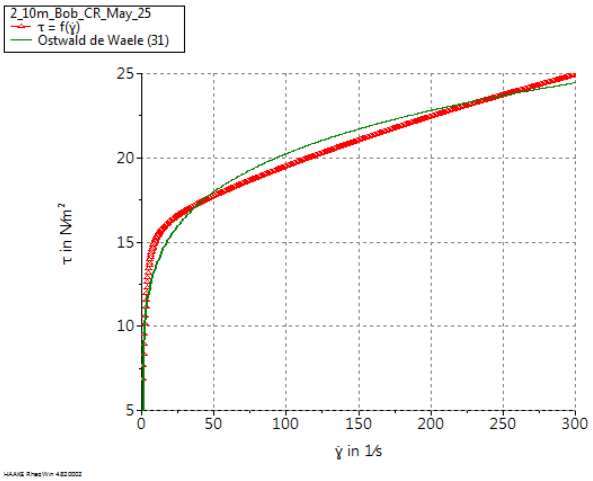

(a) Power law curve fitting to the ramp-down flow curve of Fluid mud-2 and sample no 4 (Test number 169)

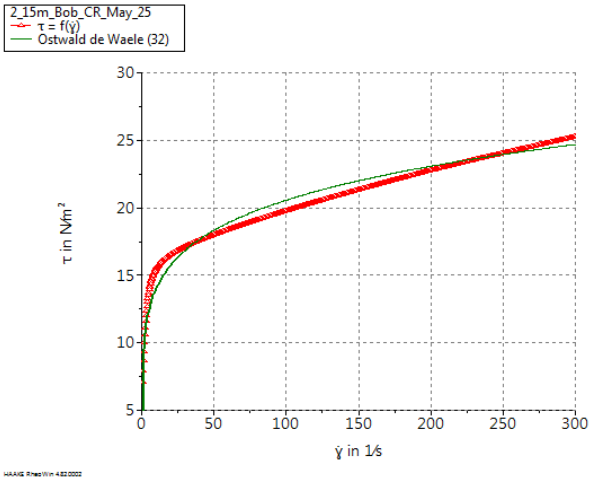

(b) Power law curve fitting to the ramp-down flow curve of Fluid mud-2 and sample no 5 (Test number 170)

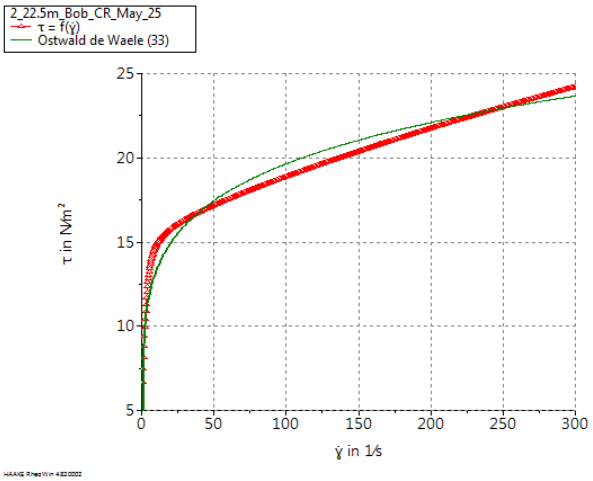

(c) Power law curve fitting to the ramp-down flow curve of Fluid mud-2 and sample no 6 (Test number 171)

Figure B.49: Ostwald-de Waele (Power-law) model curve fitting to the ramp-down flow curves of the fluid mud collected after the second set of flume experiments.

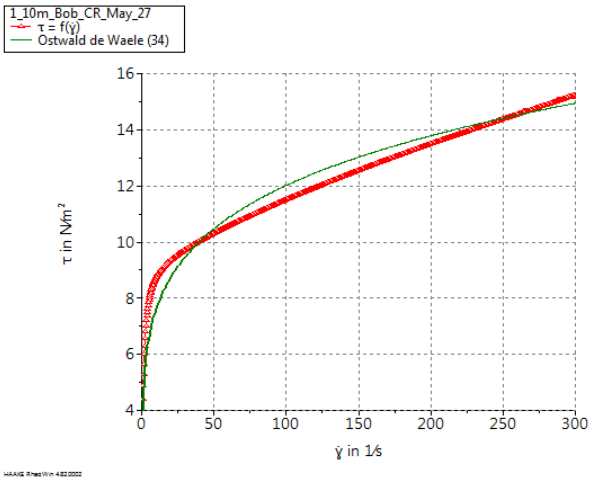

(a) Power law curve fitting to the ramp-down flow curve of Fluid mud-3 and sample no 1 (Test no 178)

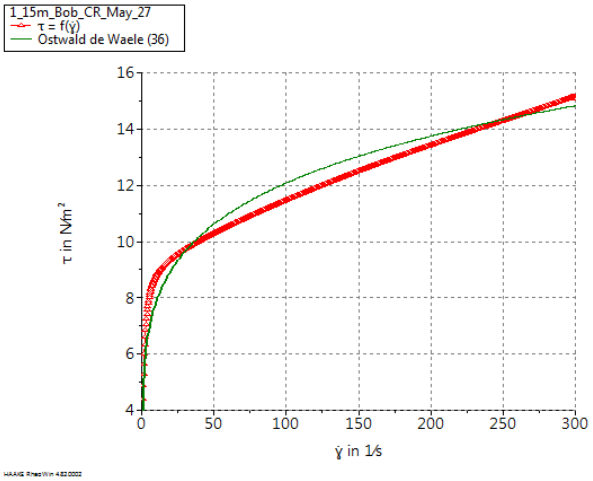

(b) Power law curve fitting to the ramp-down flow curve of Fluid mud-3 and sample no 2 (Test number 179)

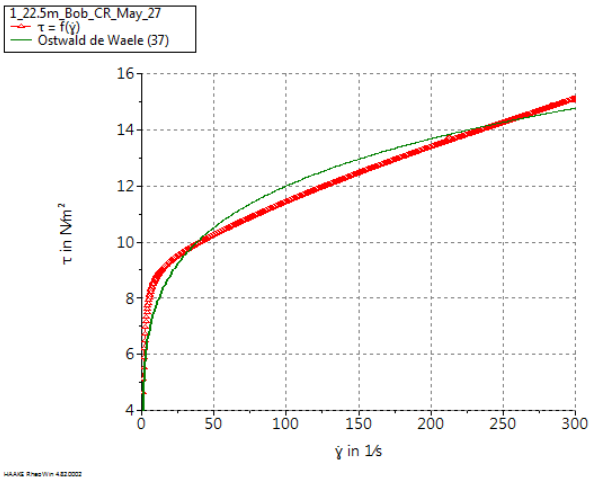

(c) Power law curve fitting to the ramp-down flow curve of Fluid mud-3 and sample no 3 (Test number 180)

Figure B.50: Ostwald-de Waele (Power-law) model curve fitting to the ramp-down flow curves of the fluid mud collected before the third set of flume experiments.

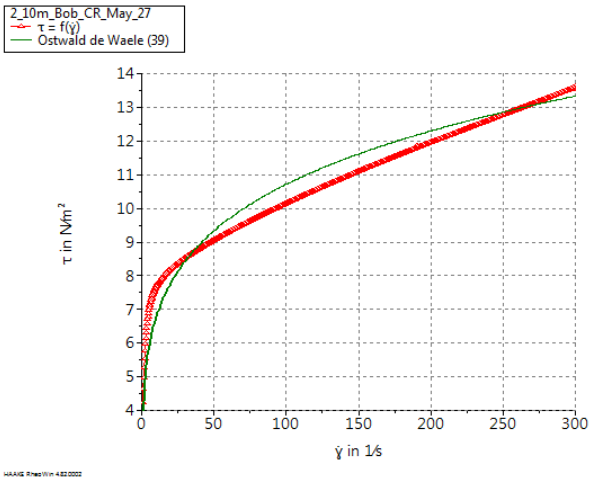

(a) Power law curve fitting to the ramp-down flow curve of Fluid mud-3 and sample no 4 (Test number 187)

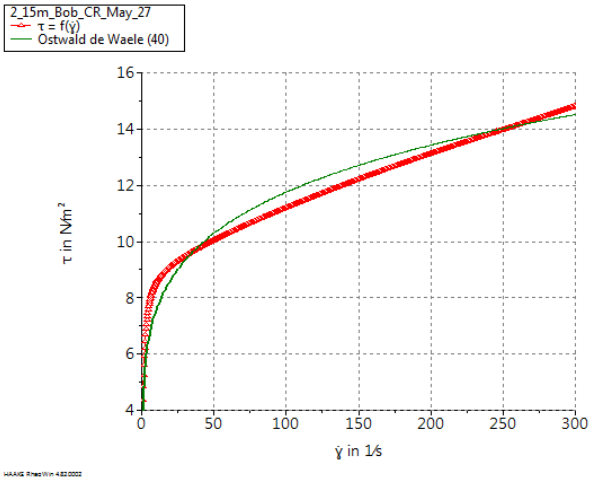

(b) Power law curve fitting to the ramp-down flow curve of Fluid mud-3 and sample no 5 (Test number 188)

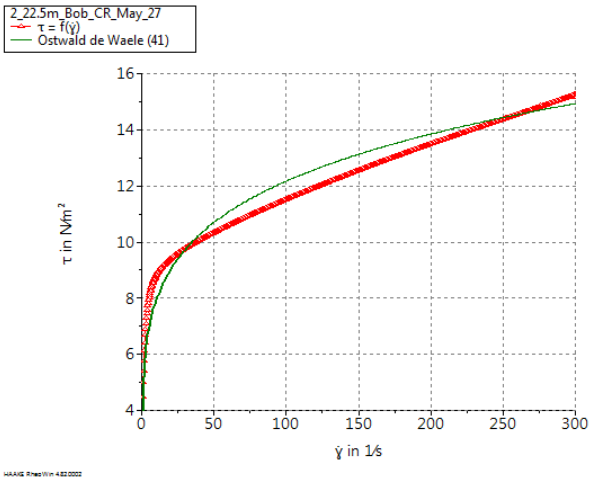

(c) Power law curve fitting to the ramp-down flow curve of Fluid mud-3 and sample no 6 (Test number 189)

Figure B.51: Ostwald-de Waele (Power-law) model curve fitting to the ramp-down flow curves of the fluid mud collected after the third set of flume experiments.

The frictional force exerted on a plate when dragged in Bingham fluids is calculated using the analytical

formulas, see Table B.7.

Table B.7: Calculations of frictional forces exerted on a plate dragged in Bingham fluids

Fluid mud	Velocity [m/s]	Reynolds number (Eq. 2.12)	Bingham number (Eq. 2.15)	Drag coefficient (Eq. 2.14)	Frictional force [N] (Eq. 2.16)
Fluid mud-1	0.25	4674	0.558	0.577	33.3
	0.5	9348	0.139	0.153	35.3
	0.75	14023	0.062	0.073	37.9
	1.0	18697	0.035	0.044	41.0
Fluid mud-2	0.25	8670	0.438	0.452	27.2
	0.5	17340	0.109	0.119	28.8
	0.75	26010	0.049	0.057	30.7
	1.0	34680	0.027	0.034	33.1
Fluid mud-3	0.25	12709	0.251	0.262	15.6
	0.5	25418	0.063	0.071	16.8
	0.75	38126	0.028	0.034	18.4
	1.0	50835	0.016	0.021	20.3

List of Tables

List of Figures

References

Abril, G., Commarieu, M.-V., Maro, D., Fontugne, M., Guérin, F., & Etcheber, H. (2004, 5). A massive dissolved inorganic carbon release at spring tide in a highly turbid estuary. *Geophysical Research Letters*, *31*(9), n/a-n/a. Retrieved from http://doi.wiley.com/10.1029/2004GL019714 doi: 10.1029/2004GL019714

Ahuja, A., Potanin, A., & Joshi, Y. M. (2020, 8). Two step yielding in soft materials. *Advances in Colloid and Interface Science*, *282*, 102179. Retrieved from https://doi.org/10.1016/j.cis.2020.102179https://linkinghub.elsevier.com/retrieve/pii/S0001868620301755 doi: 10.1016/j.cis.2020.102179

Allen, J. (1991, 12). Fine sediment and its sources, Severn Estuary and inner Bristol Channel, southwest Britain. *Sedimentary Geology*, *75*(1-2), 57–65. Retrieved from https://linkinghub.elsevier.com/retrieve/pii/003707389190050N doi: 10.1016/0037-0738(91)90050-N

Barnes, H. A. (1997). *Thixotropy - A review.* doi: 10.1016/S0377-0257(97)00004-9

Barnes, H. A. (1999, 2). The yield stress-a review or '$\pi\alpha\nu\tau\alpha\ \rho\epsilon\iota$'-everything flows? *Journal of Non-Newtonian Fluid Mechanics*, *81*(1-2), 133–178. doi: 10.1016/S0377-0257(98)00094-9

Barth, R., van der Made, C. J. A. W., Bourgonjen, L., van Dijken, J., Vantorre, M., & Verwilligen, J. (2016). MANOEUVRING WITH NEGATIVE UNDERKEEL CLEARANCE : 2 ND FULL SCALE FIELD TEST IN THE PORT OF DELFZIJL. In *Proceedings of the 4th international conference on ship manoeuvring in shallow and confined water (mashcon), 23 - 25 may 2016, hamburg, germany* (Vol. 0, pp. 262–271). Bundesanstalt für Wasserbau (BAW). doi: 10.18451/978-3-939230-38-0{_}30

Bezuijen, A., Den Hamer, D. A., Vincke, L., & Geirnaert, K. (2018, 7). Free fall cone tests in kaolin clay. *Physical Modelling in Geotechnics*, *1*, 285–291. Retrieved from https://www-taylorfrancis-com.tudelft.idm.oclc.org/chapters/edit/10.1201/9780429438660-37/free-fall-cone-tests-kaolin-clay-bezuijen-den-hamer-vincke-geirnaert doi: 10.1201/9780429438660-37

Bingham, E. C. (1922). Fluidity and plasticity. *Engineering*, 440. Retrieved from http://orton.catie.ac.cr/cgi-bin/wxis.exe/?IsisScript=BFHIA.xis&method=post&formato=2&cantidad=1&expresion=mfn=011959

Bird, R. B., & Marsh, B. D. (2000, 7). Viscoelastic Hysteresis. Part I. Model Predictions. *Transactions of the Society of Rheology*, *12*(4), 479. Retrieved from https://sor.scitation.org/doi/abs/10.1122/1.549096 doi: 10.1122/1.549096

Birk, L. (2019). Fundamentals of ship hydrodynamics : fluid mechanics, ship resistance and propulsion / Lothar Birk, University of New Orleans. In (p. 634).

Boger, D. V. (2009, 11). Rheology and the resource industries. *Chemical Engineering Science*, *64*(22), 4525–4536. Retrieved from www.wise-uranium.org/mdaf.htmlhttps://linkinghub.elsevier.com/retrieve/pii/S0009250909001705 doi: 10.1016/j.ces.2009.03.007

Brossard, C., Delouis, A., Galichon, P., Granboulan, J., & Monadier, P. (1991). Navigability in channels subject to siltation physical scale model experiments. In *Proceedings of the coastal engineering conference.* doi: 10.1061/9780872627765.236

Chandran, N., C, S., & Thomas, S. (2020). Introduction to rheology. In *Rheology of polymer blends and nanocomposites* (pp. 1–17). Elsevier. Retrieved from https://linkinghub.elsevier.com/retrieve/pii/B978012816957500001X doi: 10.1016/B978-0-12-816957-5.00001-X

Cheng, D. C.-H. (1986, 9). Yield stress: A time-dependent property and how to measure it. *Rheologica Acta*, *25*(5), 542–554. Retrieved from http://link.springer.com/10.1007/BF01774406 doi: 10.1007/BF01774406

Chhabra, R. P., & Richardson, J. F. (2008). *Non-Newtonian Flow and Applied Rheology*. Elsevier. Retrieved from https://linkinghub.elsevier.com/retrieve/pii/B9780750685320X00017 doi: 10.1016/B978-0-7506-8532-0.X0001-7

Delefortrie, G. (2007). *Manoeuvring behaviour of container vessels in muddy navigation areas* (Unpublished doctoral dissertation).

Dzuy, N. Q., & Boger, D. V. (1983, 8). Yield Stress Measurement for Concentrated Suspensions. *Journal of Rheology*, *27*(4), 321–349. Retrieved from http://sor.scitation.org/doi/10.1122/1.549709 doi: 10.1122/1.549709

Eberli, G. P., Swart, P. K., Malone, M. J., & et al. (1997). *Proceedings, initial reports, Ocean Drilling Program, Leg 166; Bahamas transect*.

Fitton, T., Williams, M., Seddon, K., Bhattacharya, S., & Chryss, A. (2007, 3). Simulation of Thickened Tailings Stacks. *Paste 2007: Tenth International Seminar on Paste and Thickened Tailings, 2007 13-15 March, Perth*, 305–313. Retrieved from https://papers.acg.uwa.edu.au/p/702_30_Fitton/

Foda, M. A., Hunt, J. R., & Hsien-Ter Chou. (1993). A nonlinear model for the fluidization of marine mud by waves. *Journal of Geophysical Research*. doi: 10.1029/92jc02797

Gao, Z., Yang, H., & Xie, M. (2015). Computation of flow around wigley hull in shallow water with muddy seabed. *Journal of Coastal Research*. doi: 10.2112/SI73-086.1

Gleißle, W. (1993). Rate- or Stress-Controlled Rheometry. In *Techniques in rheological measurement.* doi: 10.1007/978-94-011-2114-9{_}9

Goodeve, C. F. (1939, 1). A general theory of thixotropy and viscosity. *Transactions of the Faraday Society*, *35*(0), 342–358. Retrieved from https://pubs.rsc.org/en/content/articlehtml/1939/tf/tf9393500342https://pubs.rsc.org/en/content/articlelanding/1939/tf/tf9393500342 doi: 10.1039/TF9393500342

Google Maps. (n.d.). Retrieved from https://www.google.com/maps/@51.9631738,4.116197,15z?hl=en

Granboulan, J., Feral, A., Villerot, M., & Jouanneau, J. M. (1989, 1). Study of the sedimentological and rheological properties of fluid mud in the fluvio-estuarine system of the Gironde estuary. *Ocean and Shoreline Management*, *12*(1), 23–46. doi: 10.1016/0951-8312(89)90041-6

Green, H., & Weltmann, R. N. (1946). Equations of Thixotropic Breakdown for the Rotational Viscometer. *Industrial and Engineering Chemistry - Analytical Edition*. doi: 10.1021/i560151a004

Herschel, W. H., & Bulkley, R. (1926). Konsistenzmessungen von Gummi-Benzollösungen. *Kolloid-Zeitschrift*. doi: 10.1007/BF01432034

The IUPAC Compendium of Chemical Terminology. (2019). *The IUPAC Compendium of Chemical Terminology*. doi: 10.1351/GOLDBOOK

Jacobs, W., Kesteren, W. V., & Winterwerp, J. C. (2008). Chapter 8 Strength of sediment mixtures as a function of sand content and clay mineralogy. *Proceedings in Marine Science*, *9*. doi: 10.1016/S1568-2692(08)80010-1

Kaidi, S., Lefrançois, E., & Smaoui, H. (2020). Numerical modelling of the muddy layer effect on Ship's resistance and squat. *Ocean Engineering*. doi: 10.1016/j.oceaneng.2020.106939

Kineke, G., Sternberg, R., Trowbridge, J., & Geyer, W. (1996, 1). Fluid-mud processes on the Amazon continental shelf. *Continental Shelf Research*, *16*(5-6), 667–696. Retrieved from https://linkinghub.elsevier.com/retrieve/pii/027843439500050X doi: 10.1016/0278-4343(95)00050-X

Kirichek, A., Chassagne, C., Winterwerp, J., & Vellinga, T. (2018). How Navigable Are Fluid Mud Layers? *Terra et Aqua*(August), 7–18.

Kirichek, A., Shakeel, A., & Chassagne, C. (2020, 6). Using in situ density and strength measurements for sediment maintenance in ports and waterways. *Journal of Soils and Sediments*, *20*(6), 2546–2552. Retrieved from https://doi.org/10.1007/s11368-020-02581-8http://link.springer.com/10.1007/s11368-020-02581-8 doi: 10.1007/s11368-020-02581-8

Kranenburg, C. (1994). The fractal structure of cohesive sediment aggregates. *Estuarine, Coastal and Shelf Science*, *39*(6). doi: 10.1016/S0272-7714(06)80002-8

Leijs, K. (2021). *CFD simulations of the flow around a tanker in shallow water with muddy seabed* (Doctoral dissertation, Delft University of Technology). Retrieved from https://repository.tudelft.nl/islandora/object/uuid%3Aa7c7e1ae-e7f0-4e15-9a03-0901af9e8959

Liepsch, D. (2016). A Basic Introduction to Rheology Shear Flow. *J Biomech*.

McAnally, W. H., Friedrichs, C., Hamilton, D., Hayter, E., Shrestha, P., Rodriguez, H., ... Teeter, A. (2007, 1). Management of Fluid Mud in Estuaries, Bays, and Lakes. I: Present State of Understanding on Character and Behavior. *Journal of Hydraulic Engineering*, *133*(1), 9–22. Retrieved from http://ascelibrary.org/doi/10.1061/%28ASCE%290733-9429%282007%29133%3A1%289%29 doi: 10.1061/(ASCE)0733-9429(2007)133:1(9)

Mehta, A. J. (2013). *An Introduction to Hydraulics of Fine Sediment Transport* (Vol. 38; A. Mehta, Ed.). WORLD SCIENTIFIC. Retrieved from https://www.worldscientific.com/worldscibooks/10.1142/8708 doi: 10.1142/8708

Mehta, A. J., Samsami, F., Khare, Y. P., & Sahin, C. (2014, 3). Fluid Mud Properties in Nautical Depth Estimation. *Journal of Waterway, Port, Coastal, and Ocean Engineering*, *140*(2), 210–222. Retrieved from https://ascelibrary-org.tudelft.idm.oclc.org/doi/abs/10.1061/%28ASCE%29WW.1943-5460.0000228 doi: 10.1061/(ASCE)WW.1943-5460.0000228

Mewis, J., & Wagner, N. J. (2009, 3). Thixotropy. *Advances in Colloid and Interface Science*, *147-148*(C), 214–227. doi: 10.1016/J.CIS.2008.09.005

Nichols, M. M., Thompson, G. S., & Faas, R. W. (1978, 7). *A Field Study of Fluid Mud Dredged Material. Its Physical Nature and Dispersal.* (Tech. Rep.). Retrieved from https://apps.dtic.mil/sti/citations/ADA058952

PIANC. (2014). *Harbour Approach Channels Design Guidelines* (Tech. Rep.).

Rodrigue, J.-P. (2020). *Port terminals section updated | The Geography of Transport Systems*. Retrieved from https://transportgeography.org/port-terminals-section-updated-2/ doi: 10.4324/9780429346323

Schramm, G. (1994). A Practical Approach to Rheology and Rheometry. *Rheology*.

Schultz, M. P., Bendick, J. A., Holm, E. R., & Hertel, W. M. (2011). Economic impact of biofouling on a naval surface ship. *Biofouling*. doi: 10.1080/08927014.2010.542809

Sellmeijer, R., & van Oortmerssen, G. (1984). EFFECT OF MUD ON TANKER MANOEUVRES. *Naval Architect*, *126*, 7.

Šesták, J., Žitný, R., & Houška, M. (1983, 1). Simple rheological models of food liquids for process design and quality assessment. *Journal of Food Engineering*, *2*(1), 35–49. Retrieved from https://linkinghub.elsevier.com/retrieve/pii/0260877483900055 doi: 10.1016/0260-8774(83)90005-5

Shakeel, A., Kirichek, A., & Chassagne, C. (2020a, 6). Rheological analysis of mud from Port of Hamburg, Germany. *Journal of Soils and Sediments*, *20*(6), 2553–2562. Retrieved from https://doi.org/10.1007/s11368-019-02448-7http://link.springer.com/10.1007/s11368-019-02448-7 doi: 10.1007/s11368-019-02448-7

Shakeel, A., Kirichek, A., & Chassagne, C. (2020b, 9). Yield stress measurements of mud sediments using different rheological methods and geometries: An evidence of two-step yielding. *Marine Geology*, *427*(September 2019), 106247. Retrieved from https://doi.org/10.1016/j.margeo.2020

.106247https://linkinghub.elsevier.com/retrieve/pii/S0025322720301353 doi: 10.1016/j.margeo.2020.106247

Shakeel, A., MacIver, M., van Kan, P. J., Kirichek, A., & Chassagne, C. (2021, 9). A rheological and microstructural study of two-step yielding in mud samples from a port area. *Colloids and Surfaces A: Physicochemical and Engineering Aspects*, *624*, 126827. Retrieved from https://linkinghub.elsevier.com/retrieve/pii/S0927775721006968 doi: 10.1016/j.colsurfa.2021.126827

Song, S., Dai, S., Demirel, Y. K., Atlar, M., Day, S., & Turan, O. (2021). Experimental and Theoretical Study of the Effect of Hull Roughness on Ship Resistance. *Journal of Ship Research*. doi: 10.5957/josr.07190040

Steffe, J. F. (1967). *Rheological Methods IN FOOD PROCESS ENGINEERING, Second Edition*. Freeman press.

Stieger, M. (2019). The Rheology Handbook - For users of rotational and oscillatory rheometers. *Applied Rheology*. doi: 10.1515/arh-2002-0029

Teeter, A. (1992). *Evaluation on new fluid mud survey system at field sites.* (Tech. Rep.).

Ten Brummelhuis, E. (2021). *Modelling of high concentration fluid mud water injection dredging density currents* (Tech. Rep.). Retrieved from https://repository.tudelft.nl/islandora/object/uuid%3Ae4b50eee-adce-4847-9ed5-4528b58658c0

Toorman, E. A. (1997). Modelling the thixotropic behaviour of dense cohesive sediment suspensions. *Rheologica Acta 1997 36:1*, *36*(1), 56–65. Retrieved from https://link-springer-com.tudelft.idm.oclc.org/article/10.1007/BF00366724 doi: 10.1007/BF00366724

Van Kessel, T., & Blom, C. (1998). Rheology of cohesive sediments: Comparison between a natural and an artificial mud. *Journal of Hydraulic Research*, *36*(4), 591–612. Retrieved from https://iahr.tandfonline.com/doi/abs/10.1080/00221689809498611 doi: 10.1080/00221689809498611

Vantorre, M. (1991). Ship behaviour and control at low speed in layered fluids. In *Hadmar '91, international symposium hydro- and aerodynamics in marine engineering.*

Winterwerp, J. C., & van Kesteren, W. G. M. (2004). *Introduction to the Physics of Cohesive Sediment Dynamics in the Marine Environment*.

Zander, F., Heimovaara, T., & Gebert, J. (2020). Spatial variability of organic matter degradability in tidal Elbe sediments. *Journal of Soils and Sediments*, *20*(6). doi: 10.1007/s11368-020-02569-4